# Advances in Hybrid Thin Film Composite Membranes:
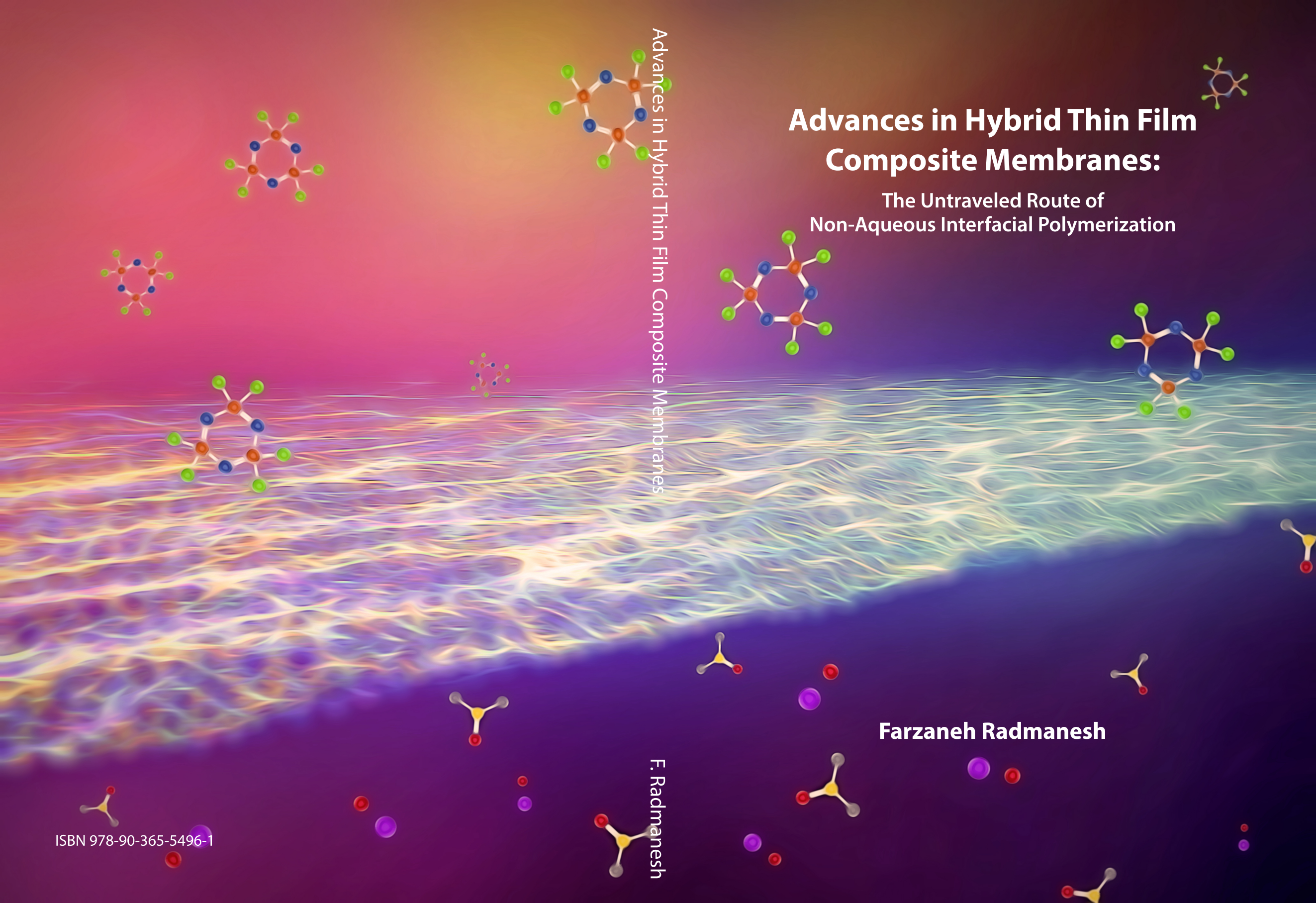
## The Untraveled Route of Non-Aqueous Interfacial Polymerization

**Farzaneh Radmanesh**

# ADVANCES IN HYBRID THIN FILM COMPOSITE MEMBRANES:

# THE UNTRAVELED ROUTE OF NON-AQUEOUS INTERFACIAL POLYMERIZATION

*Farzaneh Radmanesh*

# ADVANCES IN HYBRID THIN FILM COMPOSITE MEMBRANES:

# THE UNTRAVELED ROUTE OF NON-AQUEOUS INTERFACIAL POLYMERIZATION

DISSERTATION

to obtain
the degree of doctor at the Universiteit Twente,
on the authority of the rector magnificus,
prof. dr. ir. A. Veldkamp,
on account of the decision of the Doctorate Board
to be publicly defended
on Friday 16 December 2022 at 12.45 hours

by

**Farzaneh Radmanesh**

born on the 29th of August, 1989
in Esfahan, Iran

This dissertation has been approved by:

Supervisors

prof. dr. ir. N.E. Benes
prof. dr. ir. E.J.R. Sudhölter

**Graduation Committee:**

| | |
|---|---|
| Chair / secretary: | prof.dr. J.L. Herek |
| Supervisors: | prof.dr.ir. N.E. Benes<br>Universiteit Twente, TNW, Inorganic<br>Membranes |
| | prof.dr.ir. E.J.R. Sudhölter<br>Universiteit Twente, TNW, Films in Fluids |
| Committee Members: | dr. M.A. Hempenius<br>Universiteit Twente, TNW, Sustainable Polymer<br> Chemistry |
| | prof.dr. C.A. Nijhuis<br>Universiteit Twente, TNW, Hybrid Materials<br>for Opto-Electronics |
| | prof.dr.ir. G. Bargeman<br>Nobian Chemicals B.V |
| | dr.ir. T.A. Peters<br>Sintef |
| | prof.dr. K.U. Loos<br>University of Groningen |
| | prof.dr. S.P. Nunes<br>KAUST, Environmental Science and Engineering |

*To my father….*

# Table of contents

# Summary

Interfacial polymerization is a very flexible technique in which polymerization occurs at the interface between two immiscible phases. It allows for fabrication of thin and defect-free membrane films that can be used in various applications, such as nanofiltration, gas separation and gas barriers. Normally, the polymerization reaction takes place between two reactive monomers, one in water and one in an organic solvent. However, many interesting reactants, including amines and alcohols with complex topologies, are difficult to dissolve in water. This thesis focuses on non-aqueous interfacial polymerization techniques for new thin film materials from monomer combinations that previously could not be used in interfacial polymerization. With the proposed technique, a series of cyclomatrix polyphosphazene networks are synthesized and their properties and performance are tuned for various industrial application demands.

**Chapter 1** gives an overview of interfacial polymerization and the parameters that influence the properties and performance of the film. Furthermore, the challenges and restrictions of classical aqueous interfacial polymerization are discussed. The second part of this chapter argues the limitation of aqueous interfacial polymerization and proposes a new non-aqueous platform to broaden the number of monomers and synthesis chemistries with this technique. It is followed by a discussion of the industrial needs and challenges for thermally stable gas separation membranes, organic solvent nanofiltration membranes, and gas barriers.

**Chapter 2** covers a systematic study of the effects of cations on membrane properties and performance. For this, two distinct POSS molecules were used: one functionalized with $-NH_3^+Cl^-$ and one, so far unexplored, with $-NH_2$. The ammonium groups are partially deprotonated by using three different bases, LiOH, NaOH, and KOH. We demonstrate that the introduced cations affect the film thickness but not the molecular composition of the polyamic acid. All the obtained polyamic acids can be imidized, but the cations reduce the imidization kinetics as well as the loss of organic crosslinkers. For flat disc membranes, at 200 °C, the absence of cations results in comparable permeability combined with higher selectivity for $H_2/N_2$. This, and the possibility to discard the fabrication step of a adding a base, motivates a scale-up study of the new POSS. For tubular membranes, much higher ideal and mixed gas selectivities are found for $-NH_2$ functionalized POSS than for membranes where NaOH was added. Results indicate that the new route allows more reproducible production of defect-free membranes and has the potential for larger-scale polyPOSS-imide fabrication.

In the next chapter, another hybrid network is assessed for gas separation at high temperatures. **Chapter 3** reports on the formation of thin-film composite cyclomatrix polyphosphazene membranes via the interfacial polymerization reaction between polyhedral oligomeric silsesquioxane and hexachlorocyclotriphosphazene, on top of ceramic support. The prepared polyphosphazene networks are highly cross-linked and show excellent thermal stability until 340 °C. Single gas permeation experiments at temperatures ranging from 50 to 250 °C reveal a molecular sieving behavior, with permselectivities as high as 130 for $H_2/CH_4$ at low temperatures. The permselectivities of the membranes persist at higher temperatures; at 250 °C $H_2/N_2$ (40), $H_2/CH_4$ (31), $H_2/CO_2$ (7), and $CO_2/CH_4$ (4), respectively, while maintaining permeances in the order of $10^{-7}$ to $10^{-8}$ mol m$^{-2}$ s$^{-1}$ Pa$^{-1}$. Compared to other types of polymer-based membranes, especially the $H_2/N_2$ and $H_2/CH_4$ selectivities are high, with similar permeances. Consequently, hybrid polyphosphazene membranes have great potential for use in high-temperature gas separation applications.

In need to find a more stable network at high temperatures with facile preparation, **Chapter 4** reports a  non-aqueous interfacial polymerization

platform to prepare a series of thermally stable cyclomatrix poly(phenoxy)phosphazenes thin film composite membranes that can sieve hydrogen from hot gas mixtures. By replacing the conventionally used aqueous phase with dimethyl sulfoxide/potassium hydroxide, a variety of biphenol molecules are deprotonated to aryloxide anions that react with hexachlorocyclotriphosphazene dissolved in cyclohexane to form a thin film of a highly cross-linked polymer film. The film membranes have persisting permselectivities for hydrogen over nitrogen and methane at temperatures as high as 260 °C and do not lose their performance after exposure to 450 °C. The unprecedented thermal stability of these polymer membranes opens potential to industrial membrane gas separations at elevated temperatures.

In **Chapter 5**, a series of cyclomatrix polyphosphazene films has been prepared by non-aqueous interfacial polymerization of small aromatic hydroxyl compounds in a potassium hydroxide dimethylsulfoxide solution and hexachlorocyclotriphosphazene in cyclohexane, on top of ceramic supports. Via the amount of dissolved potassium hydroxide, the extent of deprotonation of the aromatic hydroxyl compounds can be changed, in turn affecting the molecular structure and permselective properties of the thin polymer networks ranging from hydrogen/oxygen barriers to membranes with persisting hydrogen permselectivities at high temperatures. Barrier films are obtained with high potassium hydroxide concentration, revealing permeabilities as low as $9.4\times10^{-17}$ cm$^3$ cm cm$^{-2}$ s$^{-1}$ Pa$^{-1}$ for hydrogen and $1.1\times10^{-16}$ cm$^3$ cm cm$^{-2}$ s$^{-1}$ Pa$^{-1}$ for oxygen. For films obtained with a lower concentration of potassium hydroxide, single gas permeation experiments reveal a molecular sieving behavior, with hydrogen permeance around $10^{-8}$ mol m$^{-2}$ s$^{-1}$ Pa$^{-1}$ and permselectivities of $H_2/N_2$ (52.8), $H_2/CH_4$ (100), and $H_2/CO_2$ (10.1), at 200 °C. Thus, the results presented in **Chapter 5** reveal the versatility of this non-aqueous interfacial polymerization technique, where numerous tuning parameters are available to produce films/membranes with various properties and performances.

**Chapter 6**, we use the fascinating flame-retardant properties of polyphosphazene to prepare well-defined highly hydrogen selective thin-film composite membranes. The membranes are prepared via the interfacial polymerization reaction between 1,3,5-trihydroxybenzene or *m*-dihydroxybenzene and HCCP on top of the ceramic support. It is followed by pyrolysis of the prepared membranes under $N_2$. In-depth characterization

shows that pyrolysis is started at 350 °C. At 450 °C, the prepared pyrolyzed polyphosphazene networks show the best hydrogen selectivity. It has a compact structure mostly made of disordered carbon accompanied by P-O-C and P-O-P bonds. Single gas permeation experiments at 200 °C reveal a molecular sieving behavior, with permselectivities above 100 for $H_2/N_2$, $H_2/CH_4$, and $H_2/CO_2$, with acceptable hydrogen permeance $2 \times 10^{-10}$ mol m$^{-2}$ s$^{-1}$ Pa$^{-1}$. The $H_2/CO_2$ permselectivities outperformed other CMS membranes using a lower pyrolysis temperature. Finally, the pyrolyzed thin-film composite membranes have a great potential for use in high-temperature applications, such as the selective separation of hydrogen in precombustion.

In **Chapter 7,** we report the synthesis of cyclomatrix polyphosphazene membrane with interfacial polymerization between 1,1-Tris(4 hydroxyphenyl)ethane and hexachlorocyclotriphosphazene on top of ceramic and polymeric supports to design tight organic solvent nanofilteration membranes. The potential of ceramic-supported thin film composite membranes as organic solvent nanofiltration membranes is confirmed with a polyethylene glycol molecular weight cutoff of $463 \pm 137$ g mol$^{-1}$ in water and polystyrene molecular weight cutoff of $347 \pm 120$ g mol$^{-1}$ and $503 \pm 220$ g mol$^{-1}$ in acetone and ethanol, respectively. Also, the resulting ceramic-supported TFC membrane shows a methylene blue rejection with Mw of 319 g mol$^{-1}$ of 99.5±0.2%, 95±0.2 %, and 93±0.5% in water, ethanol, and acetone, respectively. Compared to the other thin film composite ceramic-based membranes, the rejection for dyes with $M_w$<400 Da is higher with similar permeances. Furthermore, the network is made on top of the porous polyacrylonitrile supports with interfacial polymerization to validate the preparation technique and facilitate the industrial implementation. FE-SEM pictures reveal the formation of layers with a few defects. It results in higher permeance and a lower rejection. Consequently, our result clearly shows the great potential of cyclomatrix polyphosphazene membranes as organic solvent nanofiltration membranes, as well as the importance of the choice of support.

The last chapter of this thesis, **Chapter 8**, reflects on the obtained results in the previous chapters. In addition, this chapter suggests some monomers that could be interesting for non-aqueous interfacial polymerization. Finally, some perspectives for future research are given.

# Samenvatting

Grensvlakpolymerisatie is een breed toepasbare methode waarbij polymerisatie plaatsvindt op het grensvlak tussen twee niet-mengbare fasen. Het resultaat is een dunne en defect-vrije laag, die onder andere gebruikt kan worden als membraan voor gasscheiding en nanofiltratie, en als gasbarrière. De conventionele grensvlakpolymerisatiemethode maakt gebruik van twee reactieve monomeren, waarvan het ene monomeer zich in water bevindt en het andere monomeer zich bevindt in een organisch oplosmiddel. Echter, veel uiterst interessante reactanten, zoals amines en alcoholen met complexe topologie, zijn slecht oplosbaar in water. Dit proefschrift introduceert een niet-watergebaseerde grensvlakpolymerisatiemethode, waarmee meer monomeer combinaties en materialen mogelijk zijn. De synthese van een serie van cyclische polyfosfazeen lagen wordt beschreven, waarvan de eigenschappen en prestaties geoptimaliseerd zijn aan de hand van industriële eisen.

**Hoofdstuk 1** geeft een overzicht van grensvlakpolymerisatie en de parameters die een effect hebben op de eigenschappen en prestaties van de betreffende laag. Daarnaast worden de uitdagingen en de beperkingen van de klassieke water-gebaseerde grensvlakpolymerisatie besproken. In het tweede gedeelte van dit hoofdstuk wordt een nieuwe methode voor grensvlakpolymerisatie gepresenteerd. Deze methode maakt gebruik van niet-waterige oplossingen, waardoor het mogelijk wordt om veel meer monomeren te gebruiken voor grensvlakpolymerisatie. Hierdoor wordt de deur geopend voor nieuwe laagsamenstellingen. Het hoofdstuk eindigt met een bespreking van de behoeften en uitdagingen met betrekking tot industriële toepassing van thermisch stabiele gasscheidingsmembranen, gasbarrières, en nanofiltratie van organische oplosmiddelen.

**Hoofdstuk 2** presenteert een systematische studie van het effect van het type kation op de membraaneigenschappen en membraanprestaties. De twee verschillende polyoctaëdrische oligomere silsesquioxaan (POSS) moleculen die hiervoor gebruikt zijn, onderscheiden zich door verschillende functionele groepen. Het ene molecuul is gefunctionaliseerd met $-NH_3^+Cl^-$, terwijl het andere molecuul is gefunctionaliseerd met $-NH_2$. Dit laatste molecuul is nog niet eerder in deze context onderzocht. De ammoniumgroep is van het eerstgenoemde molecuul is gedeprotoneerd met behulp van drie verschillende basen, LiOH, NaOH en KOH. In dit hoofdstuk laten we zien dat de geïntroduceerde kationen de dikte van de laag beïnvloeden, terwijl de moleculaire compositie van het polyamidezuur onveranderd blijft. Alle polyamidezuren kunnen worden geïmidiseerd, alhoewel de kationen zowel de imidisatiesnelheid, als de mate van vernetting verminderen. Wanneer de kationen afwezig zijn, laten vlakke schijfmembranen een vergelijkbare permeabiliteit en een hogere selectiviteit naar $H_2/N_2$ zien op een temperatuur van 200 °C. Dit resultaat, samen met de mogelijkheid om het gebruik van een base uit te sluiten, resulteerde in een studie van de mogelijkheden voor opschaling. Buisvormige membranen waarop de nieuwe POSS laag gesynthetiseerd is, hebben een veel hogere afzonderlijke en gemengde gas selectiviteit, in vergelijking tot de membranen waarbij NaOH was gebruikt tijdens de synthese. Het gebruik van het $-NH_2$ gefunctionaliseerde POSS molecuul resulteert in een meer reproduceerbare synthese van defect-vrije membranen en kan mogelijk ook voor de productie van polyPOSS-imide lagen op grotere schaal gebruikt worden.

Het volgende hoofdstuk beschrijft een ander type hybride laag, die onderzocht is voor hoge temperatuur gasscheiding. **Hoofdstuk 3** rapporteert de vorming van dunne film composiet membranen gemaakt van cyclische polyfosfazeen met behulp van grensvlakpolymerisatie tussen POSS en hexachloorcyclotrifosfazeen (HCCP) op een keramische drager. De verkregen polyfosfazeen lagen worden gekenmerkt door de hoge mate van vernetting en laten een erg goede thermische stabiliteit zien tot een temperatuur van 340 °C. De membranen laten gedragen zich als een moleculaire zeef, met een permselectiviteit van wel 130 voor $H_2/CH_4$ op 50 °C. Op 250 °C zijn de volgende permselectiviteiten verkregen: $H_2/N_2$ (40), $H_2/CH_4$ (31), $H_2/CO_2$ (7), and $CO_2/CH_4$ (4), met een doorlaatbaarheid in de ordergrootte tussen de $10^{-7}$ tot $10^{-8}$ mol m$^{-2}$ s$^{-1}$ Pa$^{-1}$. De gemeten $H_2/N_2$ en

H$_2$/CH$_4$ selectiviteit is hoog in vergelijking met andere polymeer-gebaseerde membranen, terwijl de doorlaatbaarheid tussen het hier beschreven membraan en andere polymeer-gebaseerde membranen vergelijkbaar is.

**Hoofdstuk 4** introduceert een nieuwe grensvlakpolymerisatiemethode waarmee gemakkelijk lagen gesynthetiseerd kunnen worden die stabiel zijn op hoge temperaturen. Om dit te bereiken is voor het eerst een niet-watergebaseerde grensvlakpolymerisatie toegepast, waarmee cyclische poly(fenoxy)fosfazeen dunne film composiet membranen gemaakt zijn. Door het vervangen van de waterige fase met een mengsel van dimethylsulfoxide (DMSO) en kaliumhydroxide (KOH), worden de aanwezige bifenol moleculen gedeprotoneerd. De verkregen aryloxide anionen reageren met HCCP opgelost in cyclohexaan en vormen een dunne laag met een hoge mate van vernetting. Deze dunne laag membranen hebben een goede H$_2$/N$_2$ en H$_2$/CH$_4$ permselectiviteit op 260 °C en laten dezelfde prestaties zien na blootstelling aan 450 °C. Deze ongekende thermische stabiliteit maakt het mogelijk om de membranen te gebruiken voor industriële hoge temperatuur gasscheiding.

In **Hoofdstuk 5** wordt niet-watergedragen grensvlakpolymerisatie gebruikt voor de bereiding van cyclische polyfosfazeen lagen op een keramische drager, door aromatische hydroxylverbindingen in een KOH-DMSO oplossing te laten reageren met HCCP opgelost in cyclohexaan. De mate van deprotonatie van de aromatische hydroxylverbinding hangt af van de concentratie KOH in de DMSO oplossing. Afhankelijk van de concentratie KOH zijn de verkregen lagen te gebruiken als waterstof/zuurstof barrièrelaag of als waterstof-selectief membraan met hoge permselectiviteit op hoge temperatuur. Hoge KOH concentraties zijn nodig voor het maken van de barrièrelagen met een permeatie van $9.4 \times 10^{-17}$ cm$^3$ cm cm$^{-2}$ s$^{-1}$ Pa$^{-1}$ voor waterstof en $1.1 \times 10^{-16}$ cm$^3$ cm cm$^{-2}$ s$^{-1}$ Pa$^{-1}$ voor zuurstof. Een lagere KOH concentratie resulteert in lagen die te gebruiken zijn als een moleculaire zeef, waarbij de doorlaatbaarheid voor waterstof rond de $10^{-8}$ mol m$^{-2}$ s$^{-1}$ Pa$^{-1}$ bedraagt. De gemeten permselectiviteit, verkregen doormiddel van permeatie van afzonderlijke gassen, bedraagt 52.8 voor H$_2$/N$_2$, 100 voor H$_2$/CH$_4$, en 10.1 voor H$_2$/CO$_2$ op 200 °C. **Hoofdstuk 5** laat de veelzijdigheid van de niet-watergebaseerde grensvlakpolymerisatiemethode, waarbij veel verschillende parameters gebruikt kunnen worden om zowel dunne lagen als membranen te fabriceren met uiteenlopende eigenschappen en prestaties.

**Hoofdstuk 6** bespreekt de synthese van dunne laag composiet membranen voor selectieve waterstofscheiding op hoge temperatuur. Voor het verkrijgen van deze membranen wordt gebruik gemaakt van de niet-watergedragen grensvlakpolymerisatiemethode, door HCCP te laten reageren met 1,3,5-trihydroxybenzeen of m-dihydroxybenzeen. Omdat de cyclische fosfazeenring onderdeel uitmaakt van een weinig vertakte polymeer wordt een uniek thermisch degradatieprofiel verkregen. De thermisch degradatie begint op ongeveer 200 °C. De films vertonen de hoogste waterstofpermselectiviteit wanneer deze op 450 °C gepyrolyseerd zijn. Op deze temperatuur ontstaat er een compacte structuur, die voornamelijk bestaat uit ongeordende koolstof met P-O-C en P-O-P verbindingen. Gaspermeatie experimenten met afzonderlijke gassen laten een doorlaatbaarheid zien van waterstof van $2 \times 10^{-10}$ mol m$^{-2}$ s$^{-1}$ Pa$^{-1}$. De verkregen permselectiviteit van dit type membraan, voor zowel $H_2/N_2$, $H_2/CH_4$, als $H_2/CO_2$, is hoger dan 100. Daarmee is vooral de gemeten $H_2/CO_2$ permselectiviteit veel hoger in vergelijking met andere koolstof moleculaire zeef (CMS) membranen. Het gemak waarmee de dunne laag composiet membranen te synthetiseren zijn, gecombineerd met de lage kosten en het uniek thermische degradatieprofiel, maakt dat de dunne laag komposieten een grote potentie kunnen hebben voor gebruik in industriële hoge-temperatuur toepassingen, zoals de scheiding van waterstof tijdens voorverbranding, alsmede als gasbarrière.

**Hoofdstuk 7** bespreekt de synthese van dichte organisch oplosmiddel nanofiltratie (OSN) membranen met behulp van grensvlakpolymerisatie. In dit geval vindt de polymerisatie plaats tussen 1,1-tri(4-hydroxyfenyl)ethaan en HCCP op zowel een keramische als polymeer drager. De geschiktheid voor OSN van de gesynthetiseerde laag op de keramische drager is bevestigd aan de hand van molecuulgewichtsgrens (MWCO) metingen. De verkregen MWCO bedraagt 463 ± 137 Da voor polyethyleenglycol in water, en respectievelijk 347 ± 120 Da en 503± 220 Da voor polystyreen in aceton en ethanol. De methyleenblauw retentie bedraagt 99.5±0.2%, 95±0.2 %, en 93±0.5% in respectievelijk water, ethanol en aceton. Deze retentie is hoger in vergelijking met andere dunne laag composiet membranen, terwijl de doorlaatbaarheid vergelijkbaar is. De toepasbaarheid van de verkregen dunne laag in industriële toepassing is onderzocht door de laag op een poreuze polyacrylonitril drager te synthetiseren. De verkregen laag bezit een aantal

defecten, waardoor de doorlaatbaarheid van de laag hoger is en haar retentie lager is. De resultaten gepresenteerd in **Hoofdstuk 7** laten de potentie van cyclische polyfosfazeenmembranen als OSN membranen zien.

Ten slotte wordt een reflectie op de verkregen resultaten gegeven in **Hoofdstuk 8**. Ook bespreekt dit hoofdstuk een aantal monomeren welke interessant zijn voor niet-watergebaseerde grensvlakpolymerisatie. Daarnaast worden een aantal mogelijkheden voor toekomstig onderzoek in dit hoofdstuk besproken.

x

# Chapter 1

# Introduction

# 1.1 Membrane separation

Membrane separation is a technique that allows us to separate one or more specific molecular components from a homogeneous mixture. The membrane is a permselective barrier that allows passage of the specific components at faster rates than those of the other components in the mixture. The performance of the membrane is generally described with two criteria: permeance and selectivity. The permeance is a measure of the amount of components passing through a surface area of the membranes, per unit of time and per unit of driving force. The selectivity is determined from the relative change in mixture composition when comparing the retained phase (the retentate) and permeated phase (the permeate). Often the selectivity is based on the ratio of permeances of two pure components; this is referred to as permselectivity or ideal selectivity, and this is generally different from the actual process selectivity that is based on mixture experiments.

## 1.1.1 Historical perspective

The first experiment for membranes was recorded in the $18^{th}$ century when Abbe Jean Antoine Nollet developed the term osmosis to describe water permeation through natural membranes.[1] Through the $19^{th}$ century, membranes were only used in the laboratory to test theories, for instance, related to osmotic pressure and the diffusion laws of Fick. Early researchers used natural membranes, including bladders of mammals and fish and animal intestines. It was in 1907 when Collodion (nitrocellulose) membranes became preferred because these could be manufactured in a consistent manner. In 1930 microporous collodion membranes became commercially available. The fabrication method was extended to other polymers, most notably cellulose acetate. Over the following years, membranes were still primarily used in a few laboratories and specialized industrial applications because they were costly and showed low performance. In the 1960s, Loeb and Sourirajan proposed a fabrication method that paved the way to extend the use of membranes in industrial processes. This technique made the membranes an order of magnitude more permeable than previous ones. The

Loeb-Sourirajan technique strongly accelerated the development and commercialization of membranes.[2]

## 1.1.2. Membrane classification

Membranes can be classified in many different ways. From a structural perspective, they can be categorized as porous or as dense.

Porous membranes are mainly used in fluid separation and purification processes, including ultrafiltration (UF) and microfiltration (MF). Porous membranes have a solid matrix with defined holes or pores ranging from 1 nm to 20 μm.[3] The fluid transport through these membranes is predominantly governed by viscous flow, and the separation is based on the molecular size of the solute relative to the membrane pore size distribution.[3] This allows, for instance, to separate (colloidal) particles or large molecular weight solutes from a fluid.

Dense membranes are primarily used in gas separation, reverse osmosis, electrodialysis, and pervaporation. These membranes have a dense structure with no discrete pores, and the molecular transport is governed by a combination of sorption (solution) and molecular mobility (diffusion). Nanofiltration membrane materials are a juncture between porous and dense materials, and the molecular transport in these materials has features of both viscous transport and molecular solution-diffusion. For dense membranes, the material properties affect the relative importance of solubility and diffusion for the overall transport rate. In rubbery membranes, generally, the solubility governs the separation because the diffusion of distinct components in the highly dynamic macromolecular structure is comparable. The molecular solubility is determined by the condensability of a component and its affinity toward the membrane material. Rubbery membranes can be used to remove large condensable and soluble hydrocarbons from gas mixtures. For example, polyurethane membranes with low glass transition temperature can be used to separate butane and propane from methane since the solubility of the large hydrocarbons butane and propane is much larger than that of the smaller methane.[4] In contrast, in glassy polymers, the differences in diffusivity of components govern the separation. Molecules

must pass through localized free volume elements in a rigid dense structure. In this case, bigger molecules diffuse much slower than smaller molecules. Glassy polymers are good candidates for the separation of hydrogen from gas mixtures. Examples of glassy membranes are polyimide (PI), polyethersulfone (PES), and polybenzimidazole (PBI). In summary, as compared to rubbery membranes, glassy polymers show lower permeations but higher (perm)selectivities for small molecules over larger ones.

Inherent to being a permselective barrier, membranes also pose mass transport resistance for the molecules that should preferentially permeate. In order to minimize this transport resistance while maintaining as much as possible selectivity, a membrane should be as thin as possible. A drawback of a thin membrane is its low mechanical strength. This can be overcome by making asymmetric membranes that combine a relatively thick open support structure, for mechanical strength, with a thin region or film. The thin film exclusively determines the permeance and selectivity of the membrane. Since the flux is inversely proportional to the membrane's thickness, the obtained flux in asymmetric membranes is significantly higher than in symmetrical membranes.[2] The thin layer and support may be formed from more than one material in single or multiple separate fabrication steps.

The Loeb-Sourirajan technique employs the phase-separation concept to produce asymmetric membranes. When a thin film of a polymer solution (in liquid form) is immersed in a non-solvent bath, separation of a polymer rich phase and polymer lean phase can occur. The polymer-rich phase can be a solid material, and the polymer lean phase, a liquid. Because of diffusion and mixing limitations, phase separation will be different for various locations within the polymer-solvent film, resulting in an asymmetric membrane. The method is very facile and versatile, but in general, it is limited to the production of membranes of a single weakly cross-linked polymer.[5] In another method, a distinct layer is prepared on top of a porous support, producing a thin-film composite membrane (TFC).[5] Currently, TFC are the most efficient membranes for various applications. Importantly, the TFC approach provides opportunities to tailor the properties of the support and the thin layer separately.[6] The thin layer can be produced through many techniques, among which interfacial polymerization is a frequently applied

method.[5] Interfacial polymerization allows to produce a highly cross-linked thin film on top of a support.

## 1.2 Interfacial polymerization

The liquid-liquid interface has exceptional properties that may differ from bulk.[7] Amongst these, it can provide a restricted region for chemical reactions, which can be used for synthesizing polymers in the form of thin functional films.[8] This particular process is named interfacial polymerization (IP).

IP is used in the large-scale production of highly cross-linked networks. It provides excellent flexibility regarding surface topology and chemical properties of synthesized polymers, as compared to bulk polymerizations.[9–11] As a result, it has evolved as an effective technique to synthesize an impressive collection of polymers, including polyamides, polyurethanes, polyureas, polyanilines, polyimides, polyesters, and polybenzimidazole.[11–16] The synthesized materials can be in the form of films, nanoparticles, capsules, and nanofibers.[17–21] Polymer films obtained by this method have been used for membrane applications, mostly nanofiltration (NF) and reverse osmosis (RO), and a few studies on gas separation.[8]
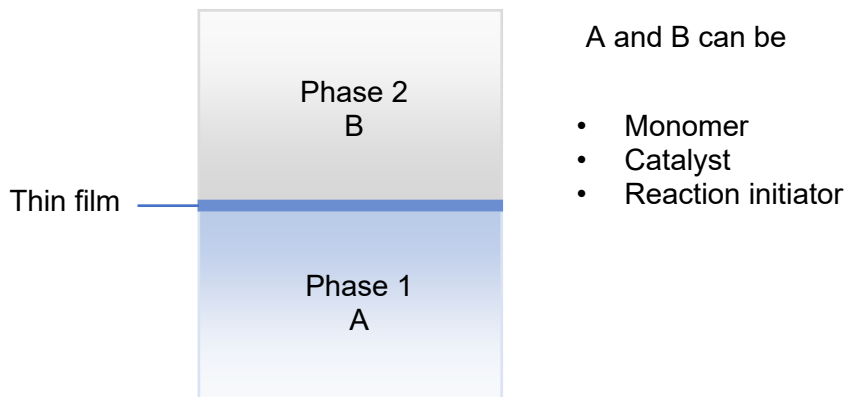


Figure 1.1 Schematic illustration of the interfacial polymerization reaction.

## 1.2.1 Basic principles of interfacial polymerization

In IP, the polymerization reaction occurs at the interface of two immiscible phases. Depending on the polymerization, two reactive monomers or monomers and initiators/catalysts are distributed in two phases.[22] The combination of phases can be categorized into three groups; liquid/solid, liquid/gas, and liquid/liquid.[23] Once the two phases come into contact, the reaction happens locally at the interface and generates a polymeric network. As a result, an ultrathin layer with high molecular weight can be formed.[24] The created films are inherently defect-free and uniform since the diffusion of the monomer is easier at the interfaces without films.[8] Figure 1.1 shows a simple schematic of an interfacial polymerization reaction between reactants A and B.

During IP, the growth of the layer is determined by the kinetics of the chemical reactions and the diffusion of monomers. At the onset of interfacial polymerization, monomer-monomer reactions occur within a reaction-diffusion boundary layer, and chemical kinetics limit the polymerization reaction. Consequently, a thin layer forms and separates the two phases. As the network grows, the polymerization rate reduces and becomes progressively more limited by the diffusion of monomers. Eventually, the film acts as a barrier that effectively hinders the diffusion of monomers and stops polymerization. The observed behavior for the thickness of the film is known as "self-limiting."[25]

## 1.2.2 Interfacial polymerization parameters

Several studies, experimental and theoretical, have explored the effects of different IP parameters on the formation and properties of films.[25–27] The parameters can affect molecular weight, branching, cross-linking, roughness, density, mechanical strength, and final performance of the polymer as a membrane.[28–31] Figure 1.2 summarizes five main categories influencing the formation and properties of the formed polymer; monomer, solvent, reaction condition, synthesized polymers, and support (membrane application). In some cases, parameters can be paired with each other to augment or alleviate the effect of each other. In brief, some of the crucial factors influencing the performance of membranes will be discussed here.
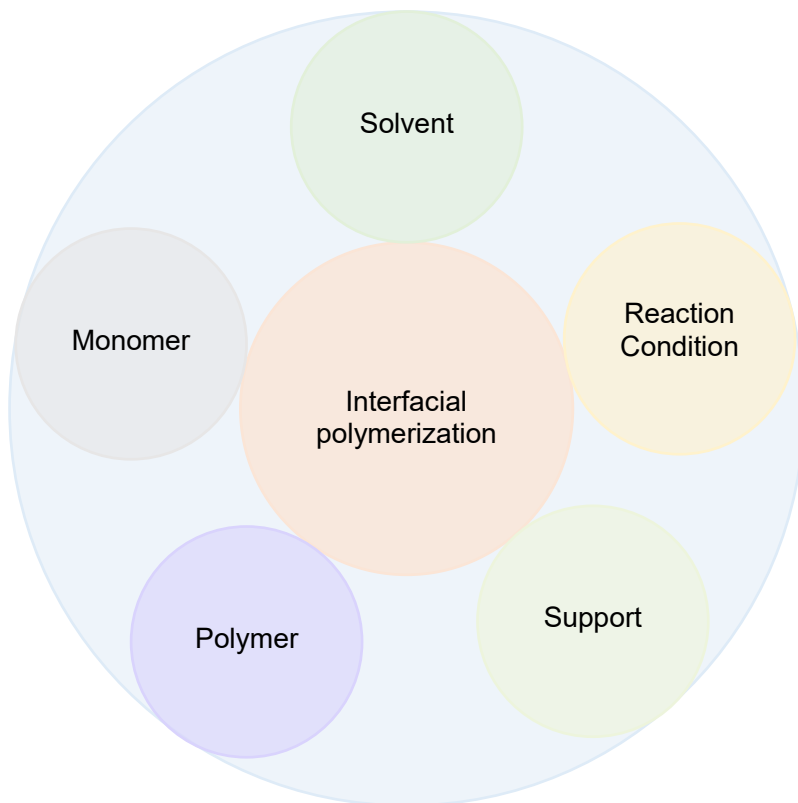
Figure 1.2 Overview of the main parameters that determine the formation and properties of thin films during interfacial polymerization. Those parameters can overlap each other.

## Monomers

Generally, IP is the reaction between a nucleophile reactant, such as amine and alcohol, in water and an electrophile, such as acid chloride, in an organic solvent. Monomers involved in IP possess two or more functional groups and determine the properties of the final polymers to a large extent. A wide variety of monomers can be used for IP. They are selected based on their final application, such as gas separation, NF, and RO. Well-known monomers used to prepare commercial polyamide NF membranes are piperazine (PIP) or *m*-phenylenediamine (MPDA) and trimesoyl chloride

(TMC).[32] Over the years, many other modified amine and acyl chloride monomers have been investigated to enhance the performance of NF membranes.[33] To this aim, researchers have incorporated different isomers of *m*-phenylenediamine, aliphatic diamine, and monomers with additional functional groups.[33–36]

Other monomers have been investigated to form membranes that can face up to the complexity of applications such as organic solvent nanofiltration (OSN) and gas permeation. For OSN, amine-functionalized monomers with particular shapes, such as cyclodextrins and trianglamine macrocycles, have been selected to react with acyl chlorides, forming 'molecularly-porous' polyamide membranes.[37–40] Also, other monomers (i.e. alcohols) and structures (i.e. polyesters) have been explored.[15,41] Similarly, monomers with reactive groups such as amine *(m*-phenylenediamine), alcohols, and hybrid functionalized polyhedral oligomeric silsesquioxanes (POSS) have been explored for gas separation. They result in polyamides, polyester, and polyimide structures.[15,42–44]

The reactivity, solubility, size, and diffusion of the monomers greatly influence the characteristics of the finally obtained thin films.[30] Monomers should be reactive enough for adequate polymerization kinetics. For highly reactive monomers, film formation can occur in a matter of seconds.[24] In contrast, monomers with low reactivity sometimes need days to react. The reactivity of monomers impacts the thickness of films; generally, less reactive the monomers produce hicker films. Some ways to increase reaction kinetics include increasing the concentrations of the monomers and changing the solvents. Higher concentrations of monomers correspond to a higher rate of polymerization. However, increasing concentrations is not always practical, and there can be concentrations above which the rate of reaction does not change with a further increase in the concentration.[25] In addition, the monomer concentrations also affect the macromolecular structure of the polymer (the extent of cross-linking, chain packing, etc.) and hence the performance of a membrane.[44] Generally, a well-defined film is obtained when the monomers are highly reactive and their solubility in another phase is low. The high solubility of monomers in the opposite phases can cause the formation of a more corrugated layer.[44] The diffusion of monomers to the opposite phase is also affected by the size and flexibility of the monomer; for

larger and more rigid molecules the augmented mass transport limitation due to film formation are more pronounced, and typically thinner films of less flexible polymer networks are obtained. In conclusion, via the selection of the monomers, the membrane performance can be tailored[15,45,46]

## Reaction conditions

The temperature and time of reaction are among the most crucial synthesis parameters that influence membrane performance.

Most of the time, IP is performed at room temperature. A few researchers have systematically investigated the effect of the temperature by performing IP with one or both phases above room temperature.[47–49] Increasing the temperature of the organic phase improves the diffusion of monomers to the opposite phase. This has two distinct effects. Firstly, it disturbs the interface and changes the morphology of the membrane. Secondly, it enhances the cross-linking density. Consequently, permeability and rejection can be affected.[47,48] Shen et al.[49] also investigated the effect of reaction temperature on the properties of the membranes. They prepared polyester TFC membranes by IP between glucose in water and TMC in heptane. Since the solubility of glucose in water is limited, the IP was performed at temperatures between 20-50 °C to increase the diffusion of glucose monomers across the water/heptane interface and facilitate the reaction rate between glucose and TMC. As a result, the cross-linking density and rejection increase while maintaining high water permeances up to 16.1 L m$^{-2}$ h$^{-1}$ bar$^{-1}$.[49]

Increasing the reaction time results in the formation of a thicker layer and a higher extent of cross-linking. At some point, the growth of film decelerates due to increased mass transfer limitations of the monomers. At this stage, there can still be a progressive formation of covalent bonds, leading to further densification of the material densifies, and affecting the film properties.[36,50,51]

In addition to temperature and time, other parameters can affect the interplay of reaction and diffusion kinetics. In particular, the use of additives has been explored for this purpose. Common additives include acid acceptors,

nanomaterials, and catalysts. Acid acceptors are used to adjust the pH of the solution and remove the acids that are formed as a by-product of an interfacial polycondensation reaction.[52,53] The incorporation of nanomaterials as additives into the polymeric matrix has been proven to be effective in the design of advanced TFC membranes.[54–56] Adding catalysts can be essential for obtaining high-performance membranes.[57–60] For example, a phase transfer catalyst is crucial for the IP reaction between diphenols in water and hexachlorocyclotriphosphazene in dichloromethane. A phase transfer catalyst facilitates the transport of a monomer to the opposite phase, thereby increasing the polymerization rate, which in turn, can influence the extent of cross-linking and final membrane selectivity.[59,60]

## Polymer

The properties of the polymer that is formed during IP are not only relevant for the final application, but already during the IP process the polymer properties will affect the very formation of the film. Upon contacting the two phases during IP, monomers diffuse to the opposite phase, react, and film formation starts. The film growth reduces the diffusion of the monomers, the extent of which is determined by the characteristics of the formed polymer network that has been formed, and ultimately film growth and cross-linking becomes very slow.[50,61] The polymer properties affect the rate of monomer transport via their mobility and solubility. Also, the solubility of the polymer in the organic solvent is important. Because the polymer is generally formed in the organic phase, its solubility in this solvent defines the precipitation point and molecular weight.[62] Specifically, higher solubility in the organic phase results in the precipitation of polymers with a higher molecular weight range.[47,63,64]

## Support

The principal function of the membrane support is to provide mechanical strength to the very thin selective IP layer. Hence, the mechanical properties of the support, under the application condition of interest, are vital. For high temperatures and pressures, porous inorganic materials can be an option; however, these supports are expensive, brittle, and in general, have a low

surface-to-volume ratio that is associated with the tubular of stiff flat sheet geometry. In contrast, porous polymeric supports provide a more inexpensive solution and can also be fabricated in the form of hollow fibers or flexible flat sheets that can be accommodated in spiral wound modules. Particularly, in gas separation, the hollow fiber geometry is favored because of its high-pressure resilience.

Yet, the morphology and physicochemical properties of the support have pronounced the formation, properties, and performance of the IP film atop it.[65] Important morphological features include surface roughness, porosity, and pore size distribution. Important physicochemical properties include surface chemistry and hydrophilicity. All these properties directly affect the characteristics of the interface and hence directly affect the IP reaction that occurs there.[66–69]

The porosity and pore size distribution affect how much monomer is available for the reaction and how fast it can diffuse to the reaction zone. Typically the support is impregnated with the aqueous phase, and a low porosity implies that less of this phase can present. When, in addition, the pores are small, the diffusion of the aqueous phase monomer will be slower. Small pores also provide a more suitable surface for a thin layer to form on top, in particular when the surface roughness is low. In addition, smaller pores will stabilize the phase-phase interface. As such, smooth supports with small pores can allow for the formation of well-defined defect-free films. It has also been observed that films that form on supports with smaller pore sizes have a higher cross-linking density. Sharabati et al.[70] and Singh et al.[71] have investigated the effect of the pore size of support on the selectivity of PA layers. Both pieces of research are in line and prove that reducing the pore size of the support enhances the rejections, which is believed can be due to the formation of a defect-free layer and improvement of cross-linking.[70,71]

The surface chemistry and hydrophilicity of the support affect the connection between the IP film and the support. It has been observed that a relatively hydrophilic surface can improve this connection and decrease film delamination.[69,72] In hydrophilic support, a concave meniscus of the

aqueous phase in the pores can result in a more pronounced layer growth inside the pores.

## Chemistries

Many classes of polymers can be synthesized with IP. This section briefly discusses the chemistries that have mainly been developed for membrane applications, such as polyamides, polyesters, polyamines, polyimides, and covalent organic frameworks (COFs).

Polyamides is the most prevalent chemistry in IP. It is the main chemistry for preparing commercial membranes for desalination and, in fewer cases, gas separation applications.[11,43,46,47,52,73] Generally, the polyamide is formed by the reaction of an acyl chloride and a (poly)amine, Figure 1.3. Both aliphatic and aromatic precursors can be used to synthesize polyamides. Polyamides can generally be used at a pH ranging from 2 to 10. However, they are not completely stable towards chlorine treatments for membrane cleaning. Several methods have been developed to overcome this issue, including changing the monomer precursors used for IP and chemical post-modification.[11,43,46,47,52,73]
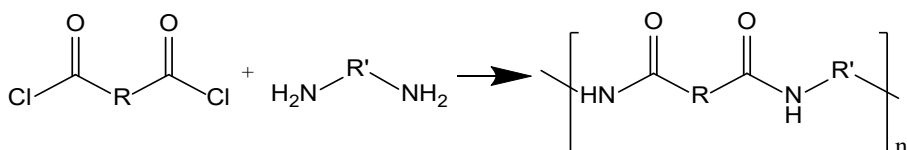


Figure 1.3 The formation of polyamide from acyl chloride and (poly)amine monomers

Polyesters are another chemistry for TFC membranes, generally for NF and gas separation applications.[15,37,74] Polyesters are typically synthesized by the reaction of acyl chloride and alcohol, Figure 1.4.[15] The main drawback of polyesters is that they are more susceptible to hydrolysis under acid and base conditions, as compared to polyamides.
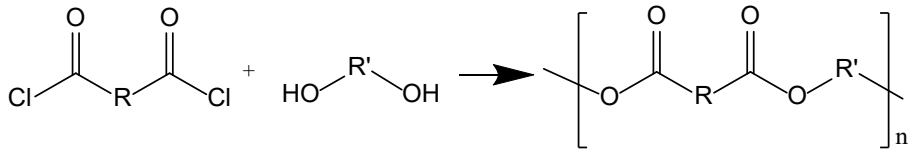
Figure 1.4 The formation of polyesters from acyl chloride and alcohol monomers

Via the reaction between a diamine, and a di- or trichloride functionalized triazine polyamine-based TFC membranes can be prepared for NF, RO, and a few gas separation applications, Figure 1.5.[75,76] The resonance structure of the triazine ring provides polymer rigidity and thermal and chemical stability.[24] One drawback of di-or trichloride triazines is the moderate reactivity of the second and third chloride groups, which might affect the cross-linking density. To overcome this issue, methods such as increasing the temperature and using monomers with a high functionality and reactivity can be applied.[77,78] Recently, Elshof et al. used alcohol instead of amine and successfully formed triazine-based TFC membranes.[78]
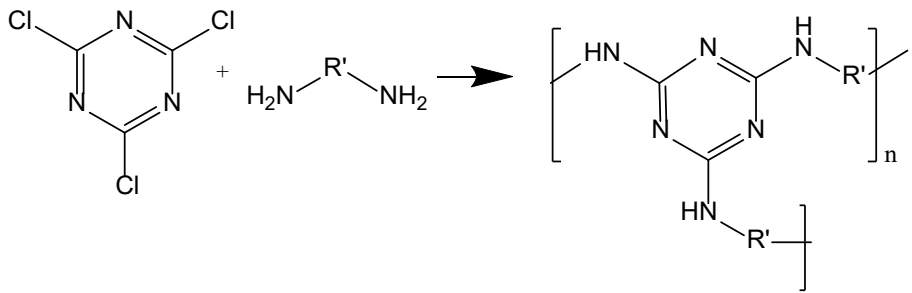


Figure 1.5 The formation of polyamine from acyl chloride and alcohol monomers

Polyimides are known for their high thermal and chemical stability. They are synthesized in a two-step procedure; IP reaction between an anhydride with a primary amine, resulting in polyamic acid, followed by chemical or thermal imidization to form polyimides, Figure 1.6. The synthesized membranes have been used for gas separation, nanofiltration, and pervaporation.[14,42,45] The imidization step is challenging since polyamic

acids are hydrolytically unstable, and the polymer molecular weight might decrease after the termination of the reaction.
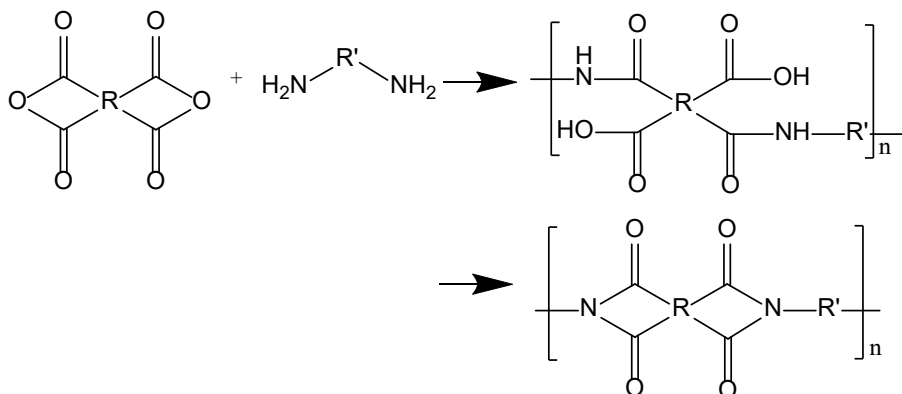


Figure 1.6 The formation of polyimide from a two-step procedure: IP between anhydride and primary amine followed by thermal or chemical imidization.

COFs are crystalline polymers with covalent bonds in two or three dimensions. They are promising candidates for molecularly engineered membranes since by careful selection of the monomer subunits, which are then polymerized into layered sheets, membranes can be engineered at the molecular level.[79] Several researchers have reported on the preparation of COFs with IP between monomers such as amine and terephthalaldehyde for membrane applications, Figure 1.7.[57,80,81]
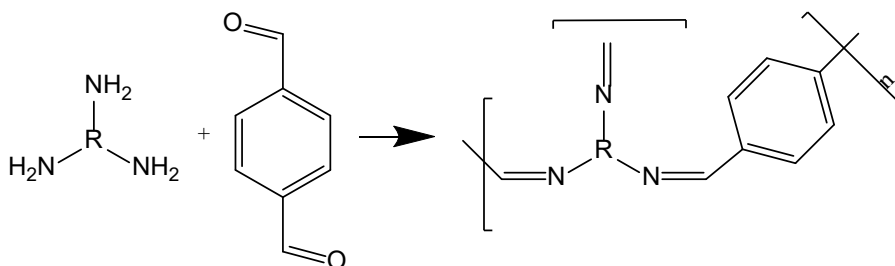


Figure 1.7 The formation of COF from amine and terephthalaldehyde monomers

The chemistries mentioned above are some of the most important chemistries to form the membrane and are therefore discussed here, but the list is not exhaustive. It is worth to mention the number of chemistries developed by IP is still limited compared to bulk polymerization.

## Solvents

Although pivotal in any IP process, here, I choose to discuss the effects of the solvents last. This is because the typical selection of IP solvents is the main reason for the limited variety of chemistries that has been explored in IP, so far. Departing from the conventional choice of using an aqueous phase, thereby significantly broadening the selection of potential nucleophile reactants, is a linchpin of this thesis.

In conventional IP, the film formation is typically via a polycondensation reaction between two monomers, one dissolved in water and one dissolved in a non-polar solvent such as an alkane. The formation of a thin film, first and foremost, requires a stable liquid-liquid interface, which can be obtained by selecting a pair of solvents that are not very miscible, such as the very polar water and the non-polar alkane. Even for such very immiscible solvents, small amounts of each solvent will dissolve in the other phase. Selecting the non-polar solvent can be based on various considerations. Critical is that the polymerization reaction typically occurs in the non-polar phase, and the solvent choice therefore directly affects, in the reaction zone, the diffusivity, the solubility, and the reactivity of the monomers, as well as the solubility of the polymer that is formed. For less viscous solvents, monomer diffusion is typically faster, facilitating the fabrication of suitable RO membranes.[47,82] Yuan et al. [44] showed that the choice of non-polar solvent affects the diffusivity of the monomers, the thickness and the extent of cross-linking of the membranes, and finally, their performance.[44] Ghosh et al. [47] controlled the diffusivity and solubility of the aqueous monomer, MPDA, to the organic phase by changing the non-polar solvent. They showed that the selection of non-polar solvent directly influences membrane performance. [47]

Almost without exception, the solvent of choice for the polar phase has been water. Water is one of the most polar solvents available, and it has many

ecological and economic advantages. In some studies, a co-solvent, such as DMSO, is added to the aqueous phase to enhance the water permeation of TFC membranes.[83–86] Numerous mechanisms have been proposed for how DMSO can influence water permeation. It can disturb the reaction zone and change the interface stability and monomer diffusivity in another phase.[24] This results in an increase in surface roughness, surface area, pore size, and, subsequently, flux enhancement.[87] Another mechanism is suggested by Lee et al.[83] who added DMSO to the aqueous phase to increase the water permeation of polyamide membranes prepared from PMD and TMC. They attributed the enhancement in water permeation to the dipole-dipole interaction between DMSO and TMC, which increases the TMC concentration at the interface and, thereby, the reaction rate. Due to the fast reaction, the films form quickly and hinder the diffusion of monomers for further reaction. As a result, the thickness and roughness of the active layer reduce. Furthermore, the cross-linking degree diminishes due to the incomplete reaction due to the interaction of acyl chloride groups interacting with $S^{\delta+}$- $O^{\delta-}$ electrostatic dipoles of DMSO at the interface. However, it could not be the only reason, and possibly the hydrolysis of acyl group matters as well.[85,87].

The addition of the co-solvents to an aqueous phase is often associated with changes in the reactivity of the acyl chloride but may also affect the reactivity of the aqueous phase monomer. For instance, as compared to water and other alcohols, dimethyl sulfoxide (DMSO) and dimethylformamide (DMF) have been shown to enhance the nucleophilicity of phenolates.[88,89] Throughout this thesis, DMSO is a co-solvent and prime solvent for the non-polar phase to enhance the reactivity of the polar phase reactant. It is explored how this broadens the reactant portfolio to include monomers that are insufficiently nucleophile for conventional (aqueous) IP.

## 1.2.3 Outlook

Interfacial polymerization is an elegant technique provides a platform to use a wide range of monomers to synthesize polymers with distinct and impressive properties. In this context, interfacial polymerization is explored as the main technique for designing and synthesizing very thin hybrid

16

organic-inorganic polymeric film, polyimide and polyphodphazene, on top of the ceramic supports and producing TFC suitable for a broad range of molecular separations, gas separation at high temperature, and solvent nanofiltration membranes, as well as hydrogen/oxygen barrier films.

Many studies have focused on developing TFC membranes based on exploring different monomers in the past years. However, most organic compounds, including aromatic amines with complex topologies, are partially soluble in water. This limits the number of monomers and chemistries used in interfacial polymerization and, subsequently, forms networks for specific membrane applications.[43] In addition, water hydrolyses monomers such as acyl chlorides during interfacial polymerization and produces by-products. As a result, it reduces the cross-linking degree and produces membranes with several defects, which primarily affects the selectivity of membranes.[90] To the best of our knowledge, few studies aimed at the formation of polyamide and polyesters with expanding non-aqueous interfacial polymerization, and no attempts have been made to expand non-aqueous interfacial polymerization to other chemistries.[43,91,92] Liu et al.[43] replaced water with a series of ionic liquids to produce polyamide membranes with interfacial polymerization. In another study, Wamser et al. showed the formation of various polyamide porphin films at the interface of DMSO/chloroform or DMSO/ethyl acetate.[91] Ogata et al. reported interfacial polymerization in non-aqueous systems for synthesizing aromatic polyesters.[93]

This thesis aims to introduce a novel non-aqueous interfacial polymerization platform aiming to broaden the functional monomers in interfacial polymerization and, in turn, form newer chemistries. In particular, we explore the potential of non-aqueous interfacial polymerization for preparing films by replacing DMSO for water in the polar phase. Similar to classical aqueous interfacial polymerization, the cross-linking degree, chain flexibility and packing can be easily controlled to obtain various types of structures. Several tuning parameters are at our disposal that can be manipulated to obtain desired film structures, such as type of monomers and base concentration. The most prominent aspect of this approach is that it can be used to form versatile structures for harsh industrial demanding conditions

such as hot gas separation, hydrogen barriers and organic solvent nanofiltration.

## 1.2   Cyclomatrix polyphoaphazene networks

**Linear polyphosphazene**

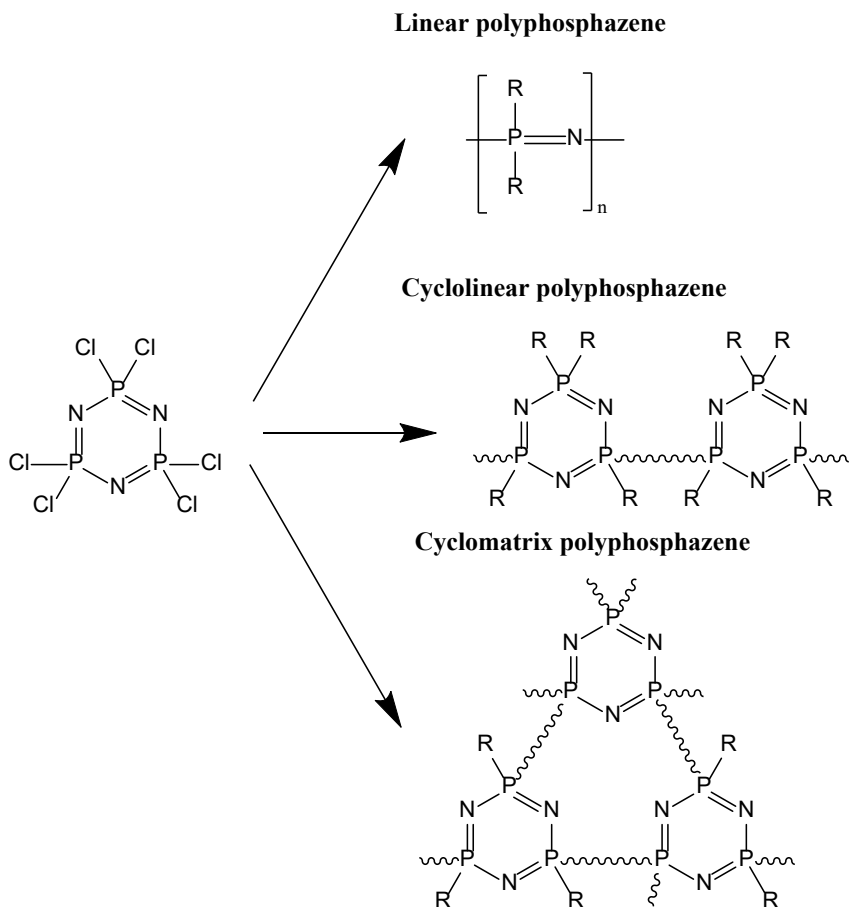**Cyclolinear polyphosphazene**

**Cyclomatrix polyphosphazene**

Figure 1.8 Three main classes of polyphosphazene. Here, R represents different organic functional groups

Polyphosphazenes are a hybrid materials including a broad range of polymers. They contains phosphorus and nitrogen atoms attached via alternatingly arranged saturated and unsaturated bonds in their backbones, providing either cyclic rings or linear chains.[94] The three main classes of

polyphosphazene are linear, cyclolinear, and cyclomatrix, Figure 1.8. With the vast substitutional potential of side groups, R, and architectures, polymers with specialized properties can be synthesized and tailored for different applications, including fire retardants, fuel cells, and various membranes.[95]

.

Linear phosphazene polymers are made from the ring opening polymerization of hexachlorocyclophosphazene (HCCP) at 250°C under a vacuum. HCCP contains two chlorines atom per repeating unit that can be substituted by organic nucleophiles such as alkoxides, aryloxides, and amines. The other two architectures, cyclolinear, and cyclomatrix, are made from HCCP rings linked via organic or inorganic groups. If HCCP reacts with di or tri-functional compounds, it forms a highly cross-linked cyclomatrix polyphosphazene network.[96] They are of high interest for their flame-retardant properties and good thermal and chemical stability.[97] The main interest of this thesis is utilizing cyclomtrix polyphophszene structure for molecular separation applications.

Depending on the structure, methods such as doctor-blade casting, drop casting, or spin coating can be used to prepare cyclomatrix polyphosphazene films, leading to the formation of relatively thick films in the order of a few hundred microns.[6,98] Even for a few structures such as 1,3,5-Trihydroxybenzene and HCCP, only the formation of micro/nanospheres is reported.[99] The mentioned studies suggest that a different approach rather than conventional bulk polymerization and film preparation is needed to prepare thin cyclomatrix polyphosphazene films; interfacial polymerization.

A few studies reported the formation of cyclomatrix polyphosphazene films via interfacial polymerization.[36,60] Maaskant et al. reported the fabrication and characterization of cyclomatrix polyphosphazene layer by interfacial polymerization of aromatic diphenols in water with HCCP and a phase transfer catalyst in dichloromethane. A phase transfer catalyst was used to facilitate the transport of less reactive monomer, HCCP, and increase the polymerization rate. However, the approach did not allow to make a thin selective film.[60] You et al. prepared NF membranes via interfacial

polymerization between branched polyethyleneimine (PEI) and HCCP. The reported method to form NF membranes could not be used for other amine-functionalized monomers, due to the specific properties of PEI, such as high reactivity.[36]

In this thesis, we report on an interfacial polymerization method to prepare, in a single step, thin and highly cross-linked cyclomatrix networks from HCCP and a broad range of monomers for various applications, such as gas separation membranes at high temperatures, gas barriers, and organic solvent nanofiltration.

## 1.4    Hydrogen    separation    membranes    at    high temperature

The history of membrane gas separation started in 1979 when *Permea*, a trademark name owned by *Monsanto*, launched the first membrane plant based on polysulfone hollow fibers to purge hydrogen in the Bosh-Haber process.[100] Since then, this technology has found its application in hydrogen separation, natural gas treatment (e.g., $CO_2/CH_4$, $H_2S/CH_4$, $He/CH_4$ separation), gas/vapor separation (e.g., $C_3H_6/N_2$, $C_2H_4/N_2$, gasoline/air) and nitrogen production (e.g., $N_2/O_2$ separation).

Recently, hydrogen separation membranes at temperatures above 100 °C have attracted immense attention. Hydrogen is an important energy source that can address issues related to global climate change, energy security, and local air pollution.[101] Most of the $H_2$ in the world is supplied using fossil fuels. This process is associated with the formation of many by-products such as $CO_2$, and other contaminants generated in the process. Most importantly, the gas streams are produced at high temperatures and must be kept at those temperatures during the process in chemical industries and cooling the stream followed by re-heating causes a waste of considerable energy. This highlights the importance of thermally stable structures for hydrogen separation.

Various membrane materials such as polymeric membranes, inorganic-based membranes (ceramics, metals, graphene oxide (GO)), and porous hybrid

materials (zeolite imidazolate framework (ZIF) and metal-organic frameworks (MOFs)) have been developed for hydrogen purification at high temperatures.[102–106] Due to the complex preparation processes (high cost and their modularizing problem) of inorganic and porous hybrid materials, numerous studies have been focused on synthesizing/modifying polymeric materials which stand at high temperatures.[107] Unfortunately, the existing commercial polymers are not suitable candidates for such applications due to their insufficient thermal stability and chain rigidity at high temperatures. Therefore, researchers have focused on developing thermally stable polymeric materials applicable to hydrogen separation including PBI, polyimide, and thermally rearranged (TR) membranes.
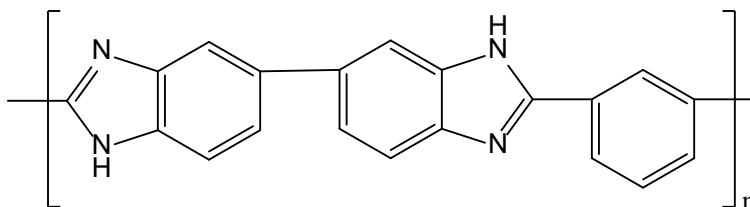


Figure 1.9 Chemical structure of the PBI-Celazole®

PBI is a rigid heterocyclic polymer exhibiting high thermal stability above 500 °C and high mechanical stability at high pressures. A commercial PBI, known as Celazole® is considered the benchmark for $H_2/CO_2$ separation at high temperatures, Figure 1.9. Celazole® exhibited mixed gas $H_2$ permeability of 13 barrer and $H_2/CO_2$ selectivity of 20 at 270 °C.[108] The substantial disadvantage of this membrane is the low gas permeability. It is the result of its tightly packed structure due to strong hydrogen bonding. Many studies have focused on increasing the gas permeabilities by introducing bulky functional groups, such as $CF_3$ and $CH_3$, in PBI and disrupting its chain packing.[109,110] However, in most studies, the increase in permeability was accompanied by a dramatic loss in selectivity. Another method to increase the permeability is incorporating ZIFs in PBIs to create mixed matrix membranes (MMMs).[111,112] Yang et al. showed that incorporation of 33 wt% ZIF-8 nanoparticles into PBI-based hollow fiber membrane led to a $H_2$ permeance of 202 GPU at 180 °C, which is more than 70 times higher than that of unmodified membranes.[112] In another report,

Lin et al. chose a completely different approach and cross-linked Celazole® with phosphoric acid ($H_3PO_4$).[113] As a result, at 180 °C, $H_2/CO_2$ selectivity was enhanced by sacrificing the permeability. They attributed the enhancement in selectivity to the favorable combination of chain rigidity with efficient chain packing caused by chemical cross-linking.[113] Another interesting chemistry for $H_2$ separation at high temperatures is polyimides (PIs). In general, PIs show moderate selectivity and higher permeance compared to PBI. To enhance the selectivity, several studies cross-linked the PI structure to restrict chain mobility.[114,115] 1,4-butanediamine (BuDA) cross-linked P84® membranes exhibited $H_2/CO_2$ permselectivity of 12 at 150 °C.[114] In other studies, PI mixed matrix membranes with ZIF7 were fabricated to enhance the permeability while retaining high $H_2/CO_2$ selectivity by cross-linking.[116] Ortho-functionalized polyimide can be thermally rearranged at 350-400 °C to form a polybenzoxazoles (PBO) structure with high thermal stability (>400 °C). They were used to separate $H_2$ at temperatures up to 300 °C and exhibited acceptable $H_2/CO_2$ selectivity.[117]

Using interfacial polymerization to prepare TFC membranes for hot gas separation reduces the complexity of the preparation process. However, the number of studies on advancing gas separation membranes with interfacial polymerization is limited. For gas separation, a precise molecular separation is required, whereas interfacial polymerization occurs with a fast reaction rate, which leads to an uncontrol packing of the polymer network and a distribution of pore diameter and free volume.[118] Raaijmakers et al.[45] prepared polyPOSS-imide membranes for $H_2$ separation up to 300 °C.[16,45] Shan et al. fabricated PBI membranes by interfacial polymerization with high $H_2/CO_2$ selectivities at 150 °C.[16]

Finally, despite all the efforts, achieving some commercially viable membranes for hot $H_2$ separation is still challenging due to a low separation performance or complex preparation processes (such as imidization or thermal rearrangement). The studies mentioned above illustrate that further developments to prepare thermally stable membranes for separating hot gases are required. In this thesis, we aim to offer a new one-step scalable interfacial polymerization approach to produce membranes for this application.

# 1.5 Organic solvent nanofiltration membranes

The second topic of interest in this thesis is the development and molecular design of organic solvent nanofiltration (OSN) membranes suitable for separating molecules with Mw below 400 Da.

Nanofiltration describes a pressure-driven membrane-based separation that will reject solutes below 1000 Da in mass. However, upon exposure to feed streams containing organic solvents, typical membranes dissolve or degrade, reducing membrane performance. NF membrane technology for organic solvents is also referred to as organic solvent nanofiltration (OSN).[119] OSN has attracted immense attention from academia and industries, because of the high application potential. Millions of tons of organic solvents are used in pharmaceutical, oil, and chemical industries, drugs, chemical products, and edible oils. The products and solvents are required to be purified and separated, and OSN membranes could be an alternative to the traditional separation method with advantages such as ease of scale-up, relatively mild operating conditions, and compatibility with heat-sensitive compounds.[119] Great efforts have been made to enhance the performance of OSN membranes by developing new polymeric membranes.[119–122] Two main types of OSN polymeric membranes are polymeric integrally skinned asymmetric (ISA) and TFC membranes. ISA membranes are typically fabricated by phase inversion followed by covalent cross-linking of the polymer chains in a polymeric membrane. ISA membranes are favoured by membrane industry due to their ease of processing. To date, many polymeric materials have been examined for ISA membranes, including PI and PBI. The main drawback of ISA membrane is the cross-linking process which increases the resistance of membranes and reduces the flux. On the other hand, TFC membranes prepared by interfacial polymerization show a significant advantage over ISA membranes. The unique layered structure of TFC, support and selective layer allow it to modify them separately.[118]

A broad range of monomers have been exploited for interfacial polymerization to design the selective layer on a molecular level to increase the performance of OSN membranes. They have modified the thickness and the micro-porosity of membranes to enhance solvent permeance.[118]

Various types of polymers, such as polyamide, polyimide, polyester, covalent organic framework (COF), and covalent organic polymer (COP), have been explored.[15,41,123] However, designing TFC OSN membranes for rejecting molecules with Mw <400 Da is still challenging since it needs better control over the interfacial polymerization process. A few works succeeded in forming those membranes.[15,39,43] Jimenez-Solomon et al. fabricated polyester TFC OSN membranes by interfacial polymerization between 1,3-benzenediol and TMC. The resulting membrane display dye (314 g mol$^{-1}$) rejection of 95% in methanol with acetone and methanol permeance around 0.3 L m$^{-2}$ h$^{-1}$ bar$^{-1}$ and 0.5 L m$^{-2}$ h$^{-1}$ bar$^{-1}$, respectively.[15] Liu et al. fabricated polyamide TFC OSN membrane with a dye rejection (327.3 g mol$^{-1}$) of 95% in methanol.[43] Villalobos et al. fabricated a cyclodextrin-based polyester TFC membrane which display a rejection of methyl orange (327.3 g mol$^{-1}$) between 91-96% in different solvents (water, acetonitrile, methanol, ethanol, and tetrahydrofuran).[39]

The above-mentioned studies demonstrate that researchers continue to develop new membranes with distinct properties for OSN. Still, further developments in this field are required to implement interfacial polymerization OSN membranes for industrial applications. In this context, we aim to design and prepare polyphosphazene selective thin films, tailored for OSN.

## 1.6 Barriers

The third topic of interest in this thesis is the development of hydrogen/oxygen barrier films with interfacial polymerization.

The hydrogen-based economy has captivated considerable attention during the past years. It is a zero-carbon fossil fuel alternative and offers more energy per mass than any other fuel. For aviation and transport applications, hydrogen should be stored and transported in lightweight materials. However, hydrogen storage is very challenging as it is highly diffusive. To store hydrogen efficiently, polymers have several advantages over metals in terms of specific strength, toughness, cost, and easy processability. In

addition, metals might suffer from severe hydrogen embrittlement and fail during the performance.

The polymeric matrix can be a good gas barrier when both solubility and diffusivity are minimized. Regarding hydrogen, the important factor is controlling diffusivity, which can be controlled by tuning the polymer structure and adding nanofillers. Adding less bulky and more planar aromatic units in the polymer backbone reduces the chain packing and improves gas barrier properties.[124,125] Liu et al. prepared an intrinsic high-barrier polyimide consisting of a planar group.[125] The resulting films exhibited excellent oxygen barrier properties.[125]  Zeng et al. fabricated polyimide containing a high planarity naphthalene ring. The obtained layer displays superior barrier properties with extremely low water vapor and oxygen transmission.[124] Other researchers used this idea for other chemistries, such as polyamide, and polyethylene terephthalate (PET).[126,127] Another effective way to improve the barrier properties of materials is by applying a high aspect ratio two-dimensional nanofillers such as silica nanosheets. The nanofiller-polymer matrix restricts the diffusion of hydrogen by introducing a long tortuous path. Also, nanofillers hinder the segmental mobility of polymer chains leading to a reduction in the free volume.[128] Habel et al. prepared a nanocomposite of silicate nanosheets and poly(vinyl alcohol).[129] Films with 50% nanofillers showed helium and hydrogen permeabilities as low as 0.8 and 0.6 $cm^3$ $\mu m$ $m^{-2}$ $day^{-1}$ $atm^{-1}$, respectively.[129] Seo et al. proposed preparing nanocomposites using covalently bonded graphene oxide (GO) and MXenes nanofillers and poly (ethylene-co-acrylic acid) (EAA). The films containing 10 wt% of nanofillers showed a very low $H_2$ permeability.[130] Although using nanofillers is an effective technique to prepare hydrogen barrier films, considering the expensive costs of synthesizing and mixing nanofiller with polymer, it can be costly to apply on larger scales. It also demonstrates that developing polymeric materials could be a safer investment by the industry.

In this context, we aim to develop a one-step scalable approach to synthesizing hydrogen barrier layers with interfacial polymerization. This aim could be achieved by using small planar monomers for interfacial polymerization reactions.
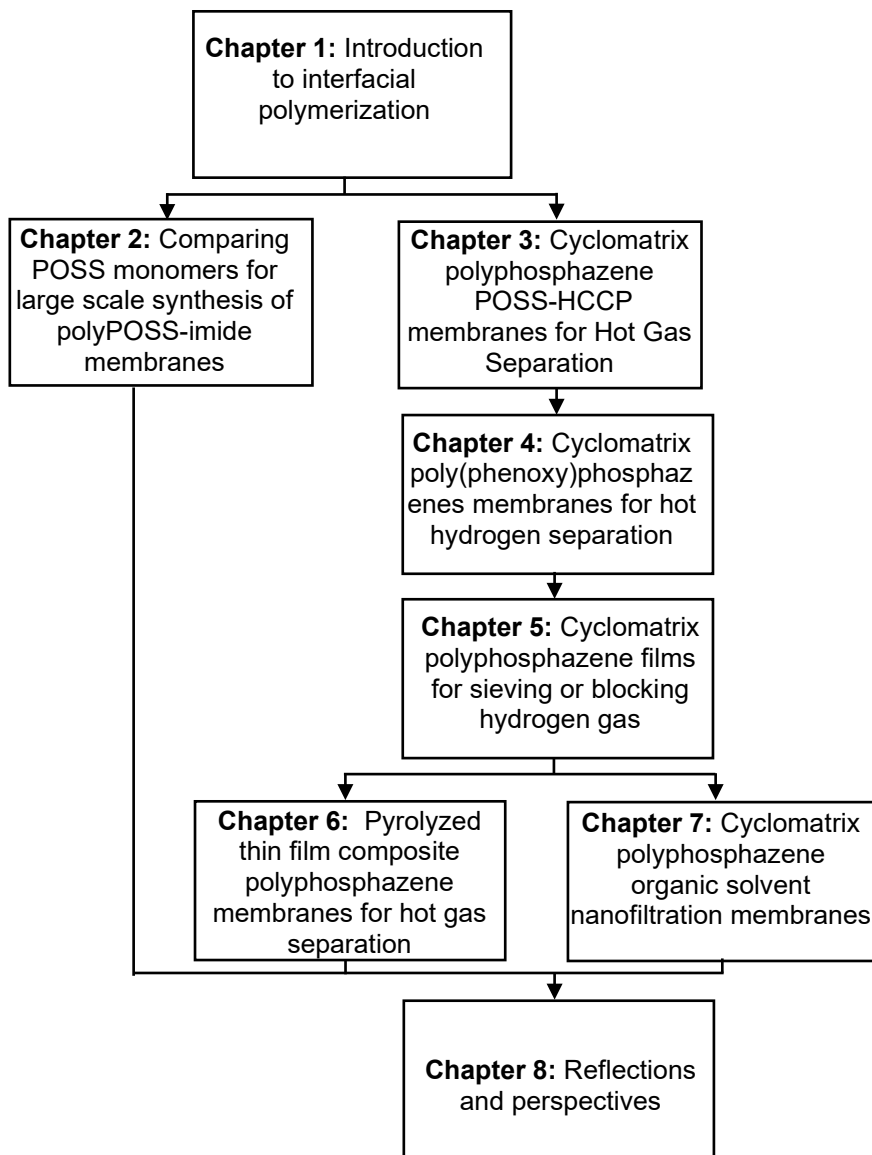
Figure 1.10 Schematic overview of the thesis outline

## 1.7 Thesis outline

The importance of different parameters on properties and performance of interfacial polymerization prepared TFC is described in the previous sections. To elaborate on this section, **Chapter 2** of this work systematically studies the effect of parameters on the composition, performance, and scaling up the potential of polyPOSS-imide membranes. The next **chapters**, **3 to 7**, aim to develop a non-aqueous interfacial polymerization platform for preparing polyphosphazene membranes/barriers based on industrial demands. This is achieved by replacing water with DMSO or a mixture of DMSO and water in an interfacial polymerization system. The flexibility of this platform is evaluated by exploring parameters that affect the properties and performance of the layer. Similar to the traditional interfacial polymerization, factors such as the monomers and reaction conditions were explored as tuning parameters to obtain layers suitable for gas separation membranes, nanofiltration membranes, and gas barriers. Chapters 3 to 7 of this thesis describe the various monomers and the tuning parameters used to produce a broad range of cyclomatrix polyphosphazene layers. An overview of the chapters is given in Figure 1.10.

**Chapter 2** investigates the effects of cations on the polyPOSS-imide properties and the performance of flat discs and tubular membranes. For this, two distinct POSS molecules were used: functionalized with $-NH_3^+Cl^-$ or, so far unexplored, $-NH_2$. The ammonium groups are partially deprotonated by using three different bases, LiOH, NaOH, and KOH. The result shows that the introduced cations via the addition of bases do not affect the molecular composition and hydrogen separation performance of flat disc membranes at 200 °C. In addition, the absence of cations provides a simpler synthesizing route by eliminating the addition of bases. For tubular membranes, much higher ideal and mixed gas selectivities are found than for membranes where the base, NaOH, was added.

**Chapter 3** reports the fabrication of cyclomatrix phosphazene POSS-HCCP network via interfacial polymerization between octa aminopropyl POSS in DMSO/water and HCCP in cyclohexane. The resulting network is highly

cross-linked. The hydrogen separation performance and stability of these membranes are tested at elevated temperatures.

**Chapter 4** reports the non-aqueous interfacial polymerization platform to prepare a series of thermally stable cyclomatrix poly(phenoxy)phosphazenes thin film composite membranes. The networks are stable at high temperatures and show persisting permselectivities for hydrogen over nitrogen and methane at temperatures as high as 260 °C.

**Chapter 5** further explores the versatility of the non-aqueous interfacial polymerization by using a series of smaller aromatic hydroxy compounds than in chapter 4 and HCCP to produce hydrogen separation membranes or hydrogen barriers. It also explores the parameters affecting the formation of the layer and the amount of KOH which dictates the conversion of the hydroxyl groups into phenolate anions. The results show that this parameter affects the molecular structure and permselective properties of the thin polymer networks ranging from hydrogen/oxygen barriers to membranes with persisting hydrogen permselectivities at high temperatures.

**Chapter 6** reports on the possibility of pyrolysis of the prepared ultrathin cyclomatrix polyphosphazene films in chapter 5 under $N_2$, at relatively low temperatures. At 450 °C, pyrolyzed polyphosphazene networks form without defect and show a good hydrogen performance at 200 °C. The final structure comprises disordered carbon and P-O-C and P-O-P bonds.

**Chapter 7** explores the possibility of using non-aqueous interfacial polymerization to prepare cyclomatrix polyphosphazene for OSN membrane applications. The TFC membranes are prepared by interfacial polymerization of a larger monomer compared to previous chapters, 1,1,1-tris(4-hydroxyphenyl)ethane (TPE), and HCCP on top of ceramic and polyacrylonitrile supports. The nanofiltration performance of these membranes in organic solvents is evaluated.

The last chapter of this thesis, **Chapter 8**, reflects on all results in the previous chapters and outlines unexplored areas of interest. In addition, it contains directions for further research.

# 1.8 References

[1] E.P. Favvas, F.K. Katsaros, S.K. Papageorgiou, A.A. Sapalidis, A.C. Mitropoulos, A review of the latest development of polyimide based membranes for $CO_2$ separations, React. Funct. Polym. 120 (2017) 104–130. https://doi.org/10.1016/j.reactfunctpolym.2017.09.002.

[2] Richard W. Baker, Membrane Technology and Applications, John Wiley & Sons, Inc., 2012.

[3] E.D. Heinrich Strathmann, Lidietta Giorno, Introduction to membrane science and technology, Wiley-VCH, Weinheim, Germany, 2011.

[4] A. Khosravi, M. Sadeghi, Separation performance of poly(urethane–urea) membranes in the separation of C2 and C3 hydrocarbons from methane, J. Memb. Sci. 434 (2013) 171–183. https://doi.org/10.1016/j.memsci.2013.01.025.

[5] A.F. Ismail, M. Padaki, N. Hilal, T. Matsuura, W.J. Lau, Thin film composite membrane — Recent development and future potential, Desalination. 356 (2015) 140–148. https://doi.org/10.1016/j.desal.2014.10.042.

[6] W.J. Lau, A.F. Ismail, N. Misdan, M.A. Kassim, A recent progress in thin film composite membrane: A review, Desalination. 287 (2012) 190–199. https://doi.org/10.1016/j.desal.2011.04.004.

[7] D.W.D. Alexander G. Volkov, Liquid-Liquid InterfacesTheory and Methods, CRC Press, 2020.

[8] F. Zhang, J. Fan, S. Wang, Interfacial Polymerization: From Chemistry to Functional Materials, Angew. Chemie Int. Ed. 59 (2020) 21840–21856. https://doi.org/10.1002/anie.201916473.

[9] J.-B. Fan, H. Liu, Y. Song, Z. Luo, Z. Lu, S. Wang, Janus Particles Synthesis by Emulsion Interfacial Polymerization: Polystyrene as Seed or Beyond?, Macromolecules. 51 (2018) 1591–1597. https://doi.org/10.1021/acs.macromol.7b02304.

[10] J.-H. Kang, E. Reichmanis, Low-Threshold Photon Upconversion Capsules Obtained by Photoinduced Interfacial Polymerization, Angew. Chemie. 124 (2012) 12011–12014. https://doi.org/10.1002/ange.201205540.

[11] Y. Liang, Y. Zhu, C. Liu, K.-R. Lee, W.-S. Hung, Z. Wang, Y. Li, M. Elimelech, J. Jin, S. Lin, Polyamide nanofiltration membrane with highly uniform sub-nanometre pores for sub-1 Å precision separation, Nat. Commun. 11 (2020) 2015. https://doi.org/10.1038/s41467-020-15771-2.

[12] P. Phoungtawee, D. Crespy, Shining a new light on the structure of polyurea/polyurethane materials, Polym. Chem. 12 (2021) 3893–3899. https://doi.org/10.1039/D1PY00649E.

[13] J. Huang, R.B. Kaner, A General Chemical Route to Polyaniline Nanofibers, J. Am. Chem. Soc. 126 (2004) 851–855. https://doi.org/10.1021/ja0371754.

[14] S. Hong, I.-C. Kim, T. Tak, Y.-N. Kwon, Interfacially synthesized chlorine-resistant polyimide thin film composite (TFC) reverse osmosis (RO) membranes, Desalination. 309 (2013) 18–26. https://doi.org/10.1016/j.desal.2012.09.025.

[15] M.F. Jimenez-Solomon, Q. Song, K.E. Jelfs, M. Munoz-Ibanez, A.G. Livingston, Polymer nanofilms with enhanced microporosity by interfacial polymerization, Nat. Mater. 15 (2016) 760–767. https://doi.org/10.1038/nmat4638.

[16] M. Shan, X. Liu, X. Wang, Z. Liu, H. Iziyi, S. Ganapathy, J. Gascon, F. Kapteijn, Novel high performance poly( p -phenylene benzobisimidazole) (PBDI) membranes fabricated by interfacial polymerization for H 2 separation, J. Mater. Chem. A. 7 (2019) 8929–8937. https://doi.org/10.1039/C9TA01524H.

[17] Y. Zhong, B. Cheng, C. Park, A. Ray, S. Brown, F. Mujid, J.-U. Lee, H. Zhou, J. Suh, K.-H. Lee, A.J. Mannix, K. Kang, S.J. Sibener, D.A. Muller, J. Park, Wafer-scale synthesis of monolayer two-dimensional porphyrin polymers for hybrid superlattices, Science (80-. ). 366 (2019) 1379–1384. https://doi.org/10.1126/science.aax9385.

[18] R. Ameloot, F. Vermoortele, W. Vanhove, M.B.J. Roeffaers, B.F. Sels, D.E. De Vos, Interfacial synthesis of hollow metal–organic framework capsules demonstrating selective permeability, Nat. Chem. 3 (2011) 382–387. https://doi.org/10.1038/nchem.1026.

[19] J. Huang, S. Virji, B.H. Weiller, R.B. Kaner, Polyaniline Nanofibers: Facile Synthesis and Chemical Sensors, J. Am. Chem. Soc. 125 (2003) 314–315. https://doi.org/10.1021/ja028371y.

[20] S. Karan, Z. Jiang, A.G. Livingston, Sub–10 nm polyamide nanofilms with ultrafast solvent transport for molecular separation, Science (80-. ). 348 (2015) 1347–1351. https://doi.org/10.1126/science.aaa5058.

[21] B. Wu, Z. Sun, J. Wu, J. Ruan, P. Zhao, K. Liu, C. Zhao, J. Sheng, T. Liang, D. Chen, Nanoparticle-Stabilized Oxygen Microcapsules Prepared by Interfacial Polymerization for Enhanced Oxygen Delivery, Angew. Chemie Int. Ed. 60 (2021) 9284–9289. https://doi.org/10.1002/anie.202100752.

[22] J. Yang, M.W. Keller, J.S. Moore, S.R. White, N.R. Sottos, Microencapsulation of Isocyanates for Self-Healing Polymers, Macromolecules. 41 (2008) 9650–9655. https://doi.org/10.1021/ma801718v.

[23] Y. Song, J.-B. Fan, S. Wang, Recent progress in interfacial polymerization, Mater. Chem. Front. 1 (2017) 1028–1040. https://doi.org/10.1039/C6QM00325G.

[24] M.J.T. Raaijmakers, N.E. Benes, Current trends in interfacial polymerization chemistry, Prog. Polym. Sci. 63 (2016) 86–142. https://doi.org/10.1016/j.progpolymsci.2016.06.004.

[25] A. Nowbahar, V. Mansard, J.M. Mecca, M. Paul, T. Arrowood, T.M. Squires, Measuring Interfacial Polymerization Kinetics Using Microfluidic Interferometry, J. Am. Chem. Soc. 140 (2018) 3173–3176. https://doi.org/10.1021/jacs.7b12121.

[26] K. Bouchemal, F. Couenne, S. Briançon, H. Fessi, M. Tayakout, Polyamides nanocapsules: Modeling and wall thickness estimation, AIChE J. 52 (2006) 2161–2170. https://doi.org/10.1002/aic.10828.

[27] V. Enkelmann, G. Wegner, Mechanism of interfacial polycondensation and the direct synthesis of stable polyamide membranes, Die Makromol. Chemie. 177 (1976) 3177–3189. https://doi.org/10.1002/macp.1976.021771106.

[28] S.K. Karode, S.S. Kulkarni, A.K. Suresh, R.A. Mashelkar, Molecular weight distribution in interfacial polymerization—model development and verification, Chem. Eng. Sci. 52 (1997) 3243–3255. https://doi.org/10.1016/S0009-2509(97)00138-3.

[29] Y. Arai, M. Watanabe, K. Sanui, N. Ogata, Effect of polycondensation methods on molecular weight distribution of nylon 610, J. Polym. Sci. Polym. Chem. Ed. 23 (1985) 3081–3093. https://doi.org/10.1002/pol.1985.170231216.

[30] A. V. Berezkin, Y. V. Kudryavtsev, Effect of Cross-Linking on the Structure and Growth of Polymer Films Prepared by Interfacial Polymerization, Langmuir. 31 (2015) 12279–12290. https://doi.org/10.1021/acs.langmuir.5b03031.

[31] A. V. Berezkin, Y. V. Kudryavtsev, Linear interfacial polymerization: Theory and simulations with dissipative particle dynamics, J. Chem. Phys. 141 (2014) 194906. https://doi.org/10.1063/1.4901727.

[32] X. Yang, Monitoring the Interfacial Polymerization of Piperazine and Trimesoyl Chloride with Hydrophilic Interlayer or Macromolecular Additive by In Situ FT-IR Spectroscopy, Membranes (Basel). 10 (2020) 12. https://doi.org/10.3390/membranes10010012.

[33] X. Li, Y. Cao, H. Yu, G. Kang, X. Jie, Z. Liu, Q. Yuan, A novel composite nanofiltration membrane prepared with PHGH and TMC by interfacial polymerization, J. Memb. Sci. 466 (2014) 82–91. https://doi.org/10.1016/j.memsci.2014.04.034.

[34] E. Maaskant, W. Vogel, T.J. Dingemans, N.E. Benes, The use of a star-shaped trifunctional acyl chloride for the preparation of polyamide thin film composite membranes, J. Memb. Sci. 567 (2018) 321–328. https://doi.org/10.1016/j.memsci.2018.09.032.

[35] T. Wang, L. Dai, Q. Zhang, A. Li, S. Zhang, Effects of acyl chloride monomer functionality on the properties of polyamide reverse osmosis (RO) membrane, J. Memb. Sci. 440 (2013) 48–57. https://doi.org/10.1016/j.memsci.2013.03.066.

[36] M. You, W. Li, Y. Pan, P. Fei, H. Wang, W. Zhang, L. Zhi, J. Meng, Preparation and characterization of antibacterial polyamine-based cyclophosphazene nanofiltration membranes, J. Memb. Sci. 592 (2019) 117371. https://doi.org/10.1016/j.memsci.2019.117371.

[37] T. Huang, T. Puspasari, S.P. Nunes, K. Peinemann, Ultrathin 2D-Layered Cyclodextrin Membranes for High- Performance Organic Solvent Nanofiltration, Adv. Funct. Mater. 30 (2020) 1906797. https://doi.org/10.1002/adfm.201906797.

[38] T. Huang, B.A. Moosa, P. Hoang, J. Liu, S. Chisca, G. Zhang, M. AlYami, N.M. Khashab, S.P. Nunes, Molecularly-porous ultrathin membranes for highly selective organic solvent nanofiltration, Nat. Commun. 11 (2020) 5882. https://doi.org/10.1038/s41467-020-19404-6.

[39] L.F. Villalobos, T. Huang, K.-V. Peinemann, Cyclodextrin Films with Fast Solvent Transport and Shape-Selective Permeability, Adv. Mater. 29 (2017) 1606641. https://doi.org/10.1002/adma.201606641.

[40] P.H.H. Duong, D.H. Anjum, K.-V. Peinemann, S.P. Nunes, Thin porphyrin composite membranes with enhanced organic solvent transport, J. Memb. Sci. 563 (2018) 684–693. https://doi.org/10.1016/j.memsci.2018.04.038.

[41] A. Asadi Tashvigh, N.E. Benes, Covalent organic polymers for aqueous and organic solvent nanofiltration, Sep. Purif. Technol. 298 (2022) 121589. https://doi.org/10.1016/j.seppur.2022.121589.

[42] M.J.T. Raaijmakers, M.A. Hempenius, P.M. Schön, G.J. Vancso, A. Nijmeijer, M. Wessling, N.E. Benes, Sieving of Hot Gases by Hyper-Cross-Linked Nanoscale-Hybrid Membranes, J. Am. Chem. Soc. 136 (2014) 330–335. https://doi.org/10.1021/ja410047u.

[43] C. Liu, J. Yang, B. Guo, S. Agarwal, A. Greiner, Z. Xu, Interfacial Polymerization at the Alkane/Ionic Liquid Interface, Angew. Chemie. 133 (2021) 14757–14764. https://doi.org/10.1002/ange.202103555.

[44] F. Yuan, Z. Wang, S. Li, J. Wang, S. Wang, Formation–structure–performance correlation of thin film composite membranes prepared by interfacial polymerization for gas separation, J. Memb. Sci. 421–422 (2012) 327–341. https://doi.org/10.1016/j.memsci.2012.07.035.

[45] M.J.T. Raaijmakers, M. Wessling, A. Nijmeijer, N.E. Benes, Hybrid Polyhedral Oligomeric Silsesquioxanes–Imides with Tailored Intercage Spacing for Sieving of Hot Gases, Chem. Mater. 26 (2014) 3660–3664. https://doi.org/10.1021/cm500691e.

[46] M.J.T. Raaijmakers, T. Schmidt, M. Barth, M. Tutus, N.E. Benes, M. Wessling, Enzymatically Active Ultrathin Pepsin Membranes, Angew. Chemie Int. Ed. 54 (2015) 5910–5914. https://doi.org/10.1002/anie.201411263.

[47] A.K. Ghosh, B.-H. Jeong, X. Huang, E.M.V. Hoek, Impacts of reaction and curing conditions on polyamide composite reverse osmosis membrane properties, J. Memb. Sci. 311 (2008) 34–45. https://doi.org/10.1016/j.memsci.2007.11.038.

[48] B. Khorshidi, T. Thundat, B.A. Fleck, M. Sadrzadeh, A Novel Approach Toward Fabrication of High Performance Thin Film Composite Polyamide Membranes, Sci. Rep. 6 (2016) 22069. https://doi.org/10.1038/srep22069.

[49] J. Shen, G. Wang, X. You, B. Shi, J. Xue, J. Yuan, Y. Li, J. Guan, Y. Ma, Y. Su, R. Zhang, Z. Jiang, Thermal-facilitated interfacial polymerization toward high-performance polyester desalination membrane, J. Mater. Chem. A. 9 (2021) 8470–8479. https://doi.org/10.1039/D0TA12283A.

[50] G.-Y. Chai, W.B. Krantz, Formation and characterization of polyamide membranes via interfacial polymerization, J. Memb. Sci. 93 (1994) 175–192. https://doi.org/10.1016/0376-7388(94)80006-5.

[51] P.S. Goh, A.F. Ismail, S.M. Sanip, B.C. Ng, M. Aziz, Recent advances of inorganic fillers in mixed matrix membrane for gas separation, Sep. Purif. Technol. 81 (2011) 243–264. https://doi.org/10.1016/j.seppur.2011.07.042.

[52] M. Dalwani, J. Zheng, M. Hempenius, M.J.T. Raaijmakers, C.M. Doherty, A.J. Hill, M. Wessling, N.E. Benes, Ultra-thin hybrid polyhedral silsesquioxane–polyamide films with potentially unlimited 2D dimensions, J. Mater. Chem. 22 (2012) 14835. https://doi.org/10.1039/c2jm31941a.

[53] D. Li, H. Wang, Recent developments in reverse osmosis desalination membranes, J. Mater. Chem. 20 (2010) 4551. https://doi.org/10.1039/b924553g.

[54] Y. Liu, X. Wang, X. Gao, J. Zheng, J. Wang, A. Volodin, Y.F. Xie, X. Huang, B. Van der Bruggen, J. Zhu, High-performance thin film nanocomposite membranes enabled by nanomaterials with different dimensions for nanofiltration, J. Memb. Sci. 596 (2020) 117717. https://doi.org/10.1016/j.memsci.2019.117717.

[55] D. Hu, Z.-L. Xu, C. Chen, Polypiperazine-amide nanofiltration membrane containing silica nanoparticles prepared by interfacial polymerization, Desalination. 301 (2012) 75–81. https://doi.org/10.1016/j.desal.2012.06.015.

[56] B. Tang, C. Zou, P. Wu, Study on a novel polyester composite nanofiltration membrane by interfacial polymerization. II. The role of lithium bromide in the performance and formation of composite membrane, J. Memb. Sci. 365 (2010) 276–285. https://doi.org/10.1016/j.memsci.2010.09.015.

[57] M. Matsumoto, L. Valentino, G.M. Stiehl, H.B. Balch, A.R. Corcos, F. Wang, D.C. Ralph, B.J. Mariñas, W.R. Dichtel, Lewis-Acid-Catalyzed Interfacial Polymerization of Covalent Organic Framework Films, Chem. 4 (2018) 308–317. https://doi.org/10.1016/j.chempr.2017.12.011.

34

[58] S.D. Naik, L.K. Doraiswamy, Phase transfer catalysis: Chemistry and engineering, AIChE J. 44 (1998) 612–646. https://doi.org/10.1002/aic.690440312.

[59] J. Xiang, Z. Xie, M. Hoang, D. Ng, K. Zhang, Effect of ammonium salts on the properties of poly(piperazineamide) thin film composite nanofiltration membrane, J. Memb. Sci. 465 (2014) 34–40. https://doi.org/10.1016/j.memsci.2014.03.074.

[60] E. Maaskant, H. Gojzewski, M.A. Hempenius, G.J. Vancso, N.E. Benes, Thin cyclomatrix polyphosphazene films: interfacial polymerization of hexachlorocyclotriphosphazene with aromatic biphenols, Polym. Chem. 9 (2018) 3169–3180. https://doi.org/10.1039/C8PY00444G.

[61] V. Freger, S. Srebnik, Mathematical model of charge and density distributions in interfacial polymerization of thin films, J. Appl. Polym. Sci. 88 (2003) 1162–1169. https://doi.org/10.1002/app.11716.

[62] Y. Zhang, N.E. Benes, R.G.H. Lammertink, Visualization and characterization of interfacial polymerization layer formation, Lab Chip. 15 (2015) 575–580. https://doi.org/10.1039/C4LC01046A.

[63] J. Jegal, S.G. Min, K.-H. Lee, Factors affecting the interfacial polymerization of polyamide active layers for the formation of polyamide composite membranes, J. Appl. Polym. Sci. 86 (2002) 2781–2787. https://doi.org/10.1002/app.11257.

[64] L. Hu, S. Zhang, R. Han, X. Jian, Preparation and performance of novel thermally stable polyamide/PPENK composite nanofiltration membranes, Appl. Surf. Sci. 258 (2012) 9047–9053. https://doi.org/10.1016/j.apsusc.2012.05.153.

[65] G.Z. Ramon, M.C.Y. Wong, E.M.V. Hoek, Transport through composite membrane, part 1: Is there an optimal support membrane?, J. Memb. Sci. 415–416 (2012) 298–305. https://doi.org/10.1016/j.memsci.2012.05.013.

[66] G. Gong, H. Nagasawa, M. Kanezashi, T. Tsuru, Facile and Scalable Flow-Induced Deposition of Organosilica on Porous Polymer Supports for Reverse Osmosis Desalination, ACS Appl. Mater. Interfaces. 10 (2018) 14070–14078. https://doi.org/10.1021/acsami.7b19075.

[67] X. Zhu, X. Zhang, J. Li, X. Luo, D. Xu, D. Wu, W. Wang, X. Cheng, G. Li, H. Liang, Crumple-textured polyamide membranes via MXene nanosheet-regulated interfacial polymerization for enhanced nanofiltration performance, J. Memb. Sci. 635 (2021) 119536. https://doi.org/10.1016/j.memsci.2021.119536.

[68] S. Wang, Y. Zhang, Y. Han, Y. Hou, Y. Fan, X. Hou, Design of Porous Membranes by Liquid Gating Technology, Accounts Mater. Res. 2 (2021) 407–419. https://doi.org/10.1021/accountsmr.1c00024.

[69] F. Liu, L. Wang, D. Li, Q. Liu, B. Deng, A review: the effect of the microporous support during interfacial polymerization on the morphology and performances of a thin film composite membrane for liquid purification, RSC Adv. 9 (2019) 35417–35428. https://doi.org/10.1039/C9RA07114H.

[70] J. A. D. Sharabati, S. Guclu, S. Erkoc-Ilter, D.Y. Koseoglu-Imer, S. Unal, Y.Z. Menceloglu, I. Ozturk, I. Koyuncu, Interfacially polymerized thin-film composite membranes: Impact of support layer pore size on active layer polymerization and seawater desalination performance, Sep. Purif. Technol. 212 (2019) 438–448. https://doi.org/10.1016/j.seppur.2018.11.047.

[71] P.S. Singh, S.V. Joshi, J.J. Trivedi, C.V. Devmurari, A.P. Rao, P.K. Ghosh, Probing the structural variations of thin film composite RO membranes obtained by coating polyamide over polysulfone membranes of different pore dimensions, J. Memb. Sci. 278 (2006) 19–25. https://doi.org/10.1016/j.memsci.2005.10.039.

[72] W.-C. Chao, Y.-H. Huang, W.-S. Hung, Q. An, C.-C. Hu, K.-R. Lee, J.-Y. Lai, Effect of the surface property of poly(tetrafluoroethylene) support on the mechanism of polyamide active layer formation by interfacial polymerization, Soft Matter. 8 (2012) 8998. https://doi.org/10.1039/c2sm25769f.

[73] X. Zhang, Z.-M. Zhan, F.-Y. Cheng, Z.-L. Xu, P.-R. Jin, Z.-P. Liu, X.-H. Ma, X.-R. Xu, B. Van der Bruggen, Thin-Film Composite Membrane Prepared by Interfacial Polymerization on the Integrated ZIF-L Nanosheets Interface for Pervaporation Dehydration, ACS Appl. Mater. Interfaces. 13 (2021) 39819–39830. https://doi.org/10.1021/acsami.1c09221.

[74] S. Yu, S. Li, Y. Liu, S. Cui, X. Shen, High-performance microporous polymer membranes prepared by interfacial polymerization for gas separation, J. Memb. Sci. 573 (2019) 425–438. https://doi.org/10.1016/j.memsci.2018.12.029.

[75] K.P. Lee, J. Zheng, G. Bargeman, A.J.B. Kemperman, N.E. Benes, pH stable thin film composite polyamine nanofiltration membranes by interfacial polymerisation, J. Memb. Sci. 478 (2015) 75–84. https://doi.org/10.1016/j.memsci.2014.12.045.

[76] C.-W. Tsai, C. Tsai, R.-C. Ruaan, C.-C. Hu, K.-R. Lee, Interfacially Polymerized Layers for Oxygen Enrichment: A Method to Overcome Robeson's Upper-Bound Limit, ACS Appl. Mater. Interfaces. 5 (2013) 5563–5568. https://doi.org/10.1021/am4008006.

[77] J.T. Thurston, J.R. Dudley, D.W. Kaiser, I. Hechenbleikner, F.C. Schaefer, D. Holm-Hansen, Cyanuric Chloride Derivatives. I. Aminochloro-s-triazines, J. Am. Chem. Soc. 73 (1951) 2981–2983. https://doi.org/10.1021/ja01151a001.

[78] M.G. Elshof, E. Maaskant, M.A. Hempenius, N.E. Benes, Poly(aryl cyanurate)-Based Thin-Film Composite Nanofiltration Membranes, ACS Appl. Polym. Mater. 3 (2021) 2385–2392. https://doi.org/10.1021/acsapm.0c01366.

[79] A.R. Corcos, G.A. Levato, Z. Jiang, A.M. Evans, A.G. Livingston, B.J. Mariñas, W.R. Dichtel, Reducing the Pore Size of Covalent Organic Frameworks in Thin-Film Composite Membranes Enhances Solute Rejection, ACS Mater. Lett. 1 (2019) 440–446. https://doi.org/10.1021/acsmaterialslett.9b00272.

[80] L. Valentino, M. Matsumoto, W.R. Dichtel, B.J. Mariñas, Development and Performance Characterization of a Polyimine Covalent Organic Framework Thin-Film Composite Nanofiltration Membrane, Environ. Sci. Technol. 51 (2017) 14352–14359. https://doi.org/10.1021/acs.est.7b04056.

[81] W. Dai, F. Shao, J. Szczerbiński, R. McCaffrey, R. Zenobi, Y. Jin, A.D. Schlüter, W. Zhang, Synthesis of a Two-Dimensional Covalent Organic Monolayer through Dynamic Imine Chemistry at the Air/Water Interface, Angew. Chemie Int. Ed. 55 (2016) 213–217. https://doi.org/10.1002/anie.201508473.

[82] M.B.M.Y. Ang, S.-H. Huang, S.-W. Wei, Y.-H. Chiao, R.R. Aquino, W.-S. Hung, H.-A. Tsai, K.-R. Lee, J.-Y. Lai, Surface Properties, Free Volume, and Performance for Thin-Film Composite Pervaporation Membranes Fabricated through Interfacial Polymerization Involving Different Organic Solvents, Polymers (Basel). 12 (2020) 2326. https://doi.org/10.3390/polym12102326.

[83] J. Lee, R. Wang, T.-H. Bae, A comprehensive understanding of co-solvent effects on interfacial polymerization: Interaction with trimesoyl chloride, J. Memb. Sci. 583 (2019) 70–80. https://doi.org/10.1016/j.memsci.2019.04.038.

[84] B. Khorshidi, T. Thundat, D. Pernitsky, M. Sadrzadeh, A parametric study on the synergistic impacts of chemical additives on permeation properties of thin film

composite polyamide membrane, J. Memb. Sci. 535 (2017) 248–257. https://doi.org/10.1016/j.memsci.2017.04.052.

[85] I. C. Kim, B.-R. Jeong, S.-J. Kim, K.-H. Lee, Preparation of high flux thin film composite polyamide membrane: The effect of alkyl phosphate additives during interfacial polymerization, Desalination. 308 (2013) 111–114. https://doi.org/10.1016/j.desal.2012.08.001.

[86] P. Liu, J. Yu, Influence of modifying interfacial polymerization compositions on the performance of composite forward osmosis hollow fiber membranes, J. Polym. Res. 26 (2019) 60. https://doi.org/10.1007/s10965-019-1730-8.

[87] S.H. Kim, S.-Y. Kwak, T. Suzuki, Positron Annihilation Spectroscopic Evidence to Demonstrate the Flux-Enhancement Mechanism in Morphology-Controlled Thin-Film-Composite (TFC) Membrane, Environ. Sci. Technol. 39 (2005) 1764–1770. https://doi.org/10.1021/es049453k.

[88] T.B. Phan, C. Nolte, S. Kobayashi, A.R. Ofial, H. Mayr, Can One Predict Changes from S N 1 to S N 2 Mechanisms?, J. Am. Chem. Soc. 131 (2009) 11392–11401. https://doi.org/10.1021/ja903207b.

[89] R.J. Mayer, M. Breugst, N. Hampel, A.R. Ofial, H. Mayr, Ambident Reactivity of Phenolate Anions Revisited: A Quantitative Approach to Phenolate Reactivities, J. Org. Chem. 84 (2019) 8837–8858. https://doi.org/10.1021/acs.joc.9b01485.

[90] Z. Yang, H. Guo, C.Y. Tang, The upper bound of thin-film composite (TFC) polyamide membranes for desalination, J. Memb. Sci. 590 (2019) 117297. https://doi.org/10.1016/j.memsci.2019.117297.

[91] C.C. Wamser, R.R. Bard, V. Senthilathipan, V.C. Anderson, J.A. Yates, H.K. Lonsdale, G.W. Rayfield, D.T. Friesen, D.A. Lorenz, Synthesis and photoactivity of chemically asymmetric polymeric porphyrin films made by interfacial polymerization, J. Am. Chem. Soc. 111 (1989) 8485–8491. https://doi.org/10.1021/ja00204a023.

[92] Y. Liu, J. Zhu, J. Zheng, X. Gao, J. Wang, X. Wang, Y.F. Xie, X. Huang, B. Van der Bruggen, A Facile and Scalable Fabrication Procedure for Thin-Film Composite Membranes: Integration of Phase Inversion and Interfacial Polymerization, Environ. Sci. Technol. 54 (2020) 1946–1954. https://doi.org/10.1021/acs.est.9b06426.

[93] N. Ogata, K. Sanui, T. Onozaki, S. Imanishi, Interfacial Polycondensation in Aqueous and Non-Aqueous Systems, J. Macromol. Sci. Part A - Chem. 15 (1981) 1059–1063. https://doi.org/10.1080/00222338108056783.

[94] H.R. Allcock, Recent developments in polyphosphazene materials science, Curr. Opin. Solid State Mater. Sci. 10 (2006) 231–240. https://doi.org/10.1016/j.cossms.2007.06.001.

[95] M. Ahmad, T. Nawaz, I. Hussain, X. Chen, M. Imran, R. Hussain, M.A. Assiri, S. Ali, Z. Wu, Phosphazene Cyclomatrix Network-Based Polymer: Chemistry, Synthesis, and Applications, ACS Omega. 7 (2022) 28694–28707. https://doi.org/10.1021/acsomega.2c01573.

[96] H.R. Allcock, Polyphosphazene elastomers, gels, and other soft materials, Soft Matter. 8 (2012) 7521. https://doi.org/10.1039/c2sm26011e.

[97] M. Rezakazemi, M. Sadrzadeh, T. Matsuura, Thermally stable polymers for advanced high-performance gas separation membranes, Prog. Energy Combust. Sci. 66 (2018) 1–41. https://doi.org/10.1016/j.pecs.2017.11.002.

[98] P. Vandezande, L.E.M. Gevers, I.F.J. Vankelecom, Solvent resistant nanofiltration: separating on a molecular level, Chem. Soc. Rev. 37 (2008) 365–405. https://doi.org/10.1039/B610848M.

[99] S. Mehmood, L. Wang, H. Yu, F. Haq, S. Fahad, Bilal-ul-Amin, M. Alim Uddin, M. Haroon, Recent Progress on the Preparation of Cyclomatrix-Polyphosphazene Based Micro/Nanospheres and Their Application for Drug Release, ChemistrySelect. 5 (2020) 5939–5958. https://doi.org/10.1002/slct.201904844.

[100] J. Deng, Z. Huang, B.J. Sundell, D.J. Harrigan, S.A. Sharber, K. Zhang, R. Guo, M. Galizia, State of the art and prospects of chemically and thermally aggressive membrane gas separations: Insights from polymer science, Polymer (Guildf). 229 (2021) 123988. https://doi.org/10.1016/j.polymer.2021.123988.

[101] S. Adhikari, S. Fernando, Hydrogen Membrane Separation Techniques, Ind. Eng. Chem. Res. 45 (2006) 875–881. https://doi.org/10.1021/ie050644l.

[102] P. Kumar, D.W. Kim, N. Rangnekar, H. Xu, E.O. Fetisov, S. Ghosh, H. Zhang, Q. Xiao, M. Shete, J.I. Siepmann, T. Dumitrica, B. McCool, M. Tsapatsis, K.A. Mkhoyan, One-dimensional intergrowths in two-dimensional zeolite

nanosheets and their effect on ultra-selective transport, Nat. Mater. 19 (2020) 443–449. https://doi.org/10.1038/s41563-019-0581-3.

[103] C. Kura, Y. Kunisada, E. Tsuji, C. Zhu, H. Habazaki, S. Nagata, M.P. Müller, R.A. De Souza, Y. Aoki, Hydrogen separation by nanocrystalline titanium nitride membranes with high hydride ion conductivity, Nat. Energy. 2 (2017) 786–794. https://doi.org/10.1038/s41560-017-0002-2.

[104] Y. Ying, M. Tong, S. Ning, S.K. Ravi, S.B. Peh, S.C. Tan, S.J. Pennycook, D. Zhao, Ultrathin Two-Dimensional Membranes Assembled by Ionic Covalent Organic Nanosheets with Reduced Apertures for Gas Separation, J. Am. Chem. Soc. 142 (2020) 4472–4480. https://doi.org/10.1021/jacs.9b13825.

[105] L. Ding, Y. Wei, L. Li, T. Zhang, H. Wang, J. Xue, L.-X. Ding, S. Wang, J. Caro, Y. Gogotsi, MXene molecular sieving membranes for highly efficient gas separation, Nat. Commun. 9 (2018) 155. https://doi.org/10.1038/s41467-017-02529-6.

[106] Y.-S. Li, F.-Y. Liang, H. Bux, A. Feldhoff, W.-S. Yang, J. Caro, Molecular Sieve Membrane: Supported Metalâ&#128;&#147;Organic Framework with High Hydrogen Selectivity, Angew. Chemie. 122 (2010) 558–561. https://doi.org/10.1002/ange.200905645.

[107] L. Lei, F. Pan, A. Lindbråthen, X. Zhang, M. Hillestad, Y. Nie, L. Bai, X. He, M.D. Guiver, Carbon hollow fiber membranes for a molecular sieve with precise-cutoff ultramicropores for superior hydrogen separation, Nat. Commun. 12 (2021) 268. https://doi.org/10.1038/s41467-020-20628-9.

[108] D.R. Pesiri, B. Jorgensen, R.C. Dye, Thermal optimization of polybenzimidazole meniscus membranes for the separation of hydrogen, methane, and carbon dioxide, J. Memb. Sci. 218 (2003) 11–18. https://doi.org/10.1016/S0376-7388(03)00129-7.

[109] S.C. Kumbharkar, U.K. Kharul, N-substitution of polybenzimidazoles: Synthesis and evaluation of physical properties, Eur. Polym. J. 45 (2009) 3363–3371. https://doi.org/10.1016/j.eurpolymj.2009.10.006.

[110] S.H. Choi, D.H. Kim, D.Y. Kim, J.Y. Han, C.W. Yoon, H.C. Ham, J.-H. Kim, H.-J. Kim, S.W. Nam, T.-H. Lim, J. Han, A highly selective polybenzimidazole-4,4′-(hexafluoroisopropylidene)bis(benzoic acid) membrane for high-temperature

hydrogen separation, J. Appl. Polym. Sci. 132 (2015) n/a-n/a. https://doi.org/10.1002/app.42371.

[111] J. Sánchez-Laínez, B. Zornoza, C. Téllez, J. Coronas, Asymmetric polybenzimidazole membranes with thin selective skin layer containing ZIF-8 for H2/CO2 separation at pre-combustion capture conditions, J. Memb. Sci. 563 (2018) 427–434. https://doi.org/10.1016/j.memsci.2018.06.009.

[112] T. Yang, G.M. Shi, T.-S. Chung, Symmetric and Asymmetric Zeolitic Imidazolate Frameworks (ZIFs)/Polybenzimidazole (PBI) Nanocomposite Membranes for Hydrogen Purification at High Temperatures, Adv. Energy Mater. 2 (2012) 1358–1367. https://doi.org/10.1002/aenm.201200200.

[113] L. Zhu, M.T. Swihart, H. Lin, Unprecedented size-sieving ability in polybenzimidazole doped with polyprotic acids for membrane H 2 /CO 2 separation, Energy Environ. Sci. 11 (2018) 94–100. https://doi.org/10.1039/C7EE02865B.

[114] M. Omidvar, C.M. Stafford, H. Lin, Thermally stable cross-linked P84 with superior membrane H2/CO2 separation properties at 100 °C, J. Memb. Sci. 575 (2019) 118–125. https://doi.org/10.1016/j.memsci.2019.01.003.

[115] C.E. Powell, X.J. Duthie, S.E. Kentish, G.G. Qiao, G.W. Stevens, Reversible diamine cross-linking of polyimide membranes, J. Memb. Sci. 291 (2007) 199–209. https://doi.org/10.1016/j.memsci.2007.01.016.

[116] S. Japip, K.-S. Liao, T.-S. Chung, Molecularly Tuned Free Volume of Vapor Cross-Linked 6FDA-Durene/ZIF-71 MMMs for H 2 /CO 2 Separation at 150 °C, Adv. Mater. 29 (2017) 1603833. https://doi.org/10.1002/adma.201603833.

[117] S.H. Han, H.J. Kwon, K.Y. Kim, J.G. Seong, C.H. Park, S. Kim, C.M. Doherty, A.W. Thornton, A.J. Hill, Á.E. Lozano, K.A. Berchtold, Y.M. Lee, Tuning microcavities in thermally rearranged polymer membranes for CO2 capture, Phys. Chem. Chem. Phys. 14 (2012) 4365. https://doi.org/10.1039/c2cp23729f.

[118] Y. Li, Z. Guo, S. Li, B. Van der Bruggen, Interfacially Polymerized Thin-Film Composite Membranes for Organic Solvent Nanofiltration, Adv. Mater. Interfaces. 8 (2021) 2001671. https://doi.org/10.1002/admi.202001671.

[119] G.M. Shi, Y. Feng, B. Li, H.M. Tham, J.-Y. Lai, T.-S. Chung, Recent progress of organic solvent nanofiltration membranes, Prog. Polym. Sci. 123 (2021) 101470. https://doi.org/10.1016/j.progpolymsci.2021.101470.

[120] S. Darvishmanesh, J.C. Jansen, F. Tasselli, E. Tocci, P. Luis, J. Degrève, E. Drioli, B. Van der Bruggen, Novel polyphenylsulfone membrane for potential use in solvent nanofiltration, J. Memb. Sci. 379 (2011) 60–68. https://doi.org/10.1016/j.memsci.2011.05.045.

[121] C. Roengpithya, D.A. Patterson, P.C. Taylor, A.G. Livingston, Development of stable organic solvent nanofiltration membranes for membrane enhanced dynamic kinetic resolution, Desalination. 199 (2006) 195–197. https://doi.org/10.1016/j.desal.2006.03.045.

[122] X.Q. Cheng, K. Konstas, C.M. Doherty, C.D. Wood, X. Mulet, Z. Xie, D. Ng, M.R. Hill, L. Shao, C.H. Lau, Hyper-Cross-Linked Additives that Impede Aging and Enhance Permeability in Thin Polyacetylene Films for Organic Solvent Nanofiltration, ACS Appl. Mater. Interfaces. 9 (2017) 14401–14408. https://doi.org/10.1021/acsami.7b02295.

[123] Y. Li, E. Wong, A. Volodine, C. Van Haesendonck, K. Zhang, B. Van der Bruggen, Nanofibrous hydrogel composite membranes with ultrafast transport performance for molecular separation in organic solvents, J. Mater. Chem. A. 7 (2019) 19269–19279. https://doi.org/10.1039/C9TA06169J.

[124] Y. Zeng, Y. Liu, J. Tan, J. Huang, J. Liu, A. Tang, C. Chen, H. Chen, Structure-Gas Barrier Property Relationship in a Novel Polyimide Containing Naphthalene and Amide Groups: Evaluation by Experiments and Simulations, Materials (Basel). 14 (2021) 1402. https://doi.org/10.3390/ma14061402.

[125] Y. Liu, J. Huang, J. Tan, Y. Zeng, J. Liu, H. Zhang, Y. Pei, X. Xiang, Y. Liu, Intrinsic high-barrier polyimide with low free volume derived from a novel diamine monomer containing rigid planar moiety, Polymer (Guildf). 114 (2017) 289–297. https://doi.org/10.1016/j.polymer.2017.03.006.

[126] K. Pang, R. Kotek, A. Tonelli, Review of conventional and novel polymerization processes for polyesters, Prog. Polym. Sci. 31 (2006) 1009–1037. https://doi.org/10.1016/j.progpolymsci.2006.08.008.

[127] Y.S. Hu, R.Y.F. Liu, L.Q. Zhang, M. Rogunova, D.A. Schiraldi, S. Nazarenko, A. Hiltner, E. Baer, Oxygen Transport and Free Volume in Cold-Crystallized and Melt-Crystallized Poly(ethylene naphthalate), Macromolecules. 35 (2002) 7326–7337. https://doi.org/10.1021/ma0205156.
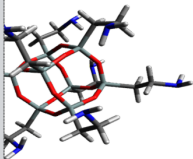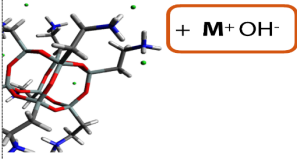
[128] O.C. Compton, S. Kim, C. Pierre, J.M. Torkelson, S.T. Nguyen, Crumpled Graphene Nanosheets as Highly Effective Barrier Property Enhancers, Adv. Mater. 22 (2010) 4759–4763. https://doi.org/10.1002/adma.201000960.

[129] C. Habel, E.S. Tsurko, R.L. Timmins, J. Hutschreuther, R. Kunz, D.D. Schuchardt, S. Rosenfeldt, V. Altstädt, J. Breu, Lightweight Ultra-High-Barrier Liners for Helium and Hydrogen, ACS Nano. 14 (2020) 7018–7024. https://doi.org/10.1021/acsnano.0c01633.

[130] O.B. Seo, S. Saha, N.H. Kim, J.H. Lee, Preparation of functionalized MXene-stitched-graphene oxide/poly (ethylene-co-acrylic acid) nanocomposite with enhanced hydrogen gas barrier properties, J. Memb. Sci. 640 (2021) 119839. https://doi.org/10.1016/j.memsci.2021.119839.

# Chapter 2

# Comparing amine- and ammonium functionalized silsesquioxanes for large scale synthesis of hybrid polyimide high-temperature gas separation membranes

# Abstract

PolyPOSS-imide membranes are promising for separating $H_2$ from larger molecules ($CO_2$, $N_2$, $CH_4$) at temperatures up to 300 °C. Their fabrication involves two steps: interfacial polymerization of POSS and 6FDA, followed by thermal imidization. This work provides a systematic study of the effects of cations on membrane properties and performance. For this, two distinct POSS molecules were used: functionalized with $-NH_3^+Cl^{-1}$ or, so far unexplored, $-NH_2$. The ammonium groups are partially deprotonated by using three different bases, LiOH, NaOH, and KOH. We demonstrate that the introduced cations affect the film thickness but not the molecular composition of the polyamic acid. All polyamic acids can be imidized, but the cations reduce the imidization kinetics as well as the loss of organic crosslinkers. For flat disc membranes, at 200 °C, the absence of cations results in comparable permeability combined with higher selectivity for $H_2/N_2$. This, and the possibility to discard adding a base, motivated a scale-up study of the new POSS. For tubular membranes, much higher ideal and mixed gas selectivities are found than for membranes where NaOH was added. Results indicate that the new route allows more reproducible production of defect free membranes and has potential for larger-scale polyPOSS-imide fabrication.

## 2.1 Introduction

Global warming, due to greenhouse gas emissions, is one of the current worldwide concerns.[1] The development of new, innovative, and flexible methods to reduce emissions of $CO_2$ in industrial processes at high temperatures is very important. Besides, in many industrial processes, gas separation at elevated temperatures is desirable to reduce efficiency losses associated with cooling and heating of gas streams.[2] Within this context, membrane separations may offer valuable alternatives for existing technologies.

Polyimide membranes are promising candidates for $H_2$ separation ($H_2/N_2$, $H_2/CH_4$, $H_2/CO_2$) at high temperatures, thanks to their exceptional thermal, chemical, and mechanical stability.[3, 4] However, conventional polyimides are not able to properly separate $H_2$ from mixtures at elevated temperatures. One way to address this issue is by improving the cross-linking density of polyimide, by introducing a highly functionalized and rigid monomer into the macromolecular structure in order to reduce the molecular dynamics.[5] Polyhedral oligomeric silsesquioxane (POSS) with a basic formula of $R_nSi_nO_{1.5n}$ (n = 6, 8, 12), providing eight functionalize groups, offers this possibility.[6]

Raaijmakers et al.[7] have used POSS cages as the main building block for synthesizing a polyimide polymeric network, resulting in hybrid membranes that can selectively separate gas molecules at elevated temperatures. They have demonstrated a two-step procedure for synthesizing a hybrid polyPOSS−imide network: the interfacial polymerization (IP) of an ammonium chloride salt functionalized POSS and anhydride, followed by thermal imidization. This results in ultrathin (<100 nm) selective films on top of ceramic supports, providing for high $H_2$ permeance (> 1000 GPU) while still retaining gas selectivity of approximately 5 for $H_2/CH_4$ and $H_2/N_2$ at 300 °C. The $CO_2/CH_4$ selectivity of approximately 60 at temperatures below 100 °C emphasizes the applicability of the polyPOSS−imide over a broad temperature range.[7]

The procedure of Raaijmakers [7] involves the addition of a base for partial deprotonation of the ammonium groups of the distinguished POSS molecule.

The extent of the deprotonation, and the reactivity of the functional groups of the POSS molecules, will be affected by the nature of the cations that are added with the alkaline base. In addition, such cations affect the electrostatics during the interfacial polycondensation reaction, both with respect to the characteristics of the interface between the two immiscible liquids phases with respect to the polymerization kinetics.[8-10] This may affect film properties, such as thickness, free volume, degree of cross-linking, amongst others.[11] Moreover, in the subsequent thermal treatment of the polyamic acid films, the presence and nature of the cations can also impact the properties of the final materials. The condensation of the amic acid bonds to form the imide groups cannot occur when the proton of the amic acid group is exchanged with another cation; the imidization requires a carboxylic acid group in the ortho position to an amide group which is blocked by the ions.[12-14] Also, the cation interferes with intra and intermolecular interactions of polyamic acid groups, for instance, diminishing hydrogen bonding. This also affects the subsequent imidization of the polyamic acid.[15] Finally, ions that remain in the final membrane could facilitate the sorption of small polar molecules such as water, affecting the transport of these and other small molecules within the matrix (e.g., competitive sorption, hindrance of diffusive pathways).

By using a proprietary approach, SINTEF is able to synthesize POSS molecules with amine groups (POSS–$(CH_2)_3NH_2$), rather than POSS with ammonium groups POSS (POSS–$(CH_2)_3NH_3^+Cl^-$) that require deprotonation.[16] This allows omitting the addition of a base in the procedure reported by Raaijmakers.[7] Here, we investigate whether such a more facile method, with the new POSS source, can be used for membrane fabrication. For this purpose, the two different types of POSS are reacted with 4,4-(hexafluoroisopropylidene) diphthalic anhydride (6FDA), atop ceramic supports. Deprotonation of the ammonium functionalized POSS is done with the addition of different bases, *i.e.*, LiOH, NaOH, and KOH, individually, introducing different cations. This allows studying the effect of the nature of the cations on the formation, imidization, and performance of polyPOSS-imide membranes for $H_2$ recovery. Finally, the scale-up potential of membranes deploying the new POSS source is investigated using porous ceramic tubular supports. The performance of these tubular membranes is

assessed by means of single and mixed gas measurements in a wide range of operating conditions.

## 2.2 Experimental

### 2.2.1. Materials

Toluene (anhydrous 99.8 wt.%), 6FDA, NaOH, LiOH, and KOH were obtained from Sigma-Aldrich. Ammonium chloride salt functionalized POSS (Octa ammonium POSS®, USA) was purchased from Hybrid Plastics, abbreviated HP-POSS. Octa aminopropyl POSS (52.6 wt.% in n-propanol) was kindly provided by SINTEF (Norway), abbreviated SF-POSS, and recently up-scaled by Funzionano AS (Norway). Porous α-alumina discs (D 39 mm, thickness 2 mm) were obtained from Pervatech B.V. (The Netherlands), coated with a 3 μm thick γ-alumina layer via a dip-coating and calcination process as described before by Karaliç et al.[17] and used as supports. Asymmetric $TiO_2/Al_2O_3$ single-channel (OD = 10 mm, ID = 6 mm, length = 250 mm) supports were provided by Céramiques Techniques Industrielles (CTI, France) and coated with a γ-alumina layer atop of an internal zirconia microfiltration layer.

### 2.2.2. Material fabrication

Table 2.1 List of Acronyms

| Acronym | Name |
|---------|------|
| $M^+$ | Metal cation, $Li^+$, $Na^+$, $K^+$ |
| PA | Polyamic acid prepared with SF-POSS |
| Li-PA | Polyamic acid prepared with HP-POSS, pH adjusted with LiOH |
| Na-PA | Polyamic acid prepared with HP-POSS, pH adjusted with NaOH |
| K-PA | Polyamic acid prepared with HP-POSS, pH adjusted with KOH |
| M-PA | Polyamic acid prepared with HP-POSS, pH adjusted with different bases (M-pH) |
| PI | Polyimide prepared from PA |
| Li-PI | Polyimide prepared from Li-PA |
| Na-PI | Polyimide prepared from Na-PA |
| K-PI | Polyimide prepared from K-PA |
| M-PI | Polyimide prepared from M-PA |

For both the preparation of freestanding films and membranes, the pH value of aqueous solution of HP-POSS (0.9 wt.%) was adjusted to 9.9 by using one of the base solutions, NaOH, LiOH, and KOH, with a concentration of 0.5M. For SF-POSS, the 0.9 wt.% aqueous solution has an initial pH of 10.5, and no additional pH adjustment was needed. Thin films were prepared by 2 step procedures reported elsewhere [18, 19]: first, the interfacial polymerization reaction between 0.9 wt.% POSS in water and 0.075 wt. % 6FDA in toluene, resulting in the formation of polyamic acid, followed by a thermal imidization.  Based on the type of POSS solution, different abbreviations were used, which can be found in Table 2.1.

## Preparing freestanding films

The freestanding films were prepared by bringing the pH adjusted aqueous solution of HP-POSS into contact with the 6FDA solution of 0.075 wt.% in toluene. After 30 minutes, the collected film was washed with acetone and water. It was followed by imidization at 300 ˚C for 2 hours with a ramp rate of 5˚C/min in air atmosphere. The collected solid might be referred to as powder in the text.

## Membranes preparation

In brief, a film was formed atop a flat disc ceramic membrane by soaking the porous support in 0.9 wt.% POSS aqueous solution for 15 minutes, followed by contacting it with the 6FDA solution in toluene. Subsequently, the membrane was imidized by heating it to 300 ˚C for 2 hours with a ramp rate of 5˚C/min in an air atmosphere.

For the tubular membranes, the same procedure as in [19] was used. The tubular membranes were pre-wetted with 0.9 wt.% aqueous SF-POSS solutions for 15 min, followed by reacting the 6FDA solution for 5 minutes. Subsequently, imidization of the membranes was carried in an oven for 2 h at 300 °C.

## 2.2.3. Material characterization

Scanning electron micrographs were obtained using a field emission scanning electron microscope (FE-SEM, JSM-7610F, Jeol) to visualize the

samples' morphology and thickness. The images were taken after applying a 5 nm Pt/Pd coating. Thermal gravimetric analysis (TGA) combined with mass spectrometer (MS) measurements were carried out using a Netsch STA 449 F3 Jupiter TGA and QMS 403 D Aelos MS under 70 mL min$^{-1}$ N$_2$ flow with a heating rate of 10°C min$^{-1}$ from 50 to 800°C. Fourier transform infrared spectroscopy (FTIR) in attenuated total reflectance (ATR) was performed to analyze the structure of the membranes in the range of 400–4000 cm$^{-1}$ using (ATR-FTIR, Spectrum Two, PerkinElmer). X-ray Photoelectron Spectroscopy (XPS) measurements were performed on the membranes with an Ultra Axis™ spectrometer (Kratos Analytical, Manchester UK). The membranes were irradiated with with monochromatic Al K$_\alpha$ radiation (1486.6 eV) with a beam size of 100 μm at a power of 25 W. X-ray diffractometer (XRD) patterns were recorded by monitoring the diffraction angle 2θ from 5° to 40° on a D2 PHASER XRD (Bruker) using copper radiation under a voltage of 45 kV and a current of 40 mA. EDX analysis was carried out at 10 kV with >1000 counts s$^{-1}$ on obtained powders (SEM, JSM-6010LA, JEOL). The experiment was repeated four times for each sample. The average value and 95% confidence interval are reported.

## 2.2.4. Membrane performance

### Flat disc membranes

Membrane single gas permeation experiments were done using Inspector Poseidon (Convergence, The Netherlands) gas permeation setup using a dead-end mode at a trans-membrane pressure of 2 bar and atmospheric pressure at the permeate side. Single gas permeation of He, N$_2$, H$_2$, CH$_4$, and CO$_2$ was measured at temperatures between 50-200 °C. Two different samples were measured, and the average data and standard deviation are reported. The ideal selectivity was calculated as the ratio of respective permeances.

### Tubular membranes

Single-channel membranes were tested in a home-build gas permeation setup available at SINTEF, in a crossflow configuration, reported elsewhere.[19] In short, the feed gas was applied on the inner side of the membranes (lumen) with an active permeation area of 23 cm$^2$. Mass flow controllers (MFC, Bronkhorst High-Tech B·V., The Netherlands) and a back-pressure

regulator (BPR, Bronkhorst High-Tech B·V., The Netherlands) were used to accurately control the gas feed flow and control its pressure, respectively. The permeate stream was kept at ambient pressure. The gas flow rates were measured with mass flowmeters (MFM, Bronkhorst High-Tech B·V., The Netherlands). Single gas permeation of $N_2$, $H_2$, $CH_4$, and $CO_2$ was measured up to 250 °C and 10 bar. For the mixed gas measurement, a gaseous mixture containing 60% $H_2$, 20% $CH_4$, 10% $N_2$, and 10% $CO_2$ was used to mimic the conditions of coke oven gas. The gas concentration in all the gaseous streams (feed, retentate, and permeate) was measured by a micro-GC (μGC, Agilent 490). The reported data is the average result of three tubular samples and denoted GEN-PI.

The gas permeance of the $i$-th gas, $P_i$, was obtained using Equation (2.1):

$$P_i = \frac{\dot{n}_p \, y_{p,i}}{A \Delta p_i} \qquad (2.1)$$

where $\dot{n}_p$ is the total mass flow of the permeate side, $y_{p,i}$ is the the $i$-th gas concentration on the permeate side, A is the membrane area, and $\Delta p_i$ is the differential $i$-th gas partial pressure between the feed and the permeate side. For gaseous mixture, the $\Delta p_i$ is calculated from Equation (2.2):

$$\Delta p_i = \frac{\left(p_{f,in} - p_p\right)_i - \left(p_{f,out} - p_p\right)_i}{\ln\left(p_{f,in} - p_p\right)_i - \ln\left(p_{f,out} - p_p\right)_i} \qquad (2.2)$$

where $p_{f,in}$ and $p_{f,out}$ are the pressure at the feed inlet and outlet, respectively. For the gas mixture, the selectivity was obtained by means of Equation (2.3):

$$\textit{Selectivity of i over j} = \frac{y_i/y_j}{x_i/x_j} \qquad (2.3)$$

where $y$ and $x$ are the gas concentration of the species i in the permeate ($y$) and in the feed ($x$) stream, respectively.

The stage cut for the separation experiment was calculated as the ratio between the gas flow on the permeate side and the feed side, as shown in Equation (2.4):

$$stage\ cut = \frac{\dot{n}_p y_{p,i}}{\dot{n}_f y_{f,i}} \qquad (2.4)$$

## 2.3 Results & Discussion

In this work, the results and discussion part is divided into three parts. Firstly, we study the effect of cations on the formation and properties of polyamic acid and polyimide networks and the imidization step. Secondly, the gas permeation performance of small flat disc membranes is characterized. Finally, in the third part, the gas separation performance of tubular membranes is evaluated.

### 2.3.1 Characterization of the polymeric network
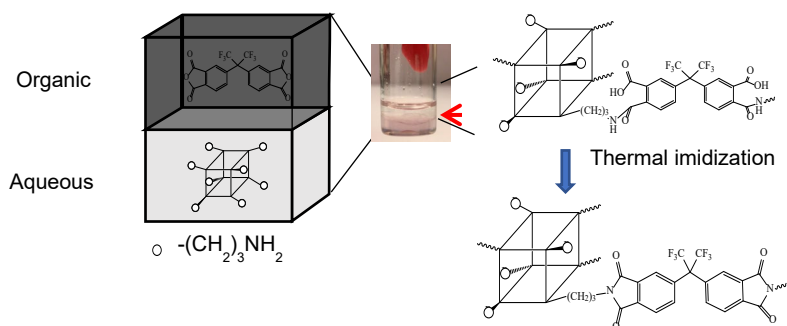


Figure 2.1 Schematic representation of the preparation of freestanding polyPOSS-imide films; for supported membrane films a porous support structure is soaked with the aqueous solution and subsequently contacted with the organic solution, the POSS cage is illustrated as a cube.

Figure 2.1 gives a schematic representation of the preparation of freestanding polyPOSS-imide films. Reactions were so rapid that the formation of the freestanding polyamic acid films between the two immiscible solutions could be easily confirmed with the bare eye in less than 1 minute. The formed polyamic acid layer was converted to polyimide by the dehydrative cyclization of the polyamide acid through thermal imidization.

Figure 2.2A represents the FTIR spectra of polyamic acid and polyimide powders normalized with respect to the symmetric stretching of $CF_3$ band at 1256 cm$^{-1}$. The bands at 1624 cm$^{-1}$ and 1555 cm$^{-1}$ exhibit N-H bending and

53

C=O stretching of the amic acid group in all samples, respectively. A single peak at 1118 cm$^{-1}$ for vSi–O–Si is expected for perfect symmetry of the Si–O skeleton, but split into two split peaks [16], mainly due to the loss of that perfect skeleton symmetry upon reaction-induced variations of the chemical environment at a certain degree of cross-linking. Two bands at 1099 cm$^{-1}$ and 1032 cm$^{-1}$ are attributed to the Si-O-Si asymmetric stretching of polyhedral silsesquioxane structures, respectively. For all the samples, except for PA, a peak appears around 1410 cm$^{-1}$ that can be attributed to the C-O stretching of carboxylic acid groups in which the proton has been exchanged for a cation.[12, 20, 21] Figure S2.1 represents a schematic illustration of the cation exchange process of polyamic acids.

Figure 2.2B shows the FTIR of polyimide powder, normalized for the CF$_3$ band. After heating the polyamic acids to 300 ˚C for 2 hr, two new peaks appear at 1778 cm$^{-1}$ and 1710 cm$^{-1}$ attributed to C=O symmetric and asymmetric stretching of the imide group. Thus, FTIR indicates the successful formation of all polyamic acid and polyimide networks. Also, for the polyamic acid networks fabricated with HP-POSS, it confirms the presence of carboxylate salts due to proton-cation exchange of the carboxylate acid groups.
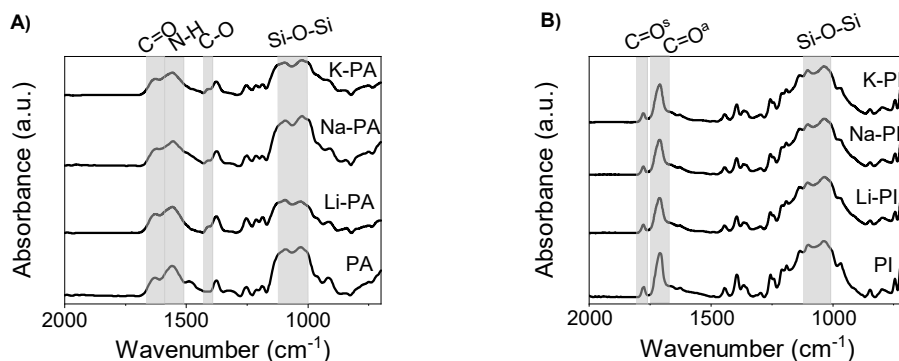


Figure 2.2 FTIR spectra of (A) polyamic acid and (B) polyimide powders. In the spectra of the polyamic acid (A), the peak at 1410 cm$^{-1}$ indicates dissociated carboxyl groups in the M-PA film. For polyimide spectra (B), the new peaks at 1778 cm$^{-1}$ and 1710 cm$^{-1}$ correspond to the imide groups.

EDX analysis is used on the formed networks to investigate the elemental composition and extent of cross-linking for polyamic acid and polyimide powders (Table 2.2). The data reveal the presence of Na, K, C, Si, Cl, O, and F. Unfortunately, Li cannot be detected with this method due to the low x-ray yield of this element.[22] Elemental analysis reveals that the PA does not contain significant amounts of cations or chloride. For the M-PA powders in which a base was added during synthesis, the corresponding cations are detected, as well as Cl$^-$. The detected cations, M$^+$, can be presented in the form of M$^+$-carboxylate groups or as the remaining MCl that was formed during the IP reaction. This is confirmed by XRD data, Figure S2.2, where distinct peaks corresponding to the salts' crystal structure indicate that MCl salt is present in an amorphous M-PI network. The similar elemental content of M$^+$ and Cl$^-$ do not necessarily imply that the cations are predominantly present as MCl; the chlorine can also be present accompanied by a proton. Also, the content of Na is higher than K, attributed to the higher affinity of carboxylic acid toward Na.[23]

The F/Si ratio is similar for all the polyamic acids. This ratio is representative for the degree of cross-linking, and the result implies that, in the interfacial polycondensation process, a similar amount of functional groups on the POSS cage will react with an anhydride group, irrespective of the presence and type of the cation and the presence of Cl$^-$. In other words, the presence of the cations does not substantially affect the molecular composition of the polymer that is formed in the interfacial polymerization reaction.

Also, in the derived polyimide material, the main elements of interest (Na, K, C, Si, Cl, O, and F) are detected. For all polyimides in which cations were added (M-PI), the changes in the concentrations of C, F, Si and O remain within experimental error, indicating no significant loss of crosslinker groups. The ratio of F over Si stays constant over the imidization process (around 1.1). This indicates that the POSS cages are, on average, connected with 3 to 4 bridges, but the experimental error is large. These results are in line with a previous study.[18] Notably, for PI samples, the percentage of C and F are slightly lower, and the content of Si and O are slightly higher than in the corresponding polyamic acid (PA). The thermal treatment reduces the ratio of F/Si to 0.5, corresponding to less than 3 imide groups per POSS cage, but again the experimental error is large. Still, these results indicate

that thermal imidization can result in the loss of more of the organic crosslinkers in the absence of the cations.

Table 2.2 EDX analysis of polyamic acid and polyimide powders.

| | Elemental Composition (%) | | | | | | | |
|---|---|---|---|---|---|---|---|---|
| | Polyamic acid | | | | Polyimide | | | |
| | PA | Li-PA | Na-PA | K-PA | PI | Li-PI | Na-PI | K-P |
| Na | 0 | 0 | 1±0.2 | 0 | 0 | 0 | 0.72±0.3 | 0 |
| K | 0 | 0 | 0 | 0.5±0.2 | 0 | 0 | 0 | 0.1 |
| Cl | 0 | 0.3±0.1 | 1.3±0.3 | 0.9±0.2 | 0 | 1.2±0.3 | 0.7±0.2 | 0.1 |
| C | 54.6±2.4 | 53.2±1.7 | 55.9±2.1 | 52.8±2.1 | 46.1±2.4 | 57.5±5.1 | 54.1±0.5 | 53.8±0 |
| N | 11.5±1.4 | 12.3±3.1 | 9±2 | 11.9±1.7 | 9.2±1.2 | 6±1.6 | 7.6±0.6 | 8.1±0. |
| Si | 7.3±2.1 | 5 ±1.8 | 7.8±2.4 | 6.4±1.2 | 10.2±2.7 | 9.5±3.1 | 8.3±0.9 | 7.4±2. |
| F | 7.7±1 | 9.3±0.9 | 7.9±0.5 | 7.7±1 | 5.1±0.4 | 8±1.5 | 9.4±0.8 | 9.5±2. |
| F/Si | 1.2±0.3 | 1.8±0.6 | 1±0.3 | 1.2±0.1 | 0.5±0.2 | 0.9±0.3 | 1.1±0.1 | 1.3±0. |
| O | 18.8±2.3 | 19.9±0.4 | 17.1±1.5 | 19.8±2.3 | 29.3±4.6 | 18.9±2.3 | 19.2±1.9 | 21.2±1 |

XPS is performed on the surface of four membranes, PA, PI, Na-PA, and Na-PI, and the results are listed in Table 2.3. The data reveal the presence of POSS and anhydride for all samples. As expected, for PA and PI no Na is detected, and Na-PA and Na-PI do contain Na. After imidization, XPS results reveal, for both samples, decreased content of C and F and increased content of Si and O. The F/Si ratios are reduced by an order of magnitude for both samples. This implies that during thermal imidization, at the outer surface of the membranes, the extent of cross-linking is significantly decreased. Such a decrease in crosslinks is in contrast with the EDX results, where only small changes in crosslinker concentration are observed, even in the absence of the cations. It should be emphasized that XPS probes only a very thin (~nm) region at the outer surface of the supported membranes, whereas EDX probes the bulk composition of the freestanding films. It has previously been observed that the degree of cross-linking in the thin outer surface region of polyPOSS-imide membranes is lower as compared to in the rest of the films.[24]

The TGA data in Figure 2.3A shows the mass loss of 4 different polyamic acids. All polyamic acids exhibit four steps of mass loss up to 800˚C, agreeing well with previous observations.[25] The mass loss between 150 to 300 ˚C is higher for the PA sample (10%) as compared to other samples (5 %). This is due to more pronounced imidization in the absence of amide

groups in which the protons have been exchanged for cations. In polyamic acid containing cations, the replacement of a proton of a carboxylic acid by an $M^+$ cation prevents from ring closure (imidization). Also, the lower mass loss of the M-PA samples can be due to lesser detachment of linker groups. This can be the result of the stabilization of the CO-NH group by a cation [12] or the reduced hydrogen bonding between the NH and OH of adjacent amide groups induced by the presence of the cations. This hydrogen bonding can lead to destabilization, and hence to an amic acid structure that is more sensitive to thermal imidization.[12, 15, 26]

Table 2.3 XPS analysis of polyamic acid and polyimide powders

| | Elemental Composition (%) | | | |
|---|---|---|---|---|
| | Polyamic acid | | Polyimide | |
| | PA | Na-PA | PI | Na-PI |
| Na | 0 | 1±0.1 | 0 | 0.6±0.1 |
| Cl | 0 | 0.7±0.2 | 0 | 0 |
| C | 65±2.7 | 59.2±1.7 | 32±3.1 | 22±3.7 |
| N | 5.7±0.5 | 5.7±0.3 | 3.3±0.5 | 2.1±0.3 |
| Si | 5.9±0.5 | 7.1±1.6 | 9.3±1.4 | 6.3±0.7 |
| F | 3.5±0.2 | 6.4±0.4 | 0.8±0 | 0.9±0.1 |
| F/Si | 0.6±0.1 | 1.2±0.2 | 0.08±0 | 0.14±0 |
| O | 19.3±1.1 | 21.1±1.1 | 45.5±1.4 | 54±0.8 |

Table 2.4 $T_d^5$, $T_d^{10}$, $T_{d,max}$, and residue at 750 °C of polyimide

| | K-PI | Na-PI | Li-PI |
|---|---|---|---|
| $T_d^5$ | 414 | 423 | 424.3 |
| $T_d^{10}$ | 472 | 471 | 473.1 |
| $T_{d,max}$ | 516.3 | 527.1 | 520.5 |

The thermal stability of the polyimide network is represented by TGA data in Figure 2.3B. It can be concluded that all polyimide polymers are thermally stable up to 300 ˚C, the onset of decomposition, and at a higher temperature, a significant decrease in mass is observed. As expected, PI has a higher amount of residue at 800 °C than the other polyimides. The results are in line with the EDX results and the TGA results for the polyamic acid. They indicate that the PI powders can have fewer organic bridges, leading to a higher final (inorganic) residue at 800 °C. The difference between the mass loss of M-PI and PI, around 7 %, is in good agreement with the ratio of

6FDA and POSS derived from the EDX data; based on this ratio, and assuming the loss of all propyl chains and fluorine groups, the difference between the residuals of polyimide powders can be calculated to be 7 %. Table 2.4 shows the $T_d{}^5$, $T_d{}^{10}$, and $T_d{}^{max}$ (subscript indicates wt% loss) of the powders. All polyimide samples decompose around 516 to 538 °C. PI has the highest $T_d{}^5$, $T_d{}^{10}$ because of the lower number of organic bridges between the POSS cages. This leads to about 10-22 °C differences between PI and M-PI.
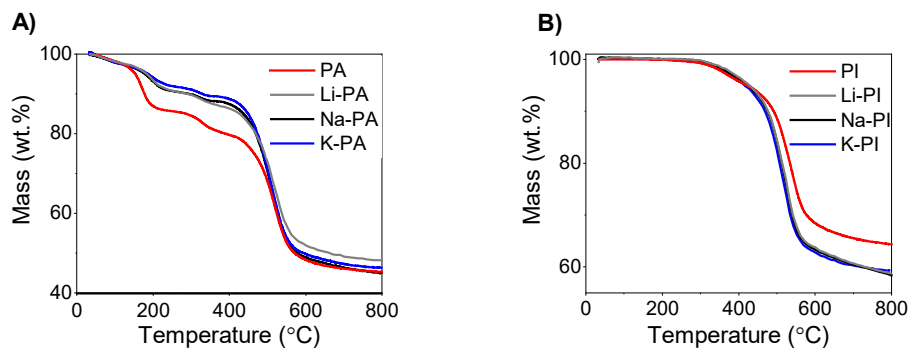


Figure 2.3 TGA scan of (A) polyamic acid and (B) polyimide powders.

In summary, all the polyimide networks are stable up to 300 °C, and the difference between the residues and $T_{d,max}$ at 800 °C, originates from the lower amount of organic bridges between the POSS cages in PI polymers.

## 2.3.2 Flat disc membrane characterization and performance

Figure 2.4 shows the FE-SEM cross-sectional images of membranes. It confirms the fabrication of the layer atop the ceramic supports. The layer thicknesses are in the range of other IP membranes [27]: Na-PI (69.4±10 nm) ≤ Li-PI (83.9±5 nm) < PI (100.3 ±3nm) < K-PI(137.8±10 nm).

Different ions induce different electrostatic charge distribution on the interface of the solvents, which is the reaction zone. They make different 'salting-out' and 'salting-in' effects, often following the Hofmeister series. For instance, in this series, $K^+$ with higher salting-out efficiency would result in a faster layer formation.[28] In addition, the presence and nature of the salt affect the nature of the interface; a less sharp interface between two

liquids will affect film thickness.[9] Because of the large experimental error (±10 nm.) and a large number of convoluted effects, here we do not analyze in detail the relation between the salt and the film thickness. Yet, the observations are essential to interpret the results in the next section.
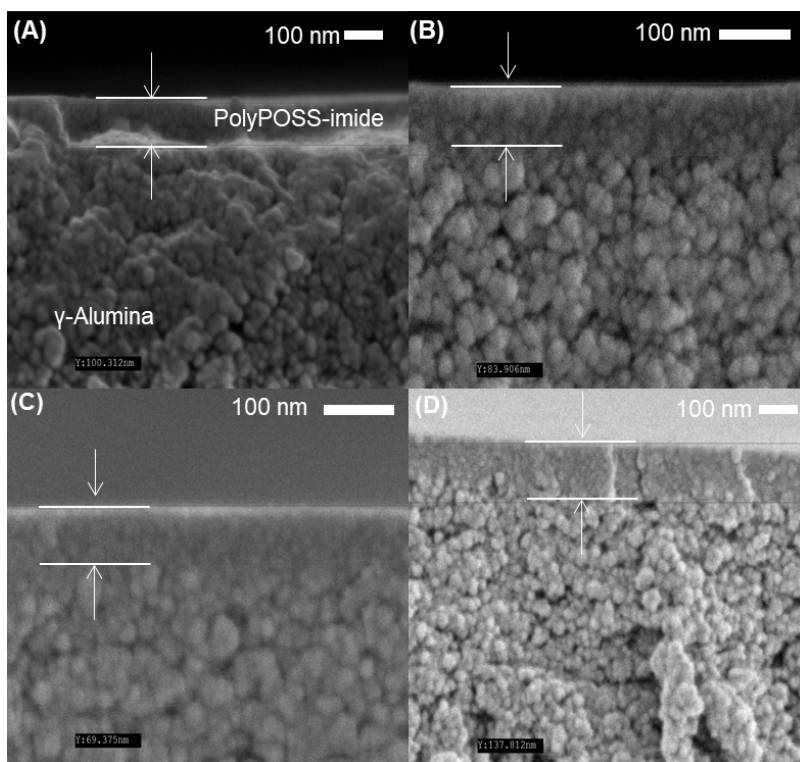


Figure 2.4 FE- SEM images of cross-section (a) Li-PI, (b) PI, (c) Na-PI, and (d) K-PI membranes.

Figure 2.5 shows the gas permeability behavior of the polyPOSS-imide membranes at 200, 100, and 50 °C. All membranes display molecular sieving behaviour; a decreasing permeability with increasing size of the permeant.[29] The persistence of this sieving behavior at elevated temperature is attributed to moderation of the dynamics of the crosslinked network, resulting from the incorporation of the rigid inorganic cages. This is in line with earlier experimental studies.[18] The order of gas permeance is Li-PI, Na-PI > PI > K-PI (Figure S2.3), which is in agreement with

thicknesses observed in the SEM micrographs. Because of the different membrane thicknesses found for the different M-PI, Figure S2.2 provides the thickness-corrected permeability values. The data in this figure reveals similar permeabilities for the different membranes, with slightly lower values for K-PI and PI as compared to Na-PI and Li-PI.
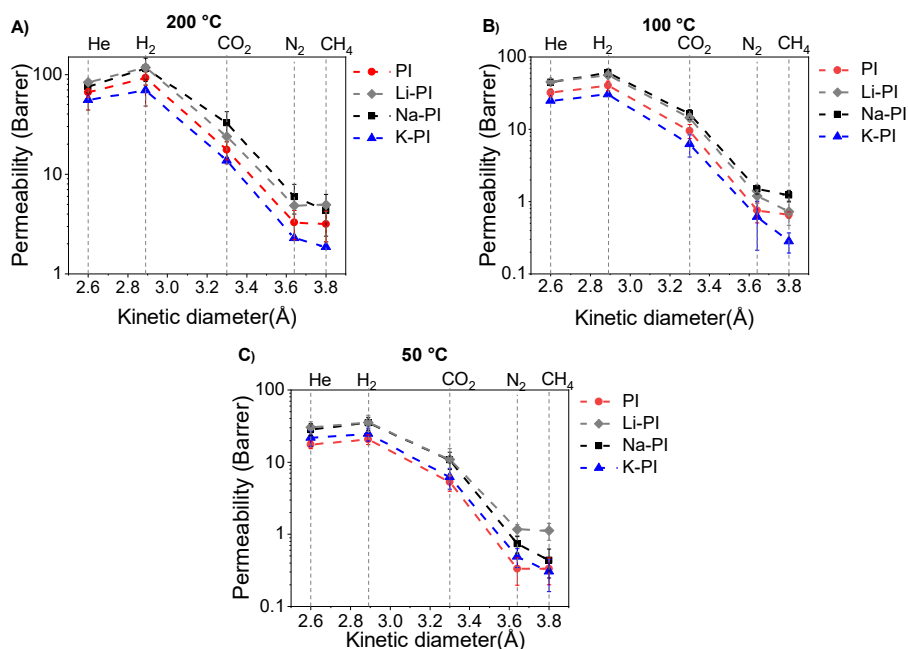


Figure 2.5 Gas permeability as a function of the gas kinetic diameter for polyimide membranes at (A) 200 °C, (B) 100 °C, and (C) 50 °C.

Table 2.5 Calculated activation energies for pure gas permeance based on Arrhenius equation.

| Gases | Activation energy (kJ mol$^{-1}$) | | |
|---|---|---|---|
| | PI | Li-PI | Na-PI |
| He | $11.2 \pm 0.2$ | $9.2 \pm 0.7$ | $8.7 \pm 0.8$ |
| H$_2$ | $12.4 \pm 0.4$ | $10.5 \pm 0.9$ | $10.4 \pm 0.7$ |
| CO$_2$ | $10 \pm 0.1$ | $8.7 \pm 1.1$ | $8.9 \pm 0.8$ |
| N$_2$ | $19.6 \pm 0.7$ | $16.9 \pm 1.5$ | $18 \pm 0.2$ |
| CH$_4$ | $21.5 \pm 0.2$ | $18.9 \pm 1.5$ | $19.8 \pm 0.5$ |

Molecular sieving typically involves a thermally activated diffusion mechanism. The corresponding activation energies obtained from fitting the

Arrhenius equation to the data are listed in Table 2.5. The values vary in the range of 8-25 kJ/mol, which is in good agreement with reported data for polyimide membranes.[30] For all membranes, the trend for activation energies is $CH_4 > N_2 > H_2 > He \geq CO_2$. Generally, gases with higher kinetic diameters have higher activation energies for diffusion. The lowest value for the energy of activation for $CO_2$, is due to the affinity of these gases with the $CF_3$ and amine groups. The relatively large sorption energy of this gas reduces the energy of activation.[31] For the other gases, the negative contribution of the enthalpy of sorption is lower.
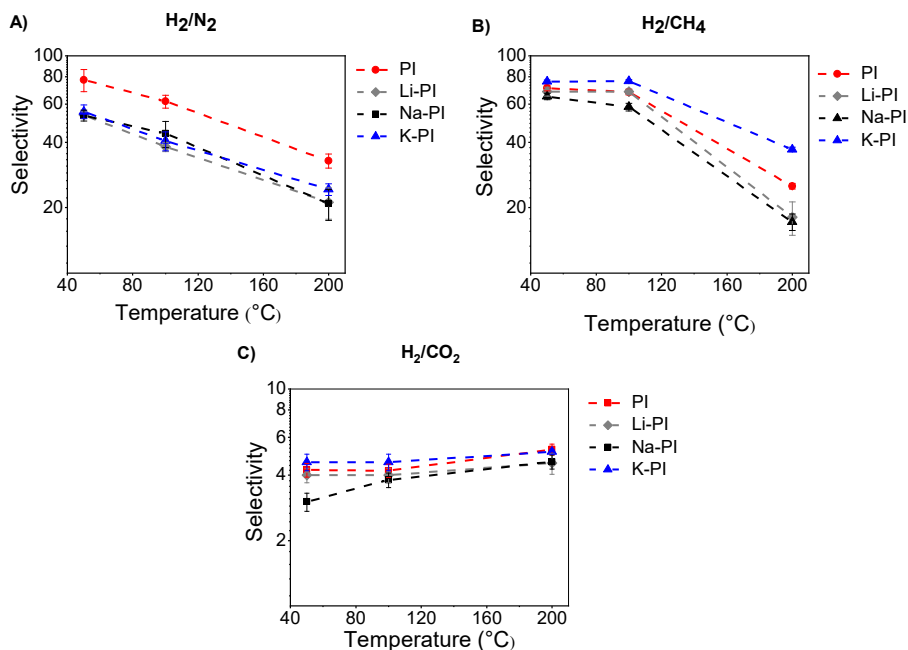


Figure 2.6 Permselectivity of (A) $H_2/N_2$, (B) $H_2/CH_4$, and (C) $H_2/CO_2$ as a function of temperature.

The PI membrane shows a slightly higher activation energy for $N_2$ and $CH_4$ than other membranes. This can be related to a lower number of organic bridges in the PI network, as was found in the EDX and TGA analysis. The only pathway for the diffusion of gases in the networks is via the organic bridges because the POSS cages are too small, even for $H_2$ molecules.[32, 33] The removal and chemical conversion of polyamic acid results in shrinkage and some cases, remove some additional free volume.[25] Fewer

organic bridges will thus lower diffusion, particularly for larger molecules. It should be mentioned that the lower concentration of $CF_3$ and corresponding higher concentration of amines may cancel out, to a certain degree, in the sorption energy of $CO_2$. As a result, all the membranes show a comparable value for $CO_2$ activation energy.[34]

Figure 2.6 depicts the (single gas) permselectivity of $H_2/N_2$, $H_2/CH_4$, and $H_2/CO_2$ as a function of temperature. The selectivity of all gas pairs decreases as a function of temperature except for $H_2/CO_2$. This is related to similar activation energies of the $H_2$ and $CO_2$.[30] The selectivity of $H_2/CO_2$ for all the membranes is comparable; it is not affected by changing the cation during interfacial polymerization.

For the other gases, the energy of activation is large compared to that of $H_2$. Sieving selectivity persists up to the highest measured temperature (200°C). This is attributed to the alternating network of organic bridges and rigid POSS cages. At 200 °C, the highest selectivity for $H_2/N_2$ is observed for the PI (32.9), as compared to Li-PI and Na-PI (both 21) and K-PI (24). For $H_2/CH_4$ at 200°C K-PI has the highest selectivity (37.1), followed by PI (25.1) and subsequently Li-PI (18.1) and Na-PI (17.2). Obtained selectivities are comparable to those of polyimide, Tröger's Base (TB)-based polyimide and poly(p-phenylenebenzobisimidazole).[29,35,36] The high selectivities for PI at high temperature result from the high activation energies, which in turn are attributed to the lower concentration of organic bridges and corresponding free volume available for diffusion.

In summary, all polyPOSS-imide membranes are thermally stable. They have comparable permeabilities with subtle differences in selectivities. Therefore, both SF-POSS and HP-POSS can be used for synthesizing polyPOSS-imide membranes on a large industrial scale. SF-POSS is an interesting monomer to use on an industrial scale to prepare polyPOSS-imide membranes since it provides a more straightforward procedure by omitting the pH adjusting step needed for HP-POSS. In view of this, we will assess the scale-up potential of polyPOSS-imide membranes by using SF-POSS as a monomer.

## 2.3.3 Tubular Membrane characterization and performance
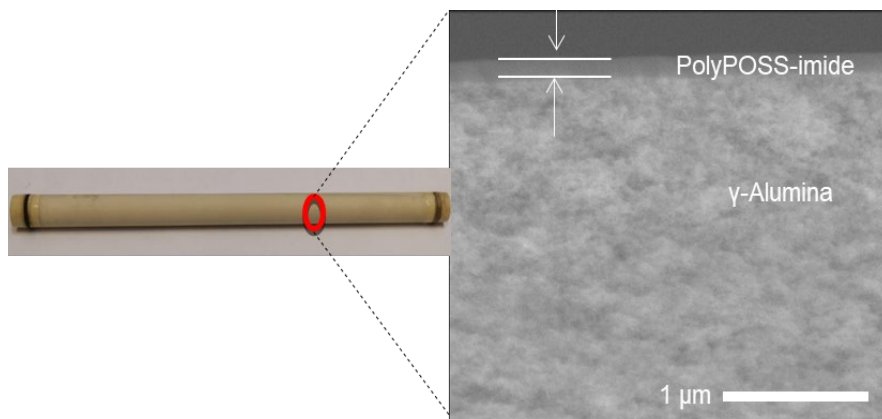


Figure 2.7 SEM images of the cross-section of a tubular polyPOSS imide-membrane, GEN-PI.

Figure 2.7 shows the cross-sectional SEM images of the inner side of the tubular membrane. The average thickness of polyPOSS-imide layer is 120 nm with thickness variation over the length of $\pm$ 30 nm, which is notable. This agrees well with the thickness obtained in the previous section for small flat disc membranes. The significant variation in the thickness of tubular membranes is related to the larger size of the support. Comparing GEN-PI and Na-PI from the literature [19] indicates that both membranes have a similar thickness in the range of 90-150 nm, unlike the flat disc membranes with a noticeable standard deviation. While producing a more homogeneous layer is more manageable for small flat disc supports (area of 11.9 cm$^2$), more effort is needed to better control the fabrication on tubular supports (area of 43 cm$^2$) or even multichannel supports.[19] It should be mentioned that more data is needed for a complete comparison between the layer's thickness atop flat and tubular supports.

Figure S2.4A shows single gas performance data of GEN-PI as a function of temperature at a transmembrane pressure of 10 bar. It can be observed that the performance of the tubular membrane agrees well with the performance of the flat disc membranes in the previous section. This is in line with earlier experimental studies.[19] The permeance decreases with increasing the kinetic diameter of the permeating gas. Also, at higher temperatures, the permeance increases, which shows the dominant diffusion mechanism of gas

transport in the membranes. Both flat disc and tubular membranes reveal remarkably similar results in terms of permeances. The activation energies are represented in Table 2.6 , and it follows the same trend as the flat disc membranes, $CH_4 > N_2 > H_2 \geq CO_2$. For all gases, the obtained activation energies are moderately higher compared to the flat disc membranes. It could be related to reduced mass transport resistance of the tubular membranes compared to their disc-shaped counterparts and higher operating pressure (10 bar).[19] Comparing the results with Na-PI tubular membranes in literature [19] reveals that the activation energies for GEN-PI are considerably higher, agreeing with flat disc membranes in section 2.3.2. As explained in the previous section, the structural changes in PI compared to Na-PI result in higher activation energies and underline the higher energy barrier for gas diffusion.

Table 2.6 Pure gas activation energies calculated based on Arrhenius equation.

| Gases | Activation energy (kJ mol$^{-1}$) |
|---|---|
| $H_2$ | 19.9±0.9 |
| $CO_2$ | 22.1±1.5 |
| $N_2$ | 30.4±1 |
| $CH_4$ | 32.9±0.9 |

Figure 2.8 shows the influence of temperature and pressure on the performance of the tubular GEN-PI membrane, and compares it with the literature data of Na-PI.[19] As mentioned before, this section aims to evaluate the performance of thin films for upscaling, and all the performance data is reported based on the membrane permeance. For all temperatures, the same $H_2$ permeance trend is observed for PI and Na-PI membranes; permeance enhancement as a function of temperature. Also, within the investigated pressure range, the transmembrane pressure has a limited effect on $H_2$ permeance. For all the measurement conditions, the $H_2$ permeance of GEN-PI membranes is lower than those of reported Na-PI membranes.[19] This is attributed to higher activation energies of GEN-PI than those reported for Na-PI tubular membranes.[19] Lower activation energies underline the lower energy barrier for gas diffusion. These results agree well with the obtained results for flat disc membranes in section 2.3.2. Unlike the results of flat membranes, which shows that lower permeance of PI membranes is related to the thicker selective layer, all GEN-PI and Na-PI membranes have

a thickness in the range of 90-150 nm, slightly higher for GEN-PI membranes, 110-120 nm compared to 90-150 nm. In summary, while GEN-PI has a higher selectivity, the permeance is lower than Na-PI, showing the distinct performance of both types of polyPOSS-imide membranes on a larger scale regardless of the thickness of the selective layer.
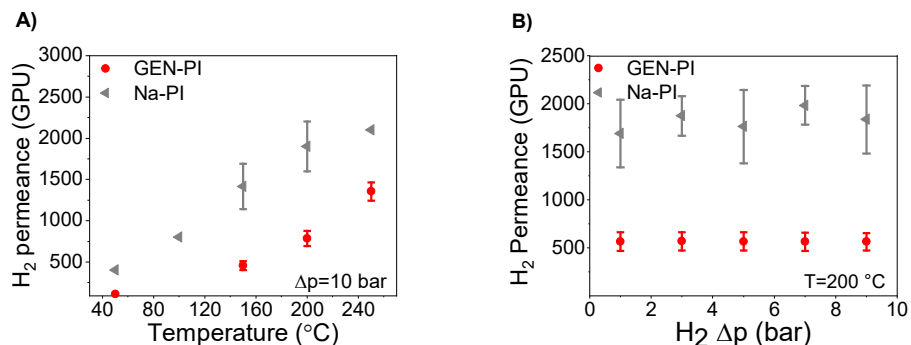


Figure 2.8 Influence of temperature and pressure on GEN-PI membranes' performance compared with literature data [19] obtained for Na-PI membranes. (A) $H_2$ permeance as a function of temperature at $\Delta p=10$ bar , (B) $H_2$ permeance as a function of $\Delta p$ at a temperature of 200 °C.

Figure 2.9 shows the mixed gas performance of GEN-PI at various temperatures (150, 200, and 250 °C) at a transmembrane pressure of 9 bar and its comparison with the literature data of Na-PI atop of tubular supports.[19] The selectivity of GEN-PI for all gas pairs decreases with increasing temperature in both pure and mixed gas, except for $H_2/CO_2$. This observation is in line with data obtained for flat disc membranes. Interestingly, in the case of pure gas selectivity of $H_2/CO_2$ and $H_2/CH_4$, a higher value is obtained for tubular membranes, 5.3 vs. 8 and 25.1 vs. 45.5, respectively, while the pure gas permeances are comparable for flat and tubular membranes (Figure S2.4A). It could be related to the reduced mass transport resistance of the tubular membrane compared to the disc resulting from morphological differences and the higher operating pressure. Similar effects were observed in.[19] Unexpectedly, all pure gas selectivities of Na-PI membranes from literature, except for one membrane, GEN 7, [19] have a different trend than those of GEN-PI and increase as a function of temperature. It implies that all membranes, except for GEN 7, have defects and their influence on the gas selectivity becomes lower at higher temperature due to the drop in gas viscosity (assuming viscous flow through

65

defects). These defects can be the result of salt formation, as shown by the XRD results, and its interference with the layer's formation during interfacial polymerization.

For all the gas pairs, the GEN-PI mixed gas selectivities are lower than pure gas selectivities. This is attributed to gas mixtures' effect on individual gas permeances, as shown in Figure S2.3B. With increasing temperature, the permeance increases, agreeing well with the pure gas performance. The $H_2$ permeance is partially affected in mixed gas measurements and is reduced by 10% at 250 °C. This is probably due to the existence of a concentration polarization effect on the feed side as previously observed for high-flux Pd-based membranes.[37] When the $H_2$ permeance is so high, and the membrane is $H_2$ selective, a reduction in $H_2$ concentration and increment in the concentration of other gases occurs in the boundary layer.[37, 38] While positive minor changes are observed in the permeance for $CO_2$ in mixed gas measurements, no remarkable changes are seen for $CH_4$. Moreover, an increase of 40% in the permeance of $N_2$ can be seen. A similar observation was also made for the Na-PI in the previous study.[19] The co-existence of $CO_2$ and $CH_4$ with other gases swells the polyPOSS imide layer and results in $N_2$ permeance enhancement.[24] All those changes in the gas permeance lead to the reduction in the mixture's gas pairs selectivity. It is noteworthy to mention that the long-term hydrothermal stability of polyPOSS-imide membranes was tested at 250 °C for 1000 hours elsewhere [39], and the obtained results suggest that membrane's performance was preserved at unchanged condition.

In conclusion, membranes synthesized with SFPOSS show a pure gas selectivity of $H_2/N_2$ (34), $H_2/N_2$ (42), and $H_2/CH_4$ (8) at 200 °C, which is higher than those produced with HPPOSS. More importantly, out of three produced PI samples, none of them have any defects. On the contrary, Na-PI tubular membranes from the previous study [19] illustrate solid proof of deficiency on the selective layer for 5 membranes out of 6. Therefore, SFPOSS may have a better potential compared to HPPOSS to be used as a reactant in synthesizing polyPOSS-imide membranes on a large scale.
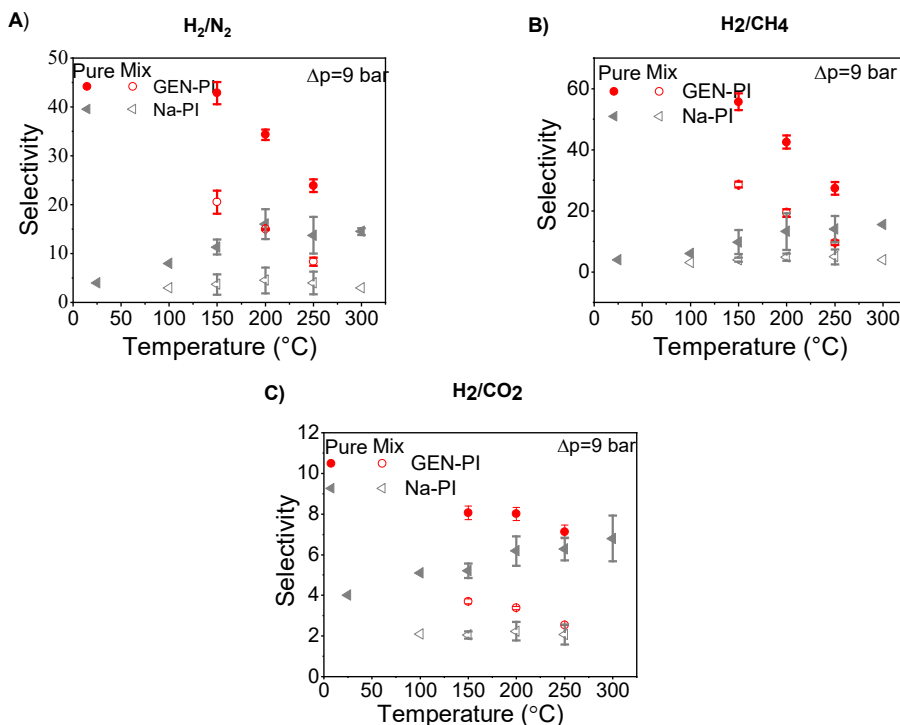
Figure 2.9 PolyPOSS-imide separation performance using pure and quaternary gas mixtures at various temperatures and transmembrane pressure of 10 bar compared with literature data [19] obtained for Na-PI networks. (A) $H_2/N_2$ selectivity, (B) $H_2/CH_4$ selectivity, and (C) $H_2/CO_2$ selectivity as a function of temperature at $\Delta p=9$ bar. The calculated stage cut for transmembrane pressure of 10 bar is 53%.

## 2.4 Conclusions

In this study, the effect of cations on the formation, imidization, and performance of polyPOSS-imide membranes atop lab-scaled flat disc and single-channel tubular supports for high temperature $H_2$ separation are investigated. Moreover, to upscale these membranes, a more straightforward fabrication procedure is assessed using SF-POSS cages rather than HP-POSS salt functionalized cages, which need deprotonation. For this purpose, three different lab-scale flat discs polyPOSS-imide membranes with HP-POSS and bases like LiOH, NaOH, and KOH, as a cation source, and one with SF-POSS, without cation, were prepared. Subsequently, to investigate the potential of SF-POSS, a tubular single-channel was fabricated. Finally, their performance was evaluated at different operating temperature and pressure.

It was found that all polyamic acid samples have the same cross-linking degree irrespective of the POSS source, and type of cations and, while each POSS cage is connected with 4 organic bridges. However, after imidization, an average number of imide groups per POSS cages reduces to 2 for PI networks, unlike M-PI, which retains the number of organic bridges. In the presence of cations, in the formed polyamic acid a carboxylic acid proton is replaced by an $M^+$ cation. This replacement prevents ring closure and reduces conversion yield during imidization. Different polyPOSS-imide layer thicknesses are obtained on top of flat disc supports, in the order Na-PI (69.4nm) ≤ Li-PI (83.9nm) < PI (100.3 nm) < K-PI(137.8 nm). This may be due to the distinct characteristics of the interface between the liquids in the presence of the salts, a diverse extent of the HP-POSS deprotonation originating from distinct strengths of the bases, and different electrostatic effects in the reaction zone. PI and K-PI membranes show higher ideal selectivity for $H_2/N_2$ and $H_2/CH_4$ with comparable $H_2/CO_2$ and have lower permeance and moderately lower permeability. These results advocate the scaling-up potential of polyPOSS-imide membranes using SF-POSS as a monomer (GEN-PI). The performance of GEN-PI membranes is in good agreement with the flat disc membranes. While the pure gas permeances are similar with the lab-scale membranes, a higher $H_2/CO_2$ and $H_2/CH_4$ are obtained, 5.3 versus 8, and 25.1 versus 45.5, respectively. This could be related to the lower mass transport resistance of tubular supports than the disc-shaped supports. Besides, GEN-PI performance is compared with previously studied Na-PI tubular membranes; in all measured conditions, GEN-PI membranes exhibit higher selectivity and lower hydrogen permeance. More importantly, the average trend for GEN-PI $H_2/N_2$ and $H_2/CH_4$ is decreasing as a function of temperature. On the contrary, those selectivities increase with temperature for Na-PI membranes. This implies that the possibility of making defect free selective layers with SF-POSS as an initial monomer is much higher due to the absence of salt formation during interfacial polymerization. The findings signify that using SF-POSS in preparing large-scale defect free membranes can be beneficial. Also, the use of SF-POSS offers a more facile and straightforward procedure by omitting the deprotonation by the addition of a base.

## 2.5 Acknowledgment

## 2.6 References

[1] A. Brunetti, F. Scura, G. Barbieri, E. Drioli, Membrane technologies for $CO_2$ separation, J. Memb. Sci., 359 (2010) 115-125, https://doi.org/10.1016/j.memsci.2009.11.040.

[2] H. Lin, B.D. Freeman, Materials selection guidelines for membranes that remove CO2 from gas mixtures, J. Mol. Struct., 739 (2005) 57-74, https://doi.org/10.1016/j.molstruc.2004.07.045.

[3] B.B. Shrestha, K. Wakimoto, Z.G. Wang, A.P. Isfahani, T. Suma, E. Sivaniah, B. Ghalei, A facile synthesis of contorted spirobisindane-diamine and its microporous polyimides for gas separation, Rsc Adv., 8 (2018) 6326-6330, https://doi.org/10.1039/C7RA12719G.

[4] L. Hu, S. Pal, H. Nguyen, V. Bui, H. Lin, Molecularly engineering polymeric membranes for $H_2/CO_2$ separation at 100–300° C, J. Polym. Sci., 58 (2020) 2467-2481, https://doi.org/10.1002/pol.20200220.

[5] S.S. Wu, J.C. Liang, Y.P. Shi, M.H. Huang, X.Y. Bi, Z.G. Wang, J. Jin, Design of interchain hydrogen bond in polyimide membrane for improved gas selectivity and membrane stability, J. Memb. Sci., 618 (2021) 118659, https://doi.org/10.1016/j.memsci.2020.118659.

[6] R.M. Laine, M.F. Roll, Polyhedral phenylsilsesquioxanes, Macromolecules, 44 (2011) 1073-1109, https://doi.org/10.1021/ma102360t.

[7] M.J. Raaijmakers, M.A. Hempenius, P.M. Schön, G.J. Vancso, A. Nijmeijer, M. Wessling, N.E. Benes, Sieving of hot gases by hyper-cross-linked nanoscale-hybrid membranes, J. Am. Chem. Soc., 136 (2013) 330-335, https://doi.org/10.1021/ja410047u.

[8] Y. Yang, C.L. Muhich, M.D. Green, Kinetics and mechanisms of polycondensation reactions between aryl halides and bisphenol A, Polym. Chem., 11 (2020) 5078-5087, https://doi.org/10.1039/D0PY00740D.

[9] Y. Mansourpanah, S.S. Madaeni, A. Rahimpour, Fabrication and development of interfacial polymerized thin-film composite nanofiltration membrane using different surfactants in organic phase; study of morphology and performance, J. Memb. Sci., 343 (2009) 219-228, https://doi.org/10.1016/j.memsci.2009.07.033.

[10] X.C. Fan, Y.L. Su, X.T. Zhao, Y.F. Li, R.N. Zhang, J.J. Zhao, Z.Y. Jiang, J.N. Zhu, Y.Y. Ma, Y. Liu, Fabrication of polyvinyl chloride ultrafiltration membranes with stable antifouling property by exploring the pore formation and surface modification capabilities of polyvinyl formal, J. Memb. Sci., 464 (2014) 100-109, https://doi.org/10.1016/j.memsci.2014.04.005.

[11] J. Lee, R. Wang, T.H. Bae, A comprehensive understanding of co-solvent effects on interfacial polymerization: Interaction with trimesoyl chloride, J. Memb. Sci., 583 (2019) 70-80, https://doi.org/10.1016/j.memsci.2019.04.038.

[12] H.G. Linde, R.T. Gleason, Cation Interactions with Polyamic Acids, J. Polym. Sci. B Polym. Phys., 27 (1989) 1485-1497, https://doi.org/10.1002/polb.1989.090270710.

[13] S. Ikeda, K. Akamatsu, H. Nawafune, T. Nishino, S. Deki, Formation and growth of copper nanoparticles from ion-doped precursor polyimide layers, J. Phys. Chem. B, 108 (2004) 15599-15607, https://doi.org/10.1021/jp0478559.

[14] L.F. Villalobos, R. Hilke, F.H. Akhtar, K.V. Peinemann, Fabrication of Polybenzimidazole/Palladium Nanoparticles Hollow Fiber Membranes for Hydrogen Purification, Adv. Energy Mater., 8 (2018) 1701567, https://doi.org/10.1002/aenm.201701567.

[15] S. Serchenkova, M. Shablygin, T. Kravchenko, Z. Oprits, G. Kudryavtsev, Study of the cyclodehydration reaction of benzamido acid systems, Polym. Sci. USSR, 20 (1978) 1284-1294, https://doi.org/10.1016/0032-3950(78)90269-1.

[16] M. Dalwani, J. Zheng, M. Hempenius, M.J. Raaijmakers, C.M. Doherty, A.J. Hill, M. Wessling, N.E. Benes, Ultra-thin hybrid polyhedral silsesquioxane–polyamide films with potentially unlimited 2D dimensions, J. Mater. Chem., 22 (2012) 14835-14838, https://doi.org/10.1039/C2JM31941A.

[17] P. Karakiliç, C. Huiskes, M.W. Luiten-Olieman, A. Nijmeijer, L. Winnubst, Sol-gel processed magnesium-doped silica membranes with improved H2/CO2 separation, J. Memb. Sci., 543 (2017) 195-201, https://doi.org/10.1016/j.memsci.2017.08.055.

[18] M.J.T. Raaijmakers, M. Wessling, A. Nijmeijer, N.E. Benes, Hybrid Polyhedral Oligomeric Silsesquioxanes-Imides with Tailored Intercage Spacing for Sieving of Hot Gases, Chem. Mater., 26 (2014) 3660-3664, https://doi.org/10.1021/cm500691e.

[19] L. Ansaloni, E. Louradour, F. Radmanesh, H. van Veen, M. Pilz, C. Simon, N.E. Benes, T.A. Peters, Upscaling polyPOSS-imide membranes for high temperature H2 upgrading, J. Memb. Sci., 620 (2021) 118875, https://doi.org/10.1016/j.memsci.2020.118875

[20] H. Fukuzumi, S. Fujisawa, T. Saito, A. Isogai, Selective Permeation of Hydrogen Gas Using Cellulose Nanofibril Film, Biomacromolecules, 14 (2013) 1705-1709, https://doi.org/10.1021/bm400377e.

[21] M. Shimizu, T. Saito, A. Isogai, Water-resistant and high oxygen-barrier nanocellulose films with interfibrillar cross-linkages formed through multivalent metal ions, J. Memb. Sci., 500 (2016) 1-7, https://doi.org/10.1016/j.memsci.2015.11.002.

[22] J.I. Goldstein, D.E. Newbury, J.R. Michael, N.W. Ritchie, J.H.J. Scott, D.C. Joy, Scanning electron microscopy and X-ray microanalysis, Springer, 2017.

[23] A. Sthoer, J. Hladílková, M. Lund, E. Tyrode, Molecular insight into carboxylic acid–alkali metal cations interactions: Reversed affinities and ion-pair formation revealed by non-linear optics and simulations, Phys. Chem. Chem. Phys., 21 (2019) 11329-11344, https://doi.org/10.1016/10.1039/C9CP00398C.

[24] M.J.T. Raaijmakers, W. Ogieglo, M. Wiese, M. Wessling, A. Nijmeijer, N.E. Benes, Sorption Behavior of Compressed $CO_2$ and $CH_4$ on Ultrathin Hybrid Poly(POSS-imide) Layers, ACS Appl. Mater. Interfaces, 7 (2015) 26977-26988, https://doi.org/10.1021/acsami.5b08286.

[25] M.J.T. Raaijmakers, E.J. Kappert, A. Nijmeijer, N.E. Benes, Thermal Imidization Kinetics of Ultrathin Films of Hybrid Poly(POSS-imide)s, Macromolecules, 48 (2015) 3031-3039, https://doi.org/10.1021/acs.macromol.5b00473.

[26] B. Thomson, Y. Park, P.C. Painter, R.W. Snyder, Hydrogen-Bonding in Poly(Amic Acid)s, Macromolecules, 22 (1989) 4159-4166, https://doi.org/10.1021/ma00201a005.

[27] Q. Li, Z.P. Liao, X.F. Fang, J. Xie, L.H. Ni, D.P. Wang, J.W. Qi, X.Y. Sun, L.J. Wang, J.S. Li, Tannic acid assisted interfacial polymerization based loose thin-film composite NF membrane for dye/salt separation, Desalination, 479 (2020) 114343, https://doi.org/10.1016/j.desal.2020.114343.

[28] W.M. Nielen, J.D. Willott, Z.M. Esguerra, W.M. de Vos, Ion specific effects on aqueous phase separation of responsive copolymers for sustainable membranes, J. Colloid Interface Sci., 576 (2020) 186-194, https://doi.org/10.1016/j.jcis.2020.04.125.

[29] M. Omidvar, C.M. Stafford, H. Lin, Thermally stable cross-linked P84 with superior membrane H2/CO2 separation properties at 100° C, J. Memb. Sci., 575 (2019) 118-125, https://doi.org/10.1016/j.memsci.2019.01.003.

[30] K.A. Stevens, J.D. Moon, H. Borjigin, R. Liu, R.M. Joseph, J.S. Riffle, B.D. Freeman, Influence of temperature on gas transport properties of tetraaminodiphenylsulfone (TADPS) based polybenzimidazoles, J. Memb. Sci., 593 (2020) 117427, https://doi.org/10.1016/j.memsci.2019.117427.

[31] X. Li, R.P. Singh, K.W. Dudeck, K.A. Berchtold, B.C. Benicewicz, Influence of polybenzimidazole main chain structure on H2/CO2 separation at elevated temperatures, J. Memb. Sci., 461 (2014) 59-68.

[32] D. Brown, S. Neyertz, M.J.T. Raaijmakers, N.E. Benes, Sorption and permeation of gases in hyper-cross-linked hybrid poly(POSS-imide) networks: An in silico study, J. Memb. Sci., 577 (2019) 113-128, https://doi.org/10.1016/j.memsci.2014.03.008.

[33] M. Kanezashi, Y. Tomarino, H. Nagasawa, T. Tsuru, Tailoring the molecular sieving properties and thermal stability of carbonized membranes containing polyhedral oligomeric silsesquioxane (POSS)-polyimide via the introduction of norbornene, J. Memb. Sci., 582 (2019) 59-69, https://doi.org/10.1016/j.memsci.2019.04.003.

[34] L. Yu, M. Kanezashi, H. Nagasawa, T. Tsuru, Role of Amine Type in CO2 Separation Performance within Amine Functionalized Silica/Organosilica Membranes: A Review, App. Sci., 8 (2018) 1032, https://doi.org/10.3390/app8071032.

[35] Y. Zhang, W.H. Lee, J.G. Seong, J.Y. Bae, Y. Zhuang, S. Feng, Y. Wan, Y.M. Lee, Alicyclic segments upgrade hydrogen separation performance of intrinsically microporous polyimide membranes, J. Memb. Sci., 611 (2020), 118363, https://doi.org/10.1016/j.memsci.2020.118363.

[36] M. Shan, X. Liu, X. Wang, Z. Liu, H. Iziyi, S. Ganapathy, J. Gascon, F. Kapteijn, Novel high performance poly( p -phenylene benzobisimidazole) (PBDI)

membranes fabricated by interfacial polymerization for H2 separation, J. Mater. Chem. A. 7 (2019) 8929–8937. https://doi.org/10.1039/C9TA01524H.

[37] T.A. Peters, M. Stange, H. Klette, R. Bredesen, High pressure performance of thin Pd–23%Ag/stainless steel composite membranes in water gas shift gas mixtures; influence of dilution, mass transfer and surface effects on the hydrogen flux, J. Memb. Sci. 316 (2008) 119–127. https://doi.org/10.1016/j.memsci.2007.08.056.

[38] Y.W. Budhi, W. Suganda, H.K. Irawan, E. Restiawaty, M. Miyamoto, S. Uemiya, N. Nishiyama, M. van Sint Annaland, Hydrogen separation from mixed gas (H2, N2) using Pd/Al2O3 membrane under forced unsteady state operations, Int. J. Hydrog. Energy, 45 (2020) 9821-9835, https://doi.org/10.1016/j.ijhydene.2020.01.235.

[39] L. Ansaloni, M. Sarić, E. Louradour, F. Radmanesh, J.W. Dijkstra, M. Pilz, D. Høvik, N. Benes, Y. van Delft, T.A. Peters, Stability investigation of polyPOSS-imide membranes for H2 purification and their application in the steel industry, Available at SSRN 3811364 (2021)

74

# 2.7 Supplementary information

In Figure S2.1, a schematic illustration of cation exchanging in polyamic acid networks and its effect on imidization are shown.
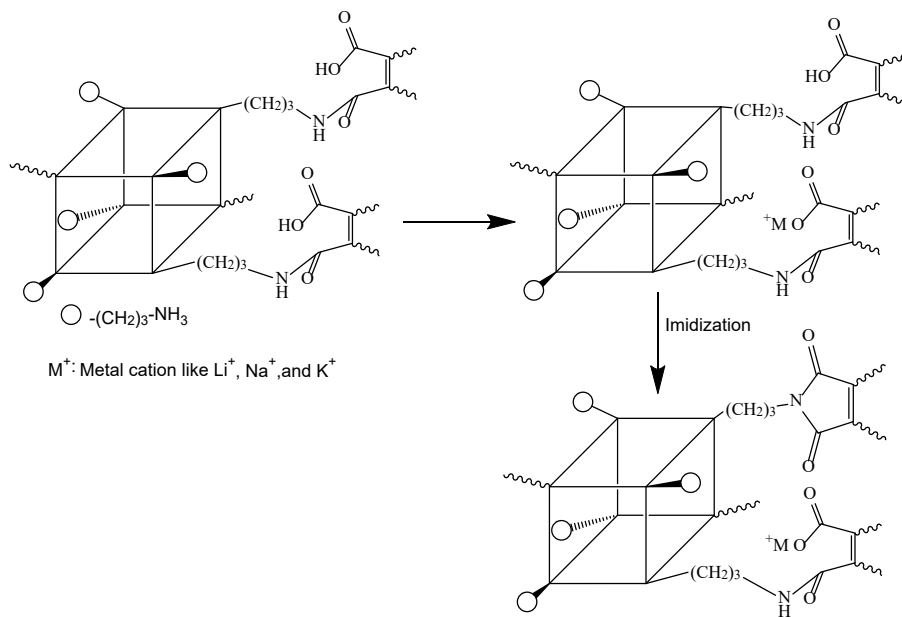


Figure S2.1 Schematic illustration of cation exchanging in polymaic acid networks and its effect on imidization.

In Figures S2.2, the XRD measurements are shown. For the permeance and selectivity, only the data at 250, 200, and 100 ºC is given. All the XRD patterns suggest a general amorphous structure of the polymers. The peaks around $2\theta= 7.37$ and 9.8 degrees correspond to the XRD pattern of POSS. The sharp peaks around $2\theta=28.4$ degrees are attributed to the KCl and (26.6 and 31.2) degrees related to NaCl crystal, implying salt formation in the free-standing layer.
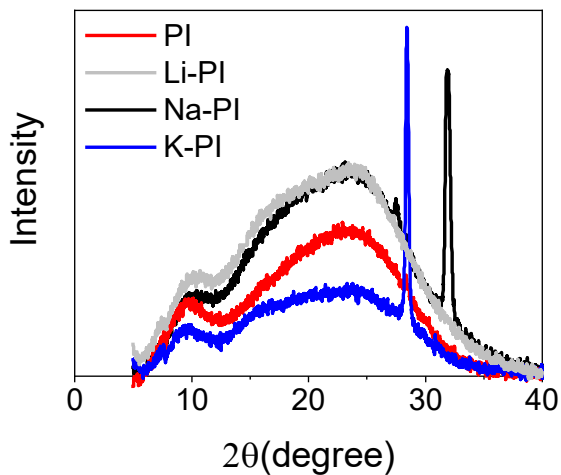


Figure S2.2 XRD patterns of polyimide.

In Figure S2.3, the flat disc membranes' gas permeance as a function of gas kinetic diameter at 200, 100, and 50 °C is shown.
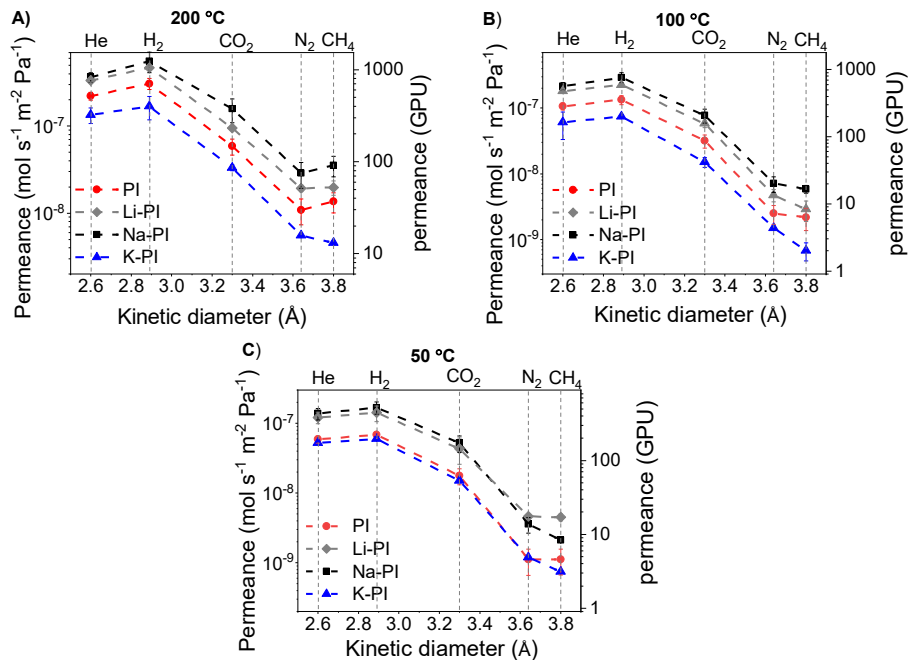


Figure S2.3 Single gas permeance of flat membranes as a function of gas kinetic diameter at (A) 200 °C, (B) 100 °C, and (C) 50 °C.

In Figure S2.4A and S2.4B, the single and mixed gas permeance of the GEN PI membranes at the transmembrane pressure of 10 bar is shown, respectively.

**A)**



**B)**
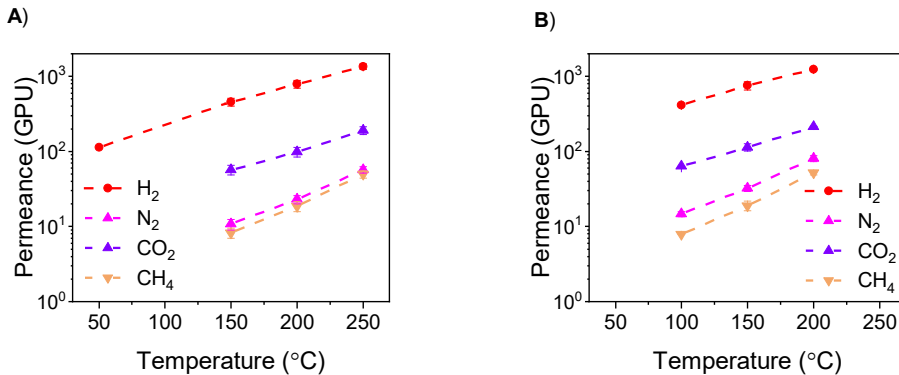
Figure S2.4 (A) Single and (B) Mixed gas permeance of GEN PI as a function of temperature for 4 different gases at the transmembrane pressure of 10 bars.

# Chapter 3

# Polyoctahedral silsesquioxane hexachlorocyclotriphosphazene membranes for hot gas separation
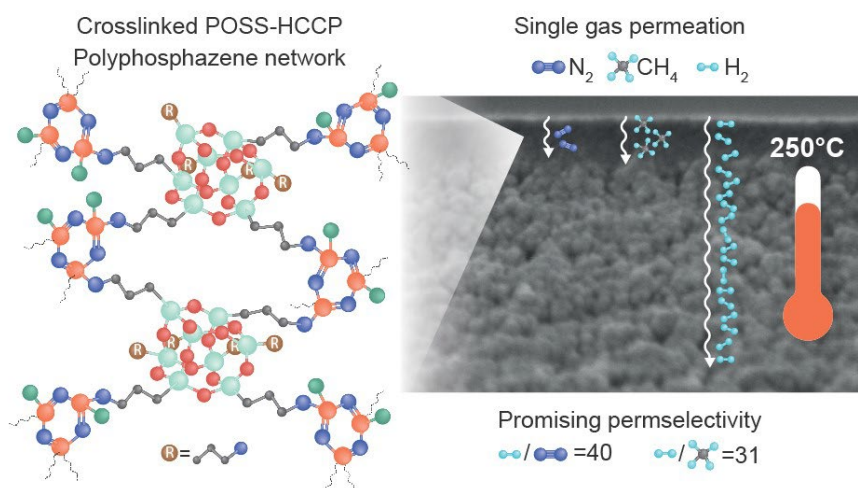
# Abstract

There is a need for gas separation membranes that can perform at high temperatures, e.g., for $CO_2$ capture in industrial processes. Polyphosphazenes classify as interesting materials for use under these conditions, because of their high thermal stability, hybrid nature, and post-functionalization options. In this work, thin-film composite cyclomatrix polyphosphazene membranes are prepared via the interfacial polymerization reaction between polyhedral oligomeric silsesquioxane and hexachlorocyclotriphosphazene on top of a ceramic support. The prepared polyphosphazene networks are highly crosslinked and show excellent thermal stability until 340 °C. Single gas permeation experiments at temperatures ranging from 50–250 °C reveal a molecular sieving behavior, with permselectivities as high as 130 for $H_2/CH_4$ at the low temperatures. The permselectivities of the membranes persist at the higher temperatures; at 250 °C $H_2/N_2$ (40), $H_2/CH_4$ (31) $H_2/CO_2$ (7), and $CO_2/CH_4$ (4), respectively, while maintaining permeances in the order of $10^{-7}$–$10^{-8}$ mol m$^{-2}$ s$^{-1}$ Pa$^{-1}$. Compared to other types of polymer-based membranes, especially the $H_2/N_2$ and $H_2/CH_4$ selectivities are high, with similar permeances. Consequently, the hybrid polyphosphazene membranes have great potential for use in high-temperature gas separation applications.

## 3.1 Introduction

Membrane technology can be used for a great variety of separation processes. The gas separation market uses membranes for many molecular separations, such as for the adjustment of the $H_2/CO$-$CO_2$ ratio in syngas production, the enrichment of $N_2$, acid gas removal from natural gas, and olefin/paraffin separations [1–7]. However, at high temperatures, the separation of small gases is more difficult because of limited thermal stability and increment of molecular dynamics of polymeric membranes.[3] By improving the stability and performance of polymeric membranes at these high-temperature conditions, they can offer a promising alternative to traditional technologies, such as for $CO_2$ capture and recovery in industrial processes [8]. Therefore, over the years, research has focused on developing membranes that can perform the required separations at high temperatures, but the available number of studies are still limited.[3,9–11] For this, a range of materials has been identified that might be of use for this purpose.[12]

One of the classes of materials of interest for high-temperature applications are polyphosphazenes.[12,13] These materials are attractive because of their robustness, hybrid nature, and post-functionalization options. The basis for most polyphosphazenes is hexachlorocyclotriphosphazene (HCCP). It can be used as a building block, e.g., for the formation of supramolecular self-assemblies or crosslinked structures. When HCCP reacts with di- or trifunctional compounds, it forms a cyclomatrix poly(phosphazene) network.[14] These crosslinked structures are of high interest for their flame retardant properties and good thermal stability.[15,16]

Over the years, polyphosphazenes have gained interest for the preparation of different types of membranes. For instance, a variety of polyphosphazenes has been used as proton exchange membranes, but they also have found their application as a nanofiltration membrane.[17–19] Gas separation properties of polyphosphazene membranes have also been studied.[20] However, in most cases, the linear poly(dichlorophosphazene) has been used as a building block, and the performance has only been studied at temperatures lower than 100 °C.[21] The gas separation performance of polyphosphazene membranes at higher temperatures has not been studied.

In this work, we use HCCP to prepare a membrane that can perform at elevated temperatures. This requires a highly crosslinked network with moderate macromolecular dynamics. For this purpose, a polyhedral oligomeric silsesquioxane (POSS), specifically octa aminopropyl POSS, is chosen as an eight functionalized amine monomer. This is a unique material with an inorganic cage base structure and organic functional groups that can serve as linkers. These cages can offer additional thermal and mechanical stability to the network.[12,15] Previous studies by Raaijmakers et al. [11,22] show that using POSS cages as the main building block in a polyimide network is beneficial to get high polymer chain rigidity for effective molecular sieving.[11]

To the best of our knowledge, it is the first time that the unique features of both POSS and HCCP are combined into a cyclomatrix poly(phosphazene) thin-film composite (TFC) membrane and used for gas separation at elevated temperatures. The polyphosphazene gas separation membranes are prepared through interfacial polymerization (IP) between POSS and HCCP, directly atop of a ceramic support. The formed thin crosslinked layer on top of the support permits high permeance of small molecules, such as hydrogen, combined with a low permeance of slightly larger molecules, such as methane.[19,23] The polyphosphazene network is characterized for its stability, and the performance of the POSS-HCCP membranes is evaluated based on single gas permeance and permselectivity at a wide range of temperatures.

## 3.2 Experimental

### 3.2.1. Materials

HAPS (POSS) in *n*-propanol (solids content 52.3 wt.%) was kindly provided by Funzionano AS. Phosphonitrilic chloride trimer (HCCP, 99%) and dimethyl sulfoxide (DMSO, anhydrous, ≥99.9%) were obtained from Sigma Aldrich. Cyclohexane (EMSURE for analysis) and potassium hydroxide (KOH, pellets extra pure) were obtained from Merck kGaA. Ethanol (EtOH, 100% technical grade) was purchased from Boom. Porous α-alumina discs

(Ø 39 mm, thickness 2 mm) were obtained from Pervatech B.V. and used as support.

## 3.2.2. Material fabrication

For both the preparation of POSS-HCCP freestanding films and the preparation of the TFC membranes, thin films were prepared by the interfacial polymerization reaction between 10 w/v% POSS in DMSO (5:1 DMSO:0.3 M KOH) and 3.5 w/v% HCCP in cyclohexane.

## Synthesis of POSS-HCCP freestanding films

POSS-HCCP freestanding films were prepared as follows. A solution of the organic HCCP solution was poured atop of the aqueous POSS solution. After 10 minutes of reaction time, a thin film was obtained that could be removed from the interface (Figure S3.1). The resulting solid was filtered, washed with water and ethanol, and dried in a vacuum oven at 50 °C. The solid might also be referred to as powder.

## Preparation of POSS-HCCP thin-film composite membranes

The porous α-alumina supports were coated with a 3 µM thick γ-alumina layer via a dip-coating and calcination process as described before by Karaliç et al. [24]. This γ-alumina layer serves as an intermediate layer upon which the dense separating layer can be formed.

The TFC membranes were made by interfacial polymerization directly on top of the porous alumina support using an IP cell, as shown in Figure S3.2 (Supporting information). First, both the POSS solution and support membrane were heated to 70 °C for 30 min. After this, 10 mL POSS solution was poured on top of the support. The cell was placed in a closed box in the oven at 80 °C for 15 minutes to ensure POSS-DMSO entering the pores. After 15 minutes, it was taken out of the oven, and the POSS solution was discarded. Subsequently, the membrane surface was dried by firmly applying a rubber roller for 3 times and removing the remaining droplets with a $N_2$ gun. The drying steps are critical to avoid delamination. Then, 10 mL HCCP solution was gently poured on top. After allowing the reaction to complete for 10 minutes, the solution was discarded, and the membrane surface was

rinsed with ethanol. Before analysis, it was dried to air overnight, and after that, it was further dried in a vacuum oven at 50 °C for minimum 12 hours.

### 3.2.3. Material characterization

The thickness and morphology of the membranes were visualized with a field emission scanning electron microscope (FE-SEM, JSM-7610F). Both surface and cross-section of the membranes were evaluated. For the sample preparation, membranes were dried overnight in a vacuum oven at  50 °C, fractured in liquid nitrogen, and coated with a 5 nm Pt/Pd conductive layer. The chemistry of the powders was examined by Fourier transform infrared spectroscopy in ATR mode (ATR-FTIR, PerkinElmer Spectrum Two). Spectra were collected from 16 scans with a resolution of 4 $cm^{-1}$ over a wavelength range from 400-4000 $cm^{-1}$. X-Ray Fluorescence (XRF) measurements (S8 Tiger, Bruker) were performed on the synthesized powder to examine the elemental composition of the formed network. Combined Thermogravimetric Analysis (TGA, STA 449 F3 Jupiler®, Netzsch) and mass spectrometry (MS, QMS 403 D Aeolos MS, Netzsch) measurements were used to assess the stability of the powder upon heating (10 °C $min^{-1}$, $N_2$ atmosphere)

### 3.2.4. Membrane performance

Single gas permeance experiments were carried out in dead-end mode at a trans-membrane pressure of 2 bar, using a Convergence Inspector Poseidon gas permeation setup. The gases measured are: He, $N_2$, $CH_4$, $H_2$, and $CO_2$. The permselectivity was calculated as the ratio of the respective permeances. Measurements were carried out at temperatures between 50 and 250 °C. Error bars represent the standard deviation between two different membrane samples.
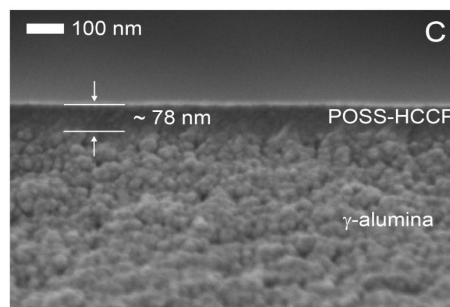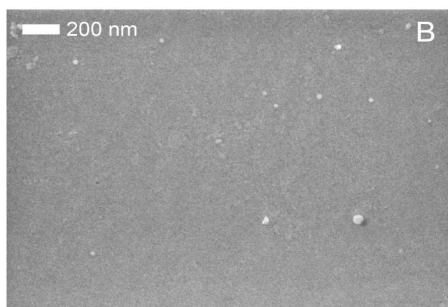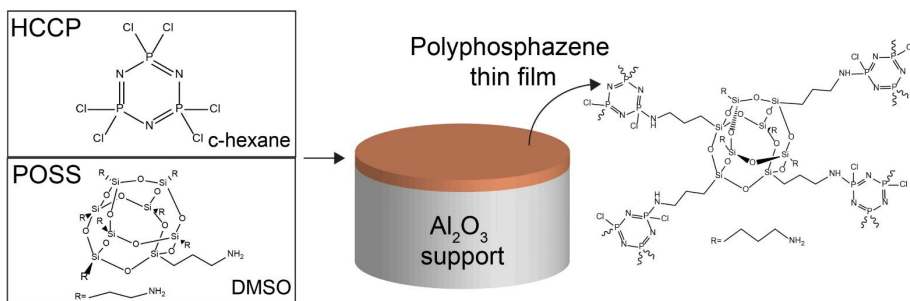
Figure 3.1 (A) Schematic representation of POSS-HCCP thin film composite membrane preparation. (B) FE-SEM picture of the POSS-HCCP membrane surface and (C) Cross-section FE-SEM image.

## 3.3 Results & Discussion

This article is divided into three parts. In the first part, the formation of thin-film composite POSS-HCCP membranes is discussed. In the second part, the polyphosphazene networks are characterized in terms of their chemistry and thermal stability. Finally, in the third part, the gas separation performance of the POSS-HCCP membranes is evaluated.

### 3.3.1. POSS-HCCP membrane preparation

Figure 3.1A gives a schematic representation of the preparation of POSS-HCCP thin-film composite membranes by the interfacial polymerization of POSS and HCCP on top of a ceramic support. The successful formation of thin POSS-HCCP polyphosphazene films is confirmed by the SEM micrograph of the surface of the membrane in Figures 3.1B and 3.1C, where both surface and cross-section images of the thin film composite membrane

are shown. The surface of the membrane appears smooth, confirming that a continuous and dense layer is formed on top of the γ-alumina layer. The cross-section image 3.1C reveals that the thickness of the layer is ~80 nm. This is a typical thickness for IP membranes. It must be noted that the spread in thickness along the sample, ± 40 nm, is rather big.

## 3.3.2. POSS-HCCP characterization

The chemistry of the formed networks is characterized by FTIR. In Figure 3.2, FTIR spectra are shown of the used monomers, POSS and HCCP, as well of the freestanding film obtained from IP. The freestanding film shows the characteristic peaks of both HCCP and POSS. The POSS cage is apparent by the peaks in the 1000-1150 cm$^{-1}$ region,[25] specifically the peak at 1100 cm$^{-1}$ that can be assigned to the Si-O-Si functional group. The broad peak around 1230 covers the peaks for asymmetric P-N-P stretching of HCCP at 1238 and 1203 cm$^{-1}$. Furthermore, at 875 cm$^{-1}$, the peak corresponding to symmetric stretching of P-N-P is observed.[26] Finally, the peak at 690 cm$^{-1}$ can be assigned to Si-C stretching of the POSS. From the presence of POSS and HCCP, combined with the mechanical integrity of the freestanding film, we conclude that a polyphosphazene network has been formed.
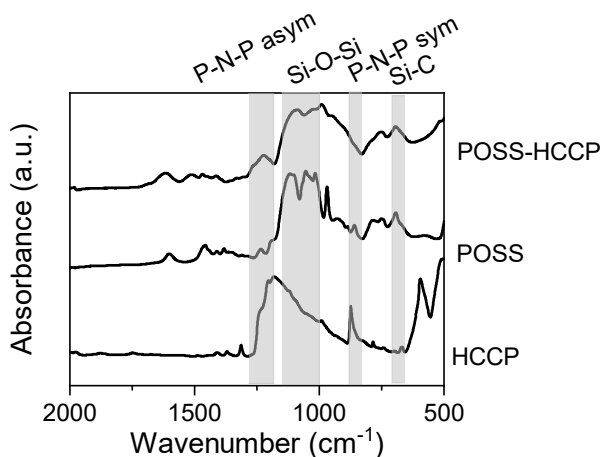


Figure 3.2 FTIR spectra of monomers POSS and HCCP and the formed polyphosphazene network.

The mechanical integrity of the polyphosphazene films requires a sufficient amount of condensation reactions between POSS and HCCP, leading to a crosslinked network. The extent of cross-linking is estimated from the XRF data in Table 3.1, showing the elemental composition of polyphosphazene powders. The data reveal the presence of Si, P, Cl, and traces of S in the powder. The traces of S are most likely due to the incomplete removal of DMSO from the sample. Unfortunately, C and N cannot be detected with this method.

The ratio of P over Cl is 1.5. This indicates that 4 out of the total 6 Cl groups per HCCP molecule are involved in the reaction with the POSS cages. This implies that most of the P atoms are covalently attached to the network. On the other hand, the ratio of Si/Cl is 2, which implies 2 reacted HCCP molecules per POSS molecule. A similar amount of HCCP molecules per POSS cage can be deduced from the the ratio of Si and P, which is roughly 4/3. From this, it can be concluded that a crosslinked polyphosphazene network has formed in which, on average, a POSS cage is connected with 4 bridges.

Table 3.1  XRF data for polyphosphazene powder

| Element | Elemental concentration (%) | Statistical error (%) |
|---|---|---|
| Si | 43.2 | 1.3 |
| P | 33.3 | 1.6 |
| Cl | 21.5 | 2.2 |
| S | 2.0 | 5.9 |

The thermal stability of the formed network is represented by the TGA-MS data of the POSS-HCCP in Figure 3.3. A limited amount of mass loss is observed below 340 °C. This is mainly attributed to the removal of physical bound water, also apparent from the $H_2O$ peak, but can partly be due to loss of trapped DMSO and unreacted monomers or further cross-linking. Beyond 340 °C a sharp and substantial ($\pm$ 40 %) decrease in mass is observed that indicates the onset of the thermal decomposition of the network. From the MS data it is apparent that fragments of the propyl chain are coming off ($C_3H_5$, $C_2H_6$ and $C_2NH$ etc.). This implies that the propyl chain is the weakest part of the network and limits the thermal stability. Besides fragments of the propyl chain, also HCl and Cl are coming off, that are

expected to come from unreacted Cl groups on the HCCP. The remaining mass is completely governed by the cyclophosphazene and the inorganic POSS cages. The mass loss of 40 % is in good agreement with the ratio of POSS and HCCP derived from the XRF data; based on this ratio, and assuming the loss of all propyl chains and unreacted chlorine groups, the mass loss can calculated to be 41 %. Concluding, the data show that the POSS-HCCP network is thermally stable up to 340 °C, which is promising for use as gas separation membrane at elevated temperatures.
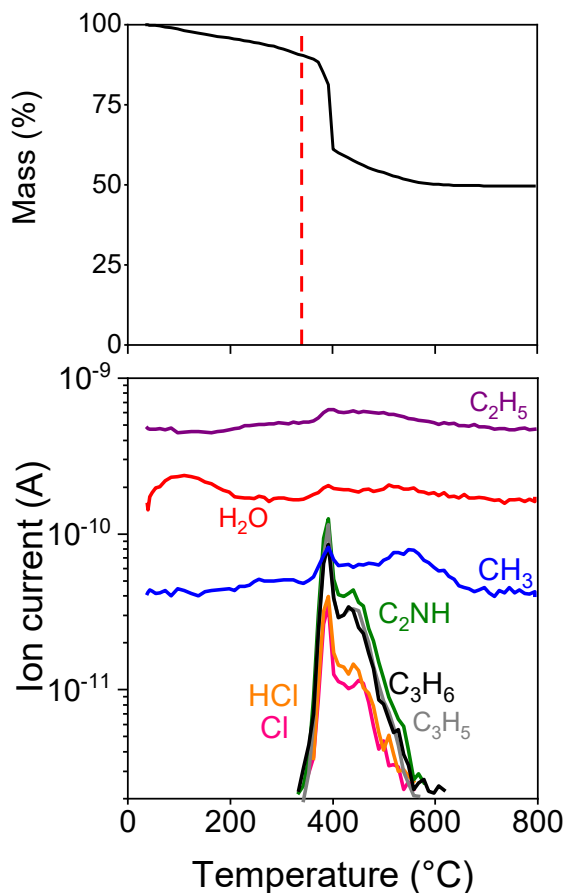


Figure 3.3 TGA-MS data from the polyphosphazene powder. TGA (top), Selected MS data (bottom).

### 3.3.3. Gas permeation

Polyphosphazenes are usually classified as thermally stable polymers.[12] Here, we report for the first time the gas permeance performance of POSS-HCCP polyphosphazenes at elevated temperatures.

Figure 3.4A shows single gas permeance data of the produced membranes as a function of gas kinetic diameter, at 250, 200, 150, 100, and 50 °C. The decrease in the permeance with an increasing kinetic diameter of the permeant is similar as the typical behavior observed for membranes consisting of glassy polymers.[27,28] It implies that the gas molecules are permeating through a rigid molecular environment in which slightly smaller molecules have a much higher mobility (diffusion coefficient) as compared to slightly larger molecules. In contrast, for elastomers generally the diffusion coefficient of permeants changes moderately with their size, and the permeation of larger molecules is actually larger due to their higher solubility. It is well-known that the substituents of polyphosphazenes have a significant effect on the final properties of these polymers, ranging from elastomers to glassy polymers [29]. In this case, the incorporation of the inorganic POSS cages results in moderation of the dynamics of the (hyper-) crosslinked network, which is manifested by molecular sieving characteristics. It should be noted that in the polyphosphaze membranes the only pathway for diffusion is via the organic regions (the alkyl chains and the HCCP) [30], because the size of the Si-O based POSS cage is too small to accommodate even the small hydrogen molecules. Consequently, the POSS cages merely act as rigid anchoring points. The molecular sieving characteristics of the membranes at the elevated temperatures imply that the dynamics of these organic bridges are moderated. This is in agreement with earlier experimental [11] and theoretical studies.[30]

Table 3.2 Comparison activation energies before and after exposure at 250 °C.

| Gases | Activation energy (kJ mol$^{-1}$) | |
|:---:|:---:|:---:|
| | Before | After 250 ºC exposure |
| He | $15.7 \pm 0.8$ | $13.1 \pm 0.7$ |
| H$_2$ | $17.9 \pm 1.1$ | $11.2 \pm 0.4$ |
| CO$_2$ | $23.5 \pm 2.4$ | $10.9 \pm 1.5$ |
| N$_2$ | $22.8 \pm 0.6$ | $19.1 \pm 0.8$ |
| CH$_4$ | $32 \pm 1.7$ | $23.8 \pm 2.6$ |

For all gases the permeance increases with increasing temperature. This is expected because diffusion is generally a thermally activated process. The Arrhenius plots of the gas permeance (Figure 3.4B) confirm that for all gases the permeance is thermally activated, with a constant activation energy over the complete temperature range from 50 to 250 °C. The activation energies follow the order CH$_4$>N$_2$>H$_2$>He, CO$_2$, corresponding to the variation in the kinetic diameter of the gas molecules. For larger molecules the activation energy for diffusion is larger, because more energy is required for successful jumps from one location to another in the polymer network. The exception to this order is CO$_2$. This different behaviour of CO$_2$ is also observed for other, glassy, polymers and results from a stronger affinity of the CO$_2$ for polar groups like amines. The presence of these groups results in a higher solubility of CO$_2$; solubility generally decreases with increasing temperature with an activation energy that is opposite in sign to that of diffusion. The combined effect of temperature on solubility and diffusion is manifested by a lower 'apparent' activation energy of CO$_2$ [2,31]. The values and order of the activation energies are comparable with other types of thermally stable membranes, such as polyimide and polybenzimidazole membranes [32]. This implies the rigidity of the polyphosphazene network and the high gas barrier properties of these membranes.
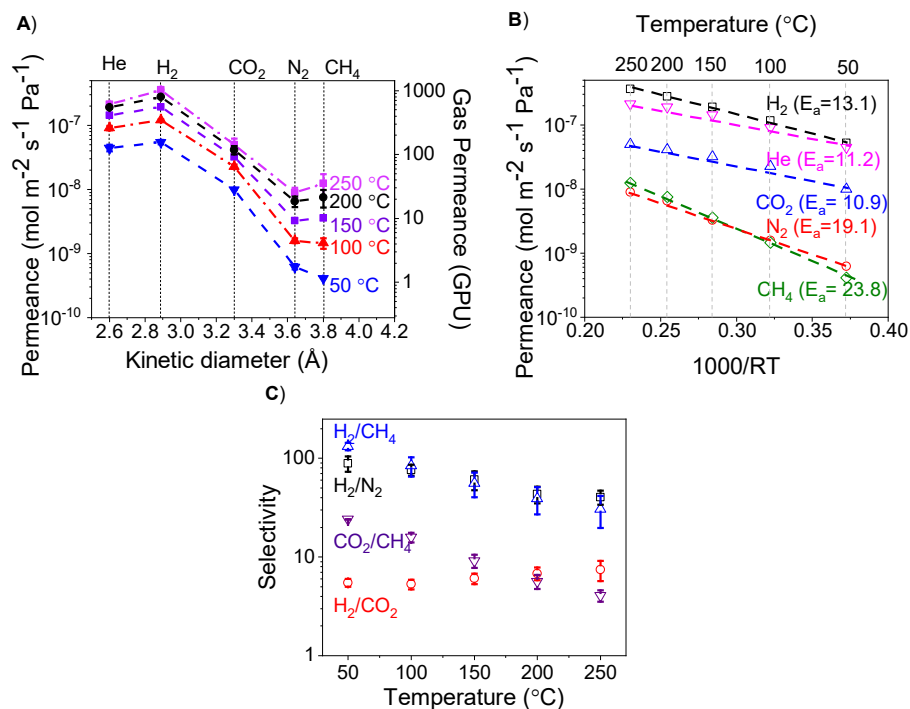
Figure 3.4 (A) Gas permeance as a function of gas kinetic diameter for 4 different temperatures. (B) Arrhenius plot of pure gas permeances. The unit of activation energies is kJ mol$^{-1}$. (C)The ideal selectivities of the membranes as a function of temperature.

The above results show the performance of the membranes from 250 to 50 °C. However, before exposure to 250 °C, the gas permeance was measured several times up to 200 °C. Figure S3.3 shows the gas performance results before exposure to 250 °C. After the exposure to 250 °C, for all gases the permeance has increased. This implies that the exposure to 250 °C has resulted in a more open network. This is further evidenced by the activation energies, in Table 3.2, before and after exposing to 250°C. The energies of activation have reduced, indicating a more open network. This effect is most pronounced for the larger gases, as a change in the openness of the network will affect their mobility more. The exception is, again, $CO_2$. For $CO_2$ the reduction in activation energy is very substantial, indicating the solubility of $CO_2$ in the network has further increased. This can be the result of (slight) thermal degradation of the network chemistry after heating to 250 °C. In particular, primary amine groups ($CNH_2$) would emerge due to the breaking

of the weakest bond (CNHP); $CO_2$ has a high affinity towards primary amines [33]. Several thermal cycles were conducted on a fresh membrane sample, to confirm these observations (Figures S3.4, S3.5 and S3.6).

The performance of the POSS-HCCP membranes is further assessed from the permselectivities of several gas combinations. In Figure 3.4C the permselectivities of $H_2/N_2$, $H_2/CH_4$, $H_2/CO_2$, and $CO_2/CH_4$ are presented as a function of temperature. Results show that at low temperatures excellent permselectivities, as high as 130 for $H_2/CH_4$, are obtained. The permselectivities of all the gas pairs decrease as a function of temperature, except for $H_2/CO_2$. This is due to differences in the activation energies of $H_2$ and $CO_2$ [32]. As temperature increases, the $H_2$ permeance enhances to a greater extent compared to the $CO_2$. Even at 250 °C, the sieving selectivity of the membrane persists. This is due to the moderated macromolecular dynamics, resulting from the high number of connections between the organic parts of the network with the rigid silica cages, as described in the XRF section.

The performance of the membranes compare favorably with other membranes tested at the same high termperature conditions, i.e., the poly(POSS imide) membranes of Rijmakers et al.[11]. At 250 °C the permselectivities of the POSS-HCCP membranes are higher than those of the poly(POSS imide) membranes; the selectivities of $H_2/N_2$, $H_2/CH_4$ and $H_2/CO_2$ are 40, 31 and 7.4, respectively, while for poly(POSS imide) membranes, the selectivities are 10, 10 and 5.5 with comparable permeances. The better selectivity of the polyphosphazene membranes is due to the use of HCCP instead of the di-anhydride (6FDA), leading to an augmented immobilizing effect.

In summary, the new POSS-HCCP polyphosphazene membranes are thermally stable and have persisting excellent selectivities and good permeances up to 250 °C. Therefore, they have a great potential for use at high temperature gas separation conditions, for example, for pre-combustion purposes.

## 3.4 Conclusion

In this work, we show for the first time the preparation of polyphosphazene thin film composite membranes via interfacial polymerization of POSS and HCCP. The synthesized polyphosphazene networks are highly crosslinked and display a great thermal stability, up to 340 ºC. The gas permeance performance of the membranes are tested at elevated high temperatures. At 250 °C permselectivities of 40, 31, 7 and 4 were obtained for the gas pairs $H_2/N_2$, $H_2/CH_4$, $H_2/CO_2$ and $CO_2/CH_4$, respectively, while maintaining permeances in the order of $10^{-7}$– $10^{-8}$ mol m$^{-2}$ s$^{-1}$ Pa$^{-1}$. At these elevated temperatures the polyphosphazene membranes outperform other types of polymer based membranes, and are therefore very promising for the use at high temperature applications, such as the selective separation of hydrogen in pre-combustion.

## 3.5 Acknowledgement

# 3.6 References

[1] W.J. Koros, R. Mahajan, Pushing the limits on possibilities for large scale gas separation: Which strategies?, J. Memb. Sci. 175 (2000) 181–196. https://doi.org/10.1016/S0376-7388(00)00418-X.

[2] X. Li, R.P. Singh, K.W. Dudeck, K.A. Berchtold, B.C. Benicewicz, Influence of polybenzimidazole main chain structure on $H_2/CO_2$ separation at elevated temperatures, J. Memb. Sci. 461 (2014) 59–68. https://doi.org/10.1016/j.memsci.2014.03.008.

[3] M. Shan, X. Liu, X. Wang, Z. Liu, H. Iziyi, S. Ganapathy, J. Gascon, F. Kapteijn, Novel high performance poly(: P -phenylene benzobisimidazole) (PBDI) membranes fabricated by interfacial polymerization for H2 separation, J. Mater. Chem. A. 7 (2019) 8929–8937. https://doi.org/10.1039/c9ta01524h.

[4] R.S. Murali, T. Sankarshana, S. Sridhar, Air Separation by Polymer-based Membrane Technology, Sep. Purif. Rev. 42 (2013) 130–186. https://doi.org/10.1080/15422119.2012.686000.

[5] F.G. Kerry, Industrial gas handbook: Gas separation and purification, CRC Press, 2007. https://doi.org/10.1201/9781420008265.

[6] C. Staudt-Bickel, W.J. Koros, Olefin/paraffin gas separations with 6FDA-based polyimide membranes, J. Memb. Sci. 170 (2000) 205–214. https://doi.org/10.1016/S0376-7388(99)00351-8.

[7] A. Iulianelli, E. Drioli, Membrane engineering: Latest advancements in gas separation and pre-treatment processes, petrochemical industry and refinery, and future perspectives in emerging applications, Fuel Process. Technol. 206 (2020). https://doi.org/10.1016/j.fuproc.2020.106464.

[8] D.Y.C. Leung, G. Caramanna, M.M. Maroto-Valer, An overview of current status of carbon dioxide capture and storage technologies, Renew. Sustain. Energy Rev. 39 (2014) 426–443. https://doi.org/10.1016/j.rser.2014.07.093.

[9] S. Kazama, M. Sakashita, Gas separation properties and morphology of asymmetric hollow fiber membranes made from cardo polyamide, J. Memb. Sci. 243 (2004) 59–68. https://doi.org/10.1016/j.memsci.2004.06.012.

[10] Weigelt, Escorihuela, Descalzo, Tena, Escolástico, Shishatskiy, Serra, Brinkmann, Novel Polymeric Thin-Film Composite Membranes for High-Temperature Gas Separations, Membranes (Basel). 9 (2019) 51. https://doi.org/10.3390/membranes9040051.

[11] M.J.T. Raaijmakers, M.A. Hempenius, P.M. Schön, G.J. Vancso, A. Nijmeijer, M. Wessling, N.E. Benes, Sieving of hot gases by hyper-cross-linked nanoscale-hybrid membranes, J. Am. Chem. Soc. 136 (2014) 330–335. https://doi.org/10.1021/ja410047u.

[12] M. Rezakazemi, M. Sadrzadeh, T. Matsuura, Thermally stable polymers for advanced high-performance gas separation membranes, Prog. Energy Combust. Sci. 66 (2018) 1–41. https://doi.org/10.1016/j.pecs.2017.11.002.

[13] E. Drioli, S.M. Zhang, A. Basile, G. Golemme, S.N. Gaeta, H.C. Zhang, Gas permeability of polyphosphazene membranes, Gas Sep. Purif. 5 (1991) 252–258. https://doi.org/10.1016/0950-4214(91)80033-2.

[14] C. Wan, X. Huang, Cyclomatrix polyphosphazenes frameworks (Cyclo-POPs) and the related nanomaterials: Synthesis, assembly and functionalisation, Mater. Today Commun. 11 (2017) 38–60. https://doi.org/10.1016/j.mtcomm.2017.02.001.

[15] R. Revathi, P. Prabunathan, M. Alagar, Synthesis and studies on phosphazene core-based POSS-reinforced polyimide nanocomposites, Polym. Bull. 76 (2019) 387–407. https://doi.org/10.1007/s00289-018-2391-1.

[16] P. Mohanty, L.D. Kull, K. Landskron, Porous covalent electron-rich organonitridic frameworks as highly selective sorbents for methane and carbon dioxide, Nat. Commun. 2 (2011) 1–6. https://doi.org/10.1038/ncomms1405.

[17] Y. Chen, Z. Li, N. Chen, Y. Zhang, F. Wang, H. Zhu, Preparation and characterization of cross-linked polyphosphazene-crown ether membranes for alkaline fuel cells, Electrochim. Acta. 258 (2017) 311–321. https://doi.org/10.1016/j.electacta.2017.11.049.

[18] S. Gao, H. Xu, T. Luo, Y. Guo, Z. Li, A. Ouadah, Y. Zhang, Z. Zhang, C. Zhu, Novel proton conducting membranes based on cross-linked sulfonated polyphosphazenes and poly(ether ether ketone), J. Memb. Sci. 536 (2017) 1–10. https://doi.org/10.1016/j.memsci.2017.04.065.

[19] M. You, W. Li, Y. Pan, P. Fei, H. Wang, W. Zhang, L. Zhi, J. Meng, Preparation and characterization of antibacterial polyamine-based cyclophosphazene

nanofiltration membranes, J. Memb. Sci. 592 (2019) 117371. https://doi.org/10.1016/j.memsci.2019.117371.

[20] C.J. Orme, J.R. Klaehn, M.K. Harrup, T.A. Luther, E.S. Peterson, F.F. Stewart, Gas permeability in rubbery polyphosphazene membranes, J. Memb. Sci. 280 (2006) 175–184. https://doi.org/10.1016/j.memsci.2006.01.009.

[21] V.A. Kusuma, J.S. McNally, J.S. Baker, Z. Tong, L. Zhu, C.J. Orme, F.F. Stewart, D.P. Hopkinson, Cross-Linked Polyphosphazene Blends as Robust CO2Separation Membranes, ACS Appl. Mater. Interfaces. 12 (2020) 30787–30795. https://doi.org/10.1021/acsami.0c06795.

[22] M.J.T. Raaijmakers, M. Wessling, A. Nijmeijer, N.E. Benes, Hybrid polyhedral oligomeric silsesquioxanes-imides with tailored intercage spacing for sieving of hot gases, Chem. Mater. 26 (2014) 3660–3664. https://doi.org/10.1021/cm500691e.

[23] E. Maaskant, H. Gojzewski, M.A. Hempenius, G.J. Vancso, N.E. Benes, Thin cyclomatrix polyphosphazene films: Interfacial polymerization of hexachlorocyclotriphosphazene with aromatic biphenols, Polym. Chem. 9 (2018) 3169–3180. https://doi.org/10.1039/c8py00444g.

[24] P. Karakiliç, C. Huiskes, M.W.J. Luiten-Olieman, A. Nijmeijer, L. Winnubst, Sol-gel processed magnesium-doped silica membranes with improved $H_2/CO_2$ separation, J. Memb. Sci. 543 (2017) 195–201. https://doi.org/10.1016/j.memsci.2017.08.055.

[25] G. Derchi, E. Manca, A. Shayganpour, A. Barone, A. Diaspro, M. Salerno, Combined characterization of the time response of impression materials via traditional and FTIR measurements, Materials (Basel). 8 (2015) 2387–2399. https://doi.org/10.3390/ma8052387.

[26] S. Türe, H. Silah, M. Tuna, Reinvestigations of the reactions of hexachlorocyclotriphosphazene with difunctional primary amines leading to novel dangler, ansa and bridged derivatives. Spectroscopic studies of the derived products, J. Mol. Struct. 1202 (2020) 127232. https://doi.org/10.1016/j.molstruc.2019.127232.

[27] M. Omidvar, C.M. Stafford, H. Lin, Thermally stable cross-linked P84 with superior membrane $H_2/CO_2$ separation properties at 100 °C, J. Memb. Sci. 575 (2019) 118–125. https://doi.org/10.1016/j.memsci.2019.01.003.

[28] S. Japip, K.-S. Liao, T.-S. Chung, Molecularly Tuned Free Volume of Vapor Cross-Linked 6FDA-Durene/ZIF-71 MMMs for $H_2/CO_2$ Separation at 150 °C, Adv. Mater. 29 (2017) 1603833. https://doi.org/10.1002/adma.201603833.

[29] H.R. Allcock, Polyphosphazenes: New polymers with inorganic backbone atoms, Science (80-. ). 193 (1976) 1214–1218. https://doi.org/10.1126/science.193.4259.1214.

[30] D. Brown, S. Neyertz, M.J.T. Raaijmakers, N.E. Benes, M. Blanc, F.-Chambéry, Sorption and permeation of gases in hyper-cross-linked hybrid poly ( POSS- imide ) networks : An in silico study, J. Memb. Sci. 577 (2019) 113–128. https://doi.org/10.1016/j.memsci.2019.01.039.

[31] J.P.G. Villaluenga, B. Seoane, J. Hradil, P. Sysel, Gas permeation characteristics of heterogeneous ODPA-BIS P polyimide membranes at different temperatures, J. Memb. Sci. 305 (2007) 160–168. https://doi.org/10.1016/j.memsci.2007.08.002.

[32] K.A. Stevens, J.D. Moon, H. Borjigin, R. Liu, R.M. Joseph, J.S. Riffle, B.D. Freeman, Influence of temperature on gas transport properties of tetraaminodiphenylsulfone (TADPS) based polybenzimidazoles, J. Memb. Sci. 593 (2020). https://doi.org/10.1016/j.memsci.2019.117427.

[33] Y.G. Ko, S.S. Shin, U.S. Choi, Primary, secondary, and tertiary amines for $CO_2$ capture: Designing for mesoporous $CO_2$ adsorbents, J. Colloid Interface Sci. 361 (2011) 594–602. https://doi.org/10.1016/j.jcis.2011.03.045.

## 3.7 Supporting information

In Figure S3.1, the interfacial polymerization reaction is visualized. The free-standing layer is formed at the interface between the two solutions.



Figure S3.1 Free-standing film POSS-HCCP.

In Figure S3.2, the interfacial polymerization setup is shown, as used for the thin film composite membrane preparation.
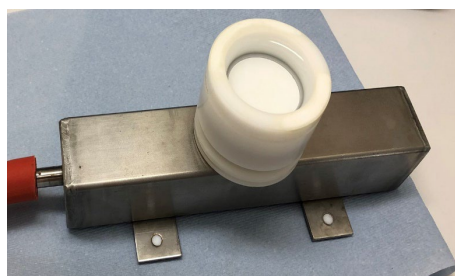


Figure S3.2 Interfacial polymerization setup.

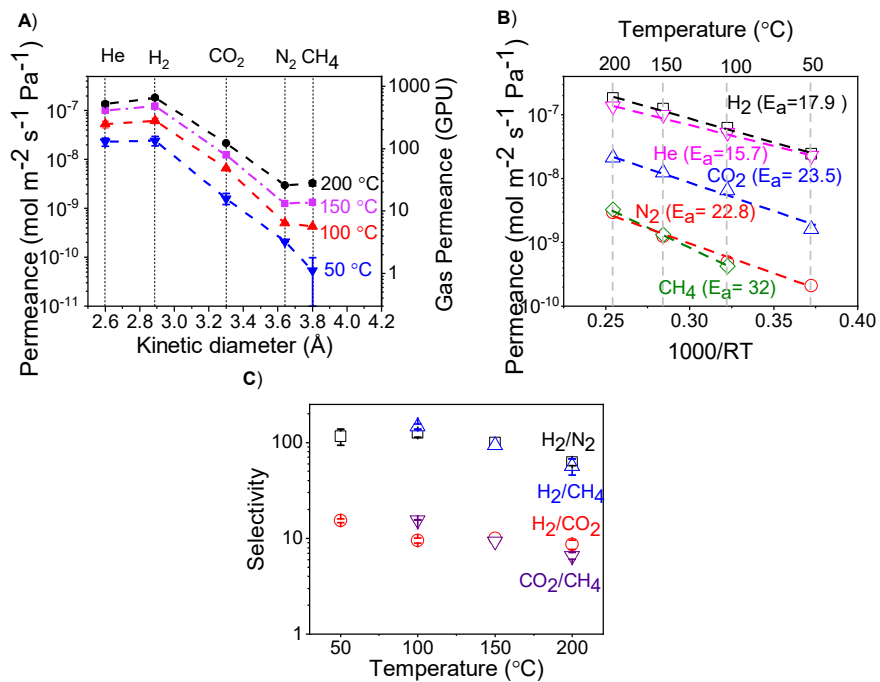In Figure S3.3, the gas permeation performance of the membranes before exposure to 250 °C is shown.



Figure S3.3 (A) Gas permeance as a function of gas kinetic diameter for 4 different temperatures. (B) Arrhenius plot of pure gas permeances. The unit of activation energies is kJ mol$^{-1}$. (C) The ideal selectivities of the membranes as a function of temperature.

Table S3.1 shows the different thermal cycles that were subjected to a freshly prepared polyphosphazene membrane. The initial cycle started at 200 °C, then in the second cycle the membrane was subjected to 250 °C and this was repeated several times. At each temperature, permeation of 5 different single gases (He, $N_2$, $CO_2$, $H_2$ and $CH_4$) was measured (for 30 minutes each, making the total duration of one temperature 2.5h).

Table S3.1 Thermal cycles.

| Cycle # | Temperature program (°C) |
|---------|--------------------------|
| 1 | 200, 150, 100 |
| 2 | 250, 200, 100, 50 |
| 3 | 250, 200, 100 |
| 4 | 250, 200, 150, 100 |
| 5 | 250, 200, 150, 100, 50 |

In Figures S3.4, S3.5 and S3.6, the results on permeance, activation energy and selectivity for the different thermal cycles and temperatures are shown. For the permeance and selectivity, only the data at 250, 200, and 100 °C is given.
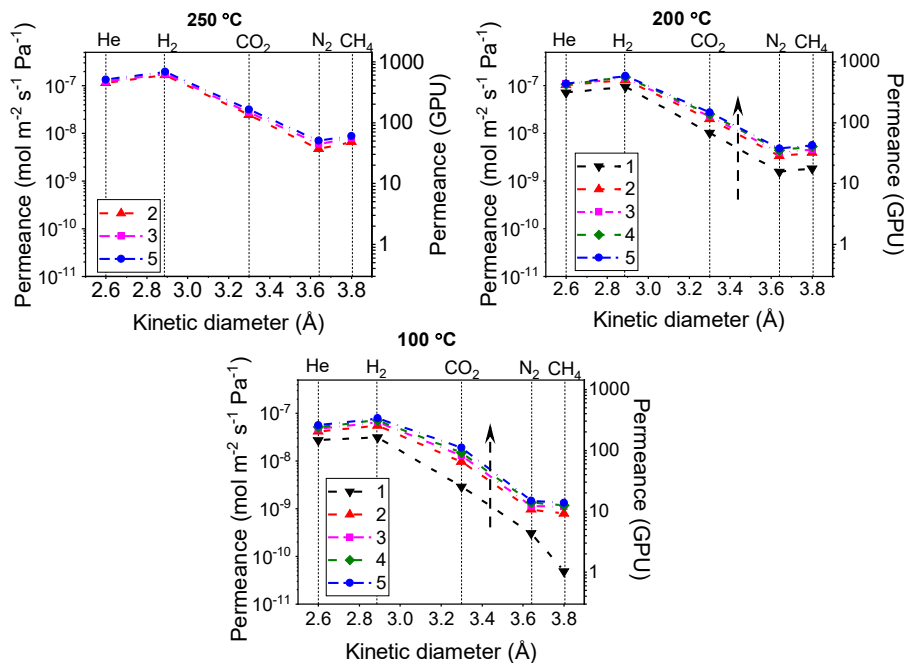
Figure S3.4 Gas permeance (y-axis) vs. kinetic diameter (x-axis) at 250 °C, 200 °C and 100 °C for different thermal cycles (the number in the legend indicates the cycle).
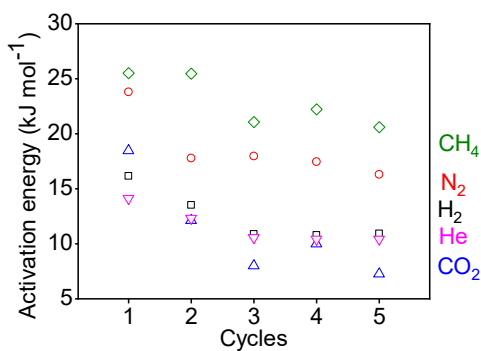
Figure S3.5 Activation energy for five different gases for each thermal cycle.
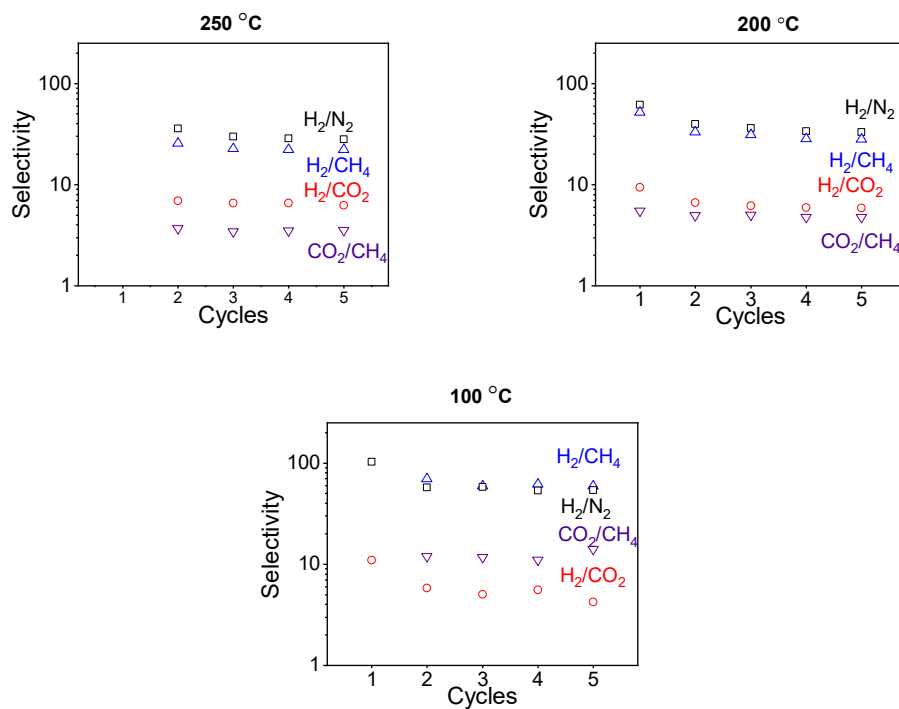


Figure S3.6 Ideal selectivity (y-axis) vs. cycle number (x-axis) at 250 ºC, 200 ºC and 100 ºC for different gas pairs.

# Chapter 4
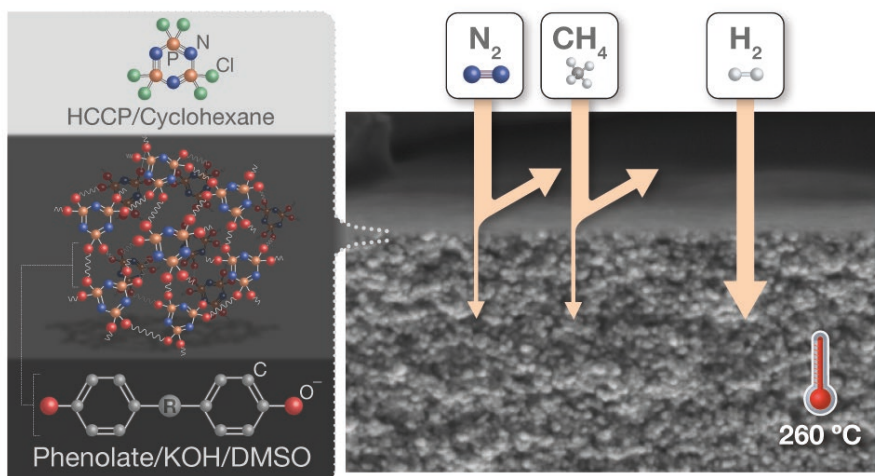
# Thin film composite cyclomatrix poly(phenoxy)phosphazene membranes for hot hydrogen separation

# Abstract

An interfacial polymerization process is introduced for the fabrication of thermally stable cyclomatrix poly(phenoxy)phosphazenes thin film composite membranes that can sieve hydrogen from hot gas mixtures. By replacing the conventionally used aqueous phase with dimethyl sulfoxide/potassium hydroxide, a variety of biphenol molecules are deprotonated to aryloxide anions that react with hexachlorocyclotriphosphazene dissolved in cyclohexane to form a thin film of highly crosslinked polymer film. The film membranes have persistent permselectivities for hydrogen over nitrogen (16-27) and methane (14-30) while maintaining hydrogen permeances in the order of ($10^{-8}$-$10^{-7}$ mol m$^{-2}$s$^{-1}$Pa$^{-1}$) at temperatures as high as 260 °C and do not lose their performance after exposure to 450 °C. The unprecedented thermal stability of these polymer membranes opens potential to industrial membrane gas separations at elevated temperatures.

## 4.1 Introduction

Molecular separations are pervasive in the large-scale chemical industry and energy production sector and denote gigantic energy requirements. More efficient separation methods can have a large impact on the process economics and, more importantly, on their sustainability. For processes that occur at high temperatures the efficiency can be substantially improved when the necessity to cool and reheat process streams is avoided. Membrane-based separations for hot gases have the potential for this, but producing membranes that have a persisting separation performance at high temperatures is challenging.[1–3] Membrane materials that have been investigated for hot gas separation include inorganic materials (metals, zeolites, carbons),[4-6] two dimensional layered materials,[7,8] covalent organic frameworks (COFs),[9] and metal-organic frameworks (MOFs).[1,2,10–13] However, their complex and costly production has hampered their industrial application.[7,14,15] Polymeric membranes would offer a more economical and scalable alternative. A limited range of polymeric materials has been investigated, including polybenzimidazole (PBI), polyimide (PI), and thermally rearranged polymers (TRP).[16–22] Shortcomings of these membranes are insufficient permeances and selectivity at high temperatures,[16,17,23] and the need for costly chemical or thermal treatment for network conversion.[23–25] Hybrid membranes, consisting of a network of inorganic polyhedral oligomeric silsesquioxane (POSS) connected via organic imide bridges, have demonstrated good separation performance at elevated temperatures.[26] Similar to the large-scale production of reverse osmosis membranes, these hybrid membranes are fabricated via the facile interfacial polymerization (IP) method, in which a thin layer is formed in-situ at the interface of two immiscible phases.[27,28] Unfortunately, these membranes require a thermal imidization step.

Recently, we developed membranes in which POSS cages are connected in a network via hexachlorocyclotriphosphazene (HCCP) bridges.[28] The cyclic phosphazene group offers exceptional inherent properties, such as natural flame retardancy and thermal stability.[29–31] Much of the current literature on cyclomatrix polyphosphazene (CPPz) reports super-macromolecular self-assemblies like nano- or micro-spheres, nanosheets, and microtubes.[29,32–

36] Limited studies report the successful formation of thin defect-free and continuous CPPz membrane films.[27,37] The IP process allows not only the formation of such films but also a high degree of cross-linking that moderates the macromolecular dynamics at the elevated temperatures of application. As such, these membranes have much potential for sieving small molecules, such as $H_2$, from hot gas streams,[26,28] where the $C(sp^3)$ bonds in the propyl groups of the POSS molecules limit the applicable temperature range to 300 °C.

Here, we demonstrate a new strikingly versatile synthesis route for highly crosslinked CPPz based thin film composite (TFC) membranes. By replacing the aqueous phase, which is typically used in conventional interfacial polymerizations, with dimethyl sulfoxide (DMSO)/potassium hydroxide (KOH) a range of different, previously non-applicable, nucleophile monomers can be used for substitution reactions with the HCCP. We focus on a selection of aromatic biphenols. Maaskant et al. reported polymerization of aromatic biphenols in water with HCCP in dichloromethane. These highly crosslinked CPPz polymers with O linking atoms exhibit higher thermal stability than materials with N linking atoms.[27,32] However, the reactivity of the phenols in water is too limited to allow the formation of thin defect-free membrane films. Meyer et al. reported enhanced reactivity of phenols in DMSO as compared to water.[38] The addition of KOH makes the DMSO solution a superbase in which the phenols can easily be deprotonated to become highly soluble and nucleophile phenolates that can react with HCCP.

To demonstrate the broad applicability of this concept, various CPPz membranes are developed from a selection of organic bridges with different ranges of flexibility. The membranes are characterized in terms of permeance of $H_2$ and the slightly larger $CO_2$, $CH_4$ and $N_2$, at elevated temperatures. The results aid molecular design of high-performance CPPz membranes, promoting advances in gas separation applications at elevated temperatures.

## 4.2 Experimental

### 4.2.1. Materials

Phosphonitrilic chloride trimer (HCCP, 99%, Sigma-Aldrich), hexaphenoxycyclotriphosphazene (ArO$_6$PP, >98%,TCI), 4,4′-Dihydroxybiphenyl (BPH, Sigma-Aldrich), 4,4′-dihydroxydiphenyl ether (DHPE Sigma-Aldrich), 4,4′-dihydroxybenzophenone (DHBP, Sigma-Aldrich), 4,4′-sulfonyldiphenol (BPS, Sigma-Aldrich), 4,4′-(Hexafluoroisopropylidene)diphenol (BPAF, Sigma-Aldrich), phenol (Sigma-Aldrich), tetrahydrofuran (anhydrous, ≥99.9%, Sigma-Aldrich), and dimethyl sulfoxide (DMSO, anhydrous, ≥99.9%, Sigma-Aldrich), cyclohexane (EMSURE for analysis, Merck), sodium hydroxide (NaOH, reagent grade, Sigma-Aldrich) and potassium hydroxide (KOH, pellets extra pure, Merck) were used as received. Porous α-alumina discs (Ø 39 mm, thickness 2 mm) were obtained from Pervatech B.V. and used as support.

### 4.2.2. Material fabrication

Freestanding polymer layers and thin film composite polymeric membranes were formed by interfacial polymerization of (1) a 10 w/v% solution of the corresponding biphenols in DMSO containing KOH ,super base[39], molar ratio of biphenol : KOH of 0.5, i.e. stoichiometric with respect to phenol groups, and 0.75, i.e. substoichiometric with respect to phenol groups and (2) a 3.5 w/v% HCCP solution in cyclohexane.

Unless otherwise mentioned, we have used a molar ratio of biphenol : KOH of 0.75. That means that maximal two of every three phenol groups can be deprotonated to phenolate anions. The used concentrations of biphenols and HCCP and the applied volumes reflect (if the solutions were perfectly mixed) a molar stoichiometry of HCCP:biphenol is 1:5. Since HCCP contains 6 reactive chlorine atoms and the biphenols have 2 phenol groups, the molar ratio of reactive chlorine to phenol is 6 : 10. Because of the molar ratio of biphenol:KOH of 0.75, the molar ratio of reactive chlorine to phenolate anion = ca 1 : 1. If all the reactive chlorine would be displaced by phenolate anion substitution, there are still unreacted phenol groups present (about 1/3 of the number of biphenol moieties). Since the performed

polymerization happens at the interface, such an ideal situation does not exist, and some heterogeneity will be present in the formed membrane layers.

## Synthesis of CCPz freestanding films

After heating biphenol solutions at 80°C for 2 hr, 10 mL was mixed with the HCCP solution (10 mL) and vigorously stirred for 10 minutes. The formed suspension was filtered, washed with water, ethanol, and acetone and dried in the vacuum oven at 50 °C.

## Preparation of biphenol-HCCP thin film composite membranes

The CCPz membranes were prepared atop of ceramic supports: α-alumina discs with a 3-μm-thick γ-alumina layer (pore size of 3-5 nm) with the setup described elsewhere.[28] First, the biphenol solution and support were heated at 80 °C for 2 hr and 30 min, respectively. After this, the preheated ceramic was soaked in preheated biphenol solution for 15 min at 80 °C. Subsequently, the support surface was dried by applying a rubber roller and $N_2$ gun, followed by contacting it with the HCCP solution for 10 min at ambient temperature. After removing the HCCP solution, the membranes were rinsed with ethanol. Before further analysis, the membrane was kept under a fume hood overnight and then dried in a vacuum oven at 50 ºC for a minimum of 24 hours.

## Synthesis of triphenoxy trichlorocycoltriphosphazene ($ArO_3Cl_3PP$)

Triphenoxy trichlorocycoltriphosphazene was prepared according to the literature, with some modifications, Figure 4.1.[40,41] HCCP was reacted with an excess amount of sodium phenolate. For this purpose, a suspension of NaOH (0.85 g, 0.02 mol), phenol (2 g, 0.02 mol), HCCP (2.5 g, 0.007 mol), and 40 mL of THF was prepared in a 100-mL three-necked round-bottom flask. The mixture was refluxed for 5 h under a nitrogen atmosphere. After the reaction was completed, the suspension was distilled under reduced pressure with a rotary evaporator, and the remaining crude product was

washed with hot deionized water to give a light yellow solid of the product. The product was dried at 50°C under vacuum overnight. ^{1}H NMR (400 MHz, chloroform) δ(11.7-12.17), ^{31}P NMR (162 MHz, Chloroform-d) δ 16.13, 15.76 (d, J = 14.8 Hz), 15.57 – 15.31 (m), 15.15, 3.82, 3.53 (d, J = 14.3 Hz), 3.28, 2.65, 2.40 – 1.95 (m), 1.90, 1.64 (d, J = 18.5 Hz), 1.27, 1.18 – 0.07 (m). The product is mostly a mixture of diphenoxy, symmetrical triphenoxy, and asymmetrical triphenoxy.[41] Besides, a small trace of phenol can be observed, ^{1}H NMR (400 MHz, chloroform) (7.22 (s, 2H), 6.55 – 6.44 (m, 3H).
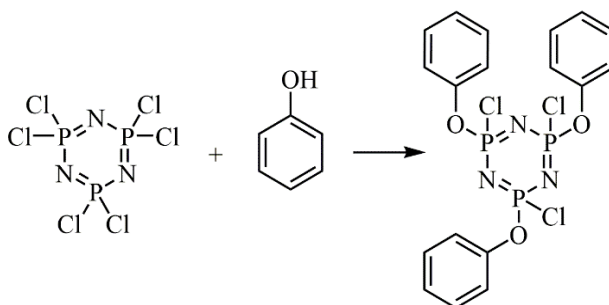


Figure 4.1 Formation of a triphenoxy trichlorocyclotriphosphazene by the reaction of phenol with HCCP

## 4.2.3. Material characterization

A field emission scanning electron microscope (FE-SEM, Zeiss MERLIN) was used to evaluate the thickness and morphology of the supported membranes. For cross-section images, samples were immersed in the liquid nitrogen for 5 minutes and carefully broken to reveal the full cross-section. All samples were mounted on an FE-SEM holder using double-sided carbon tape and coated with 5 nm Pt/Pd conductive layer using a sputter coater Quorum Q150T ES (Quorum Technologies, Ltd., UK). Energy dispersive X-ray spectra (EDX) were taken with a JEOL-JSM6010 scanning electron microscope. For this purpose, the obtained free-standing films were coated with 5 nm Pt/Pd conductive layer prior to imaging using a sputter coater Quorum Q150T ES (Quorum Technologies, Ltd., UK). EDX analysis was performed at 10 kV with >1000 counts/s. The experiment was repeated three times at different points, and the average value was reported. [1]H, ^{13}C, and ^{31}P nuclear magnetic resonance (NMR) spectroscopies were performed on

400 MHz pulsed Fourier Transform NMR spectrometer (Agilent 400-MR DD2) using Deuterated DMSO (DMSO-d6). Fourier transform infrared spectroscopy in attenuated total reflectance mode (FTIR-ATR, PerkinElmer Spectrum Two, USA) was used to characterize the free-standing films. Spectra were averaged over 16 scans with a resolution of 4 $cm^{-1}$ over a wavelength range from 400-4000 $cm^{-1}$. The elemental composition of synthesized free-standing films was measured with X-Ray Fluorescence (XRF) (S8 Tiger, Bruker) and CN elemental analysis (FLASH 2000 series analyzer). The thermal stability of the membranes was examined by heating a fixed amount of sample (10 mg) on a heating stage under an inert nitrogen atmosphere at a heating rate of 10 °C $min^{-1}$ using a Thermo Gravimetric Analysis (TGA, STA 449 F3 Jupiler®, Netzsch) in combination with mass spectrometry (MS, QMS 403 D Aeolos MS, Netzsch) to detect the released gaseous products according to their mass to charge ratios ($m/z = 1 - 110$ amu).

## 4.2.4. Membrane performance

Single gas permeance measurements were performed using a gas permeation setup in dead-end mode (Convergence Inspector Poseidon). The single gas permeance of He (0.255 nm), $H_2$ (0.289 nm), $CO_2$ (0.33 nm), $N_2$ (0.364 nm), and $CH_4$ (0.389 nm) was measured at a transmembrane pressure of 2 bar within the temperature range from 50 °C to 260 °C, which is limited by the thermal stability of the sealing. The permselectivity was calculated as the ratio of the respective permeances. The experiments were performed at least twice, and the reported results are the average of the obtained values.
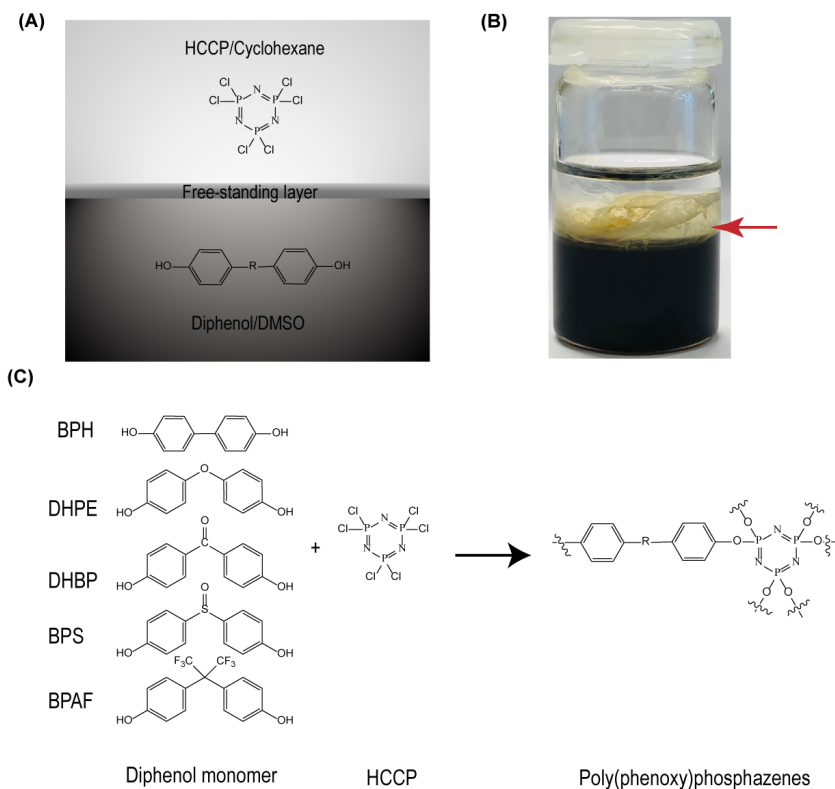
# 4.3 Results & Discussion



Figure 4.2 (A) Visualization of the interfacial polymerization between HCCP in cyclohexane and the potassium phenoxide of hydroxyl monomers in DMSO. An aromatic biphenol is dissolved in DMSO/KOH solution to convert biphenol into potassium phenoxide. Subsequently, it reacts with HCCP that is dissolved in cyclohexane. The layer forms at the interface between the two solvents. (B) Picture of the interfacial polymerization of a poly(phenoxy)phosphazene at the interface of two monomer phases. (C) Synthesis of poly(phenoxy)phosphazenes films through interfacial polymerization between five different hydroxyl compoundsand HCCP.

Thin film CPPz were formed using phosphonitrilic chloride trimer (HCCP) in cyclohexane and different aromatic biphenols in the solution of DMSO with KOH (Figure 4.2A and Figure 4.2B). The selected biphenols are 4′-dihydroxybiphenyl (BPH), 4,4′-dihydroxydiphenyl ether (DHPE), 4,4′-dihydroxybenzophenone (DHBP), 4,4′-sulfonyldiphenol (BPS), and 4,4′-

(Hexafluoroisopropylidene)diphenol (BPAF) (Figure 4.2C, Figure S4.1). The presence of KOH is necessary for the conversion of the biphenols into aryloxide anions. These anions are highly nucleophile, which aids the formation of a thin layer between the two immiscible solvents. The reaction involves the attack of the phenoxides on the P atoms of HCCP, resulting in the formation of CPPz, and KCl as a by-product.
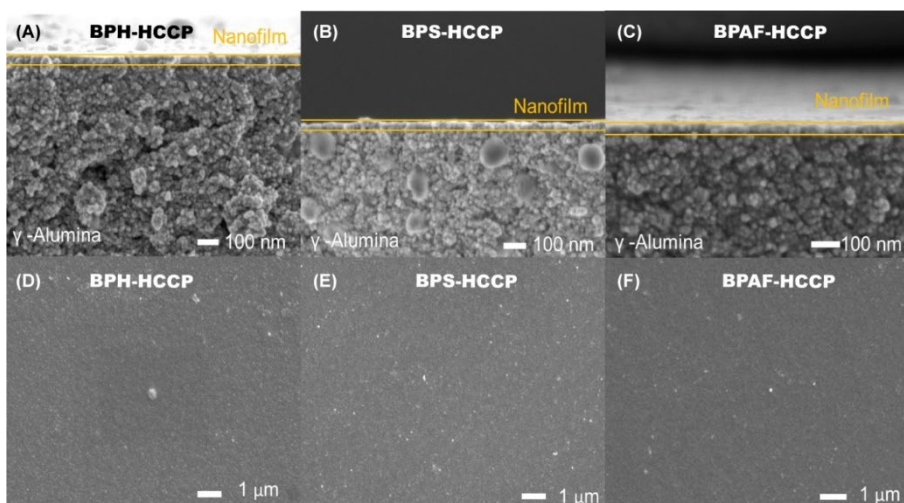


Figure 4.3 (A, B, C) Cross-sectional FE-SEM images of poly(phenoxy)phosphazenes membranes on alumina support for BPH-HCCP, BPS-HCCP, and BPAF-HCCP, respectively. (D, E, F) Surface FE-SEM images of poly(phenoxy)phosphazenes membranes on alumina support BPH-HCCP, BPS-HCCP, and BPAF-HCCP, respectively

In addition to freestanding films, the CPPz films can also be formed directly atop a porous alumina support structure to assure sufficient mechanical strength for application as a membrane. For this, the porous support is impregnated with the DMSO solution and is then contacted with the HCCP in cyclohexane. Figure 4.3A, Figure 4.3B, and Figure 4.3C depict FE-SEM images of resulting cross sections for three different biphenols and reveals that the thickness of the CPPz layer is approximately ~ 30 nm. The top-view images in Figure 4.3D, Figure 4.3E, and Figure 4.3F show that the membrane surfaces are smooth and dense, and without evident pinholes or other defects. AFM characterization (Figure S4.2, TableS4.1) reveals that the surfaces of these three samples have comparable roughness (2.5-4 nm) that

112

is, due to the low thickness of selective layers, similar to that of the unmodified ceramic support (4 nm).

The formation of the poly(phenoxy)phosphazene networks is confirmed by FTIR (Figure 4.4A), showing the characteristic peaks of P-O-Ph (950 cm$^{-1}$), the aromatic group (1400 cm$^{-1}$ and 1600 cm$^{-1}$), and two bands of HCCP (a broad peak at 1100 to 1200 cm$^{-1}$, and 875 cm$^{-1}$). Except for the DHPE-HCCP, the FTIR spectra show all typical bands of the biphenol monomers. In the DHBP-HCCP spectrum, the peak at 1650 cm$^{-1}$ is attributed to the carbonyl group of DHBP. In the BPS-HCCP spectrum, the S=O group of BPS appears at 1290 cm$^{-1}$, and in the BPAF-HCCP spectrum, the CF$_3$ band appears at 1254 cm$^{-1}$.[27]
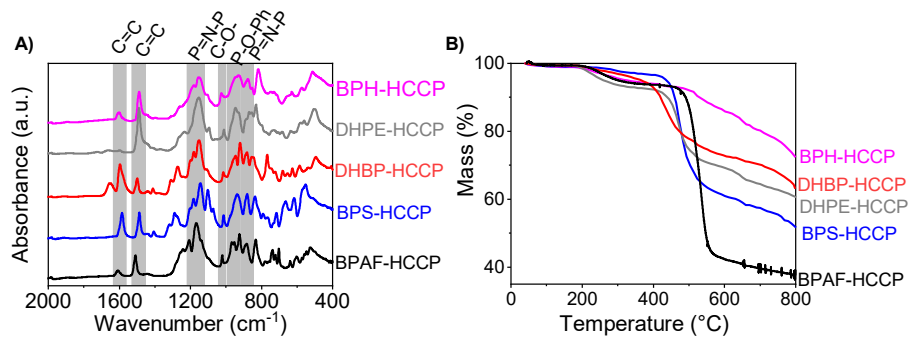


Figure 4.4 (A) FTIR spectra and (B) TGA of the formed poly(phenoxy)phosphazenes network synthesized via interfacial polymerization under N$_2$ atmosphere obtained with a heating rate of 10 °C min$^{-1}$.

The thermal stability of networks is evaluated by TGA-MS (Figure 4.4B and Figure S4.3). A limited mass loss (between 3-5 %) is detected below 400°C. This is attributed to the desorption of physically bound solvents (DMSO and water) and the removal of trapped monomers. Continuous mass loss is observed above 400 °C because of organic decomposition, evidenced by the presence of C$_3$H$_3$ and C$_4$H$_2$ in the mass spectrometer data. The thermal stability of the CPPz is higher as compared to the POSS-HCCP materials presented in our previous study. This is due to the absence of the C(sp$^3$) of the POSS-propyl group, and the Ar-O-P rather than C-NH-P connection.[28] At 450 °C minor traces of HCl evolve, indicating a small amount of unreacted Cl in the networks. Noteworthy to mention is that the amount of HCl is far lower than in the previous study by Maaskant et al.[27], evincing

the great extent of cross-linking in our networks. BPH-HCCP shows a limited continuous release of aromatic fragments and $CO_2$, and a slight reduction in the ratio of C/P (EDX, Table S4.2, Table S4.3) at 800 °C. Conversely, for BPAF-HCCP all fluorine is removed during TGA, and only C and P elements remain after the thermal procedure. The order for the residual mass of the networks at 800 °C is BPH-HCCP> DHBP-HCCP> DHPE-HCCP> BPS-HCCP> BPAF-HCCP.

Table 4.1 XRF Elemental concentration (%) for poly(phenoxy)phosphazenes free-standing films*

| Element | BPH-HCCP | DHPE-HCCP | DHBP-HCCP | BPS-HCCP | BPAF-HCCP |
|---|---|---|---|---|---|
| P | 56.4±0.8 | 45.1±0.9 | 45.7±0.9 | 27.8±0.9 | 50.9±1 |
| Cl | 5±3.6 | 18.6±2.1 | 6.4±3.7 | 1.2±10.7 | 15.8±2.5 |
| S | 0.4±0 | 20.3±2.1 | 26.1±1.2 | 56.9±0.7 | 1.6±6.6 |
| K | 36.7±1 | 14.2±2.1 | 20.2±1.6 | 2.7±4.6 | 29.3±1.6 |
| P/Cl | 11.3 | 2.4 | 7.1 | 23.3 | 3.2 |
| Unreacted Cl per HCCP | 0.3 | 1.2 | 0.4 | 0.1 | 1 |

*Reported errors for XRF data are the relative statistical errors of the peak.*

For HCCP it is well-known that the rings can be opened at a temperature exceeding 250 °C.[42] For the crosslinked materials, FTIR data does not reveal whether cyclic phosphazene rings remain after exposure to high temperatures. To unravel this, two small molecules hexaphenoxycyclotriphosphazene (ArO$_6$PP) and triphenoxy trichlorocycoltriphosphazene (ArO$_3$Cl$_3$PP)) that are representative of the molecular structure of the CPPz have been characterized by FTIR and [31]P Nuclear magnetic resonance (NMR), before and after heat treatment at 260 °C for 10 hr under $N_2$. The FTIR spectra obtained before and after thermal treatment (Figure S4.4) are very similar, with peaks corresponding to P=N-P asymmetric (1100 cm$^{-1}$ to 1200 cm$^{-1}$) and symmetric stretching (875 cm$^{-1}$), [29] and the P-O-Ph bond (950 cm$^{-1}$).[43] For ArO$_3$Cl$_3$PP, the intensity of the P-O-Ph peak increases during temperature exposure due to the substitution of Cl by ArO residues that are present in the samples. The NMR spectra for ArO$_6$PP (Figure S4.5) before and after heat treatment are interchangeable. For ArO$_3$Cl$_3$PP (Figure S4.6) the peaks at δ=0-5 disappear,

114

and the peaks from δ =14.1-18.1 ppm shift to δ =18.1-20.5, indicating the substitution of Cl by ArO.[41,44] The results imply that phosphazene rings with ArO rather than Cl groups remain cyclic at 260 ˚C.

In addition to high thermal stability, a molecular sieving ability of a polymer film at elevated temperatures requires that the macromolecular dynamics of the material under such conditions are moderated. For this, a sufficient degree of cross-linking is vital. X-ray fluorescence (XRF) spectroscopy was used to screen the extent of cross-linking from the relative presence of the elements P, Cl, S, and K (Table 4.1), combined with CN analysis for the elements C and N (Table 4.2). The XRF data reveal the presence of S and K that can be attributed to residual DMSO and KOH. The high ratios of P/Cl (2.4-23.3) indicate that almost all Cl has reacted with the biphenolates. This is confirmed by the ratio of C/N that varies between 2 and 3.5. By considering the number of C present in the biphenols this infers that highly crosslinked networks are formed with, for BPH, DHPE, BPS, and DHBP, on average, at least 5 connecting organic bridges between the phosphazene rings. For BPAF, the degree of cross-linking is slightly less, and a relatively high Cl concentration is observed.

Table 4.2 CN elemental analysis (%) for poly(phenoxy)phosphazenes free-standing films.

| Element | BPH-HCCP | DHPE-HCCP | DHBP-HCCP | BPS-HCCP | BPAF-HCCP |
|---|---|---|---|---|---|
| C | 40.1±0.5 | 51.6±0.5 | 53.7±0.3 | 47.4±0.3 | 36.3±0.3 |
| N | 2.8±0 | 4.7±0.1 | 4.1±0 | 3.8±0 | 3.8±0 |
| C/N | 14.3±0.2 | 11±0.3 | 13.1±0.1 | 12.5±0.1 | 9.6±0.1 |
| Organic bridges per HCCP | 3.5±0.1 | 2.7±0.1 | 3±0 | 3±0.1 | 2±0 |

The permeance of small gas molecules through the thin film membranes, reveals persisting molecular sieving ability; for all membranes, a decrease of permeance with increasing kinetic diameter of the molecule is observed at temperatures from 50 to 260 °C (Figure 4.5, Figure S4.7). This behavior is similar to that of glassy polymers, and originates from large differences in the diffusion rates for molecules of slightly different sizes and shapes.[45,46] In essence, for slightly larger molecules, the jump rate between bordering open spaces in a rigid glassy polymer decreases strongly.

For polyphosphazene polymers, it has been demonstrated that the $T_g$ can be affected by introducing different substitution groups.[47–50] In our case, the high degree of cross-linking aids moderating the dynamics of the macromolecular network, enabling molecular sieving at high temperatures.

The $H_2$ permeances are in the range $2.3 \times 10^{-8}$ to $3.2 \times 10^{-7}$ mol m$^{-2}$ s$^{-1}$ Pa$^{-1}$ (69 to 943 GPU) at 260 °C. For all gasses, the permeance follows the order BPH-HCCP, DHPE-HCCP> DHBP-HCCP > BPS-HCCP > BAF-HCCP. Strikingly, the permselectivities are quite similar for all membranes. In Figure 4.5B, the permselectivity of $H_2/N_2$ is plotted versus temperature. The permselectivity of $H_2/CH_4$ is of a similar order as that of $H_2/N_2$ (Figure S4.8). The permselectivities decrease with temperature because the activation energies of the diffusion coefficients of larger molecules in rigid polymer matrices are generally larger. In the BPH, BHDP, and BPS-based membranes, the activation energies of the small $H_2$ and He are in the range 14.2-17.9 kJ/mol, while those of the bigger $N_2$ and $CH_4$ are in the range 21.3-23.7 kJ/mol (Figure S4.9, Table S4.6). These values are comparable to those of polyimide and poly(p-phenylene benzobisimidazole) membranes.[17,51] For the BPAF-based membrane, the values are somewhat lower. It should be noted that even at 260 °C the $H_2/N_2$ and $H_2/CH_4$ permselectivities of all membranes still exceed the value of 10, which is remarkable for polymer-based membranes. The permselectivities of $H_2/CO_2$ are in the range 2-10, which is lower as compared to the other gas pairs, and do not show a decrease with temperature. For $CO_2$ the energy of activation is relatively low because of the more pronounced dispersion interactions of this molecule with the polymer materials; the heat of sorption of the $CO_2$ will be larger and the slope of Arrhenius type temperature dependence of sorption has the opposite sign as compared to diffusion.
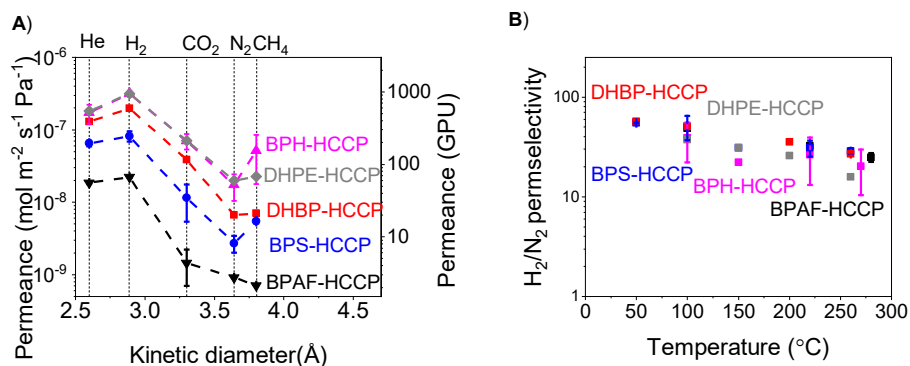
Figure 4.5 (A) Gas permeance as a function of gas kinetic diameter derived from BPH-HCCP, DHPE-HCCP, DHBP-HCCP, BPS-HCCP, and BAF-HCCP. All the measurements were done at a transmembrane pressure of 2 bar and a temperature of 260 °C. (B) The ideal $H_2/N_2$ permselectivity of the membranes as a function of temperature.

The similar activation energies and permselectivities of the membranes imply that differences in their permeance values result from differences in the morphology and thicknesses of the membranes, affecting the distances that the molecules must travel, rather than from distinct molecular structures of the materials, affecting the diffusion rate. SEM images reveal no substantial differences in thicknesses of the films atop the porous support structure that can explain the permeance differences. Likely, polymerization also occurs inside the small pores of the support, strongly reducing the permeance values. In classical interfacial processes, polymerization is known to occur predominantly in the non-polar phase rather than in the aqueous phase. By using DMSO instead of water, the location of the polymerization reaction may shift to the polar phase, resulting in a more pronounced growth in the pores of the support. The extent of film growth is strongly affected by the conditions of the process, impacting the evolution of reaction kinetics and transport kinetics during film formation. By increasing the amount of KOH, such effects can become evident.[52] When the KOH concentration is increased around twofold, the permeances of the gases decrease several orders of magnitude (Table S4.5). Compared to the lower KOH concentration, FE-SEM does not show any variations in the thickness atop ceramic supports, and XRF and CN analysis reveal a similar extent of cross-linking for freestanding films (Table S4.6, Table S4.7). This agrees

with the possibility of more pronounced growth into the porous structure. It is also observed that by lowering the KOH concentration, higher permeances can be achieved, but obtaining a defect-free thin film for these lower concentrations is more challenging.

The persisting permselectivities at 260 °C are exceptional. In Table 4.3, the performance of different membranes at elevated temperatures is summarized. As compared to the CPPz membranes, the very elegant Covalent Organic Nanosheet (CON)-based membranes[7] have higher permeance values up to 150 °C, but no data are available for their performance at higher temperatures. For temperatures exceeding 200 °C, the polyPOSSimide membranes [26,53] show comparable selectivity and lower permeances, while the polyPOSS-HCCP membranes[28] show similar permeance with about twofold higher permselectivity.

In contrast to the POSS-based membranes, the CCPz membranes are prepared from more inexpensive and more readily available monomers in a single step reaction. Also, the membranes lack the $C(sp^3)$ bond of the POSS-propyl group and have Ar-O-P rather than C-NH-P connections, providing inherently higher thermal stability. For the POSS-based membranes, the maximum application temperature is 300 °C.[28] Figure S4.10 and Figure S4.11 show that the permeance and permselectivity of the CCPz membranes is unaffected after the membranes have been exposed to 350 °C and 450 °C for 10 hours.

Table 4.3 Summary of the performance of different membranes

| Membrane material | Thickness (nm) | T(°C) | Analysis | $H_2$ permeance (GPU) | $H_2/CO_2$ | $H_2/N_2$ | Ref |
|---|---|---|---|---|---|---|---|
| PBDI[1] | 1300 | 100 | pure | 71.7 | 18.9 | 59.7 | [17] |
| PBI-Pd NPs | 800 | 200 | Mixture | 1.25 | 40 | - | [54] |
| TRP | 30000-40000 | 210 | Pure | 0.03 | 6.2 | - | [18] |
| CON | 41 | 150 | Pure | 2566 | 26.2 | 40.5 | [7] |
| 2D COF | 2000 | 200 | Mixture | ~5500 | 16 | - | [9] |
| MOFs (ZIF-8) | 20000 | 150 | Pure | 648 | 10.3 | 17.6 | [13] |
| PolyPOSS-imide | 100 | 250 | Pure | 600 | 5 | 10 | [26] |
| PolyPOSS-imide | 100 | 200 | Pure | 180 | 10 | 100 | [53] |
| Cross-linked PI | 15000 | 150 | Pure | ~7 | 10 | - | [55] |
| PI | 30000-50000 | 100 | Pure | $1.8 \times 10^{-10}$ | ~5.2 | 80 | [56] |
| POSS-HCCP | 78 | 250 | Pure | 1000 | 7.1 | 40 | [28] |
| BPH-HCCP | 20-30 | 260 | Pure | 950 | 4 | 20 | This work |
| BPS-HCCP | 20-30 | 260 | Pure | 300 | 8 | 30 | This work |

## 4.4 Conclusion

In conclusion, we have developed ultrathin (~20-30 nm) cyclomatrix poly(phenoxy)phosphazene membranes for the first time via interfacial polymerization using several biphenols including 4,4′-Dihydroxybiphenyl (BPH), 4,4′-dihydroxydiphenyl ether (DHPE), 4,4′-dihydroxybenzophenone (DHBP, Sigma-Aldrich), 4,4′-sulfonyldiphenol (BPS), 4,4′-(Hexafluoroisopropylidene)diphenol (BPAF), and hexachlorocyclotriphosphazene. The membranes are highly crosslinked, and thermally stable up to 450 ˚C. They show persisting molecular sieving behaviour up to 260 ˚C, which is the temperature limit of our sealings, with permselectivities of $H_2$ over $N_2$ and $CH_4$. The performance of the membranes remains unchanged after exposing them to 350 °C and 450 °C for 10 hours. There are currently very limited alternative polymer-based membranes that have comparable performance at this high temperature, and these require more complex and expensive fabrication. Our facile fabrication process allows for using monomers that cannot be used in conventional interfacial polymerizations, granting access to a broader assortment of membrane materials with the potential for industrial separations under harsh conditions.

## 4.5 Acknowledgement

## 4.6 References

[1] Y. Wang, H. Jin, Q. Ma, K. Mo, H. Mao, A. Feldhoff, X. Cao, Y. Li, F. Pan, Z. Jiang, A MOF Glass Membrane for Gas Separation, Angew. Chemie Int. Ed. 59 (2020) 4365–4369. https://doi.org/10.1002/anie.201915807.

[2] H. Fan, M. Peng, I. Strauss, A. Mundstock, H. Meng, J. Caro, MOF-in-COF molecular sieving membrane for selective hydrogen separation, Nat. Commun. 12 (2021) 38. https://doi.org/10.1038/s41467-020-20298-7.

[3] M.G. Schultz, Air Pollution and Climate-Forcing Impacts of a Global Hydrogen Economy, Science (80-. ). 302 (2003) 624–627. https://doi.org/10.1126/science.1089527.

[4] P. Kumar, D.W. Kim, N. Rangnekar, H. Xu, E.O. Fetisov, S. Ghosh, H. Zhang, Q. Xiao, M. Shete, J.I. Siepmann, T. Dumitrica, B. McCool, M. Tsapatsis, K.A. Mkhoyan, One-dimensional intergrowths in two-dimensional zeolite nanosheets and their effect on ultra-selective transport, Nat. Mater. 19 (2020) 443–449. https://doi.org/10.1038/s41563-019-0581-3.

[5] C. Kura, Y. Kunisada, E. Tsuji, C. Zhu, H. Habazaki, S. Nagata, M.P. Müller, R.A. De Souza, Y. Aoki, Hydrogen separation by nanocrystalline titanium nitride membranes with high hydride ion conductivity, Nat. Energy. 2 (2017) 786–794. https://doi.org/10.1038/s41560-017-0002-2.

[6] W.-H. Chen, Z.-Y. Chen, S. Lim, Y.-K. Park, P.-L. Show, Hydrogen permeation in a palladium membrane tube: Impacts of outlet and vacuum degree, Int. J. Hydrogen Energy. (2021). https://doi.org/10.1016/j.ijhydene.2021.07.182.

[7] Y. Ying, M. Tong, S. Ning, S.K. Ravi, S.B. Peh, S.C. Tan, S.J. Pennycook, D. Zhao, Ultrathin Two-Dimensional Membranes Assembled by Ionic Covalent Organic Nanosheets with Reduced Apertures for Gas Separation, J. Am. Chem. Soc. 142 (2020) 4472–4480. https://doi.org/10.1021/jacs.9b13825.

[8] L. Ding, Y. Wei, L. Li, T. Zhang, H. Wang, J. Xue, L.-X. Ding, S. Wang, J. Caro, Y. Gogotsi, MXene molecular sieving membranes for highly efficient gas separation, Nat. Commun. 9 (2018) 155. https://doi.org/10.1038/s41467-017-02529-6.

[9] H. Fan, M. Peng, I. Strauss, A. Mundstock, H. Meng, J. Caro, High-Flux Vertically Aligned 2D Covalent Organic Framework Membrane with Enhanced Hydrogen Separation, J. Am. Chem. Soc. 142 (2020) 6872–6877. https://doi.org/10.1021/jacs.0c00927.

[10] Y. S. Li, H. Bux, A. Feldhoff, G. L. Li, W.S. Yang, J. Caro, Controllable Synthesis of Metal-Organic Frameworks: From MOF Nanorods to Oriented MOF Membranes, Adv. Mater. 22 (2010) 3322–3326. https://doi.org/10.1002/adma.201000857.

[11] Y. S. Li, F.-Y. Liang, H. Bux, A. Feldhoff, W.S. Yang, J. Caro, Molecular Sieve Membrane: Supported Metal Organic Framework with High Hydrogen Selectivity, Angew. Chemie. 122 (2010) 558–561. https://doi.org/10.1002/ange.200905645.

[12] A. Huang, J. Caro, Covalent Post-Functionalization of Zeolitic Imidazolate Framework ZIF-90 Membrane for Enhanced Hydrogen Selectivity, Angew. Chemie Int. Ed. 50 (2011) 4979–4982. https://doi.org/10.1002/anie.201007861.

[13] Q. Liu, N. Wang, J. Caro, A. Huang, Bio-Inspired Polydopamine: A Versatile and Powerful Platform for Covalent Synthesis of Molecular Sieve Membranes, J. Am. Chem. Soc. 135 (2013) 17679–17682. https://doi.org/10.1021/ja4080562.

[14] M.A. Habib, A. Harale, S. Paglieri, F.S. Alrashed, A. Al-Sayoud, M.V. Rao, M.A. Nemitallah, S. Hossain, M. Hussien, A. Ali, M.A. Haque, A. Abuelyamen, M.R. Shakeel, E.M.A. Mokheimer, R. Ben-Mansour, Palladium-Alloy Membrane Reactors for Fuel Reforming and Hydrogen Production: A Review, Energy & Fuels. 35 (2021) 5558–5593. https://doi.org/10.1021/acs.energyfuels.0c04352.

[15] S. Yuan, X. Li, J. Zhu, G. Zhang, P. Van Puyvelde, B. Van der Bruggen, Covalent organic frameworks for membrane separation, Chem. Soc. Rev. 48 (2019) 2665–2681. https://doi.org/10.1039/C8CS00919H.

[16] Y. Jin, B. Gao, C. Bian, X. Meng, B. Meng, S.I. Wong, N. Yang, J. Sunarso, X. Tan, S. Liu, Elevated-temperature H 2 separation using a dense electron and proton mixed conducting polybenzimidazole-based membrane with 2D sulfonated graphene, Green Chem. 23 (2021) 3374–3385. https://doi.org/10.1039/D0GC04077K.

[17] M. Shan, X. Liu, X. Wang, Z. Liu, H. Iziyi, S. Ganapathy, J. Gascon, F. Kapteijn, Novel high performance poly( p -phenylene benzobisimidazole) (PBDI)

membranes fabricated by interfacial polymerization for $H_2$ separation, J. Mater. Chem. A. 7 (2019) 8929–8937. https://doi.org/10.1039/C9TA01524H.

[18] S.H. Han, H.J. Kwon, K.Y. Kim, J.G. Seong, C.H. Park, S. Kim, C.M. Doherty, A.W. Thornton, A.J. Hill, Á.E. Lozano, K.A. Berchtold, Y.M. Lee, Tuning microcavities in thermally rearranged polymer membranes for CO2 capture, Phys. Chem. Chem. Phys. 14 (2012) 4365. https://doi.org/10.1039/c2cp23729f.

[19] Y.S. Do, J.G. Seong, S. Kim, J.G. Lee, Y.M. Lee, Thermally rearranged (TR) poly(benzoxazole-co-amide) membranes for hydrogen separation derived from 3,3′-dihydroxy-4,4′-diamino-biphenyl (HAB), 4,4′-oxydianiline (ODA) and isophthaloyl chloride (IPCl), J. Memb. Sci. 446 (2013) 294–302. https://doi.org/10.1016/j.memsci.2013.06.059.

[20] L. Zhu, M.T. Swihart, H. Lin, Unprecedented size-sieving ability in polybenzimidazole doped with polyprotic acids for membrane H 2 /CO 2 separation, Energy Environ. Sci. 11 (2018) 94–100. https://doi.org/10.1039/C7EE02865B.

[21] Y. Zhuang, J.G. Seong, Y.S. Do, W.H. Lee, M.J. Lee, Z. Cui, A.E. Lozano, M.D. Guiver, Y.M. Lee, Soluble, microporous, Tröger's Base copolyimides with tunable membrane performance for gas separation, Chem. Commun. 52 (2016) 3817–3820. https://doi.org/10.1039/C5CC09783E.

[22] K. Mizrahi Rodriguez, S. Lin, A.X. Wu, G. Han, J.J. Teesdale, C.M. Doherty, Z.P. Smith, Leveraging Free Volume Manipulation to Improve the Membrane Separation Performance of Amine-Functionalized PIM-1, Angew. Chemie Int. Ed. 60 (2021) 6593–6599. https://doi.org/10.1002/anie.202012441.

[23] J. Lee, J.S. Kim, S. Moon, C.Y. Park, J.F. Kim, Y.M. Lee, Dimensionally-controlled densification in crosslinked thermally rearranged (XTR) hollow fiber membranes for CO2 capture, J. Memb. Sci. 595 (2020) 117535. https://doi.org/10.1016/j.memsci.2019.117535.

[24] D. Lin, Y. Liu, Z. Jia, S. Qi, D. Wu, Structural Evolution of Macromolecular Chain During Pre-imidization Process and Its Effects on Polyimide Film Properties, J. Phys. Chem. B. 124 (2020) 7969–7978. https://doi.org/10.1021/acs.jpcb.0c05146.

[25] S. Kim, J. Hou, Y. Wang, R. Ou, G.P. Simon, J.G. Seong, Y.M. Lee, H. Wang, Highly permeable thermally rearranged polymer composite membranes with a graphene oxide scaffold for gas separation, J. Mater. Chem. A. 6 (2018) 7668–7674. https://doi.org/10.1039/C8TA02256A.

[26] M.J.T. Raaijmakers, M.A. Hempenius, P.M. Schön, G.J. Vancso, A. Nijmeijer, M. Wessling, N.E. Benes, Sieving of Hot Gases by Hyper-Cross-Linked Nanoscale-Hybrid Membranes, J. Am. Chem. Soc. 136 (2014) 330–335. https://doi.org/10.1021/ja410047u.

[27] E. Maaskant, H. Gojzewski, M.A. Hempenius, G.J. Vancso, N.E. Benes, Thin cyclomatrix polyphosphazene films: interfacial polymerization of hexachlorocyclotriphosphazene with aromatic biphenols, Polym. Chem. 9 (2018) 3169–3180. https://doi.org/10.1039/C8PY00444G.

[28] F. Radmanesh, M.G. Elshof, N.E. Benes, Polyoctahedral Silsesquioxane Hexachlorocyclotriphosphazene Membranes for Hot Gas Separation, ACS Appl. Mater. Interfaces. 13 (2021) 8960–8966. https://doi.org/10.1021/acsami.0c21968.

[29] P. Mohanty, L.D. Kull, K. Landskron, Porous covalent electron-rich organonitridic frameworks as highly selective sorbents for methane and carbon dioxide, Nat. Commun. 2 (2011) 401. https://doi.org/10.1038/ncomms1405.

[30] A.-M. Caminade, A. Hameau, J.-P. Majoral, The specific functionalization of cyclotriphosphazene for the synthesis of smart dendrimers, Dalt. Trans. 45 (2016) 1810–1822. https://doi.org/10.1039/C5DT03047A.

[31] M. Zhang, Y. Li, C. Bai, X. Guo, J. Han, S. Hu, H. Jiang, W. Tan, S. Li, L. Ma, Synthesis of Microporous Covalent Phosphazene-Based Frameworks for Selective Separation of Uranium in Highly Acidic Media Based on Size-Matching Effect, ACS Appl. Mater. Interfaces. 10 (2018) 28936–28947. https://doi.org/10.1021/acsami.8b06842.

[32] X. Guo, Y. Li, M. Zhang, K. Cao, Y. Tian, Y. Qi, S. Li, K. Li, X. Yu, L. Ma, Colyliform Crystalline 2D Covalent Organic Frameworks (COFs) with Quasi-3D Topologies for Rapid $I_2$ Adsorption, Angew. Chemie. 132 (2020) 22886–22894. https://doi.org/10.1002/ange.202010829.

[33] X. Wei, D. Zheng, M. Zhao, H. Chen, X. Fan, B. Gao, L. Gu, Y. Guo, J. Qin, J. Wei, Y. Zhao, G. Zhang, Cross-Linked Polyphosphazene Hollow Nanosphere-Derived N/P-Doped Porous Carbon with Single Nonprecious Metal Atoms for the Oxygen Reduction Reaction, Angew. Chemie Int. Ed. 59 (2020) 14639–14646. https://doi.org/10.1002/anie.202006175.

[34] X. Wei, D. Zheng, M. Zhao, H. Chen, X. Fan, B. Gao, L. Gu, Y. Guo, J. Qin, J. Wei, Y. Zhao, G. Zhang, Cross-Linked Polyphosphazene Hollow

Nanosphere-Derived N/P-Doped Porous Carbon with Single Nonprecious Metal Atoms for the Oxygen Reduction Reaction, Angew. Chemie. 132 (2020) 14747–14754. https://doi.org/10.1002/ange.202006175.

[35] R. Jiang, B. Deng, L. Pi, L. Hu, D. Chen, Y. Dou, X. Mao, D. Wang, Molten Electrolyte-Modulated Electrosynthesis of Multi-Anion Mo-Based Lamellar Nanohybrids Derived from Natural Minerals for Boosting Hydrogen Evolution, ACS Appl. Mater. Interfaces. 12 (2020) 57870–57880. https://doi.org/10.1021/acsami.0c17137.

[36] L. Zhu, X. Huang, X. Tang, One-Pot Synthesis of Novel Poly(cyclotriphosphazene- co -sulfonyldiphenol) Microtubes without External Templates, Macromol. Mater. Eng. 291 (2006) 714–719. https://doi.org/10.1002/mame.200600015.

[37] M. You, W. Li, Y. Pan, P. Fei, H. Wang, W. Zhang, L. Zhi, J. Meng, Preparation and characterization of antibacterial polyamine-based cyclophosphazene nanofiltration membranes, J. Memb. Sci. 592 (2019) 117371. https://doi.org/10.1016/j.memsci.2019.117371.

[38] R.J. Mayer, M. Breugst, N. Hampel, A.R. Ofial, H. Mayr, Ambident Reactivity of Phenolate Anions Revisited: A Quantitative Approach to Phenolate Reactivities, J. Org. Chem. 84 (2019) 8837–8858. https://doi.org/10.1021/acs.joc.9b01485.

[39] A.S. Bobkov, N.M. Vitkovskaya, B.A. Trofimov, Cascade Assembly of 4,5,6,7-Tetrahydroindole from Cyclohexanone Oxime and Acetylene in the KOH/DMSO Superbase Medium: A Quantum Chemical Study, J. Org. Chem. 85 (2020) 6463–6470. https://doi.org/10.1021/acs.joc.0c00353.

[40] N. N. Tian, L.-S. Wang, M.-Y. Li, Y. Li, R.-Y. Jiang, Solubilities of Phenylphosphinic Acid, Methylphenylphosphinic Acid, Hexachlorocyclotriphosphazene, and Hexaphenoxycyclotriphosphazene in Selected Solvents, J. Chem. Eng. Data. 56 (2011) 661–670. https://doi.org/10.1021/je1009812.

[41] M. Sunitha, C.. Reghunadhan Nair, K. Krishnan, K. Ninan, Kinetics of Alder-ene reaction of Tris(2-allylphenoxy)triphenoxycyclotriphosphazene and bismaleimides — a DSC study, Thermochim. Acta. 374 (2001) 159–169. https://doi.org/10.1016/S0040-6031(01)00502-0.

[42] H.R. Allcock, C. Chen, Polyphosphazenes: Phosphorus in Inorganic–Organic Polymers, J. Org. Chem. 85 (2020) 14286–14297. https://doi.org/10.1021/acs.joc.0c01710.

[43] A.M. Turner, A. Bergantini, M.J. Abplanalp, C. Zhu, S. Góbi, B.-J. Sun, K.-H. Chao, A.H.H. Chang, C. Meinert, R.I. Kaiser, An interstellar synthesis of phosphorus oxoacids, Nat. Commun. 9 (2018) 3851. https://doi.org/10.1038/s41467-018-06415-7.

[44] H.R. Allcock, A.A. Dembek, J.L. Bennett, I. Manners, M. Parvez, Synthesis and structure of phosphazene(.eta.6-arene)chromium tricarbonyl derivatives, Organometallics. 10 (1991) 1865–1874. https://doi.org/10.1021/om00052a036.

[45] R.C. Dutta, S.K. Bhatia, Atomistic Investigation of Mixed-Gas Separation in a Fluorinated Polyimide Membrane, ACS Appl. Polym. Mater. 1 (2019) 1359–1371. https://doi.org/10.1021/acsapm.9b00146.

[46] Z. Liu, Y. Liu, W. Qiu, W.J. Koros, Molecularly Engineered 6FDA-Based Polyimide Membranes for Sour Natural Gas Separation, Angew. Chemie. 132 (2020) 14987–14993. https://doi.org/10.1002/ange.202003910.

[47] X. Zhou, S. Qiu, W. Xing, C.S.R. Gangireddy, Z. Gui, Y. Hu, Hierarchical Polyphosphazene@Molybdenum Disulfide Hybrid Structure for Enhancing the Flame Retardancy and Mechanical Property of Epoxy Resins, ACS Appl. Mater. Interfaces. 9 (2017) 29147–29156. https://doi.org/10.1021/acsami.7b08878.

[48] Z. Wang, Y. Zhang, C. Wang, X. Zheng, Y. Zheng, L. Gao, C. Yang, Y. Li, L. Qu, Y. Zhao, Color-Tunable Polymeric Long-Persistent Luminescence Based on Polyphosphazenes, Adv. Mater. 32 (2020) 1907355. https://doi.org/10.1002/adma.201907355.

[49] A.K. Sekizkardes, V.A. Kusuma, J.S. McNally, D.W. Gidley, K. Resnik, S.R. Venna, D. Hopkinson, Microporous polymeric composite membranes with advanced film properties: pore intercalation yields excellent $CO_2$ separation performance, J. Mater. Chem. A. 6 (2018) 22472–22477. https://doi.org/10.1039/C8TA07424K.

[50] H.R. Allcock, Polyphosphazenes: New Polymers with Inorganic Backbone Atoms, Science (80-. ). 193 (1976) 1214–1219. https://doi.org/10.1126/science.193.4259.1214.

126

[51] S. Escorihuela, A. Tena, S. Shishatskiy, S. Escolástico, T. Brinkmann, J. Serra, V. Abetz, Gas Separation Properties of Polyimide Thin Films on Ceramic Supports for High Temperature Applications, Membranes (Basel). 8 (2018) 16. https://doi.org/10.3390/membranes8010016.

[52] H.-S. Wu, S.-S. Meng, Effect of NaOH concentration on a sequential phosphazene reaction by phase-transfer catalysis, Chem. Eng. Sci. 53 (1998) 4073–4084. https://doi.org/10.1016/S0009-2509(98)00207-3.

[53] M.J.T. Raaijmakers, M. Wessling, A. Nijmeijer, N.E. Benes, Hybrid Polyhedral Oligomeric Silsesquioxanes–Imides with Tailored Intercage Spacing for Sieving of Hot Gases, Chem. Mater. 26 (2014) 3660–3664. https://doi.org/10.1021/cm500691e.

[54] L. Zhu, D. Yin, Y. Qin, S. Konda, S. Zhang, A. Zhu, S. Liu, T. Xu, M.T. Swihart, H. Lin, Sorption-Enhanced Mixed Matrix Membranes with Facilitated Hydrogen Transport for Hydrogen Purification and CO 2 Capture, Adv. Funct. Mater. 29 (2019) 1904357. https://doi.org/10.1002/adfm.201904357.

[55] M. Omidvar, C.M. Stafford, H. Lin, Thermally stable cross-linked P84 with superior membrane H2/CO2 separation properties at 100 °C, J. Memb. Sci. 575 (2019) 118–125. https://doi.org/10.1016/j.memsci.2019.01.003.

[56] O.C. David, D. Gorri, A. Urtiaga, I. Ortiz, Mixed gas separation study for the hydrogen recovery from $H_2/CO/N_2/CO_2$ post combustion mixtures using a Matrimid membrane, J. Memb. Sci. 378 (2011) 359–368. https://doi.org/10.1016/j.memsci.2011.05.029.

## 4.7 Supporting information

In Figure S4.1, the interfacial polymerization reaction is visualized. An aromatic diphenol is dissolved in DMSO/KOH solution to convert biphenol into potassium phenoxide. Subsequently, it reacts with the HCCP solution in cyclohexane. The layer forms at the interphase of the two solvents.
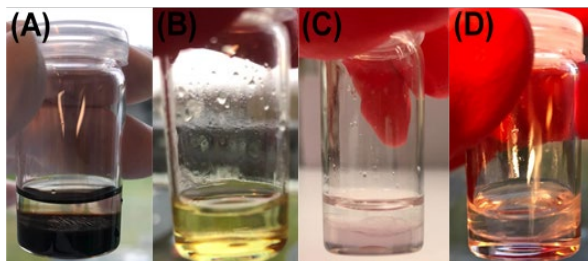


Figure S4.1 Free-standing film of poly(phenoxy) phosphazenes (A) DHPE-HCCP, (B) DHBP-HCCP, (C) BPS-HCCP, and (D) BPAF-HCCP.

Figure S4.2 shows the topographical AFM characterization of (A) Alumina support, (B) BPH-HCCP, (C) DHPE-HCCP, (D) DHBP-HCCP, (E) BPS-HCCP, and (F) BPAF-HCCP.
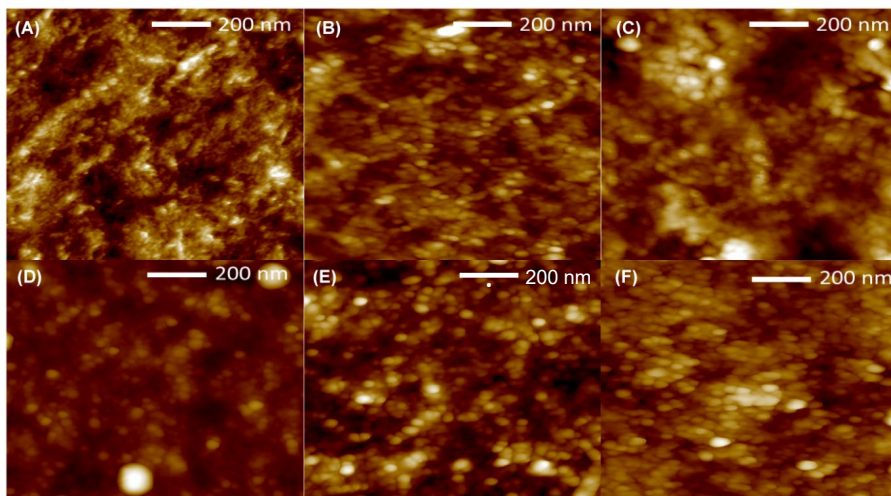


Figure S4.2 Topographical AFM images probed for (A) alumina support, (B) BPH-HCCP, (C) DHPE-HCCP, (D) DHBP-HCCP, (E) BPS-HCCP, and (F) BPAF-HCCP.

In Table S4.1, roughness of all samples calculated from AFM analysis is shown. Despite the type of used diphenols, all samples appear to have similar roughness compared to untreated alumina support.

Table S4.1 The surface roughness of  (A) alumina support, (B) BPH-HCCP, (C) DHPE-HCCP, (D) DHBP-HCCP, (E) BPS-HCCP, and (F) BPAF-HCCP

| Sample | Alumina support | BPH-HCCP | DHPE-HCCP | DHBP-HCCP | BPS-HCCP | BPAF-HCCP |
|---|---|---|---|---|---|---|
| $R_a$(nm) | 4.16±0.1 | 2.5±0 | 4.8±0.7 | 4±0.6 | 3.5±0.1 | 3.8±1 |
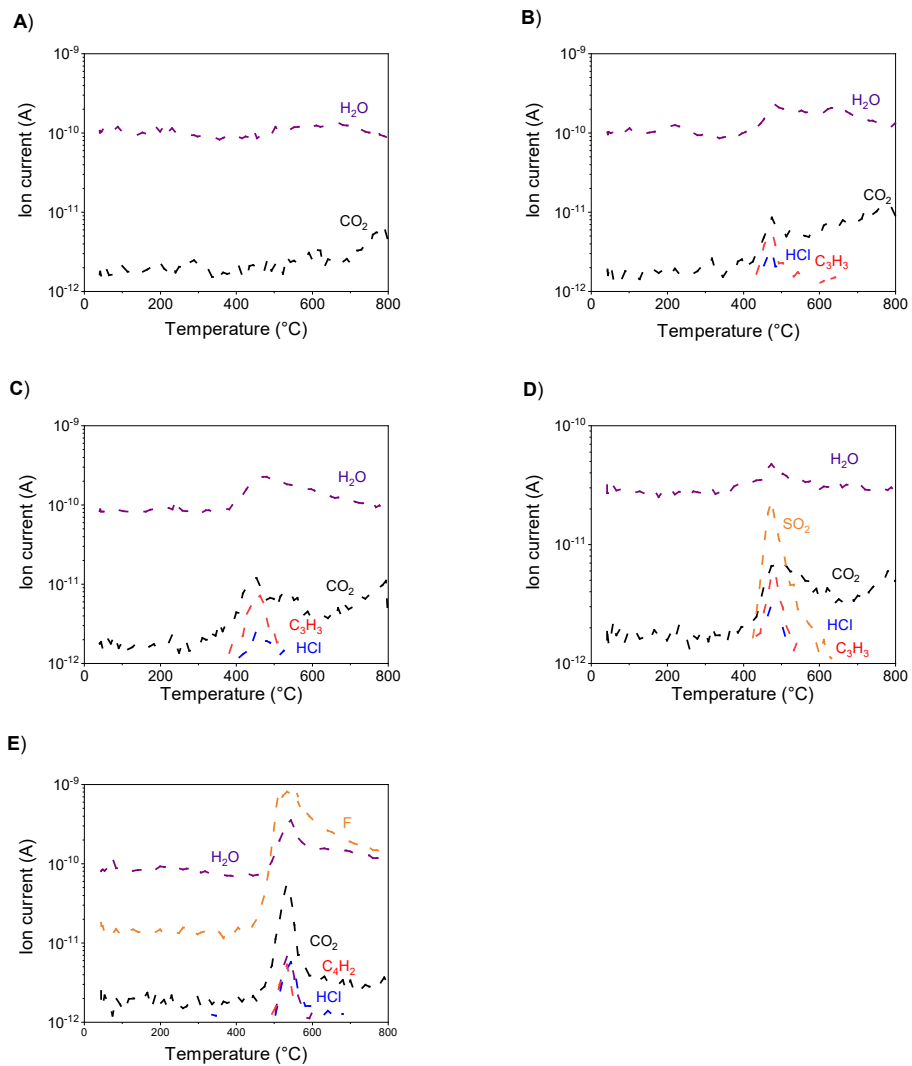
Figure S4.3 Selected MS data for synthesized networks (A)BPH-HCCP, (B) DHPE-HCCP, (C) DHBP-HCCP, (D) BPS-HCCP, and (E) BPAF-HCCP.

Table S4.2 EDX elemental analysis (%) of free-standing films before TGA analysis.

| Element | BPH-HCCP | DHPE-HCCP | DHBP-HCCP | BPAF-HCCP |
|---------|----------|-----------|-----------|-----------|
| C | 74.6±1.2 | 71.5±0.6 | 72.3±3.2 | 62.2±1.7 |
| P | 5±0.4 | 5.4±0.2 | 6.1±1 | 8.1±2.8 |
| N | 3.1±0.4 | 4.1±0.4 | 4±0.3 | 4.3±0 |
| S | 1.1±0.1 | 0.9±0.1 | 0.8±0.2 | 2.1±0.9 |
| F | 0 | 0 | 0 | 14.7±0 |
| Cl | 0.8±0.1 | 1±0.1 | 0.5±0.1 | 1±0.5 |
| C/P | 14.9±1.2 | 13.2±0.5 | 11.9±2 | 7.7±2.7 |

Table S4.3 EDX elemental analysis (%) of free-standing films after TGA analysis up to 800 °C.

| Element | BPH-HCCP | DHPE-HCCP | DHBP-HCCP | BPAF-HCCP |
|---------|----------|-----------|-----------|-----------|
| C | 81.9±0.3 | 78.2±1.7 | 79.6±1.4 | 89.2±1.7 |
| P | 7.4±0.4 | 11.4±3 | 6.5±1.5 | 1.1±0 |
| N | 0 | 0 | 0 | 0 |
| S | 0.4±0.1 | 0 | 0 | 2.3±0.1 |
| F | 0 | 0 | 0 | 0 |
| Cl | 0 | 0 | 0 | 0 |
| C/P | 11.1±0.6 | 6.8±1.8 | 12.2±2.6 | 81.1±1.5 |
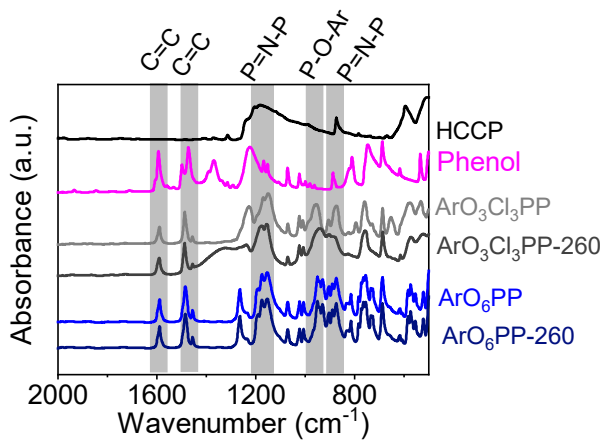
Figure S4.4 FTIR spectra of the reactants (HCCP and phenol), and model materials, hexaphenoxycyclotriphosphazene (ArO$_6$PP) and triphenoxy trichlorocycoltriphosphazene (ArO$_3$Cl$_3$PP)), before and after heat treatment at 260 ˚C for 10 hr under N$_2$.

A)



8.73
8.73
8.72
8.48

A (m)
8.72

$^{31}$P NMR (162 MHz, Chloroform-*d*) δ 8.82 − 8.63 (m).

3.00

18  16  14  12  10  8  6  4  2  0  -2  -4  -6  -8  -10  -12  -14  -16  -18  -20
f1 (ppm)

B)



18  16  14  12  10  8  6  4  2  0  -2  -4  -6  -8  -10  -12  -14  -16  -18  -20
f1 (ppm)
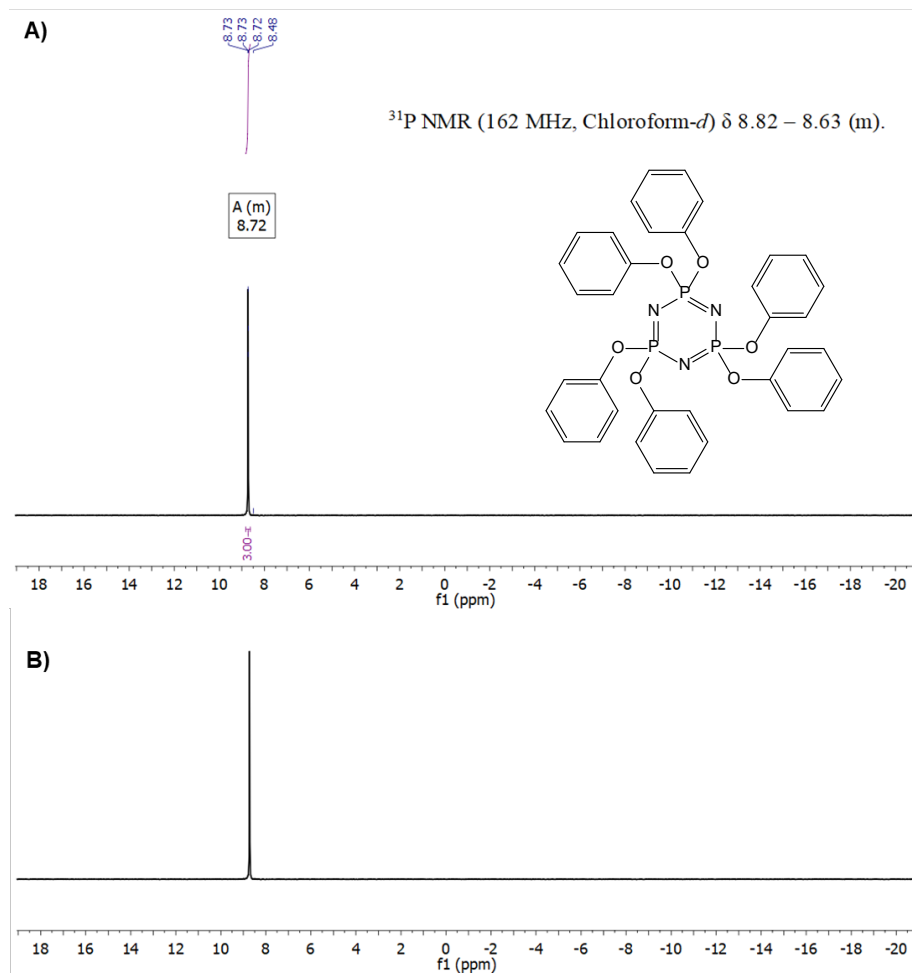
Figure S4.5 $^{31}$P liquid NMR spectrum (162 MHz) of ArO₆PP in Chloroform-d. (A) before heat treatment (B) after heat treatment at 260 °C under N₂ for 10 h. Both spectra show δ 8.82 – 8.63 (m).

**A)**



**B)**
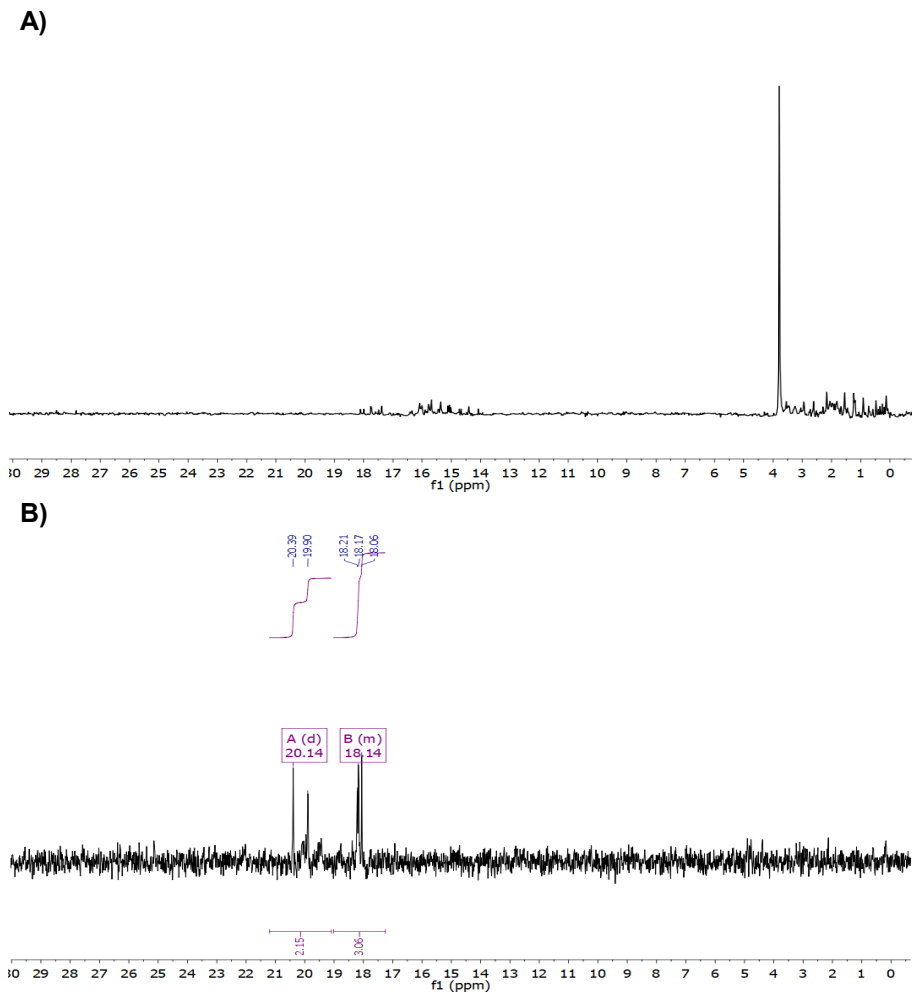


Figure S4.6 $^{31}$P liquid NMR spectrum (162 MHz) of ArO$_3$Cl$_3$PP in Chloroform-d, (A) before heat treatment. δ 16.13, 15.76 (d, J = 14.8 Hz), 15.57 – 15.31 (m), 15.15, 3.82, 3.53 (d, J = 14.3 Hz), 3.28, 2.65, 2.40 – 1.95 (m), 1.90, 1.64 (d, J = 18.5 Hz), 1.27, 1.18 – 0.07 (m), and (B) after heat treatment at 260 °C under N2 for 10 h. δ 20.14 (d, J = 80.6 Hz), 19.01 – 17.25 (m).
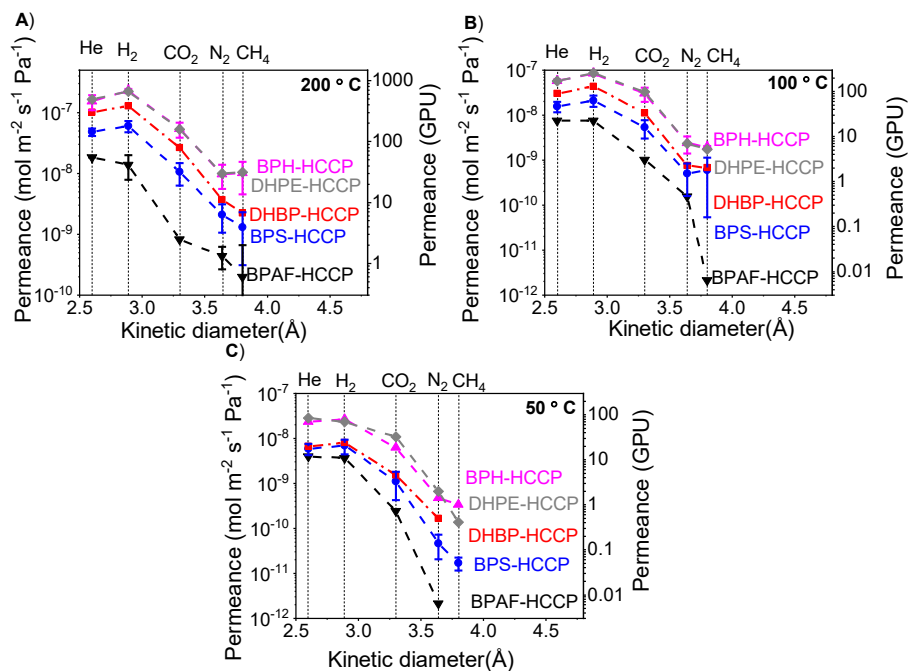
Figure S4.7 Single gas permeance at several temperatures as a function of gas kinetic diameter derived from BPH-HCCP, DHPE-HCCP, DHBP-HCCP, BPS-HCCP, and BPAF-HCCP with molar ratio of biphenol : KOH of 0.75. All the measurements were done at a transmembrane pressure of 2 bar. (A) 200 °C (B) 100 °C (C) 50 °C.
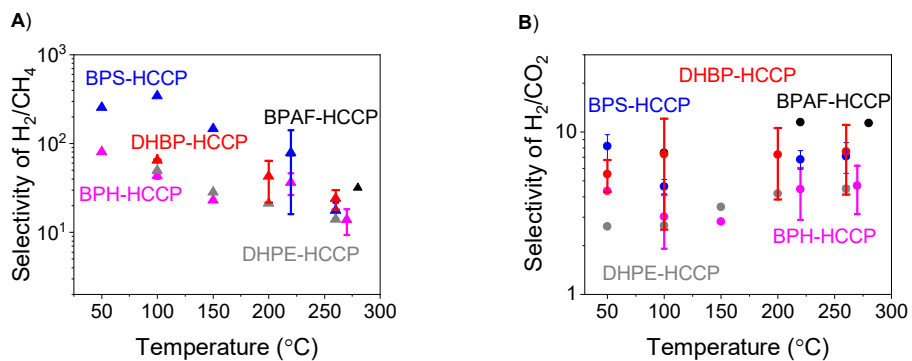
Figure S4.8 Permselectivity as a function of temperature for BPH-HCCP, DHPE-HCCP, DHBP-HCCP, BPS-HCCP, and BAF-HCCP. All the measurements were done at transmembrane pressure of 2 bar, (A) $H_2/CH_4$ (B) $H_2/CO_2$.
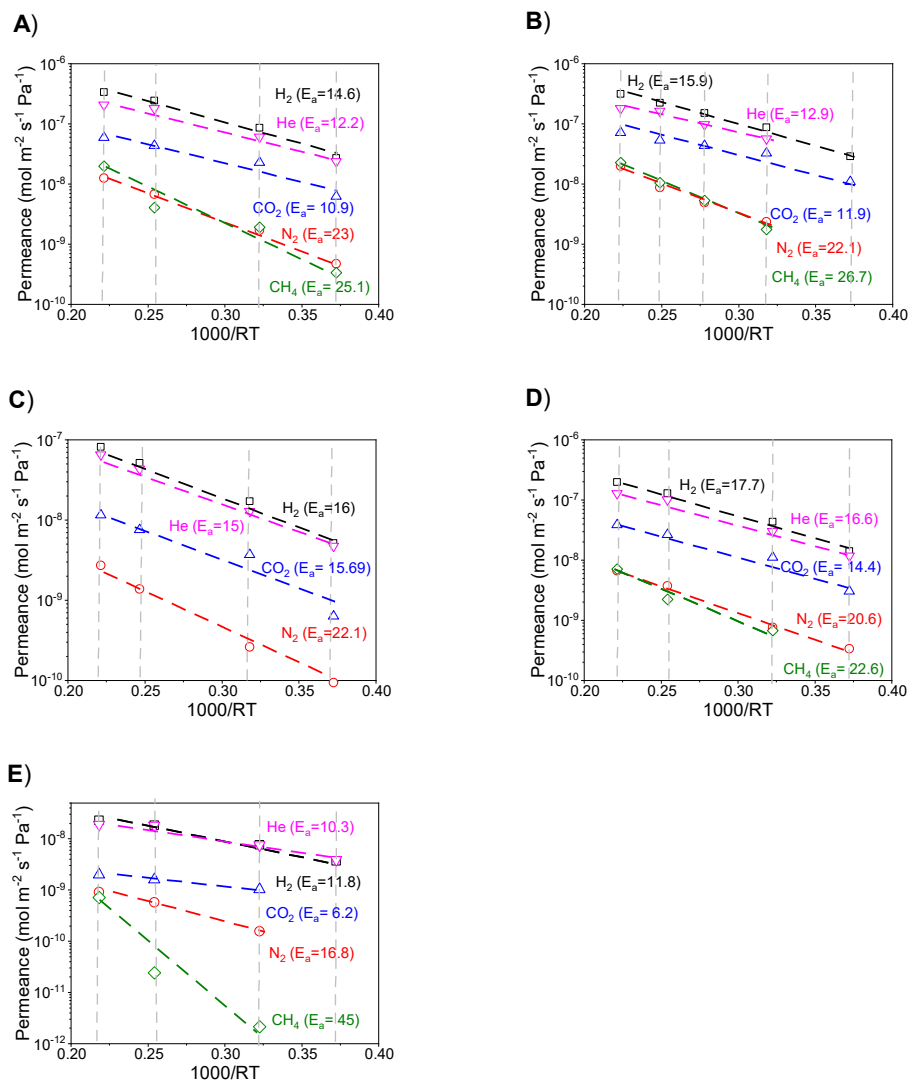
Figure S4.9 Arrhenius plot for (A) BPH-HCCP, (B) DHPE-HCCP, (C) BPS-HCCP, (D), DHBP-HCCP and E) BPAF-HCCP. The detection limit of the set-up is $1\times10^{-10}$ mol m$^{-2}$ s$^{-1}$ Pa$^{-1}$. The activation energies are shown in kJ mol$^{-1}$.

Table S4.4 Calculated Arrhenius activation energies (kJ mol$^{-1}$) for synthesized membranes in the temperature range of 50-260 °C.

| Gas | BPH-HCCP | DHPE-HCCP | DHBP-HCCP | BPS-HCCP | BPAF-HCCP |
|---|---|---|---|---|---|
| He | 12.2±2.8 | 12.9 | 16.6 | 15±2.1 | 11.8 |
| H$_2$ | 14.6±3.7 | 15.9 | 17.7 | 16±1.5 | 10.3 |
| CO$_2$ | 10.9±3 | 11.9 | 14.4 | 15.6±3.3 | 6.2 |
| N$_2$ | 23±1.3 | 22.1 | 20.6 | 19.5+2.2 | 16.8 |
| CH$_4$ | 25.1±1.9 | 26.7 | 22.6 | 25.6±4.3 | 45 |

Table S4.5 The single gas permeances and corresponding permselectivity of membranes with with molar ratio of biphenol : KOH of 0.5.

| Membrane | P$_{H2}$ (GPU) | P$_{CO2}$ (GPU) | P$_{N2}$ (GPU) | P$_{CH4}$ (GPU) | H$_2$/CO$_2$ | H$_2$/N$_2$ | H$_2$/CH$_4$ |
|---|---|---|---|---|---|---|---|
| BPH-HCCP | 35.4 | 0.7 | 1.19 | 1.12 | 49.5 | 29.7 | 31.7 |
| DHPE-HCCP | 5.8 | 0* | 0.2* | 0.1* | | | |
| BPAF-HCCP | 32.5 | 0* | 1* | 0.2* | | | |

* Permeances are lower than the detection limit of the set-up.

138

Table S4.6 Elemental concentration (%) for poly(phenoxy)phosphazenes free-standing films with molar ratio of biphenol : KOH of 0.5.

| Element | BPH-HCCP | DHPE-HCCP | DHBP-HCCP | BPS-HCCP | BPAF-HCCP |
|---|---|---|---|---|---|
| P | 56.7±1 | 56.9±0.9 | 62.9±0.8 | 27.8±0.9 | 39.6±1.1 |
| Cl | 4.9±1.3 | 7.5±3.1 | 9.1±3.1 | 2.4±5.5 | 16.5±2.2 |
| S | 0.5±0 | 15±1.7 | 5.4±3.1 | 56.6±0.6 | 12.4±1.4 |
| K | 35.8±1.3 | 19.7±1.6 | 21.8±1.6 | 12.8±1.7 | 21.4±1.7 |
| P/Cl | 11.6±0.1 | 7.5±3.1 | 6.9±2.4 | 11.6±26 | 2.4±1.3 |
| Number of Cl per HCCP | 0.3 | 0.4 | 0.4 | 0.3 | 1.3 |

Table S4.7 CN elemental analysis(%) for poly(phenoxy)phosphazenes free-standing films with  with molar ratio of biphenol : KOH of 0.5.

| Element | BPH-HCCP | DHPE-HCCP | DHBP-HCCP | BPS-HCCP | BPAF-HCCP |
|---|---|---|---|---|---|
| C | 40.8±0.6 | 44.7±1.3 | 54.7±0 | 46±0.1 | 39.6±1.6 |
| N | 2.9±0 | 3.7±0 | 4±0 | 3.5±0 | 2.9±0.2 |
| C/N | 14.1±0.2 | 12.1±0.4 | 14.4±0 | 13.1±0 | 13.7±1.1 |
| Reacted Cl per HCCP | 3.5±0.1 | 3±0.1 | 3.2 | 3.3 | 2.7±0.2 |
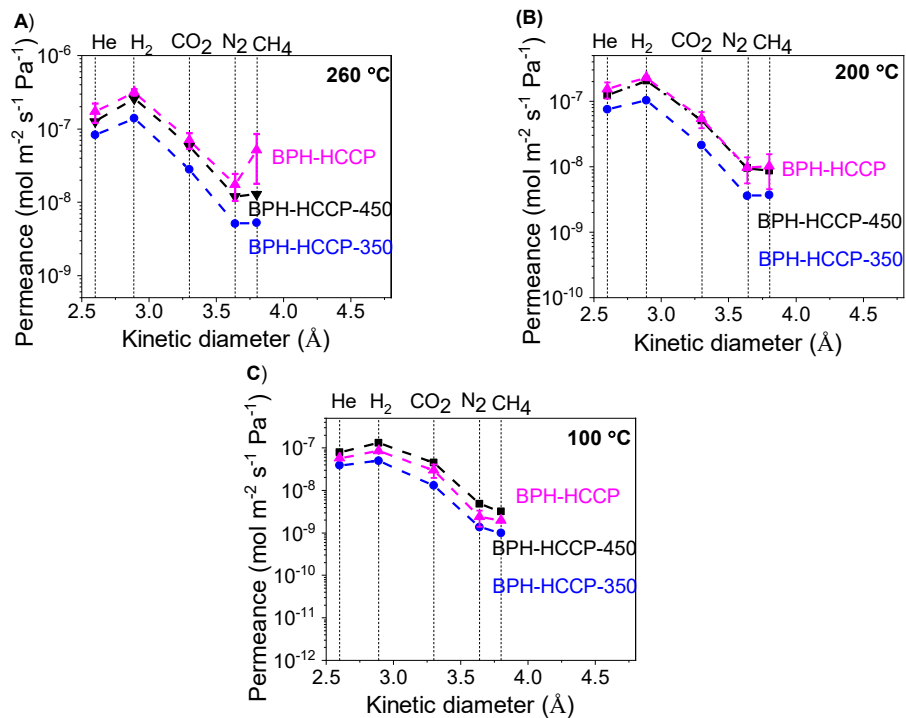
Figure S4.10 Gas permeance (y-axis) vs. kinetic diameter (x-axis) for BPH-HCCP membranes at (A) 250 °C, (B) 200 °C, and (C) 100 °C before and after exposure to 350 °C and 450 °C. Only the data at 250, 200 and 100 °C is given.
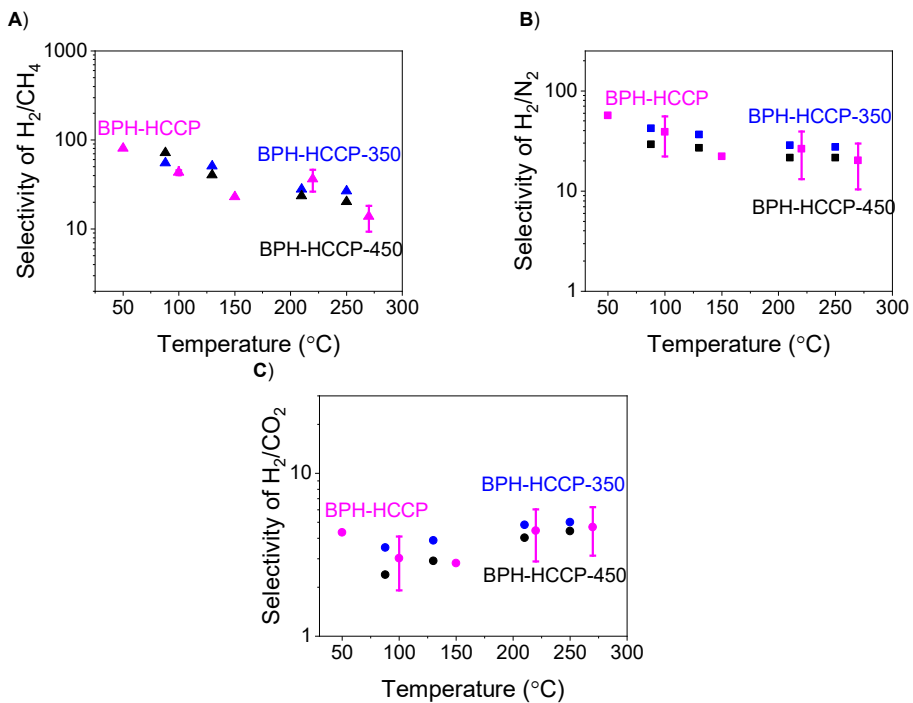
Figure S4.11 Ideal selectivity (y-axis) vs. Temperature (x-axis) for BPH-HCCP membranes before and after exposure to 350 °C and 450 °C. Only the data at 250, 200 and 100 °C is given.

# Chapter 5

# Non-aqueous interfacial polymerization derived polyphosphazene films for sieving or blocking hydrogen gas
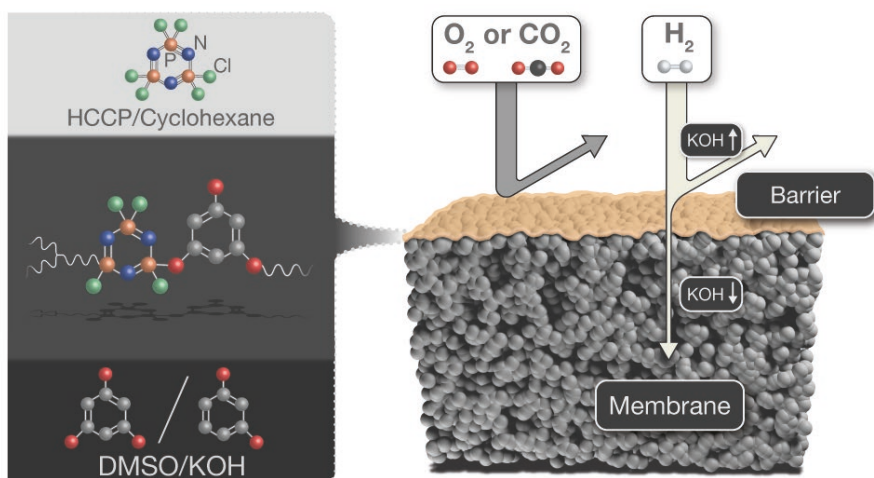
# Abstract

A series of cyclomatrix polyphosphazene films have been prepared by non-aqueous interfacial polymerization of small aromatic hydroxyl compounds in a potassium hydroxide dimethylsulfoxide solution and hexachlorocyclotriphosphazene in cyclohexane, on top of ceramic supports. Via the amount of dissolved potassium hydroxide, the extent of deprotonation of the aromatic hydroxyl compounds can be changed, in turn affecting the molecular structure and permselective properties of the thin polymer networks ranging from hydrogen/oxygen barriers to membranes with persisting hydrogen permselectivities at high temperatures. Barrier films are obtained with high potassium hydroxide concentration, revealing permeabilities as low as $9.4 \times 10^{-17}$ cm$^3$ cm cm$^{-2}$ s$^{-1}$ Pa$^{-1}$ for hydrogen and $1.1 \times 10^{-16}$ cm$^3$ cm cm$^{-2}$ s$^{-1}$ Pa$^{-1}$ for oxygen. For films obtained with a lower concentration of potassium hydroxide single gas permeation experiments reveal a molecular sieving behavior, with a hydrogen permeance around $10^{-8}$ mol m$^{-2}$ s$^{-1}$ Pa$^{-1}$ and permselectivities of H$_2$/N$_2$ (52.8), H$_2$/CH$_4$ (100), and H$_2$/CO$_2$ (10.1), at 200 °C.

# 5.1 Introduction

Interfacial polymerization (IP) is a versatile and robust technique for synthesizing functional polymers in diverse forms, including nanofibers, capsules, and ultra-thin polymer films.[1,2] In conventional IP, a polycondensation reaction takes place at the interface between two immiscible solvents. Because both of the solvents contain only one of the two highly reactive monomers for the reaction, the reaction is localized to the vicinity of the interface.[3] The film formation is affected by an intricate interplay of reaction and diffusion of the monomers. A variety of options exist to tune the morphologies and chemistries of the films that are formed, for instance, via the choice and concentrations of the monomers, the temperature, the duration of contact between the solutions, etc.

One of the key factors affecting the IP process is the selection of the solvents.[4–8] For thin film synthesis, and in particular for thin film composite membranes, generally water and an organic solvent are used. By varying the organic solvent and adding co-solvents to the aqueous phase, nanofilms with the desired properties can be obtained.[4–8] The number of studies in which water is substituted by an organic solvent is limited.[9–12] Wamser et al. showed the formation of various polyamide porphyrin films at the interface of dimethylsulfoxide (DMSO)/ chloroform and dimethylsulfoxide (DMSO)/ ethyl acetate.[9] Ogata et al. reported IP in non-aqueous systems to be useful for synthesizing aromatic polyesters and copolyesters.[10] Hessbrugge and Vaidya demonstrated the formation of highly solvent-resistant polyamide coatings at the interface of salt crystals at 7 °C.[11] Liu et al. presented IP at an alkane/ionic liquid interface to synthesize selective polyamide nanofilm membranes.[12] These studies concentrate on polyamides and polyesters; to our knowledge, no attempts have been made to expand non-aqueous IP to other chemistries, except for our recent works on POSS and poly(phenoxy) cyclomatrix phosphazenes.[13,14]

These hybrid materials comprise unsaturated rings of alternating phosphor and nitrogen atoms that are covalently connected via diphenyl oxide bridges. The organic phase monomer used in the IP process is

hexachlorocyclotriphosphazene (HCCP), a versatile building block for making polyphosphazene-based materials via reactions with a broad range of nucleophiles.[15,16] The cyclic phosphazene group offers extraordinary intrinsic properties, such as natural flame retardancy and thermal stability.[17] Most of the preparation methods involving HCCP are based on solution polymerization, and only a few studies have been dedicated to synthesizing polyphosphazene films with IP.[13–16,18] Maaskant et al. reported that the interfacial polycondensation of HCCP with diphenols in conventional IP is too slow to allow for ultrathin (~$10^8$ m) film formation. In our previous work, we replaced the water phase with a solution of KOH in dimethylsulfoxide (DMSO).[14] DMSO is a polar aprotic solvent that is immiscible with organic solvents such as cyclohexane and, in addition, facilitates nucleophilic reactions between monomers. In the solution of KOH in DMSO, the diphenols are (partly) deprotonated and become very soluble and reactive nucleophilic aryloxide anions, enabling the formation of ultrathin polymer films that have molecular sieving ability at very high temperatures.
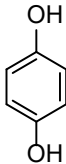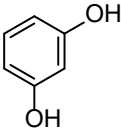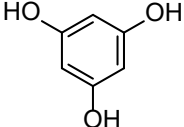
Here, we further explore the potential of non-aqueous IP for tailoring polyphosphazene films by exchanging the diphenols for the smaller aromatic hydroxy compounds (AHCs) *p*-dihydroxybenzene (PDHB) and *m*-dihydroxybenzene (MDHB), and 1,3,5-trihydroxybenzene (THB), see Table 5.1. These AHCs are planar molecules with the OH protons slightly out of the plane of the phenyl ring.[19] AHCs are affordable and easily accessible, but they show low solubility in water. Similar to diphenols, AHCs are highly soluble in DMSO, and their hydroxyl groups can be converted into anions by adding a strong base such as KOH. The structures of AHCs allow us to synthesize a tightly packed polyphosphazene network, and the adjustable parameters of IP, such as the molar ratio of hydroxyl groups of monomer to the base, provide opportunities to tune the film morphology and cover the range of applications.

Several studies have shown the potential of THB and PDHB to react with HCCP in a single solvent and form microspheres and microtubes.[20–22] To the best of our knowledge, our work is the first in which AHCs and HCCP are combined to form thin film polyphosphazene networks with properties that can be tailored from highly hydrogen selective membranes to very tight

146

gas barriers. The results can aid the further development of ultrathin membranes/barriers via non-aqueous interfacial polymerization with inexpensive monomers.

## 5.2 Experimental

Table 5.1 The chemical structure of the hydroxyl-containing monomers (AHCs) used in this study.

| Hydroxyl containing monomers | Structure |
|---|---|
| PDHB |  |
| MDHB |  |
| THB |  |

## 5.2.1. Materials

Hexachlorocyclotriphosphazene (HCCP, 99%), 1,3,5-trihydroxybenzene (THB or phloroglucinol, ≥99%), *m*-dihydroxybenzene (MDHB, ≥99.9%), *p*-dihydroxybenzene (PDHB, ≥99.9%) and dimethyl sulfoxide (DMSO, anhydrous, ≥99.9%) were obtained from Sigma-Aldrich. Cyclohexane (EMSURE for analysis), and potassium hydroxide (KOH, pellets extra pure) were supplied from Merck. All chemicals and solvents were used as received. Macroporous α-alumina discs with a diameter of 39 mm, a

thickness of 2 mm, and a pore size of 80 nm were obtained from Pervatech B.V. and used as support.

## 5.2.2. Material fabrication

Free-standing polymeric layers and thin-film composite membranes were formed by interfacial polymerization of a 10 w/v% solution of the AHCs in the super base[23] DMSO and KOH, with a 3.5 w/v% HCCP solution in cyclohexane. The molar ratio of monomer hydroxyl groups to KOH is indicated by $x$ and was kept at 4:1, 3.5:1, and 2.2:1 in DMSO, unless mentioned otherwise. A higher concentration of KOH led to the formation of salt and subsequently solid particles in AHCs/DMSO solution, and with a lower concentration of KOH ($x=6$), no layer was formed at the interface of the two immiscible phases.

### Synthesis free-standing films

Free-standing films were prepared by heating the AHC solutions at 80 °C for 2.5 h, and subsequently, HCCP solution in cyclohexane was poured on top of it. The reaction at the interface of the two solutions was confirmed by visual observation of the formation of the thin film. After 15 minutes, the film was collected, filtered, and washed with acetone, ethanol, and water, and dried in the vacuum oven at 50 °C overnight.

### Preparation of thin film composites

A mesoporous $\gamma$-$Al_2O_3$ intermediate layer with a pore size of 5 nm and a thickness of 4-5 μm was prepared on the $\alpha$-$Al_2O_3$ discs based on a previously reported procedure.[24] The IP films were prepared on top of ceramic supports, using a set-up described elsewhere.[13] First, the AHC solution and support were heated separately to 80 °C for 2.5 h and 30 min, respectively. After this, 5 ml of AHC solution was poured on top of the support and placed in a closed box in the oven at 80 °C. After 10 min, it was taken out, and its surface was dried by applying a rubber roller and $N_2$ gun. Then, 5 ml of HCCP solution was poured atop the support at ambient temperature. After the reaction for 10 min, the solution was discarded, and the resulting thin film composite (TFC) was rinsed with ethanol. The TFC

was kept in a fume hood overnight and then dried in a vacuum oven at 50 °C for a minimum of 24 h.

## 5.2.3. Material characterization

A field emission scanning electron microscope (FE-SEM, JSM-7610F) was used to visualize the thickness and morphology of the obtained TFCs. Both surface and cross-section images were acquired. Samples were prepared by immersing in liquid nitrogen for 5 min and carefully fractured to reveal the complete cross-section. Subsequently, all samples were mounted on an FE-SEM holder using double-sided carbon tape. Fourier transform infrared spectroscopy in attenuated total reflectance mode (FTIR-ATR, PerkinElmer Spectrum Two, USA) was used to characterize the free-standing film product. Spectra were averaged over 16 scans with a resolution of 4 cm$^{-1}$ over a wavenumber range of 400-4000 cm$^{-1}$. The elemental composition of synthesized free-standing films was measured with X-Ray Fluorescence (XRF) (S8 Tiger, Bruker) and CN elemental analysis (FLASH 2000 series analyzer). The thermal stability of the materials was measured by heating a fixed amount of sample (10 mg) on a heating stage under an inert nitrogen atmosphere at a heating rate of 10 ºC min$^{-1}$ using Thermo Gravimetric Analysis (TGA, STA 449 F3 Jupiler®, Netzsch) in combination with mass spectrometry (MS, QMS 403 D Aeolos MS, Netzsch). UV-vis spectra of THB and MDHB solutions with different concentrations of KOH were recorded on a Perkin-Elmer λ12 UV−vis spectrophotometer.

## 5.2.4. Membrane performance

Single gas permeance measurements were performed in dead-end mode using a commercially available Convergence Inspector Poseidon gas permeation set-up. The single gas permeance of He (0.255 nm diameter), H$_2$ (0.289 nm diameter), CO$_2$ (0.330 nm diameter), N$_2$ (0.364 nm diameter), and CH$_4$ (0.389 nm diameter) and was measured at a transmembrane pressure of 2 bar within the temperature ranges from 50 to 250 ºC. The detection limit of the Convergence set-up was limited to $10^{-10}$ mol m$^{-2}$ s$^{-1}$ Pa$^{-1}$. For this reason, TFC samples with low permeance were measured with a different set-up[25], at ambient temperature and a higher transmembrane pressure of 3 bars. In this set-up, the permeate side of known volume $V$ [m$^3$], was placed

under vacuum ($p_{start}$), and the gas was collected until an end pressure ($p_{end}$) was achieved. The amount of collected gas $n$ was calculated based on the ideal gas law: $n=(p_{end}-p_{start})V/(RT)$, where $R$ is the ideal gas constant [J mol K$^{-1}$], and $T$ is the temperature [K]. The permeance is calculated from $n/(A \cdot t \cdot \Delta p)$ [mol m$^{-2}$ s$^{-1}$ Pa$^{-1}$], where $A$ is the surface area [m$^2$], $t$ is the time [s] and $\Delta p$ is the transmembrane pressure difference [Pa]. The permeance can also be converted to permeability [cm$_{STP}^3$ cm cm$^{-2}$ s$^{-1}$ Pa$^{-1}$ ] by multiplying it with the thickness of the IP film (neglecting the resistance to transport of the support). The permselectivity for a given gas pair was calculated from the ratio of their pure gas permeance values. Experiments were performed at least twice, and the reported results are the average of the obtained values.

## 5.3 Results & Discussion

Figure 5.1A and Figure S5.1 are representatives of the visual observation of the localized formation of free-standing films from a reaction of THB, PDHB, or MDHB dissolved in DMSO/KOH, with HCCP dissolved in cyclohexane. In all studied cases, a stable and sharp interface forms between the two solutions. As an example, Figure 5.1B schematically depicts the formation of THB-HCCP film. Here, the hydroxyl groups of THB are partially deprotonated by KOH at 80 °C to form the reactive phenolate anions in DMSO, causing a change in the color of the solution from light yellow to dark brown (Figure S5.2). During IP, phenolate anions attack the phosphor atoms of the HCCP rings, displacing the chlorine atoms in a nucleophilic aromatic substitution process. The formation and properties of the network depend strongly on the extent of conversion of the hydroxyl groups into phenolate anions that can be controlled by adjusting the molar ratio of hydroxyl groups of monomers and KOH.
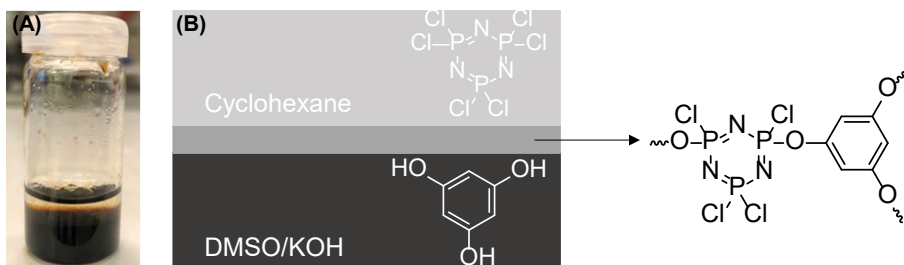
Figure 5.1 (A)Photograph of a free-standing THB-HCCP film formed at the DMSO-cyclohexane interface. (B) Illustration of the THB-HCCP network formation by the reaction of THB and HCCP.

Sufficient conversion of AHCs into nucleophile phenolate anions is necessary for successful network formation. UV-vis spectroscopic measurements reveal that the extent of phenolate formation and the type of phenolate species obtained (mono, di, or trianions) depend strongly on the concentration of KOH and the structure of the employed phenols (Figure 5.2). In the absence of KOH ($x=0$), the AHCs are protonated, and in the UV-vis absorption spectrum, they exhibit a characteristic sharp band below 300 nm representing an aromatic ring, which agrees with data from the literature.[26–29] With the addition of KOH to a PDHB solution (Figure 5.2A), new absorptions at longer wavelengths appear (325, 400, 425, and 455 nm), which are attributed to aromatic monoanions.[30–32] Absorptions of dianion species should appear at a wavelength of around 370 nm. This peak is not visible in the spectra due to the overlapping absorption bands that clutter the overall spectrum.[26] Adding KOH to the MDHB solution leads to higher and broader adsorption peaks between 260 nm to 350 nm that are ascribed to the formation of monoanion and dianion species (Figure 5.2B).[28] In addition, a new band appears at 400–600 nm. For THB (Figure 5.2C) addition of KOH gives rise to new peaks around 275, 335 and 367 nm. These peaks can be attributed to the deprotonation of the hydroxyl group and the presence of dianions and trianions.[33] For all compounds increasing the KOH concentration (from $x=3.5$ to $x=2.2$) causes a substantial increase in the intensity of peaks, implying a higher concentration of phenolate species in the solution. It is noteworthy to mention that even at the highest concentration of KOH ($x=2.2$) only a maximum 45-50% of all the hydroxyl groups are converted.
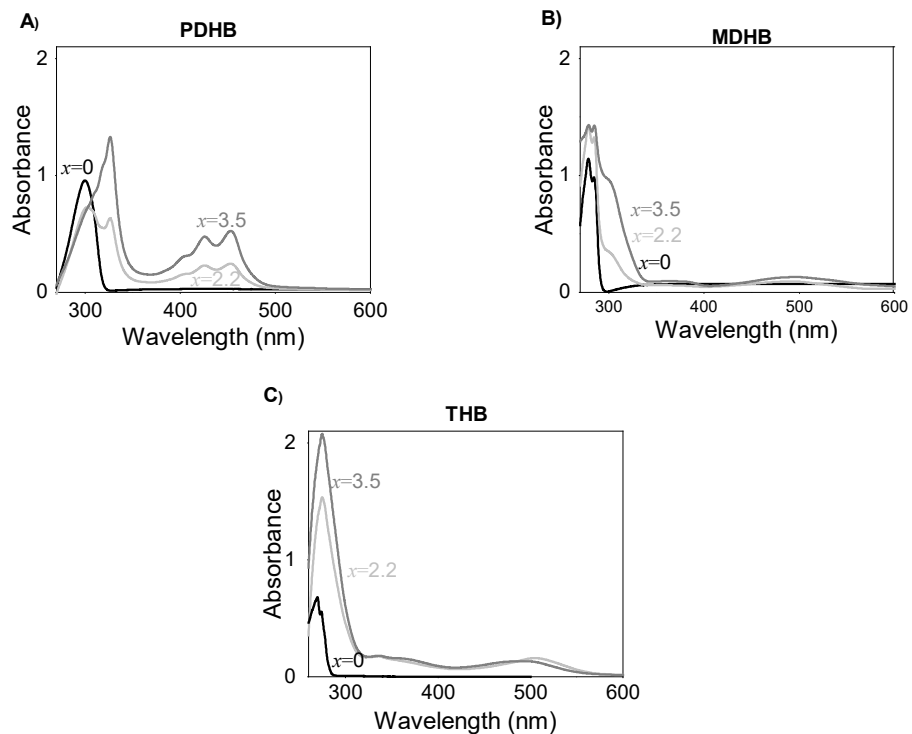
Figure 5.2 UV-vis absorption spectra of (A) 726 μM PDHB, (B) 1500 μM MDHB, and (C) 1300 μM THB in DMSO with different concentrations of KOH.

Figure 5.3 and Figure S5.3 show FE-SEM images of the cross-section and surface of TFC samples, for the three different AHCs. The images reveal relatively corrugated defect-free films atop of the ceramic supports, with thicknesses in the range 20-30 nm. These thicknesses are not substantially affected by the amount of KOH in the DMSO solution, and are comparable with those of IP-derived polyester nanofilms (20 nm) atop anodized alumina supports.[34]
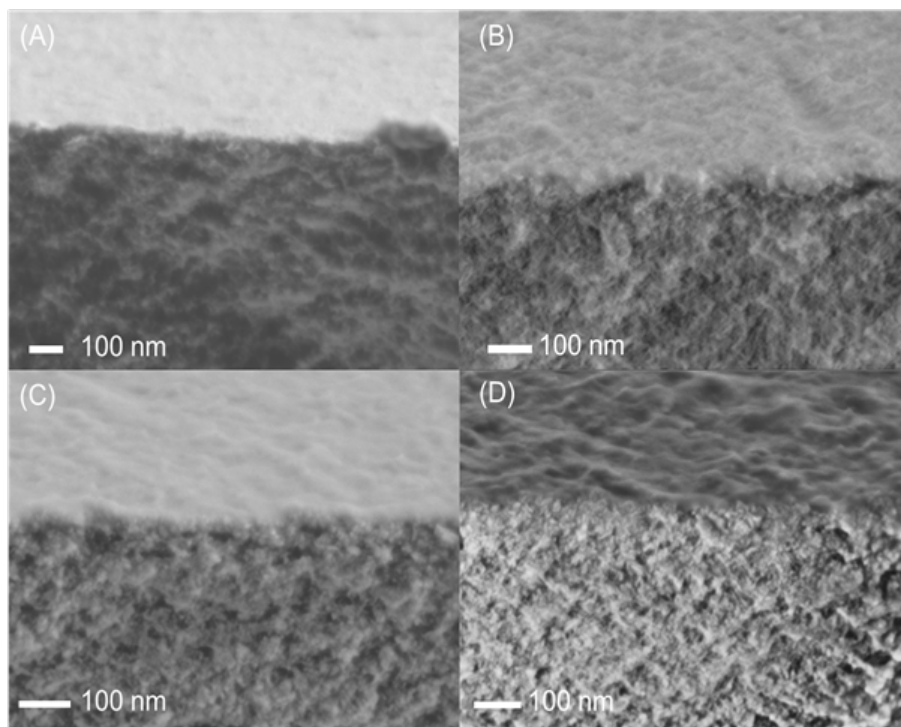
Figure 5.3 Cross-sectional FE-SEM pictures of polyphosphazene membranes. Membranes were prepared by IP of THB or MDHB in DMSO/KOH with HCCP in cyclohexane (A) THB-HCCP, $x$=2.2. (B) THB-HCCP, $x$=3.5. (C) MDHB-HCCP, $x$=2.2. (D) MDHB-HCCP, $x$=3.5.
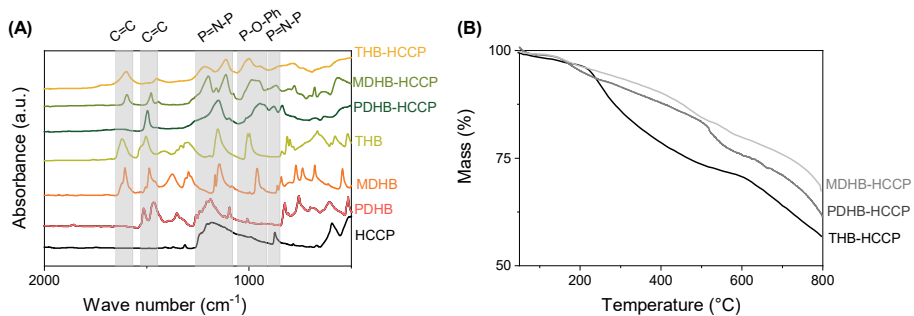


Figure 5.4 (A) FTIR spectra of free-standing polymer films formed by the IP process, collected at the interface of two solvents.(B) Mass loss up to 800 °C as a function of temperature for the polyphosphazene free-standing films prepared using different hydroxyl-containing monomers.

Figure 5.4A depicts FTIR spectra of the monomers and IP-derived free-standing films ($x$=2.2). Compared to the AHC monomers, in the films, the presence of the HCCP is confirmed by the additional absorption peak in the range 1100 to 1250 cm$^{-1}$ due to the asymmetric P=N stretching vibration of HCCP,[20] and the peaks around 870 cm$^{-1}$ due to the symmetric P=N stretching vibration. The phenyl ring is apparent by the two intense peaks about 1480 and 1600 cm$^{-1}$.[35] Covalent connection of the AHCs and HCCP is evidenced by peaks due to the stretching vibration of Ar-O-P, at 950 cm$^{-1}$ for PDHB-HCCP, and 950 and 1003 cm$^{-1}$ MDHB-HCCP and THB-HCCP.[36]

Figure 5.4B shows the mass loss of the polyphosphazene networks upon heating under $N_2$. All three materials show a monotonous decrease in weight, with an onset temperature of around 200 °C. The first part of this decrease, up to ~300 °C, is attributed to mainly the removal of adsorbed water and residual solvent (DMSO) and some further cross-linking reactions between unreacted Cl and OH groups. This is evidenced by the release of $H_2O$, $CH_3S$, and Cl (Figure S5.4). The decrease in weight at temperatures exceeding 300 °C is distinct from the behavior of the diphenol-based materials of our previous study.[14] For those materials, it was shown that the almost complete substitution of the Cl groups on the HCCP by Ar-O groups prevents the HCCP ring from opening at elevated temperatures, and no appreciable weight loss of these materials is observed for temperatures below 400 °C. Because the extent of substitution of Cl groups for the AHC-HCCP materials is much lower, the thermally induced opening of HCCP rings is more probable, causing the distinct thermal evolution of the mass. Hence, as a consequence of the lower degree of cross-linking and less substitution of Cl, the thermal stability of the AHC-HCCP materials is lower as compared to the diphenol-based material. By increasing the KOH concentration from $x$=3.5 to 2.2, the extent of deprotonation of AHCs is increased, in turn affecting the polycondensation reaction kinetics. For THB-HCCP, this results in a substantially lower loss in mass with temperature (Figure S5.5).

154

Table 5.2 XRF data for the polyphosphazene free-standing films.

| Sample | | Elemental composition (%)[a] | | | | Number of reacted Cl[b] |
|---|---|---|---|---|---|---|
| | | P | Cl | K | S | |
| PDHB- | $x$=2.2 | 32.5 | 48 | 14.5 | 4.6 | 1-2 |
| HCCP | $x$=3.5 | 34.9 | 53.1 | 9.34 | 2.7 | 1-2 |
| MDHB- | $x$=2.2 | 37.1 | 47.9 | 11.1 | 2.9 | 2 |
| HCCP | $x$=3.5 | 36.4 | 49.4 | 12 | 2.17 | 2 |
| THB- | $x$=2.2 | 36.8 | 48.9 | 8.8 | 4.7 | 2 |
| HCCP | $x$=3.5 | 37.1 | 41.5 | 13.7 | 7.7 | 2-3 |

[a] *The statistical error for the data is found to be between 0.7% to 4%.*
[b] *The number of reacted Cl per HCCP is equal to the number of reacted hydroxyl containing monomers per HCCP. This number is calculated based on the ratio of P/Cl, tacitly neglecting the presence of Cl in the form of KCl.*

XRF data (Table 5.2) for free-standing AHC-HCCP films confirms the presence of the atoms of the AHCs and HCCP, as well as some traces of K and S. The potassium can be present as counterions of aryloxides, and/or in the form of KCl. The traces of sulfur are probably due to the incomplete removal of DMSO. The number of reacted chlorine groups, based on the ratio of Cl/P, is 1-3 out of the total of 6 Cl groups per HCCP molecule. This indicates that the AHC-HCCP networks have a low degree of cross-linking compared to our previous study.[13,14] The fact that the materials do not readily dissolve in a variety of solvents is evidence of some degree of cross-linking. The crosslink density of the networks will be affected by the extent of deprotonation of the aryl alcohols.[18] In our previous study, the biphenols possess well-separated OH groups that, compared to the AHCs, display lower $pK_a$ values for the first and second deprotonation steps. This is especially the case when the bisphenols contain electron-withdrawing moieties. The more pronounced deprotonation, resulting from the lower pKa values, results in a larger number of organic bridges in the network. In fact, for the biphenol-based materials, almost all Cl groups on the HCCP are substituted by an aryloxide group. For the AHC-HCCP materials, the number of organic bridges is much lower and follows the order PDHB-HCCP < MDHB-HCCP≃THB-HCCP. This may be explained by the higher $pK_a$ values of PDHB ($pK_1$ = 9.9, $pK_2$ = 11.6) compared to MDHB ($pK_1$ = 9.2, $pK_2$ = 10.9) and THB ($pK_1$ = 8.0, $pK_2$ = 9.2, $pK_3$ = 14).[33,37]

Since the atomic percentages of O and Cl can be influenced by the presence of KCl and the hydrolysis of P−Cl to P−OH in the presence of $H_2O$, C,N elemental analysis was used to confirm the extent of cross-linking (Table S5.1). The number of reacted Cl per HCCP, calculated based on the ratio of C/N, is higher as compared to the XRF data, but also confirms incomplete conversion of the HCCP-Cl groups.
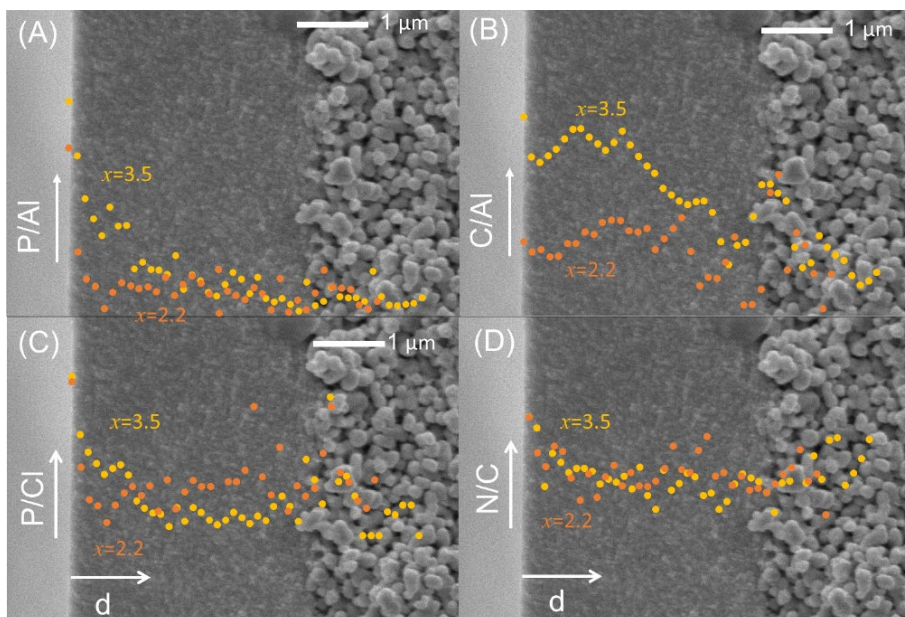


Figure 5.5 Distribution of ratios of elements over the membrane's cross-section for THB-HCCP $x$=2.2 and $x$=3.5.(A) P/Al, (B) C/Al, and (C) P/C.

Because of the intricate interplay of reaction and diffusion kinetics, in IP-prepared thin film composites, the polymer density and the degree of cross-linking can vary with location. The EDX data in Figure 5.5 reveal the impact of the KOH concentration on the distribution of different elements over the cross-section of a THB-HCCP thin film composite. The ratios P/Cl and N/C are representative of the degree of cross-linking; both these ratios are highest at the outer interface of the sample, accordant with the existence of a thin crosslinked film at this interface. The extent of cross-linking within the rest of the γ-alumina layer is similar for both KOH concentrations. The amount of polymer in the γ -alumina layer is more significant for the lowest KOH

concentration. This can be rationalized by the faster reaction kinetics and hence faster film formation at high KOH concentration, sooner resulting in impeded transport of the monomers to the reaction zone.
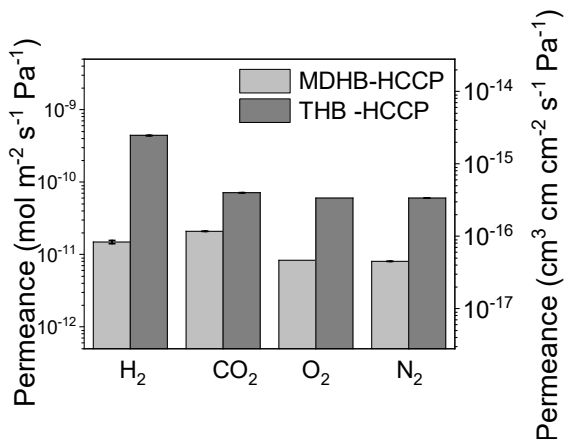


Figure 5.6 Gas permeance results of MDHB-HCCP and THB-HCCP with $x$=2.2 at a temperature of 30 °C and transmembrane pressure of 3 bar. To aid comparison with open literature, the data are converted into $cm^3$ cm $cm^{-2}$ $s^{-1}$ $Pa^{-1}$ and shown on the right axis.

The EDX data does not provide conclusive information on the effect of KOH on permselectivity or barrier properties of the thin film at the interface of the TFC. This is more evident from the gas permeance of He, $H_2$, $N_2$, $CO_2$, and $CH_4$ in the temperature range 30-200 °C, for TFCs with $x$=2.2, 3.5, and 4. For all KOH concentrations, the PDHB-HCCP films show gas permeances that are comparable to those of the bare supports (Table S5.2). This is attributed to a too low degree of substitution of Cl by Ar-O (Table 5.2), resulting in a weakly connected non-selective network. For the other two networks, the gas permeance is strongly affected by the value of $x$. For high KOH concentration, $x$=2.2, the THB-HCCP and MDHB-HCCP films exhibit gas barrier properties that may offer the potential for, e.g., confining the highly diffusive hydrogen gas in case of transportation and storage.[38–40] Figure 5.6 shows the $H_2$ and $O_2$ permeance of the two materials at 30 °C. The MDHB-HCCP films exhibit lower permeance as compared to THB-HCCP films. This is due to the higher molar concentration of MDHB during IP, increasing the thickness of the layer and hence the barrier properties.[41] To aid comparison with open literature, the data are converted into $cm^3$ cm

cm$^{-2}$ s$^{-1}$ Pa$^{-1}$ and listed in Table 5.3. Both for H$_2$ and O$_2$, the very thin TFCs have comparable performance to existing barrier coatings or even surpass their performances.[38,42–44] Moreover, the barrier properties of our thin film persist at elevated temperatures, as even at 200 °C, the H$_2$ permeance through THB-HCCP films is 10$^{-9}$ mol m$^{-2}$s$^{-1}$Pa$^{-1}$ (Figure S5.6). For ambient temperatures, Su et al.[43] and Tzeng et al.[42] reports lower hydrogen permeabilities of 6.9×10$^{-19}$ cm$^3$ cm cm$^{-2}$ s$^{-1}$ Pa$^{-1}$ and 3×10$^{-19}$ cm$^3$ cm cm$^{-2}$ s$^{-1}$ Pa$^{-1}$. These authors use completely different measurement methods and low transmembrane pressure. More importantly, they use more complex fabrication techniques involving graphene oxide and nanoclay nanosheets with high aspect ratios; the scalability of these materials is unknown. The facile IP technique used in our study is compatible with the existing large-scale industrial fabrication of reverse osmosis membranes.[45]

Table 5.3 Comparison of different published barriers with respect to their oxygen and hydrogen permeabilities.

| Film matrix | Gas | Permeability | Thickness | Ref. |
|---|---|---|---|---|
| poly(lactic acid)/graphene | $O_2$ | $1.1\times10^{-14}$ cm$^3$ cm cm$^{-2}$ s$^{-1}$ Pa$^{-1}$ | 210 µm | [46] |
| Cellulose/Graphen | $O_2$ | $0.8\times10^{-14}$ cm$^3$ cm cm$^{-2}$ s$^{-1}$ Pa$^{-1}$ | 35 µm | [47] |
| HDPE/GO | $O_2$ | $1.75\times10^{-14}$ cm$^3$ cm cm$^{-2}$ s$^{-1}$ Pa$^{-11}$ | - | [48] |
| Cellulose nanocrystal | $O_2$ | $1.75\times10^{-11}$ cm$^3$ cm cm$^{-2}$ s$^{-1}$ Pa$^{-1}$ | <15µm[1] | [49] |
| polyelectrolyte complex | $O_2$ | 0.013 cm$^3$ m$^{-2}$ day$^{-1}$ | 1.9 µm | [50] |
| Polyimide (FAPPI) | $O_2$ | 0.43 cm$^3$ m$^{-2}$ day$^{-1}$ | - | [51] |
| PMDA-FDA polyimide | $O_2$ | 1.01 cm$^3$ m$^{-2}$ day$^{-1}$ | 75 µm | [52] |
| PMDA-AAPPI polyimide | $O_2$ | 1.7 cm$^3$ m$^{-2}$ day$^{-1}$ | - | [53] |
| **THB-HCCP-2.2** | **$O_2$** | **$3.8\times10^{-16}$ cm$^3$ cm cm$^{-2}$ s$^{-1}$ Pa$^{-1}$** | **30 nm** | **This work** |
| **MDHB-HCCP-2.2** | **$O_2$** | **$1.1\times10^{-16}$ cm$^3$ cm cm$^{-2}$ s$^{-1}$ Pa$^{-1}$** | **30 nm** | **This work** |
| MXene-GO/poly (ethylene-co-acrylic acid) | $H_2$ | $3.5\times10^{-12}$ cm$^3$ cm cm$^{-2}$ s$^{-1}$ Pa$^{-1}$ | ~10 µm | [39] |
| PEI/Graphene oxide | $H_2$ | $1.8\times10^{-16}$ cm$^3$ cm cm$^{-2}$ s$^{-1}$ Pa$^{-1}$ | 91 nm | [54] |
| PDDA/Graphene oxide | $H_2$ | $3.6\times10^{-15}$ cm$^3$ cm cm$^{-2}$ s$^{-1}$ Pa$^{-1}$ | 120 µm | [55] |
| PEN/Graphite | $H_2$ | $2.3\times10^{-14}$ cm$^3$ cm cm$^{-2}$ s$^{-1}$ Pa$^{-1}$ | 70 µm | [40] |
| Chitin | $H_2$ | $1.3\times10^{-8}$ cm$^3$ cm cm$^{-2}$ s$^{-1}$ Pa$^{-1}$ | 50 µm | [44] |
| PVA/silicate nanosheets | $H_2$ | $6.9\times10^{-19}$ cm$^3$ cm cm$^{-2}$ s$^{-1}$ Pa$^{-1}$ | 1.5 µm | [38] |
| Reduced Graphene oxide | $H_2$ | $3\times10^{-19}$ cm$^3$ cm cm$^{-2}$ s$^{-1}$ Pa$^{-1}$ | 30 nm | [43] |
| polyelectrolyte complex/clay | $H_2$ | $4\times10^{-15}$ cm$^3$ cm cm$^{-2}$ s$^{-1}$ Pa$^{-1}$ | 122 nm | [42] |
| **THB-HCCP-2.2** | **$H_2$** | **$2.4\times10^{-15}$ cm$^3$ cm cm$^{-2}$ s$^{-1}$ Pa$^{-1}$** | **30 nm** | **This work** |
| **MDHB-HCCP-2.2** | **$H_2$** | **$9.4\times10^{-17}$ cm$^3$ cm cm$^{-2}$ s$^{-1}$ Pa$^{-1}$** | **30 nm** | **This work** |

[1] *Because it is an anisotropic film with a flexible thickness*

A lower concentration of KOH directly affects the kinetics of the polycondensation reaction and hence affects the permselective properties of the films. In Figure 5.7A, single gas permeance data of THB-HCCP films, with $x=4$, are presented as a function of gas kinetic diameter in the temperature range 50-200 °C. The increased value of $x$ reduces the $H_2$ barrier properties of the films. The permeance of the small gases decreases with increasing gas kinetic diameter. This gas sieving behavior is also observed for glassy polymers such as aromatic polyimides.[56,57] For all gases, the permeance increases with increasing temperature, confirming that permselectivity arises from diffusion. For THB-HCCP the activation energies, obtained from the Arrhenius plots in Figure 5.7B, follow the order $N_2 > He, H_2 > CO_2$. This complies with the order of the kinetic diameters of the gas molecules, except for $CO_2$. The distinct behavior of $CO_2$ is due to its quadrupole moment and the resulting affinity for polar groups such as amines and hydroxyl groups.[58] Increasing temperature lowers the interactions between $CO_2$ and the material. The trade-off between the temperature effect on the solution and diffusion is manifested by the lower "apparent" activation energy for $CO_2$.[59] This is in line with observations for other membranes, such as thermally stable polyimide and polybenzimidazole membranes.[60–62] The permeance of $CH_4$ is below the detection limit of the set-up and the activation energy of $CH_4$ could not be calculated.
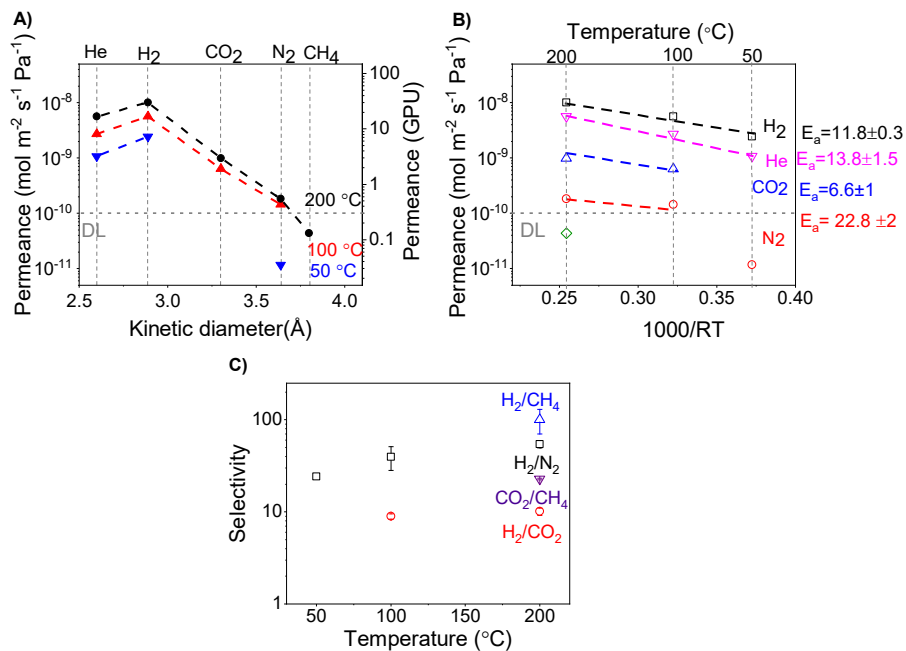
Figure 5.7 (A) Gas permeance of THB-HCCP with $x=4$ as a function of gas kinetic diameter for three different temperatures. (B) Arrhenius plot of pure gas permeances; the unit of activation energies in kJ mol$^{-1}$. (C) Ideal selectivities of the membranes as a function of temperature.

The membranes show high permselectivities, even at 200 °C: 10.1, 52.8, and 100 for $H_2/CO_2$, $H_2/N_2$, and $H_2/CH_4$. The $H_2/N_2$ selectivity increases with temperature, and the $H_2/CO_2$ selectivities are around 10 over the complete temperature range of 50-200 °C. Relatively few polymeric membranes have been characterized by permeation at high temperatures, due to often limited membrane stability. The observed performance of THB-HCCP membranes is comparable with the performance of the poly(PMDA-POSS imide) membranes and polybenzimidazole.[62–65] In addition, these new membranes have the following advantages: (1) They are made by interfacial polymerization, a simple and convenient technique that readily allows upscaling.[66] (2) The THB-HCCP membranes are formed in one step; where no additional thermal treatment is needed, as is the case for polyimides.[56] (3) Very cheap and readily accessible monomers are used for the preparation of the membranes.

## 5.4 Conclusion

Thin film cyclomatrix polyphosphazene networks are prepared by non-conventional interfacial polymerization of hexachlorocyclotriphosphazene with small aromatic hydroxy compounds. As polar phase, DMSO is used instead of water. By varying the amount of KOH in the DMSO the extent of deprotonation of the hydroxy compounds can be changed, allowing for the tailoring of the permselective properties of the thin film composites, all the way from hydrogen/oxygen barriers to membranes with persisting hydrogen permselectivities at high temperatures. The barrier properties are obtained with high KOH concentration, allowing for more pronounced deprotonation of the hydroxy compounds. A lower concentration of KOH results in materials with a larger free volume and faster transport of the small hydrogen molecules. These tunable materials show excellent potential for use in a broad landscape of applications, ranging from barriers for hydrogens storage and transport to high-temperature gas separation processes.

## 5.5 Acknowledgement

# 5.6 References

[1] B.E. Logan, M. Elimelech, Membrane-based processes for sustainable power generation using water, Nature. 488 (2012) 313–319. https://doi.org/10.1038/nature11477.

[2] P.W. Morgan, Interfacial Polymerization, in: Encycl. Polym. Sci. Technol., John Wiley & Sons, Inc., Hoboken, NJ, USA, 2011. https://doi.org/10.1002/0471440264.pst168.

[3] M.J.T. Raaijmakers, N.E. Benes, Current trends in interfacial polymerization chemistry, Prog. Polym. Sci. 63 (2016) 86–142. https://doi.org/10.1016/j.progpolymsci.2016.06.004.

[4] J. Lee, R. Wang, T.-H. Bae, A comprehensive understanding of co-solvent effects on interfacial polymerization: Interaction with trimesoyl chloride, J. Memb. Sci. 583 (2019) 70–80. https://doi.org/10.1016/j.memsci.2019.04.038.

[5] L. Hu, S. Zhang, R. Han, X. Jian, Preparation and performance of novel thermally stable polyamide/PPENK composite nanofiltration membranes, Appl. Surf. Sci. 258 (2012) 9047–9053. https://doi.org/10.1016/j.apsusc.2012.05.153.

[6] S. M. Kim, S. Hong, B.-T. Duy Nguyen, H.-Y. Nguyen Thi, S.-H. Park, J.-F. Kim, Effect of Additives during Interfacial Polymerization Reaction for Fabrication of Organic Solvent Nanofiltration (OSN) Membranes, Polymers (Basel). 13 (2021) 1716. https://doi.org/10.3390/polym13111716.

[7] A.K. Ghosh, B.-H. Jeong, X. Huang, E.M.V. Hoek, Impacts of reaction and curing conditions on polyamide composite reverse osmosis membrane properties, J. Memb. Sci. 311 (2008) 34–45. https://doi.org/10.1016/j.memsci.2007.11.038.

[8] F. Yuan, Z. Wang, S. Li, J. Wang, S. Wang, Formation–structure–performance correlation of thin film composite membranes prepared by interfacial polymerization for gas separation, J. Memb. Sci. 421–422 (2012) 327–341. https://doi.org/10.1016/j.memsci.2012.07.035.

[9] C.C. Wamser, R.R. Bard, V. Senthilathipan, V.C. Anderson, J.A. Yates, H.K. Lonsdale, G.W. Rayfield, D.T. Friesen, D.A. Lorenz, Synthesis and photoactivity of chemically asymmetric polymeric porphyrin films made by interfacial

polymerization, J. Am. Chem. Soc. 111 (1989) 8485–8491. https://doi.org/10.1021/ja00204a023.

[10] N. Ogata, K. Sanui, T. Onozaki, S. Imanishi, Interfacial Polycondensation in Aqueous and Non-Aqueous Systems, J. Macromol. Sci. Part A - Chem. 15 (1981) 1059–1063. https://doi.org/10.1080/00222338108056783.

[11] B.J. Heßbrügge, A.M. Vaidya, Preparation and characterization of salt hydrates encapsulated in polyamide membranes, J. Memb. Sci. 128 (1997) 175–182. https://doi.org/10.1016/S0376-7388(96)00307-9.

[12] C. Liu, J. Yang, B. Guo, S. Agarwal, A. Greiner, Z. Xu, Interfacial Polymerization at the Alkane/Ionic Liquid Interface, Angew. Chemie Int. Ed. 60 (2021) 14636–14643. https://doi.org/10.1002/anie.202103555.

[13] F. Radmanesh, M.G. Elshof, N.E. Benes, Polyoctahedral Silsesquioxane Hexachlorocyclotriphosphazene Membranes for Hot Gas Separation, ACS Appl. Mater. Interfaces. 13 (2021) 8960–8966. https://doi.org/10.1021/acsami.0c21968.

[14] F. Radmanesh, E. J.R. Sudhölter, A. Tena, M. G. Elshof, N.E. Benes,Thin film composite cyclomatrix poly(phenoxy)phosphazenes membranes for hot hydrogen separation, Submitted. (n.d.).

[15] H.R. Allcock, Hybrids of hybrids: nano-scale combinations of polyphosphazenes with other materials, Appl. Organomet. Chem. 24 (2010) 600–607. https://doi.org/10.1002/aoc.1636.

[16] Z. Ali, M. Basharat, Z. Wu, A Review on the Morphologically Controlled Synthesis of Polyphosphazenes for Electrochemical Applications, ChemElectroChem. 8 (2021) 759–782. https://doi.org/10.1002/celc.202001352.

[17] Z. Miao, D. Yan, T. Zhang, F. Yang, S. Zhang, W. Liu, Z. Wu, High-Efficiency Flame Retardants of a P–N-Rich Polyphosphazene Elastomer Nanocoating on Cotton Fabric, ACS Appl. Mater. Interfaces. 13 (2021) 32094–32105. https://doi.org/10.1021/acsami.1c05884.

[18] E. Maaskant, H. Gojzewski, M.A. Hempenius, G.J. Vancso, N.E. Benes, Thin cyclomatrix polyphosphazene films: interfacial polymerization of hexachlorocyclotriphosphazene with aromatic biphenols, Polym. Chem. 9 (2018) 3169–3180. https://doi.org/10.1039/C8PY00444G.

164

[19] D.E. Braun, D.A. Tocher, S.L. Price, U.J. Griesser, The Complexity of Hydration of Phloroglucinol: A Comprehensive Structural and Thermodynamic Characterization, J. Phys. Chem. B. 116 (2012) 3961–3972. https://doi.org/10.1021/jp211948q.

[20] M. Zhang, Y. Li, C. Bai, X. Guo, J. Han, S. Hu, H. Jiang, W. Tan, S. Li, L. Ma, Synthesis of Microporous Covalent Phosphazene-Based Frameworks for Selective Separation of Uranium in Highly Acidic Media Based on Size-Matching Effect, ACS Appl. Mater. Interfaces. 10 (2018) 28936–28947. https://doi.org/10.1021/acsami.8b06842.

[21] R. Jiang, B. Deng, L. Pi, L. Hu, D. Chen, Y. Dou, X. Mao, D. Wang, Molten Electrolyte-Modulated Electrosynthesis of Multi-Anion Mo-Based Lamellar Nanohybrids Derived from Natural Minerals for Boosting Hydrogen Evolution, ACS Appl. Mater. Interfaces. 12 (2020) 57870–57880. https://doi.org/10.1021/acsami.0c17137.

[22] M. Gao, J. Fu, M. Wang, K. Wang, S. Wang, Z. Wang, Z. Chen, Q. Xu, A self-template and self-activation co-coupling green strategy to synthesize high surface area ternary-doped hollow carbon microspheres for high performance supercapacitors, J. Colloid Interface Sci. 524 (2018) 165–176. https://doi.org/10.1016/j.jcis.2018.04.027.

[23] A.S. Bobkov, N.M. Vitkovskaya, B.A. Trofimov, Cascade Assembly of 4,5,6,7-Tetrahydroindole from Cyclohexanone Oxime and Acetylene in the KOH/DMSO Superbase Medium: A Quantum Chemical Study, J. Org. Chem. 85 (2020) 6463–6470. https://doi.org/10.1021/acs.joc.0c00353.

[24] X. Wang, P. Karakiliç, X. Liu, M. Shan, A. Nijmeijer, L. Winnubst, J. Gascon, F. Kapteijn, One-Pot Synthesis of High-Flux b -Oriented MFI Zeolite Membranes for Xe Recovery, ACS Appl. Mater. Interfaces. 10 (2018) 33574–33580. https://doi.org/10.1021/acsami.8b12613.

[25] J. Li, G. van Ewijk, D.J. van Dijken, J. van der Gucht, W.M. de Vos, Single-Step Application of Polyelectrolyte Complex Films as Oxygen Barrier Coatings, ACS Appl. Mater. Interfaces. 13 (2021) 21844–21853. https://doi.org/10.1021/acsami.1c05031.

[26] D. Zhang, C. Wang, L. Shen, H.-C. Shin, K.B. Lee, B. Ji, Comparative analysis of oxidative mechanisms of phloroglucinol and dieckol by electrochemical,

spectroscopic, cellular and computational methods, RSC Adv. 8 (2018) 1963–1972. https://doi.org/10.1039/C7RA10875C.

[27] M.R. Maurya, L. Rana, N. Jangra, F. Avecilla, Bis{ cis -[MoO 2 ]} Complexes of 4,6-Diacetyl Resorcinol Bis(hydrazone)and Their Catalytic Application for the Three Components Dynamic Covalent Assembly via Hantzsch Reaction, ChemistrySelect. 2 (2017) 6767–6777. https://doi.org/10.1002/slct.201701629.

[28] S.E. Blanco, M.C. Almandoz, F.H. Ferretti, Determination of the overlapping pKa values of resorcinol using UV-visible spectroscopy and DFT methods, Spectrochim. Acta Part A Mol. Biomol. Spectrosc. 61 (2005) 93–102. https://doi.org/10.1016/j.saa.2004.03.020.

[29] C. Y. Cheng, Y.-T. Chan, Y.-M. Tzou, K.-Y. Chen, Y.-T. Liu, Spectroscopic Investigations of the Oxidative Polymerization of Hydroquinone in the Presence of Hexavalent Chromium, J. Spectrosc. 2016 (2016) 1–8. https://doi.org/10.1155/2016/7958351.

[30] V.K. La Mer, E.K. Rideal, THE INFLUENCE OF HYDROGEN CONCENTRATION ON THE AUTO-OXIDATION OF HYDROQUINONE. A NOTE ON THE STABILITY OF THE QUINHYDRONE ELECTRODE, J. Am. Chem. Soc. 46 (1924) 223–231. https://doi.org/10.1021/ja01666a030.

[31] R.S.K.A. Gamage, S. Umapathy, A.J. McQuillan, OTTLE cell study of the UV-visible and FTIR spectroelectrochemistry of the radical anion and dianion of 1,4-benzoquinone in DMSO solutions, J. Electroanal. Chem. Interfacial Electrochem. 284 (1990) 229–235. https://doi.org/10.1016/0022-0728(90)87075-U.

[32] Y.O. Kim, Y.M. Jung, S. Bin Kim, S.-M. Park, Two-Dimensional Correlation Analysis of Spectroelectrochemical Data for p -Benzoquinone Reduction in Acetonitrile, Anal. Chem. 76 (2004) 5236–5240. https://doi.org/10.1021/ac049587g.

[33] D. Wang, K. Hildenbrand, J. Leitich, H. P. Schuchmann, C. von Sonntag, pH-Dependent Tautomerism and pK a Values of Phloroglucinol (1,3,5-Trihydroxybenzene), Studied by 13 C NMR and UV Spectroscopy, Zeitschrift Für Naturforsch. B. 48 (1993) 478–482. https://doi.org/10.1515/znb-1993-0413.

[34] M.F. Jimenez-Solomon, Q. Song, K.E. Jelfs, M. Munoz-Ibanez, A.G. Livingston, Polymer nanofilms with enhanced microporosity by interfacial polymerization, Nat. Mater. 15 (2016) 760–767. https://doi.org/10.1038/nmat4638.

[35] L. Sun, T. Liu, H. Li, L. Yang, L. Meng, Q. Lu, J. Long, Fluorescent and Cross-linked Organic–Inorganic Hybrid Nanoshells for Monitoring Drug Delivery, ACS Appl. Mater. Interfaces. 7 (2015) 4990–4997. https://doi.org/10.1021/acsami.5b00175.

[36] G. Tang, X. Zeng, L. Hou, T. Song, S. Yin, B. Long, A. Ali, G.-J. Deng, Cross-linked ultrathin polyphosphazene-based nanosheet with promoted charge separation kinetics for efficient visible light photocatalytic CO2 reforming to CH4, Appl. Catal. B Environ. 306 (2022) 121090. https://doi.org/10.1016/j.apcatb.2022.121090.

[37] S. Suresh, V.C. Srivastava, I.M. Mishra, Adsorption of catechol, resorcinol, hydroquinone, and their derivatives: a review, Int. J. Energy Environ. Eng. 3 (2012) 32. https://doi.org/10.1186/2251-6832-3-32.

[38] C. Habel, E.S. Tsurko, R.L. Timmins, J. Hutschreuther, R. Kunz, D.D. Schuchardt, S. Rosenfeldt, V. Altstädt, J. Breu, Lightweight Ultra-High-Barrier Liners for Helium and Hydrogen, ACS Nano. 14 (2020) 7018–7024. https://doi.org/10.1021/acsnano.0c01633.

[39] O.B. Seo, S. Saha, N.H. Kim, J.H. Lee, Preparation of functionalized MXene-stitched-graphene oxide/poly (ethylene-co-acrylic acid) nanocomposite with enhanced hydrogen gas barrier properties, J. Memb. Sci. 640 (2021) 119839. https://doi.org/10.1016/j.memsci.2021.119839.

[40] H. Kim, C.W. Macosko, Morphology and Properties of Polyester/Exfoliated Graphite Nanocomposites, Macromolecules. 41 (2008) 3317–3327. https://doi.org/10.1021/ma702385h.

[41] Y.-Y. Su, X. Yan, Y. Chen, X.-J. Guo, X.-F. Chen, W.-Z. Lang, Facile fabrication of COF-LZU1/PES composite membrane via interfacial polymerization on microfiltration substrate for dye/salt separation, J. Memb. Sci. 618 (2021) 118706. https://doi.org/10.1016/j.memsci.2020.118706.

[42] P. Tzeng, E.L. Lugo, G.D. Mai, B.A. Wilhite, J.C. Grunlan, Super Hydrogen and Helium Barrier with Polyelectolyte Nanobrick Wall Thin Film, Macromol. Rapid Commun. 36 (2015) 96–101. https://doi.org/10.1002/marc.201400559.

[43] Y. Su, V.G. Kravets, S.L. Wong, J. Waters, A.K. Geim, R.R. Nair, Impermeable barrier films and protective coatings based on reduced graphene oxide, Nat. Commun. 5 (2014) 4843. https://doi.org/10.1038/ncomms5843.

[44] B. Duan, C. Chang, B. Ding, J. Cai, M. Xu, S. Feng, J. Ren, X. Shi, Y. Du, L. Zhang, High strength films with gas-barrier fabricated from chitin solution dissolved at low temperature, J. Mater. Chem. A. 1 (2013) 1867–1874. https://doi.org/10.1039/C2TA00068G.

[45] X. Lu, M. Elimelech, Fabrication of desalination membranes by interfacial polymerization: history, current efforts, and future directions, Chem. Soc. Rev. 50 (2021) 6290–6307. https://doi.org/10.1039/D0CS00502A.

[46] H.-D. Huang, P.-G. Ren, J.-Z. Xu, L. Xu, G.-J. Zhong, B.S. Hsiao, Z.-M. Li, Improved barrier properties of poly(lactic acid) with randomly dispersed graphene oxide nanosheets, J. Memb. Sci. 464 (2014) 110–118. https://doi.org/10.1016/j.memsci.2014.04.009.

[47] S. Mahmoudian, M.U. Wahit, M. Imran, A.F. Ismail, H. Balakrishnan, A Facile Approach to Prepare Regenerated Cellulose/Graphene Nanoplatelets Nanocomposite Using Room-Temperature Ionic Liquid, J. Nanosci. Nanotechnol. 12 (2012) 5233–5239. https://doi.org/10.1166/jnn.2012.6351.

[48] P. G. Ren, H. Wang, H.-D. Huang, D.-X. Yan, Z.-M. Li, Characterization and performance of dodecyl amine functionalized graphene oxide and dodecyl amine functionalized graphene/high-density polyethylene nanocomposites: A comparative study, J. Appl. Polym. Sci. 131 (2014) n/a-n/a. https://doi.org/10.1002/app.39803.

[49] R.A. Chowdhury, M. Nuruddin, C. Clarkson, F. Montes, J. Howarter, J.P. Youngblood, Cellulose Nanocrystal (CNC) Coatings with Controlled Anisotropy as High-Performance Gas Barrier Films, ACS Appl. Mater. Interfaces. 11 (2019) 1376–1383. https://doi.org/10.1021/acsami.8b16897.

[50] R.J. Smith, C.T. Long, J.C. Grunlan, Transparent Polyelectrolyte Complex Thin Films with Ultralow Oxygen Transmission Rate, Langmuir. 34 (2018) 11086–11091. https://doi.org/10.1021/acs.langmuir.8b02391.

[51] Y. Liu, A. Tang, J. Tan, C. Chen, D. Wu, H. Zhang, Structure and Gas Barrier Properties of Polyimide Containing a Rigid Planar Fluorene Moiety and an Amide Group: Insights from Molecular Simulations, ACS Omega. 6 (2021) 4273–4281. https://doi.org/10.1021/acsomega.0c05278.

[52] J. Tan, Q. Wang, Y. Liu, Y. Zeng, Q. Ding, R. Wu, Y. Liu, X. Xiang, Synthesis, gas barrier and thermal properties of polyimide containing rigid planar

fluorene moieties, J. Macromol. Sci. Part A. 55 (2018) 75–84. https://doi.org/10.1080/10601325.2017.1387492.

[53] L.D. Wen, Qian, Ao Tang, Chengliang Chen, Yiwu Liu, Chunguang Xiao, Jinghua Tan, Synthesis, barrier performance, and molecular simulation of a high-barrier polyimide that contains amide groups, Mater. Res. Express. 8 (2021) 045305. https://iopscience.iop.org/article/10.1088/2053-1591/abf45f/meta.

[54] Y. H. Yang, L. Bolling, M.A. Priolo, J.C. Grunlan, Super Gas Barrier and Selectivity of Graphene Oxide-Polymer Multilayer Thin Films, Adv. Mater. 25 (2013) 503–508. https://doi.org/10.1002/adma.201202951.

[55] R. Rajasekar, N.H. Kim, D. Jung, T. Kuila, J.K. Lim, M.J. Park, J.H. Lee, Electrostatically assembled layer-by-layer composites containing graphene oxide for enhanced hydrogen gas barrier application, Compos. Sci. Technol. 89 (2013) 167–174. https://doi.org/10.1016/j.compscitech.2013.10.004.

[56] H. Sanaeepur, A. Ebadi Amooghin, S. Bandehali, A. Moghadassi, T. Matsuura, B. Van der Bruggen, Polyimides in membrane gas separation: Monomer's molecular design and structural engineering, Prog. Polym. Sci. 91 (2019) 80–125. https://doi.org/10.1016/j.progpolymsci.2019.02.001.

[57] Z. Liu, W. Qiu, W. Quan, Y. Liu, W.J. Koros, Fine-tuned thermally cross-linkable 6FDA-based polyimide membranes for aggressive natural gas separation, J. Memb. Sci. 635 (2021) 119474. https://doi.org/10.1016/j.memsci.2021.119474.

[58] A. Torrisi, R.G. Bell, C. Mellot-Draznieks, Functionalized MOFs for Enhanced CO 2 Capture, Cryst. Growth Des. 10 (2010) 2839–2841. https://doi.org/10.1021/cg100646e.

[59] S. Escorihuela, A. Tena, S. Shishatskiy, S. Escolástico, T. Brinkmann, J. Serra, V. Abetz, Gas Separation Properties of Polyimide Thin Films on Ceramic Supports for High Temperature Applications, Membranes (Basel). 8 (2018) 16. https://doi.org/10.3390/membranes8010016.

[60] S. Kang, Z. Zhang, L. Wu, S. Xu, G. Huo, X. Ma, N. Li, Synthesis and gas separation properties of polyimide membranes derived from oxygencyclic pseudo-Tröger's base, J. Memb. Sci. 637 (2021) 119604. https://doi.org/10.1016/j.memsci.2021.119604.

[61] E. Lasseuguette, R. Malpass-Evans, M. Carta, N.B. McKeown, M.-C. Ferrari, Temperature and Pressure Dependence of Gas Permeation in a Microporous Tröger's Base Polymer, Membranes (Basel). 8 (2018) 132. https://doi.org/10.3390/membranes8040132.

[62] M. Shan, X. Liu, X. Wang, Z. Liu, H. Iziyi, S. Ganapathy, J. Gascon, F. Kapteijn, Novel high performance poly( p -phenylene benzobisimidazole) (PBDI) membranes fabricated by interfacial polymerization for H 2 separation, J. Mater. Chem. A. 7 (2019) 8929–8937. https://doi.org/10.1039/C9TA01524H.

[63] L. Hu, S. Pal, H. Nguyen, V. Bui, H. Lin, Molecularly engineering polymeric membranes $H_2/CO_2$ separation at 100–300 °C, J. Polym. Sci. 58 (2020) 2467–2481. https://doi.org/10.1002/pol.20200220.

[64] M.J.T. Raaijmakers, M. Wessling, A. Nijmeijer, N.E. Benes, Hybrid Polyhedral Oligomeric Silsesquioxanes–Imides with Tailored Intercage Spacing for Sieving of Hot Gases, Chem. Mater. 26 (2014) 3660–3664. https://doi.org/10.1021/cm500691e.

[65] L.F. Villalobos, R. Hilke, F.H. Akhtar, K.-V. Peinemann, Fabrication of Polybenzimidazole/Palladium Nanoparticles Hollow Fiber Membranes for Hydrogen Purification, Adv. Energy Mater. 8 (2018) 1701567. https://doi.org/10.1002/aenm.201701567.

[66] F. Zhang, J. Fan, S. Wang, Interfacial Polymerization: From Chemistry to Functional Materials, Angew. Chemie Int. Ed. 59 (2020) 21840–21856. https://doi.org/10.1002/anie.201916473

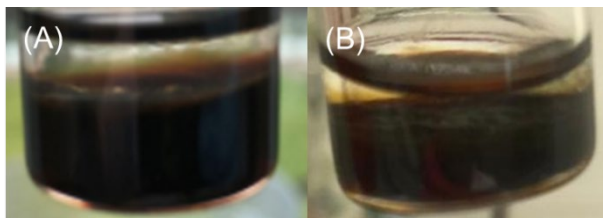## 5.7 Supporting information



Figure S5.1 Photograph of free-standing (A) MDHB-HCCP and (B) PDHB-HCCP films formed at the DMSO-cyclohexane interface.
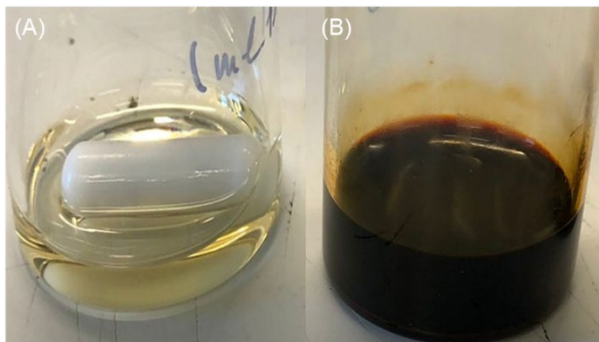


Figure S5.2 Solution of THB in DMSO (A) before addition of KOH and (B) after addition of KOH and solution at 80°C for 2.5 hr.
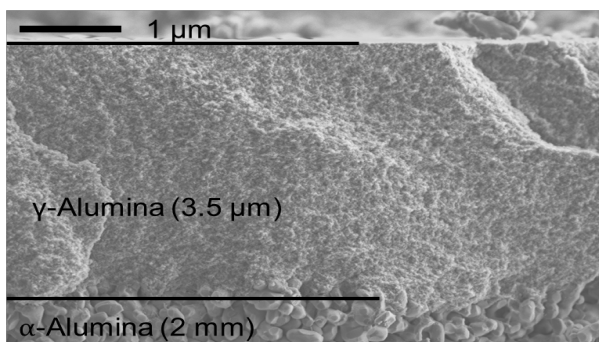
Figure S5.3 Cross-section scanning electron micrograph of the support used in this study. It shows the 3 .5 µm γ-Alumina layer and the 2 mm microporous α-Alumina.

Table S5.1 C,N elemental analysis(%) for polyphosphazene powders.

| Sample | | Elemental concentration (%) | | Number of reacted Cl[a] |
|---|---|---|---|---|
| | | C | N | |
| PDHB-HCCP | $x$=2.2 | 30.9±0.8 | 8.9±0.2 | 3-4 |
| | $x$=3.6 | 30.1±0.9 | 8.7±0.2 | 3-4 |
| MDHB-HCCP | $x$=2.2 | 32.7±0.2 | 8.2±0.3 | 4 |
| | $x$=3.6 | 32.5±0.2 | 8.1±0.3 | 4 |
| THB-HCCP | $x$=2.2 | 19.9±0.5 | 8.8±0.2 | 2-3 (2.3±0.1) |
| | $x$=3.6 | 22±0.4 | 8.4±0.1 | 2-3(2.6±0.1) |

[a]*The number of reacted Cl groups is equal to the number of reacted hydroxyl contained monomers per HCCP. This number is calculated based on the ratio of C/N.*

172
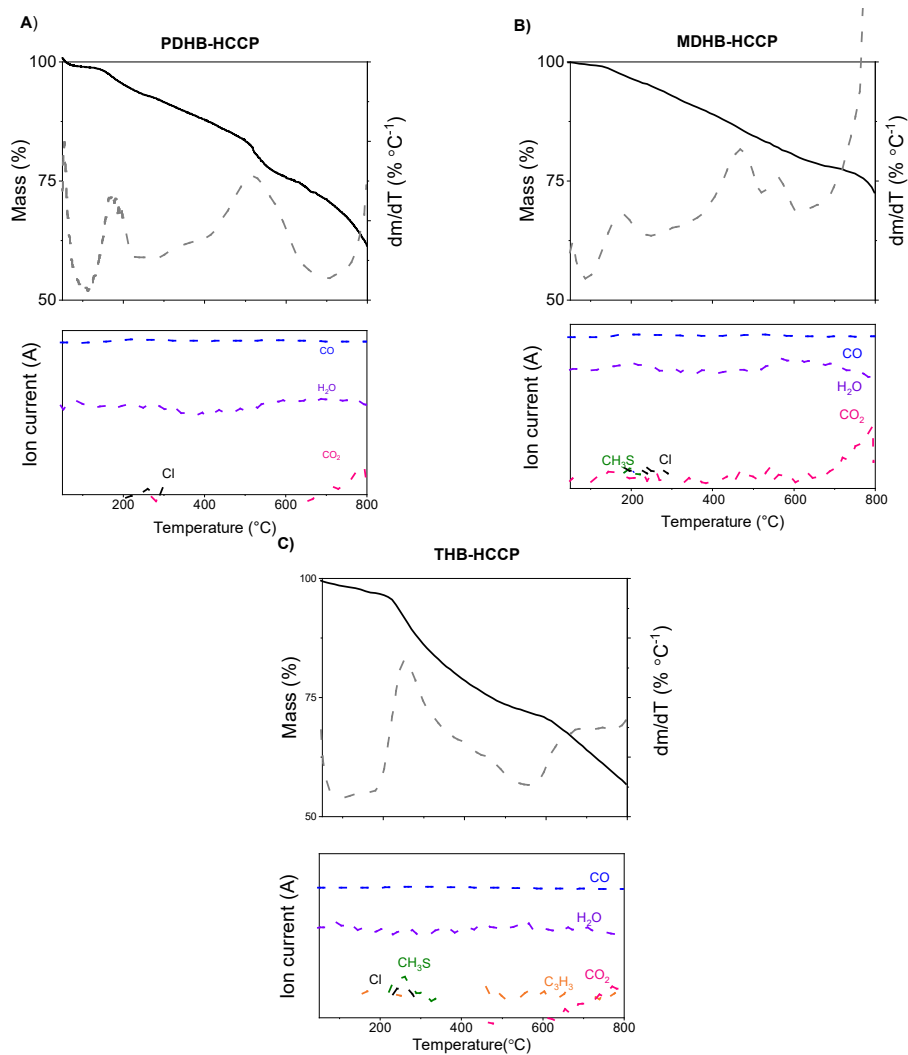
Figure S5.4 The mass loss (top panels) and the evolved gases (bottom panels) as a function of temperature for the polyphosphazene free-standing films prepared using different hydroxyl-containing monomers, obtained with a heating rate of 10 °C min$^{-1}$. (A) PDHB-HCCP, (B) MDHB -HCCP, and (C) THB-HCCP.
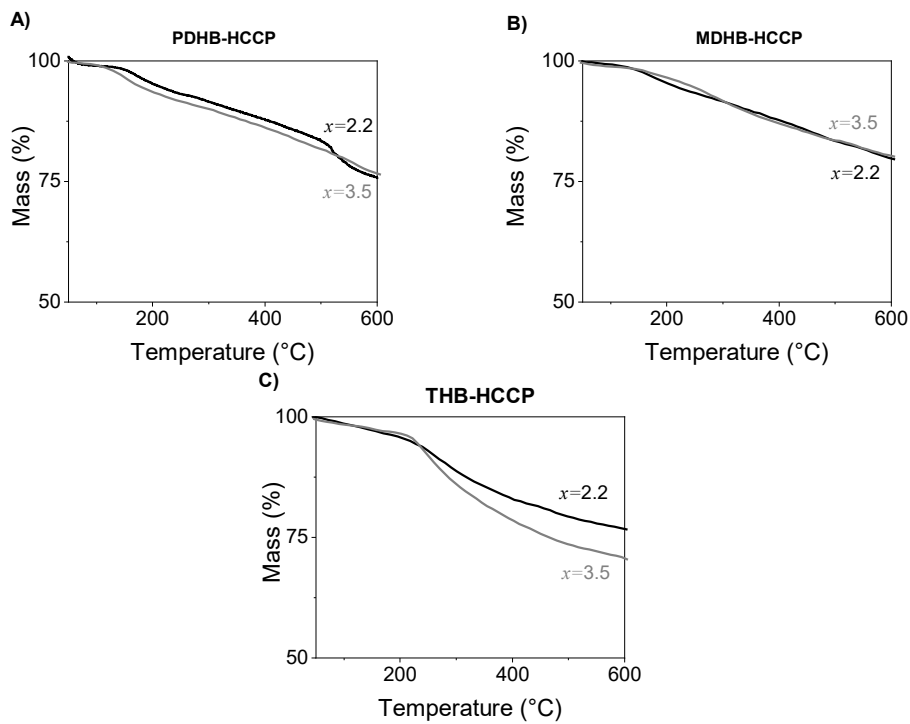
Figure S5.5 Comparison of the changes in sample mass of prepared free-standing films as a function of the temperature for the different KOH concentrations, $x$, A) PDHB-HCCP, (B) MDHB -HCCP, and (C) THB-HCCP. All samples were heated under N2 at 10 °C min$^{-1}$.

Table S5.2 Comparing the single gas separation properties of the supports and PDHB-HCCP membrane at 2 bar and 30 °C.

| Gases | Gas permeance (mol m$^{-2}$ s$^{-1}$ Pa$^{-1}$) | |
|---|---|---|
| | Support | PDHB-HCCP |
| He | $1.1 \times 10^{-6}$ | $1.1 \times 10^{-6} \pm 4.2 \times 10^{-9}$ |
| H$_2$ | $2 \times 10^{-6}$ | $2 \times 10^{-6} \pm 1.3 \times 10^{-8}$ |
| CO$_2$ | $6.1 \times 10^{-7}$ | $6.2 \times 10^{-7} \pm 1.9 \times 10^{-8}$ |
| N$_2$ | $5.7 \times 10^{-7}$ | $5.8 \times 10^{-7} \pm 5 \times 10^{-9}$ |
| CH$_4$ | $9.7 \times 10^{-7}$ | $9.8 \times 10^{-7} \pm 1.5 \times 10^{-9}$ |
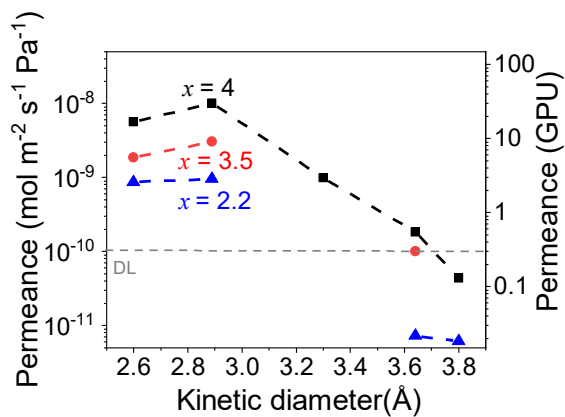


Figure S5.6  Gas permeance of THB-HCCP as a function of gas kinetic diameter at 200 ˚C for three different *x*.

# Chapter 6
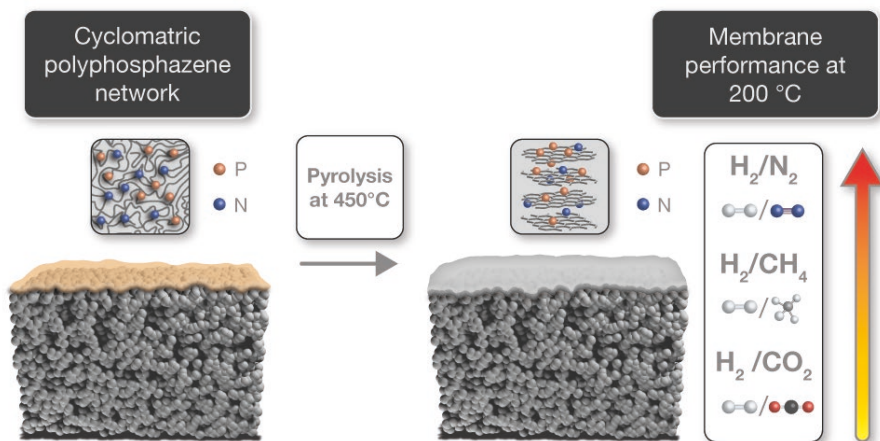
# Low temperature pyrolysis of thin film composite polyphosphazene membranes for hot gas separation

# Abstract

Highly selective thin-film composite membranes for hot hydrogen sieving are prepared via the pyrolysis of thin cyclomatric polyphenoxy phosphazene films that are prepared via non-conventional interfacial polymerization of hexachlorocyclotriphosphazene with 1,3,5-trihydroxybenzene or $m$-dihydroxybenzene. The presence of the cyclic phosphazene ring within the weakly branched polymer films gives rise to a distinct thermal degradation evolution, with an onset temperature around 200 °C. For the trihydroxybenzene derived material the hydrogen permselectivity of the films shows a maximum around a pyrolysis temperature of 450 °C. At this temperature, a compact atomic structure is obtained that comprises mostly disordered carbon and accommodates P-O-C and P-O-P bonds. These films reveal molecular sieving with permselectivities exceeding 100 for $H_2/N_2$, $H_2/CH_4$, and $H_2/CO_2$, and a hydrogen permeance of $2 \times 10^{-10}$ mol m$^{-2}$s$^{-1}$Pa$^{-1}$, at 200 °C. In particular, the $H_2/CO_2$ permselectivity at elevated temperatures is superior to that of other CMS membranes that have been presented in the literature. At ambient temperatures, the thin films are very effective barriers for small gas molecules. Because of the inexpensive facile synthesis and low temperature pyrolysis, the polyphosphazene films have potential for use in high-temperature industrial gas separations, as well as for use as barriers such as liners in high pressure hydrogen storage vessels at ambient temperature.

# 6.1 Introduction

Establishing a hydrogen-based economy has widespread momentum in many climate strategies.[1–3] This will require, amongst others, industrial-scale technology for molecular separation of hydrogen from other gases, such as CO, $CO_2$, and $CH_4$.[3–5] Membrane-based separation technology can contribute to this.[5–7] Carbon molecular sieve (CMS) membranes have been reported to exhibit good performance in selective $H_2$ separation processes.[5–7] CMS materials are fabricated via pyrolysis, under an inert atmosphere, of polymer networks comprising condensed hexagonal rings without a three-dimensional crystalline order.[8] The resulting materials have sub-nanometer pores with sizes and shapes that depend strongly on the type of polymer precursors and the applied thermal treatment conditions. Polymers including polybenzimidzole (PBI), Matrimid®, cellulose, polypyrrole, and polyimide with intrinsic microporosity have been pyrolyzed to develop membranes containing the elements C, N, and F.[5,8–11] For example, Matrimid® pyrolyzed at 675 °C has a $H_2/CO_2$ permselectivity of 1.3 at room temperature,[11] and polybenzimidzole (PBI) pyrolyzed at 900 °C has a $H_2/CO_2$ permselectivity of 80 at 150 °C.[8] Cellulose-based hollow fiber membranes pyrolyzed at 850 °C have $H_2/CO_2$ permselectivity of 83.9, $H_2/N_2$ permselectivity >800, and $H_2/CH_4$ selectivity >5700, at 130 °C.[5] CMS membranes can have a self-supporting asymmetric structure or can consist of a thin layer atop a porous ceramic or steel support. For the latter so-called thin film composite (TFC) membranes, preserving a continuous defect-free permselective thin film during pyrolysis is a challenge.[12–15] Richter et al. report a 125 nm thick carbon layer inside an asymmetric alumina tube through pyrolysis of a cross-linked unsaturated polyester, with $H_2/CO_2$ permselectivity of ~3 at 25 °C.[12] Another study reports alumina-supported CMS membranes via pyrolysis of phenol-formaldehyde resins at 500 °C, with permselectivities for $H_2/CO_2$ (~3), $H_2/N_2$ (~17), and $H_2/CH_4$ (~36.6), at 80 °C.

Recently, our group pioneered with a non-conventional interfacial polymerization (IP) technique for the fabrication of ultrathin cyclomatrix polyphosphazene films.[16] Central in this method is the replacement of the aqueous phase with a DMSO/KOH solution. In this superbase, the aromatic

hydroxy compounds can be partly converted to highly soluble and nucleophilic aryloxide anions. This allows for the fast nucleophilic substitution of the Cl groups in the hexachlorocyclotriphosphazene (HCCP) that is dissolved in the non-polar cyclohexane phase. The obtained thin film polyphosphazene networks have tuneable gas permeance, ranging from gas-tight barriers to molecular sieves for hydrogen at temperatures well above 200 °C.[16] The thermal stability of the films is exceptional. In part, this is due to the strong Ar-O bonds between the organic bridges and the HCCP molecules; these bonds are stronger than the amide or ester bonds that are prevalent for IP-derived materials. In addition, the cyclic HCCP has inherent high thermal stability and heat resistance due to the symmetrically distributed P atoms and the unvarying N-P bond length resulting from the dπ-pπ hybrid orbital overlap.[17] The thermal decomposition of the HCCP ring is an endothermic process. In addition, HCCP has a high limiting oxygen index (minimum percentage of oxygen in a mixture of oxygen and nitrogen needed for flaming combustion) and, when added as an additive to polymers, gives rise to cross-linked phosphorus oxynitride and carbonized aromatic networks in the solid phase.[18–20] The various phosphates formed in the combustion form non-volatile protective obstructions that impede the transport of oxygen and non-flammable combustion products, as well as the transport of heat. These properties make cyclomatrix polyphosphazene a popular non-halogenated additive for enhanced flame retardancy.[19]

In our previous studies, we have demonstrated that the almost complete substitution of the Cl groups by diphenol bridges results in an abrupt thermal degradation behavior, with a high onset temperature of ~400 °C.[16] In contrast, materials in which a limited number of the Cl groups are substituted by small aromatic hydroxyls exhibit a gradual thermal degradation, with an onset temperature around ~250 °C.[21] This gradual degradation facilitates controlled pyrolysis at relatively mild conditions, resulting in thin films with final atomic compositions (many heteroatoms) and structures that are distinct from other CMS materials. Here, we explore the pyrolysis of moderately cross-linked cyclomatrix polyphosphazene membranes with various temperature trajectories under $N_2$ atmosphere.

## 6.2 Experimental

### 6.2.1. Materials

Phosphonitrilic chloride trimer (HCCP, 99%), 1,3,5-trihydroxybenzene (THB, ≥99%), *m*-dihydroxybenzene (MDHB, ≥99.9%), and dimethyl sulfoxide (DMSO, anhydrous, ≥99.9%) were supplied from Sigma-Aldrich. Cyclohexane (EMSURE for analysis), and potassium hydroxide (KOH, pellets extra pure) were obtained from Merk. Macroporous α-alumina discs with a diameter of 39 mm, a thickness of 2 mm, and a pore size of 80 nm were purchased from Pervatech B.V. and used as support.

### 6.2.2. Material fabrication

Free-standing polymer membrane layers and thin-film composite polymeric membranes were formed by interfacial polymerization of a 10 w/v% solution of the THB or MDHB, aromatic hydroxy compounds (AHC), in DMSO and KOH, super base[22], and a 3.5 w/v% HCCP solution in cyclohexane. The mol ratio of hydroxyl groups (monomers: KOH) is denoted $x$ and was kept at 3.5:1. This hydroxyl ratio was chosen based on the earlier experiments and it is close to minimum amount of KOH for making a free-standing layer. THB or MDHB is partly deprotonated by using KOH. Nucleophilic substitution takes place by the attack of the phenolate anions on the phosphor atoms of the HCCP rings, displacing the chlorine atoms. The formed networks are denoted THB-HCCP and MDHB-HCCP.

The TPE-HCCP free-standing layer was prepared in the following way. A 3.5 wt.% HCCP solution in cyclohexane was gently poured atop the TPE solution to minimize disturbances of the top layer of the TPE solution. A thin layer formed at the interface of the two phases as the two solutions contacted. After 30 min, the films were collected, filtered, and washed 3 times with ethanol, acetone, and water. Then, the solid films were dried in a vacuum oven at 50°C.

## Synthesis of free-standing films

Free-standing films were prepared as follows. First, the AHC solutions were heated at 80°C for 2.5 hr. Next, the HCCP solution in cyclohexane was poured atop the AHC solution while still hot. The reaction happened as soon as the two solutions were brought into contact, and it was confirmed by visual observation of the formation of a thin layer. After 10 min, the formed thin film at the interface was collected, filtered, and washed with acetone, ethanol, and water and dried in a vacuum oven at 50 °C.

## Preparation of thin-film composite membranes

The α-alumina discs were coated with a 3 μm thick γ-alumina (porosity of ~40 % and pore size of 2-3 nm) based on the reported procedure.[23] The ceramic supports were heated to 80 °C for 2.5 h. After this, the support was impregnated with 5 ml of AHC solution in the oven at 80 °C for 10 min. Next, it was taken out, and its surface was dried by applying a rubber roller and $N_2$ gun. Then, the support was submerged into 5 ml of HCCP solution at ambient temperature. After 10 min reaction time, the solution was discarded from the surface, and the membranes were rinsed with ethanol to remove any residual reactant. The membrane was kept under a fume hood overnight and then dried in a vacuum oven at 50 ºC for a minimum of 24 h.

## Thermal treatment

Table 6.1 Overview of the used protocols and their label for thermal treatment of the membranes.

| Name | Treatment |
|---|---|
| Network-200 | 10 h at 200 ˚C |
| Network -250 | Network-200 + 10 h at 260 ˚C |
| Network-300 | Network -250 + 10 h at 300 ˚C |
| Network-350 | Network-300 + 10 h at 350 ˚C |
| Network-450 | Network-350 + 10 h at 450 ˚C |
| Network-550 | Network-450 + 10 h at 550 ˚C |
| Network-650 | Network-550 + 10 h at 650 ˚C |

Thermal treatment was done in an STF (single zone furnace) 16/610 tubular furnace (Carbolite) equipped with an alumina working tube under $N_2$

atmosphere. The membrane was thermally treated according to the protocols given in Table 6.1. The final temperature was reached at a ramp rate of 2 ˚C min$^{-1}$. The furnace was evacuated and refilled with $N_2$ two times before treatment, followed by thermal treatment under a $N_2$ flow of 200 mL min$^{-1}$. The thermally treated samples are labeled as network's name-*xxx*, where *xxx* represents the final temperature (°C) used in the thermal treatment process.

## 6.2.3. Material characterization

A field emission scanning electron microscope (FE-SEM, Zeiss MERLIN) was used to envision the thickness and morphology of the membranes. To obtain a clean fracture, samples were prepared by immersion into liquid nitrogen for 5 min before breaking them. For EDX analysis, all samples were dried and coated with a 5 nm Pt/Pd conductive layer using a sputter coater Quorum Q150T ES (Quorum Technologies, Ltd., UK) and was done at 10 kV with >1000 counts/s. Fourier transform infrared spectroscopy in attenuated total reflectance mode (FTIR-ATR, PerkinElmer Spectrum Two, USA) was used to characterize the powder product formed over 16 scans with a resolution of 4 cm$^{-1}$ over a wavelength range of 400-4000 cm$^{-1}$. The elemental composition of synthesized powders was measured with X-Ray Fluorescence (XRF) (S8 Tiger, Bruker) and C,N elemental analysis (FLASH 2000 series analyzer). X-ray photoelectron spectroscopy (XPS) measurements were performed on PHI Quantes scanning XPS/HAXPES microprobe using a monochromatic Al Kα source (1486.6 eV). The binding energies of the benzene ring (from the aromatic hydroxy compounds) were fixed in the carbon elemental fit of the prepared powders. Thermo Gravimetric Analysis (TGA, STA 449 F3 Jupiler®, Netzsch) in combination with mass spectrometry (MS, QMS 403 D Aeolos MS, Netzsch) was used to evaluate the thermal stability of the membranes. A fixed amount of sample (10 mg) was heated on a heating stage under an inert nitrogen atmosphere at a heating rate of 10 ºC min$^{-1}$.

## 6.2.4. Membrane performance

Single gas permeance measurements were carried out using a dead-end mode set-up (Inspector Poseidon, Convergence). The single gas permeance of He, $N_2$, $CH_4$, $H_2$, and $CO_2$ was measured at a transmembrane pressure of 2

bar within the temperature ranges from 50 to 250 ºC. The lower detection limit of the set-up was $10^{-10}$ mol m$^{-2}$ s$^{-1}$ Pa$^{-1}$. Permselectivity was calculated as the ratio of the respective permeances. The experiments were performed at least twice, and the reported results are the average of the obtained values.
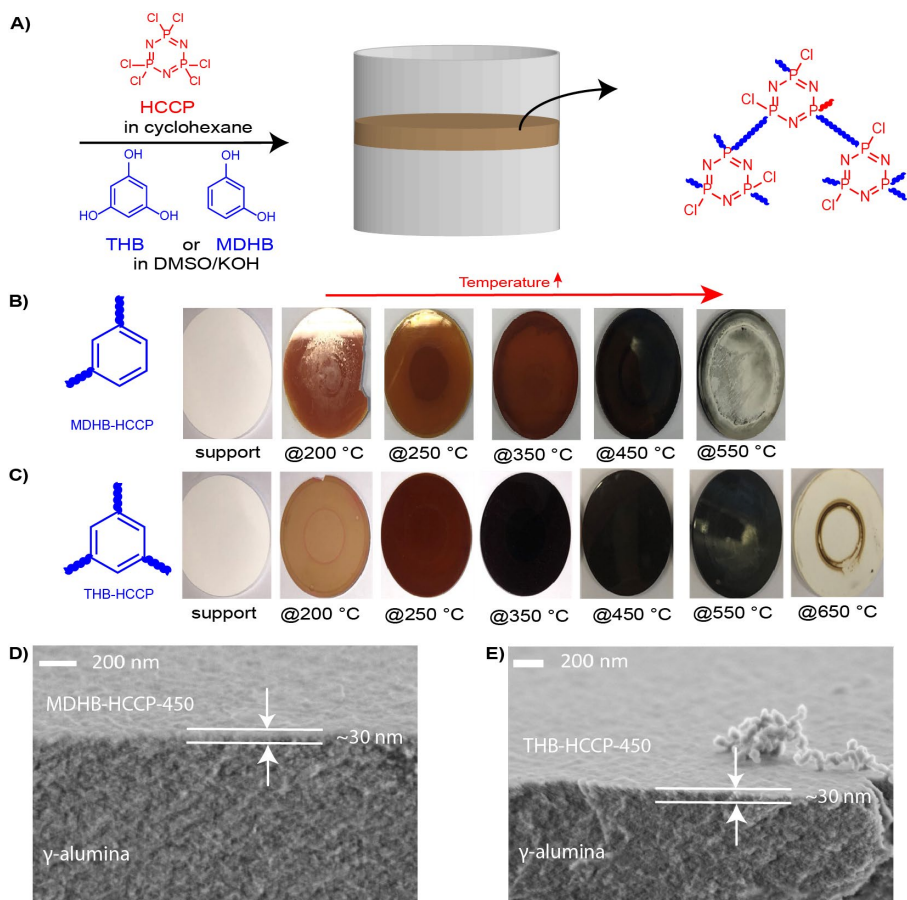
## 6.3 Results & Discussion



Figure 6.1 (A) Schematic representation of MDHB-HCCP and THB-HCCP membrane preparation. (B) Effect of thermal treatment on the appearance of THB-HCCP membranes. (C) Effect of thermal treatment on the appearance of MDHB-HCCP membranes. (D) FE-SEM picture of MDHB-HCCP-450 membrane. (E) FE-SEM picture of THB-HCCP-450 membrane. The dark rings in the centers of the

samples are a consequence of the sealing rings that were used in permeation experiments.

Figure 6.1A gives a schematic representation of the preparation of polyphosphazene networks on top of ceramic supports, using the approach reported in the earlier report.[21] Figure 6.1B and Figure 6.1C show top views of the thin film composites obtained after pyrolysis at various temperatures under an inert atmosphere. The color of samples changes with temperature. Both the MDHB and THB-derived samples have an orange color after treatment at 200 °C, and change to black after treatment at 450 °C. After treatment at 550 °C, the color of the MDHB-HCCP sample becomes white, indicating that the layer is gone. For THB-HCCP, the dark color after 550 °C is evidence that a layer is still present; after 650 °C, this layer is also gone. The SEM micrographs in Figure 6.1D and Figure 6.1E show the cross-sections of the samples treated at 450 °C and reveal the presence of thin layers, even after exposure to these high temperatures. The thicknesses of the layers, ~30 nm, are comparable to those of the untreated samples.[21] This is distinct from other CMS membranes that generally reveal substantial changes in dimensions and mass.[5,8]

Table 6.2 EDX data, elemental concentrations for pyrolyzed THB-HCCP powders

| | Elemental concentration(%) | | | |
|---|---|---|---|---|
| | THB-HCCP | THB-HCCP-200 | THB-HCCP-350 | THB-HCCP-450 |
| C | 41.5±2.8 | 39.5±1.1 | 54.8±1.8 | 51.1±0.6 |
| N | 14.2±0.5 | 13.0±2.3 | 3.0±0.1 | 2.3±0.3 |
| O | 27.9±2.9 | 23.8±2 | 31.8±1.5 | 33.0±1.1 |
| P | 9.2±1.1 | 18.4±3.8 | 9.3±0.3 | 12.0±1.1 |
| S | 0.8±0.1 | 1.3±0.3 | 0.6±0.1 | 0.7±0.1 |
| Cl | 3.8±1.5 | 3.1±1.3 | 0.1±0 | 0.2±0 |
| K | 2.6±1.0 | 1.1±0.3 | 0.4±0.2 | 0.6±0.1 |
| C/N | 2.9±0.2 | 3±0.5 | 18±0.8 | 22±2.7 |
| P/N | 0.6±0.1 | 1.4±0.4 | 3.1±0.2 | 5.2±0.8 |
| P/C | 0.1±0 | 0.5±0.1 | 0.2±0 | 0.2±0 |

Figure 6.2A and Figure 6.2B depict FTIR spectra of the monomers and the free-standing layers before and after pyrolysis. The spectra for the untreated free-standing films confirm network formation during the IP process. The broad peak in the range of 1100 to 1250 $cm^{-1}$ belongs to the asymmetric P=N stretching vibration of HCCP[24], and the peak around 873 $cm^{-1}$ is ascribed to the symmetric P=N stretching vibration.[24] Covalent connection is confirmed by the peaks at 950 $cm^{-1}$ and 1003 $cm^{-1}$ that are assigned to the stretching vibration of Ar-O-P.[25] After treating the samples at 200 °C, their spectra become less discrete. The Ar-O-P peaks intensify for both networks, implying further cross-linking of the networks. There is an overall increase in the intensity of adsorption in the range 1079 $cm^{-1}$ that can be attributed to the formation of P-O bonds, such as P–O–P  and other phosphates.[26–28] This becomes progressively more pronounced after treatment at higher temperatures. After treatment at 350 °C, peaks at 1400 and 1600 $cm^{-1}$, corresponding to the C=C bond becomes broadening. This suggests that at these temperatures, both materials consist of phosphorus-rich carbonaceous structures.[28]

EDX data in Table 6.2 and Table S6.1 confirm that, after treatment at  350 °C and 450 °C, the elemental composition of the materials comprises mainly carbon, oxygen, and phosphor. At these temperatures, most nitrogen is removed from the material. This is consistent with the decline in N/C ratio with temperature in Figure 6.2C and Table S6.2, as determined from C,N elemental analysis. For both samples, the N/C ratio decreases slightly upon treatment at 200 °C, which is attributed to an increase in the extent of cross-linking at this temperature. This is shown by an increase in the P/Cl ratio observed by XRF (Table S6.3) upon treatment at 200 °C, indicating that the thermal treatment increases the connection from an average of 2 to an average of 4-5 organic bridges per HCCP core. Further cross-linking can originate from reactions between unreacted phenolates and P-Cl moieties and reactions between P-Cl and P-OH groups of hydrolyzed HCCP.[29] A further increase in the pyrolysis temperature from 200-250 °C causes a strong further decline in the N/C ratio due to the loss of N from the collapsing HCCP core.[24,30] This removal of nitrogen progresses further to 350 °C and 450°C.
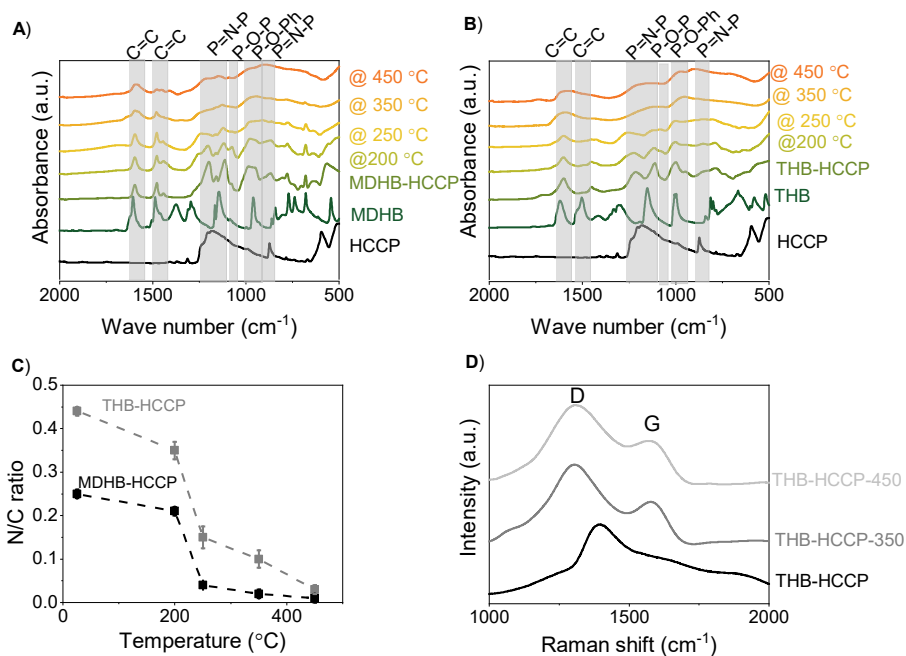
Figure 6.2 FTIR spectra of monomers and formed networks before and after heat treatment (A) MDHB-HCCP, (B) THB-HCCP, (C) effect of thermal treatment temperature on the N/C ratio in the synthesized powders see also Table S6.1, and (D) Raman spectra of THB-HCCP, THB-HCCP-350, and THB-HCCP-450 with D and G bands representing disordered carbon and highly oriented graphitic carbon, respectively.

The Raman spectra in Figure 6.2D give an indication of changes in the atomic order/disorder in THB-HCCP, before and after pyrolysis at temperatures of 350 °C and 450 °C.[31] The two broad peaks that appear at ~1310 and ~1580 cm$^{-1}$ correspond to the $D$ and $G$ bands, respectively.[18] The $D$ band is assigned to the $A_{1g}$ in-plain vibration mode of disordered carbon.[5] The $G$ band is associated with the $E_{2g}$ in-plain vibration mode of ordered carbon with an sp$^2$ electronic configuration and associates with the degree of graphitization.[32] The ratio of the two types of carbon ($I_D/I_G$, Figure S6.1) is calculated from the deconvoluted peak area. It is 3.6 for TPE-HCCP-350 and 2.7 for TPE-HCCP-450. The decrease indicates more ordering of carbon at higher temperatures.[33] The graphitic crystallite size, estimated from the Tuinstra−Koenig equation $L_a = 4.4\ I_G/I_D$, [34] is 1.13 nm for THB-HCCP-350 and 1.19 nm for THB-HCCP-450, confirming a slightly

more defective graphitic carbon in TPE-HCCP-350.[8] These observations are in line with the decomposition of the P-N rings at 350 °C and 450 °C derived from EDX and C,N elemental analysis. This explains why pyrolysis in our materials already occurs at lower temperatures than for other polymers.[38] The relatively low pyrolysis temperatures result in $I_D/I_G$ values exceeding 1, indicative of relatively disordered carbon.[35] This is in contrast to polyphosphazene carbonized at a high temperature of 950 °C.[36,37]

The thermally induced collapse of the HCCP ring is also evident from XPS data. In figure S6.2, the N1s spectrum of THB-HCCP reveals two peaks corresponding to nitrogen in the HCCP ring. For THB-HCCP-200, the position and surface area under these peaks is changed, which we attribute to an increased extent of cross-linking. A further increase of the temperature to 250 °C and higher results in a completely different spectrum, implying that the ring opening of HCCP takes place and nitrogen is no longer accommodated in the ring structure of HCCP. The P2p spectrum exhibited nearly identical curves at different processing steps of samples, Figure S6.3. In Figure S6.4, the 1s spectrum of THB-HCCP-350 shows two pronounced peaks located around 284.7 eV and 286.3 eV, corresponding to C=C/C-C and C-O/C-N, respectively. The percentage of functional groups can be calculated based on the area under each fitted peak. With increasing the pyrolysis temperature to 450 °C, the ratio of deconvoluted peak area of (C-O/C-N) to (C=C/C-C) decreases, indicating the conversion of C-O/C-N to more C=C/C-C groups, graphite-like carbon.[35,38] We can conclude an increase in the degree of graphitization which is in line with Raman spectroscopy. Also, it confirmed the results of the high-resolution N1s XPS spectrum.
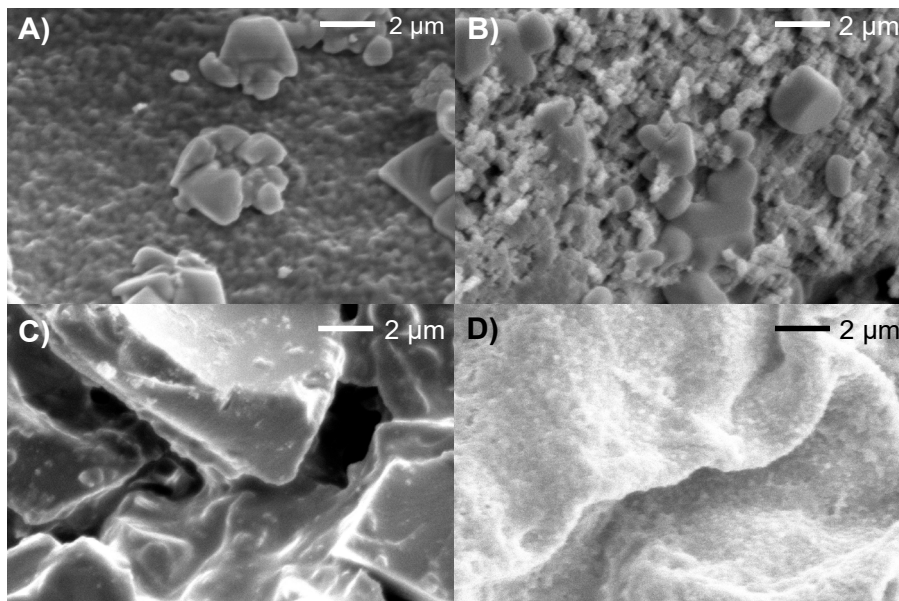
Figure 6.3 SEM images of prepared powders. (A) THB-HCCP, (B) THB-HCCP-200, (C) THB-HCCP-350, and (D) THB-HCCP-450.

The thermal stability of prepared polyphosphazene networks was evaluated by TGA-MS under $N_2$ and the detailed data are shown in Figure S6.5. The untreated networks exhibit a three-step weight loss between 50-600 °C.[21] The removal of the trapped solvents and enhancing the extent of cross-linking happens from room temperature to ~250°C. The second stage, between 250 °C to 400 °C, is attributed to the collapsing of the HCCP ring and partially carbonization of the network. Above 400 °C, further decomposition of aromatic rings and carbonization occurs.[24] In addition, Figure S6.5 shows that increasing the pyrolysis temperature decreases the mass of remaining char at 600 °C and enhances the onset of degradation due to removing the unstable bonds.

Figure 6.3 reveals the changes in the microstructure of THB-HCCP free-standing films upon pyrolysis. Prior to pyrolysis, a regular continuous film covers the ceramic support. This morphology is reported in only a few other studies, all of which are based on a single-solvent polymerization technique.[24,39,40] Heating the sample to 200 °C does not substantially change this morphology. Exposure to 350 °C results in a completely distinct

structure. This is partly caused by graphitization, but it is also due to the soft intumescent characteristics of the polyphosphazene in which materials swell when exposed to fire or heat to form a porous foamed mass. Pyrolysis leads to the formation of $PO_x$ and phosphoric acid derivatives. These derivatives can react further to form P-O-C and P-O-P complexes.[18] Another study considers the formation of cross-linked phosphorus oxynitride and carbonized aromatic networks during combustion.[19,20] Increasing the temperature to 450 °C further affects the structure of the layer. The thermal degradation of the material creates a layer that can inhibit the transport of gaseous products, and shields part of the material from heat and air.[18,19] Figure S6.6 shows the digital photos of the THB-HCCP-200 and THB-HCCP-450 powders from top and side views. The structure of THB-HCCP changes from flakes to porous structures after raising the treatment temperature from 200 °C to 450 °C. It confirms that at 450 °C the materials are indeed soft intumescent and the size of the powder increases during thermal treatment.
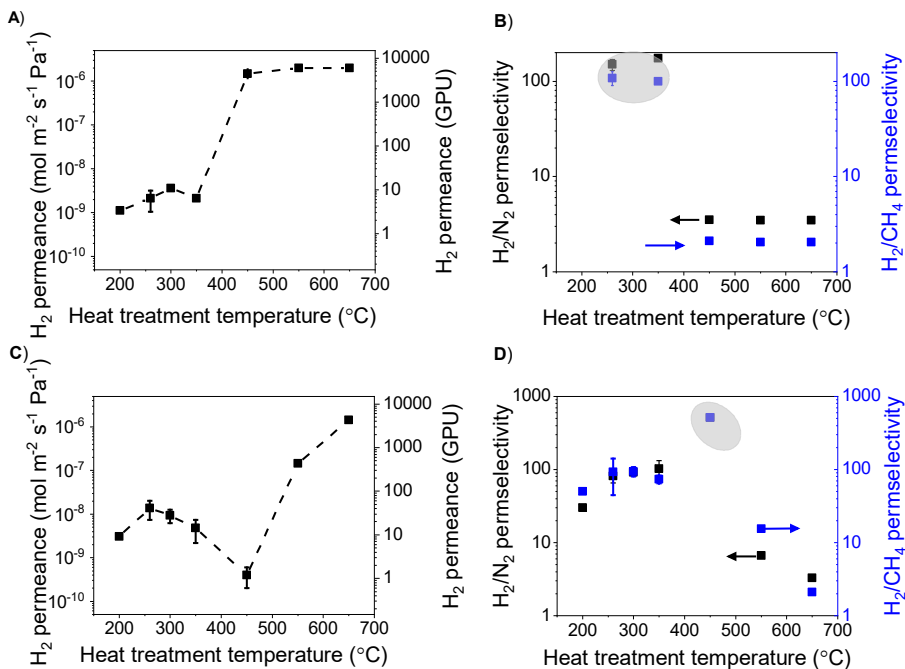
Figure 6.4 Effect of pyrolysis temperature on the performance of MDHB-HCCP at 200 ˚C (A) $H_2$ permeance, (B) $H_2/N_2$ and $H_2/CH_4$ permselectivity. Effect of the pyrolysis temperature on the performance of THB-HCCP at 200 ˚C, (C) $H_2$ permeance and (D) $H_2/N_2$ and $H_2/CH_4$ permselectivity. The gray circles show permselectivity data calculated based on the gas permeance obtained by the setup; however, $N_2$ and $CH_4$ permeances were below the detection limit of the setup.

The changes in the structure and morphology of the thin film composites affect their permselective properties. The gas separation performances of the prepared membranes were tested with pure He, $H_2$, $CO_2$, $N_2$, and $CH_4$ at a temperature between 50 to 200 °C and at a transmembrane pressure of 2 bar. Figure 6.4A and Figure 6.4B present the effects of pyrolysis temperature on the performance of MDHB-HCCP at 200 °C. For the MDHB-HCCP films, the exposure to higher temperatures results in a monotonous increase in the permeance of hydrogen at 200 °C, combined with an almost complete loss in permselectivity of hydrogen over nitrogen of methane. This observed trade-off suggests that pyrolysis leads to defects in the thin film. At a pyrolysis temperature of 450 °C, the surface colour of the sample is still black, as can be seen in Figure 6.1, but the permeances are comparable to those of the

191

ceramic supports. It is good to mention that the calculated permselectivity shown in the gray circle is based on the gas permeance of $N_2$ and $CH_4$ obtained by the set-up; however, those permeances are under the setup's detection limit, which is $1\times10^{-10}$ mol m$^{-2}$ s$^{-1}$ Pa$^{-1}$.

For THB-HCCP membranes, another behaviour is observed, Figure 6.4C and Figure 6.4D. The permeance of hydrogen at 200 °C shows a substantial increase when the sample is thermally treated at 250 °C instead of 200 °C. This increase in permeance is accompanied by an increase in permselectivity of hydrogen over nitrogen or methane. The treatment at 250 °C causes enhanced cross-linking within the polymer network, enhancing its rigidity and changing the size and the shape of the free volume elements that it contains.[41] As a result, the diffusion mobility of hydrogen in the network becomes more significant. This is substantiated by the lower activation energy of the hydrogen permeance (Figure S6.7), indicating the reduction in energy barriers for the diffusion of hydrogen molecules. For the larger molecules, nitrogen and methane, this effect is less and an enhancement in permeance is less pronounced.[41] The hydrogen permeance and its activation energy are comparable to those of very tight polybenzimidazole membranes at 39 bar 200 °C.[42] An increase in pyrolysis temperature to 300 °C does not significantly affect the permeance of hydrogen, while the activation energy reduces further. This can be explained by a lower amount of slightly larger free-volume elements. When the pyrolysis is performed at 350 °C, the activation energy is further reduced, but the permeance of 200 °C hot hydrogen does not significantly increase. This is attributed to the graphitization of part of the material, reducing the number of pathways that are available for diffusive transport. This is even more pronounced for a pyrolysis temperature of 450 °C, where the lowest $H_2$ permeance is observed, consistent with large extent of graphitization observed with Raman for this temperature. For this film, the highest permselectivity is observed, where the permeances of nitrogen and methane are below the detection limit of the set-up. Pyrolysis at temperatures of 550 °C and higher results in a strong decrease in permselectivities, due to the formation of defects.

Because of the positive values of the activation energy for transport, the permeances of the gases reduce when their temperatures are lower. The

result is that, at ambient temperature, the thin THB-HCCP-450 films are very good barriers for small gases, including hydrogen.
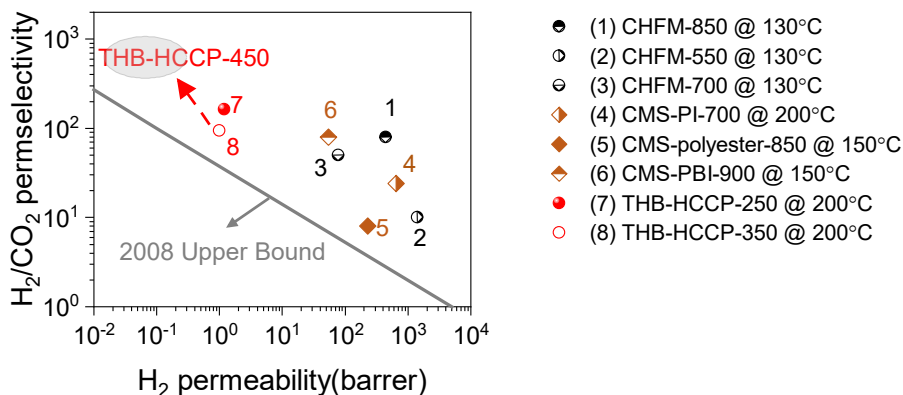


Figure 6.5 Comparison of the $H_2/CO_2$ gas performance of the prepared membranes with state-of-the-art $H_2/CO_2$ carbonized and inorganic membrane materials tested in the temperature range of 130-200 °C. The performance of THB-HCCP-450 is predicted at 200 °C. The $H_2/CO_2$ line is drawn based on the 2008 Robeson upper bond.

The $H_2/CO_2$ permselectivity of THB-HCCP is compared with that of other carbonized membranes, including carbon hollow fiber (CHFM) [5], carbonized polyimide [43], carbonized polyester [12], carbonized polybezimidazole [8] at temperatures above 130 °C in a Robeson plot (Figure 6.5). For THB-HCCP-250 and THB-HCCP-350, the $CO_2$ permeance is below the detection limit and the calculation is based on a $CO_2$ permeance of $1 \times 10^{-10}$ mol m$^{-2}$ s$^{-1}$ Pa$^{-1}$. The THB-HCCP-250 and THB-HCCP-350 show similar $H_2/CO_2$ permselectivity compared to the other studies. The predicted $H_2/CO_2$ permselectivity of THB-HCCP-450, at 200 °C, surpasses that of the carbonized membranes. In addition, the low permeability is compensated by the low thickness that can be achieved by the IP technique. Considering the separation performance for $H_2/CO_2$, $H_2/CH_4$ and $H_2/N_2$, the thermally treated TPE-HCCP-350 and TPE-HCCP-450 can be suitable for $H_2$ purification on industrial scales.

## 6.4 Conclusion

Pyrolysis of ultra-thin (~30 nm) cyclomatrix polyphosphazene membranes is used to tailor their gas separation performance. The thin film composites are prepared by interfacial polymerisation between a small aromatic hydrocarbon (in dimethyl sulfoxide with potassium hydroxide) and hexachlorocyclotriphosphazene in cyclohexane, followed by pyrolysis at temperatures between 200 to 650 °C. A combination of characterization techniques reveals that the onset of carbonization is as low as ~350 °C. The low pyrolysis temperatures, as compared to those employed in other membrane carbonization studies, result from the distinct thermal degradation of the phosphazene ring. For 1,3,5-trihydroxybenzene based polyphosphazene, pyrolysis at 450 °C gives the lowest observed hydrogen permeance of 200 °C, combined with the highest observed permselectivity of hydrogen over nitrogen or methane. This is due to the unique hybrid material that is formed during pyrolysis, combining ordered and disordered graphitized structures and accommodating P-O-P and P-O-C bonds. Hydrogen permeance at 200 °C is of the order of $2 \times 10^{-10}$ mol m$^{-2}$ s$^{-1}$ Pa$^{-1}$, and at least 100 higher as compared to permeance of nitrogen, methane, and carbon monoxide. The higher permselectivity for hydrogen over other gases, as compared to other CMS membranes, makes the pyrolyzed polyphosphazene membranes promising for use in high-temperature applications. At ambient temperatures, the thin film composites have very low gas permeance, making them potential barriers for small gas molecules, including hydrogen.

## 6.5 Acknowledgement

194

# 6.6 References

[1] A. Midilli, H. Kucuk, M.E. Topal, U. Akbulut, I. Dincer, A comprehensive review on hydrogen production from coal gasification: Challenges and Opportunities, Int. J. Hydrogen Energy. 46 (2021) 25385–25412. https://doi.org/10.1016/j.ijhydene.2021.05.088.

[2] H. Lin, E. Van Wagner, B.D. Freeman, L.G. Toy, R.P. Gupta, Plasticization-Enhanced Hydrogen Purification Using Polymeric Membranes, Science (80-. ). 311 (2006) 639–642. https://doi.org/10.1126/science.1118079.

[3] M. Noussan, P.P. Raimondi, R. Scita, M. Hafner, The Role of Green and Blue Hydrogen in the Energy Transition—A Technological and Geopolitical Perspective, Sustainability. 13 (2020) 298. https://doi.org/10.3390/su13010298.

[4] H.W. Kim, H.W. Yoon, S.-M. Yoon, B.M. Yoo, B.K. Ahn, Y.H. Cho, H.J. Shin, H. Yang, U. Paik, S. Kwon, J.-Y. Choi, H.B. Park, Selective Gas Transport Through Few-Layered Graphene and Graphene Oxide Membranes, Science (80-. ). 342 (2013) 91–95. https://doi.org/10.1126/science.1236098.

[5] L. Lei, F. Pan, A. Lindbråthen, X. Zhang, M. Hillestad, Y. Nie, L. Bai, X. He, M.D. Guiver, Carbon hollow fiber membranes for a molecular sieve with precise-cutoff ultramicropores for superior hydrogen separation, Nat. Commun. 12 (2021). https://doi.org/10.1038/s41467-020-20628-9.

[6] C. Zhang, W.J. Koros, Ultraselective Carbon Molecular Sieve Membranes with Tailored Synergistic Sorption Selective Properties, Adv. Mater. 29 (2017) 1701631. https://doi.org/10.1002/adma.201701631.

[7] W. Qiu, J. Vaughn, G. Liu, L. Xu, M. Brayden, M. Martinez, T. Fitzgibbons, G. Wenz, W.J. Koros, Hyperaging Tuning of a Carbon Molecular-Sieve Hollow Fiber Membrane with Extraordinary Gas-Separation Performance and Stability, Angew. Chemie Int. Ed. 58 (2019) 11700–11703. https://doi.org/10.1002/anie.201904913.

[8] M. Omidvar, H. Nguyen, Liang Huang, C.M. Doherty, A.J. Hill, C.M. Stafford, X. Feng, M.T. Swihart, H. Lin, Unexpectedly Strong Size-Sieving Ability in Carbonized Polybenzimidazole for Membrane H 2 /CO 2 Separation, ACS Appl. Mater. Interfaces. 11 (2019) 47365–47372. https://doi.org/10.1021/acsami.9b16966.

[9] W. Ogieglo, T. Puspasari, M.K. Hota, N. Wehbe, H.N. Alshareef, I. Pinnau, Nanohybrid thin-film composite carbon molecular sieve membranes, Mater. Today Nano. 9 (2020) 100065. https://doi.org/10.1016/j.mtnano.2019.100065.

[10] J.W.F. To, J. He, J. Mei, R. Haghpanah, Z. Chen, T. Kurosawa, S. Chen, W.-G. Bae, L. Pan, J.B.-H. Tok, J. Wilcox, Z. Bao, Hierarchical N-Doped Carbon as CO 2 Adsorbent with High CO 2 Selectivity from Rationally Designed Polypyrrole Precursor, J. Am. Chem. Soc. 138 (2016) 1001–1009. https://doi.org/10.1021/jacs.5b11955.

[11] M. Rungta, G.B. Wenz, C. Zhang, L. Xu, W. Qiu, J.S. Adams, W.J. Koros, Carbon molecular sieve structure development and membrane performance relationships, Carbon N. Y. 115 (2017) 237–248. https://doi.org/10.1016/j.carbon.2017.01.015.

[12] H. Richter, H. Voss, N. Kaltenborn, S. Kämnitz, A. Wollbrink, A. Feldhoff, J. Caro, S. Roitsch, I. Voigt, High-Flux Carbon Molecular Sieve Membranes for Gas Separation, Angew. Chemie Int. Ed. 56 (2017) 7760–7763. https://doi.org/10.1002/anie.201701851.

[13] M.L. Jue, Y. Ma, R.P. Lively, Streamlined Fabrication of Asymmetric Carbon Molecular Sieve Hollow Fiber Membranes, ACS Appl. Polym. Mater. 1 (2019) 1960–1964. https://doi.org/10.1021/acsapm.9b00567.

[14] M. Acharya, H.C. Foley, Spray-coating of nanoporous carbon membranes for air separation, J. Memb. Sci. 161 (1999) 1–5. https://doi.org/10.1016/S0376-7388(99)00173-8.

[15] L. Forster, C. D'Agostino, M.A. Llosa-Tanco, V. Spallina, C. Brencio, F. Gallucci, M. Lindley, S.J. Haigh, D.A. Pacheco-Tanaka, Tailoring pore structure and surface chemistry of microporous Alumina-Carbon Molecular Sieve Membranes (Al-CMSMs) by altering carbonization temperature for optimal gas separation performance: An investigation using low-field NMR relaxation measurements, Chem. Eng. J. 424 (2021) 129313. https://doi.org/10.1016/j.cej.2021.129313.

[16] F. Radmanesh, Ernst J.R. Sudhölter, A. Tena, M. G. Elshof, N. E. Benes, Thin film composite cyclomatrix poly(phenoxy)phosphazenes membranes for hot hydrogen separation, Submitted. (n.d.).

196

[17] X. Zhou, S. Qiu, X. Mu, M. Zhou, W. Cai, L. Song, W. Xing, Y. Hu, Polyphosphazenes-based flame retardants: A review, Compos. Part B Eng. 202 (2020) 108397. https://doi.org/10.1016/j.compositesb.2020.108397.

[18] S. Qiu, Y. Zhou, X. Zhou, T. Zhang, C. Wang, R.K.K. Yuen, W. Hu, Y. Hu, Air-Stable Polyphosphazene-Functionalized Few-Layer Black Phosphorene for Flame Retardancy of Epoxy Resins, Small. 15 (2019). https://doi.org/10.1002/smll.201805175.

[19] S. Qiu, X. Wang, B. Yu, X. Feng, X. Mu, R.K.K. Yuen, Y. Hu, Flame-retardant-wrapped polyphosphazene nanotubes: A novel strategy for enhancing the flame retardancy and smoke toxicity suppression of epoxy resins, J. Hazard. Mater. 325 (2017) 327–339. https://doi.org/10.1016/j.jhazmat.2016.11.057.

[20] S. Qiu, W. Xing, X. Feng, B. Yu, X. Mu, R.K.K. Yuen, Y. Hu, Self-standing cuprous oxide nanoparticles on silica@ polyphosphazene nanospheres: 3D nanostructure for enhancing the flame retardancy and toxic effluents elimination of epoxy resins via synergistic catalytic effect, Chem. Eng. J. 309 (2017) 802–814. https://doi.org/10.1016/j.cej.2016.10.100.

[21] F. Radmanesh, E. J.R. Sudhölter, A. Tena, M. A. Hempenius, N. Benes, Non-aqueous interfacial polymerization derived polyphosphazene films for sieving or blocking hydrogen gas, Submitted. (n.d.).

[22] A.S. Bobkov, N.M. Vitkovskaya, B.A. Trofimov, Cascade Assembly of 4,5,6,7-Tetrahydroindole from Cyclohexanone Oxime and Acetylene in the KOH/DMSO Superbase Medium: A Quantum Chemical Study, J. Org. Chem. 85 (2020) 6463–6470. https://doi.org/10.1021/acs.joc.0c00353.

[23] X. Wang, P. Karakiliç, X. Liu, M. Shan, A. Nijmeijer, L. Winnubst, J. Gascon, F. Kapteijn, One-Pot Synthesis of High-Flux b -Oriented MFI Zeolite Membranes for Xe Recovery, ACS Appl. Mater. Interfaces. 10 (2018) 33574–33580. https://doi.org/10.1021/acsami.8b12613.

[24] M. Zhang, Y. Li, C. Bai, X. Guo, J. Han, S. Hu, H. Jiang, W. Tan, S. Li, L. Ma, Synthesis of Microporous Covalent Phosphazene-Based Frameworks for Selective Separation of Uranium in Highly Acidic Media Based on Size-Matching Effect, ACS Appl. Mater. Interfaces. 10 (2018) 28936–28947. https://doi.org/10.1021/acsami.8b06842.

[25] G. Tang, X. Zeng, L. Hou, T. Song, S. Yin, B. Long, A. Ali, G.-J. Deng, Cross-linked ultrathin polyphosphazene-based nanosheet with promoted charge separation kinetics for efficient visible light photocatalytic $CO_2$ reforming to $CH_4$, Appl. Catal. B Environ. 306 (2022) 121090. https://doi.org/10.1016/j.apcatb.2022.121090.

[26] S.J. Maynard, T.R. Sharp, J.F. Haw, Thermal degradation chemistry of poly(diphenoxyphosphazene), Macromolecules. 24 (1991) 2794–2799. https://doi.org/10.1021/ma00010a024.

[27] M. El Gouri, A. El Bachiri, S.E. Hegazi, M. Rafik, A. El Harfi, Thermal degradation of a reactive flame retardant based on cyclotriphosphazene and its blend with DGEBA epoxy resin, Polym. Degrad. Stab. 94 (2009) 2101–2106. https://doi.org/10.1016/j.polymdegradstab.2009.08.009.

[28] H. Liu, X. Wang, D. Wu, Synthesis of a novel linear polyphosphazene-based epoxy resin and its application in halogen-free flame-resistant thermosetting systems, Polym. Degrad. Stab. 118 (2015) 45–58. https://doi.org/10.1016/j.polymdegradstab.2015.04.009.

[29] Y.W. Chen-Yang, S.J. Cheng, B.D. Tsai, Preparation of the partially substituted (phenoxy)chlorocyclotriphosphazenes by phase-transfer catalysis, Ind. Eng. Chem. Res. 30 (1991) 1314–1319. https://doi.org/10.1021/ie00054a036.

[30] M. Lv, C. Yao, D. Yang, H. Zeng, Synthesis of a melamine-cyclotriphosphazene derivative and its application as flame retardant on cotton gauze, J. Appl. Polym. Sci. 133 (2016). https://doi.org/10.1002/app.43555.

[31] J. Fu, Y. Huang, Y. Pan, Y. Zhu, X. Huang, X. Tang, An attempt to prepare carbon nanotubes by carbonizing polyphosphazene nanotubes with high carbon content, Mater. Lett. 62 (2008) 4130–4133. https://doi.org/10.1016/j.matlet.2008.06.020.

[32] K.N. Kudin, B. Ozbas, H.C. Schniepp, R.K. Prud'homme, I.A. Aksay, R. Car, Raman Spectra of Graphite Oxide and Functionalized Graphene Sheets, Nano Lett. 8 (2008) 36–41. https://doi.org/10.1021/nl071822y.

[33] X. Chen, Y. Fan, L. Wu, L. Zhang, D. Guan, C. Ma, N. Li, Ultra-selective molecular-sieving gas separation membranes enabled by multi-covalent-crosslinking of microporous polymer blends, Nat. Commun. 12 (2021) 1–12. https://doi.org/10.1038/s41467-021-26379-5.

198

[34] A.C. Ferrari, D.M. Basko, Raman spectroscopy as a versatile tool for studying the properties of graphene, Nat. Nanotechnol. 8 (2013) 235–246. https://doi.org/10.1038/nnano.2013.46.

[35] M. Gao, J. Fu, M. Wang, K. Wang, S. Wang, Z. Wang, Z. Chen, Q. Xu, A self-template and self-activation co-coupling green strategy to synthesize high surface area ternary-doped hollow carbon microspheres for high performance supercapacitors, J. Colloid Interface Sci. 524 (2018) 165–176. https://doi.org/10.1016/j.jcis.2018.04.027.

[36] X. Zhang, S. He, X. Wo, T. Han, J.A.N.N. Kambonde, J. Wu, X. Qiu, L. Zhao, Enhanced specific capacity and cycle stability of hybrid supercapacitors using carbonized polyphosphazene-based nanocomposites, Electrochim. Acta. 397 (2021) 139297. https://doi.org/10.1016/j.electacta.2021.139297.

[37] J.G. Seong, J.C. Lewis, J.A. Matteson, E. Craddock, U. Martinez, H. Thakkar, A.D. Benavidez, K.A. Berchtold, R.P. Singh, Polybenzimidazole-derived carbon molecular sieve hollow fiber membranes with tailored oxygen selective transport, Carbon N. Y. 192 (2022) 71–83. https://doi.org/10.1016/j.carbon.2022.02.033.

[38] K. Rhili, S. Chergui, A.S. ElDouhaibi, M. Siaj, Hexachlorocyclotriphosphazene Functionalized Graphene Oxide as a Highly Efficient Flame Retardant, ACS Omega. 6 (2021) 6252–6260. https://doi.org/10.1021/acsomega.0c05815.

[39] F. Yang, M. Qiu, Z. Miao, T. Zhang, S. Zhang, Z. Wu, N, P-Codoped Carbon Film Derived from Phosphazenes and Its Printing Integration with a Polymer Carpet Via "molecular Welding" for Flexible Electronics, ACS Appl. Mater. Interfaces. 13 (2021) 29894–29905. https://doi.org/10.1021/acsami.1c04010.

[40] R. Jiang, B. Deng, L. Pi, L. Hu, D. Chen, Y. Dou, X. Mao, D. Wang, Molten Electrolyte-Modulated Electrosynthesis of Multi-Anion Mo-Based Lamellar Nanohybrids Derived from Natural Minerals for Boosting Hydrogen Evolution, ACS Appl. Mater. Interfaces. 12 (2020) 57870–57880. https://doi.org/10.1021/acsami.0c17137.

[41] R. Xu, L. Li, X. Jin, M. Hou, L. He, Y. Lu, C. Song, T. Wang, Thermal crosslinking of a novel membrane derived from phenolphthalein-based cardo poly(arylene ether ketone) to enhance CO2/CH4 separation performance and plasticization resistance, J. Memb. Sci. 586 (2019) 306–317. https://doi.org/10.1016/j.memsci.2019.05.084.

[42] L. Zhu, M.T. Swihart, H. Lin, Tightening polybenzimidazole (PBI) nanostructure via chemical cross-linking for membrane $H_2$ /$CO_2$ separation, J. Mater. Chem. A. 5 (2017) 19914–19923. https://doi.org/10.1039/C7TA03874G.

[43] P.H.T. Ngamou, M.E. Ivanova, O. Guillon, W.A. Meulenberg, High-performance carbon molecular sieve membranes for hydrogen purification and pervaporation dehydration of organic solvents, J. Mater. Chem. A. 7 (2019) 7082–7091. https://doi.org/10.1039/C8TA09504C.

# 6.7 Supporting information

Table S6.1 EDX data for the untreated and treated MDHB-HCCP powders

| Element | Elemental concentration(%) | | | |
|---|---|---|---|---|
| | MDHB-HCCP | MDHB-HCCP-200 | MDHB-HCCP-350 | MDHB-HCCP-450 |
| C | 60.8±1.7 | 58.3±0.4 | 49.2±0.3 | 62.9±0.3 |
| N | 13.9±1.1 | 7.8±1 | 3.4±0.3 | 4.4±0.5 |
| O | 14.4±1 | 19.5±1.4 | 31.9±0.6 | 22.7±0.8 |
| P | 7.3±0.6 | 11.5±1.9 | 9.9±0.3 | 9.2±0.6 |
| S | 0.4±0.1 | 0.4±0 | 3.5±0.3 | 0.3±0.1 |
| Cl | 3±0.4 | 1.7±0.3 | 0.1±0 | 0.1±0 |
| K | 0.3±0.1 | 0.7±0.2 | 1.9±0.1 | 0.3±0.1 |
| C/N | 4.4±0.4 | 7.4±1.0 | 14.3±1.2 | 14.4±1.6 |
| P/N | 0.5±0.1 | 2.5±0.4 | 2.9±0.3 | 2.1±0.3 |

Table S6.2 CN elemental analysis for the polyphosphazene powders before and after pyrolysis.

| | Elemental concentration (%) | |
|---|---|---|
| Sample | N | C |
| MDHB-HCCP | 8.2±0.4 | 32.7±0.2 |
| MDHB-HCCP-200 | 6.4±0.3 | 30.8±0.3 |
| MDHB-HCCP-250 | 1.3±0.1 | 31.1±0.7 |
| MDHB-HCCP-350 | 0.6±0.1 | 36.1±2.2 |
| MDHB-HCCP-450 | 0.8±0.3 | 28.8±0.2 |
| THB-HCCP | 8.7±0.1 | 19.9±0.14 |
| THB-HCCP-200 | 7.6±0.4 | 21.6±0.1 |
| THB-HCCP-250 | 2±0.4 | 18.7±1 |
| THB-HCCP-350 | 1.8±0.3 | 18.5±2.2 |
| THB-HCCP-450 | 0.4±0.1 | 28.7±0.6 |

Table S6.3 XRF data for the polyphosphazene powders before and after heating to 200 ˚C

| Sample | Elemental concentration (%)[a] | | | | Number of reacted Cl[b] |
|---|---|---|---|---|---|
| | **P** | **Cl** | **K** | **S** | |
| MDHB-HCCP | 37.1 | 47.9 | 11.1 | 2.9 | ~2 |
| MDHB-HCCP-200 | 58.1 | 24.9 | 15.5 | 0 | 4-5 |
| THB-HCCP | 36.8 | 48.9 | 8.8 | 4.7 | ~2 |
| THB-HCCP-200 | 55.8 | 25.8 | 15.4 | 3.1 | 4-5 |

[a] *The statistical error for the data is measured between 0.7% to 4%*

[b] *The number of reacted Cl groups is equal to the number of reacted hydroxyl contained monomers per HCCP. This number is calculated based on the ratio of P/Cl.*
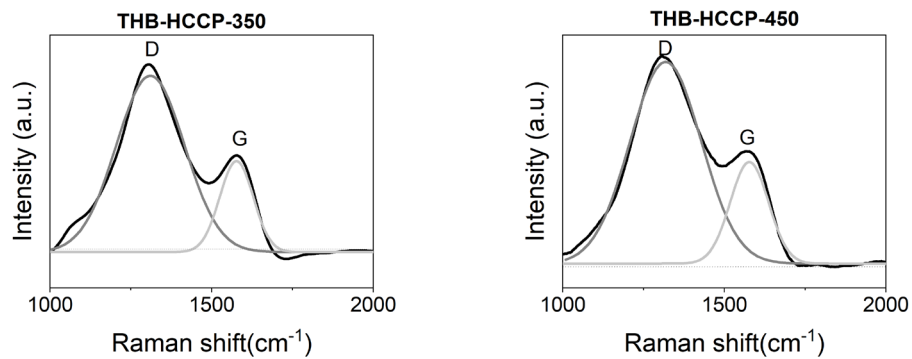
| Sample | $I_D$ | $I_G$ | $I_D/I_G$ |
|---|---|---|---|
| THB-HCCP-350 | 36.22 | 14.2 | 2.6 |
| THB-HCCP-450 | 96.85 | 26.1 | 3.7 |

Figure S6.1 Raman spectra of thermal treated THB-HCCP powders. (A) THB-HCCP-350. (B) THB-HCCP-450. The prominent peaks of D and G peaks around 1315 cm$^{-1}$ and 1580 cm$^{-1}$ correspond to the formation of disordered carbon and highly oriented graphitic carbon with a sp$^2$ electronic configuration, respectively. The ratio of $I_D/I_G$ are calculated from the corresponding deconvoluted Raman peak areas.
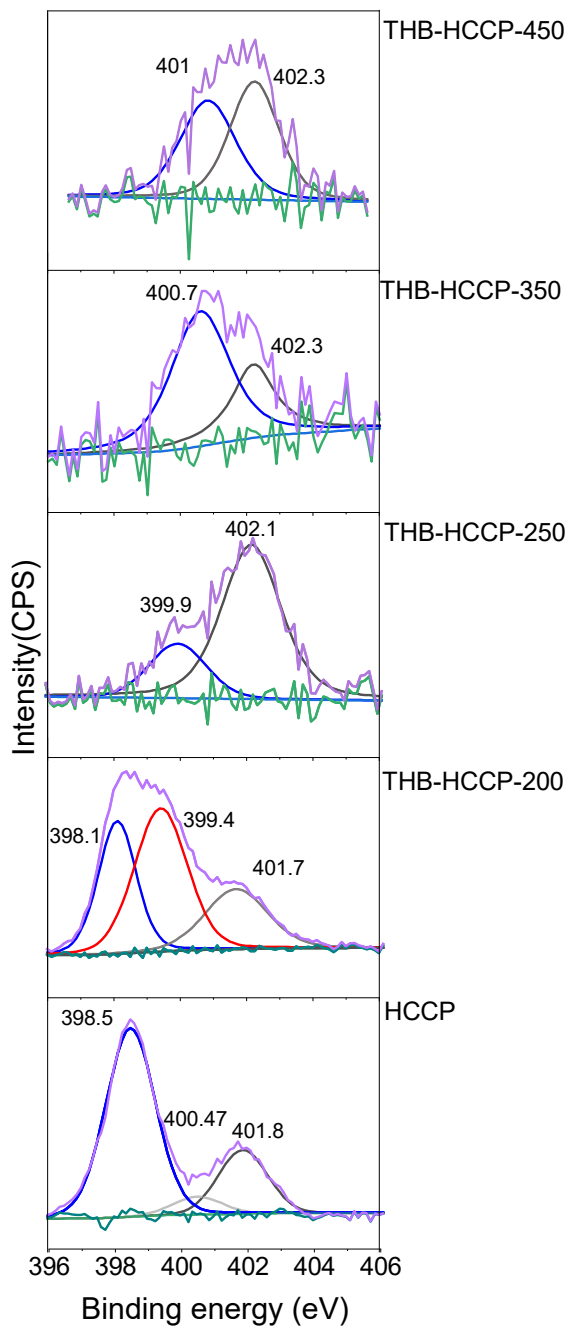
Figure S6.2 High-resolution N1s XPS spectra of HCCP, THB-HCCP-200, THB-HCCP-250, THB-HCCP-350, and THB-HCCP-450.

204
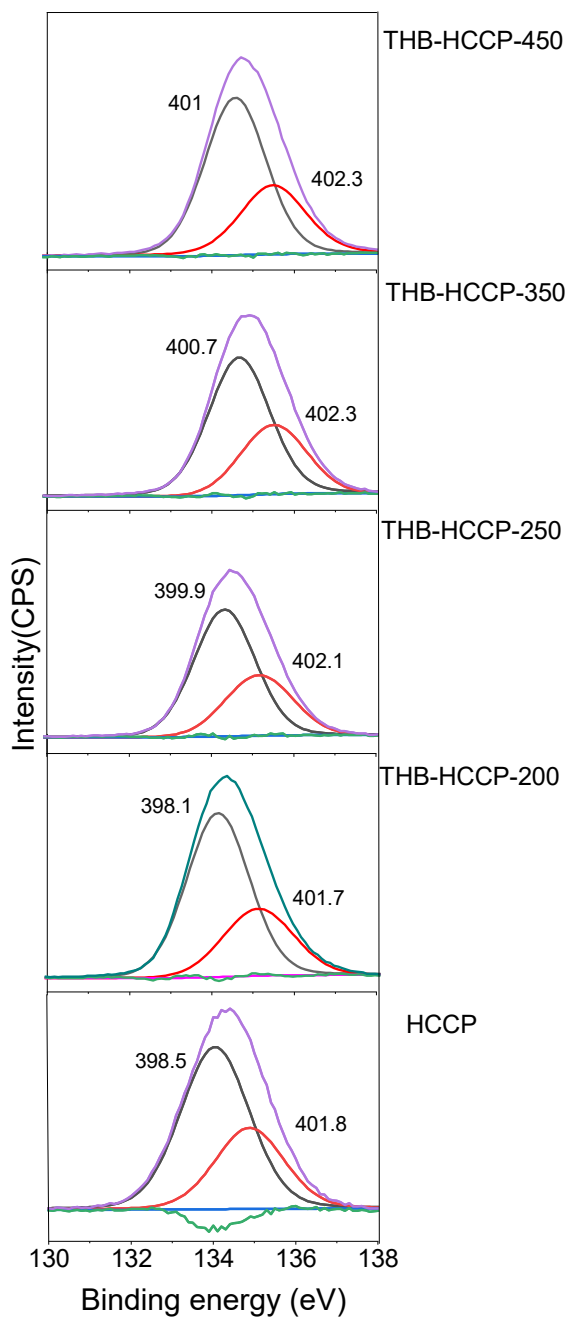
Figure S6.3 High-resolution P2p XPS spectra of HCCP, THB-HCCP-200, THB-HCCP-250, THB-HCCP-350, and THB-HCCP-450.
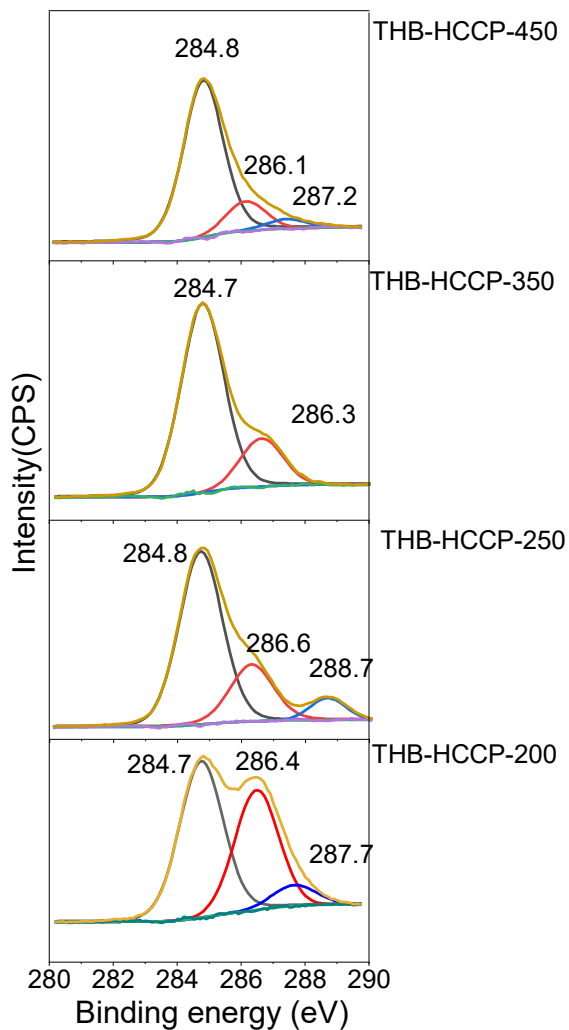
Figure S6.4 High-resolution C1s XPS spectra of HCCP, THB-HCCP-200, THB-HCCP-250, THB-HCCP-350, and THB-HCCP-450. The ratio of deconvoluted XPS peak area of peaks at $286.7\,eV$ (C-O/C-N) to $284.7\,eV$ (C=C/C-C) is 0.73, 0.34, 0.24, and 0.2 for THB-HCCP-200, THB-HCCP-250, THB-HCCP-350, and THB-HCCP-450, respectively.
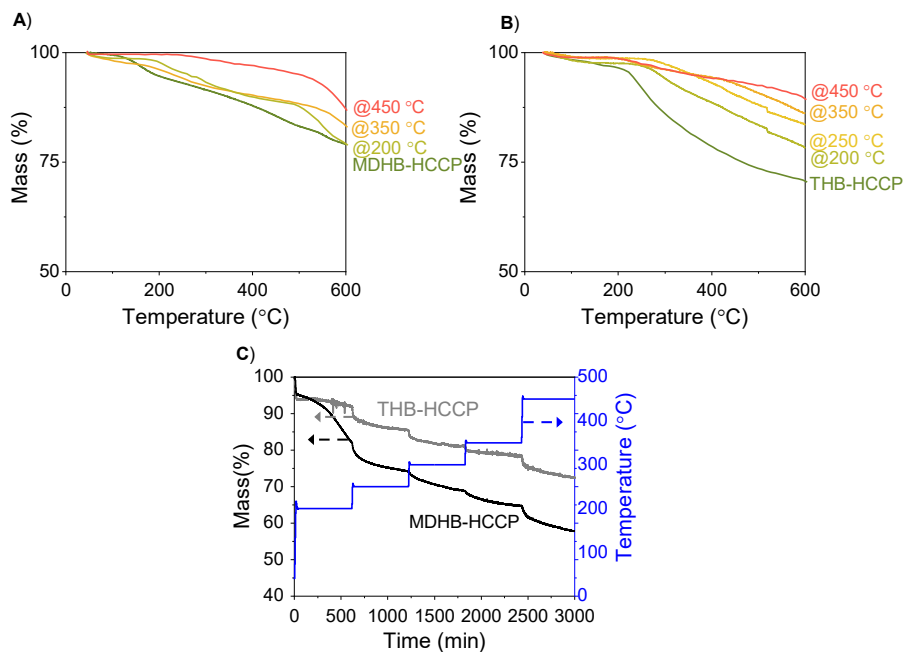
Figures S6.5 TGA data from the polyphosphazene powders before and after thermal treatments, (A) MDHB-HCCP, (B) THB-HCCP. (C) Temperature ramping and mass loss of prepared free-standing layers of MDHB-HCCP and THB-HCCP monitored by TGA.
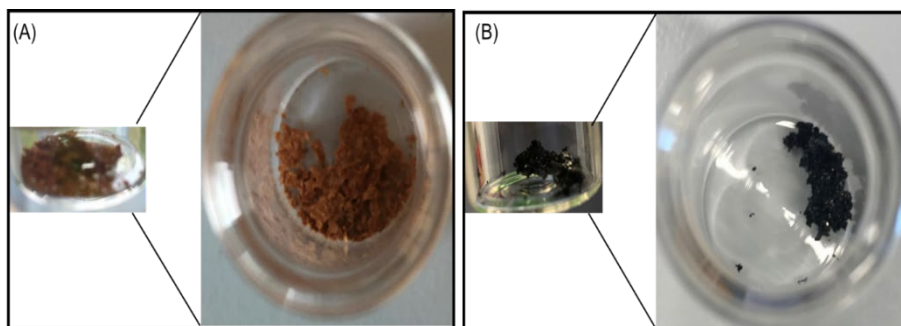
Figure 6.6 Digital photos of the prepared powders from the top and side views for (A)THB-HCCP-200, (B) THB-HCCP-450.
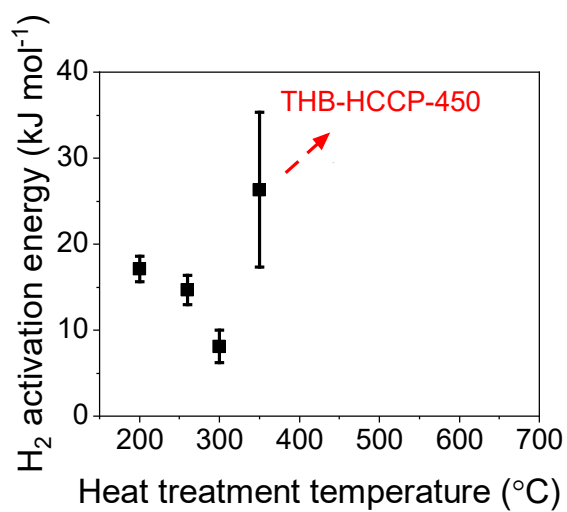


Figure S6.7 Hydrogen activation energy as a function of heat treatment temperature.

# Chapter 7

# Cyclomatrix polyphosphazene organic solvent nanofiltration membranes
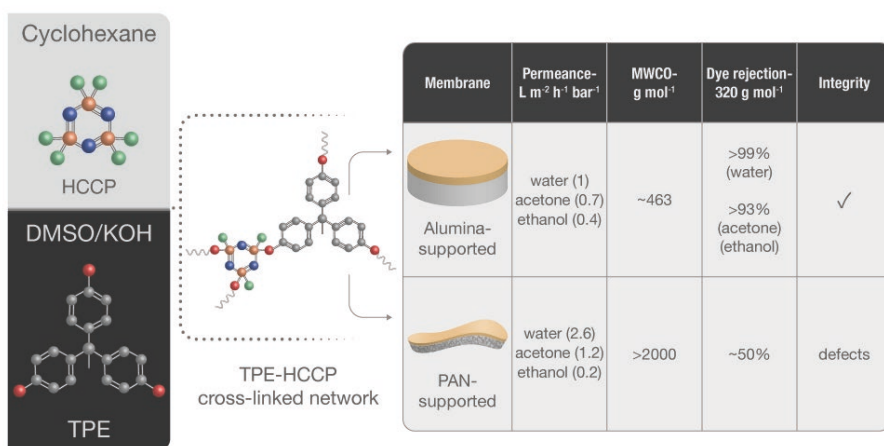
# Abstract

In this work, we report the synthesis and characteristics of cyclomatrix polyphosphazene membranes based on interfacial polymerization between 1,1-tris(4-hydroxyphenyl)ethane and hexachlorocyclotriphosphazene on top of alumina or polyacrylonitrile supports. The potential of alumina-supported thin film composite membranes as organic solvent nanofiltration membranes has been confirmed with a polystyrene-based molecular weight cutoff of 347±120 Da and 503±220 Da in acetone and toluene, respectively. Also, the resulting alumina-supported TFC membrane showed a methylene blue rejection ( Mw= 319 g mol$^{-1}$) of 98.2±2.3%, 92±1.7%, and 93±0.5% in water, ethanol, and acetone, respectively. Furthermore, a thin film composite membrane has been prepared with a polyacrylonitrile support via interfacial polymerization to validate the preparation technique for polymeric supports and facilitate industrial implementation. The resulting membrane showed higher permeance and lower rejection than the alumina-supported membrane due to the presence of pinholes in the  selective layer on top of the polyacrylonitrile supports. Our results clearly show the great potential of cyclomatrix polyphosphazene membranes as organic solvent nanofiltration membranes. However, for polyacrylonitrile-supported membranes, the preparation method needs further investigation.

# 7.1 Introduction

Nanofiltration (NF) is a pressure-driven technology that plays an indispensable role in separation processes in the industry, including water softening, food processing, and purification of primary materials and solvents.[1–5] With pore diameters of 0.5-2 nm, NF membranes are suitable for removing small organic molecules such as micropollutants and multivalent ions from liquids or separating multivalent ions from monovalent ions, even at high concentrations.[6–8] A particular category of NF membranes that can resist and perform the separation in organic solvents is referred to as organic solvent nanofiltration (OSN). To allow for this type of separation, the membrane material must be stable in organic solvents to guarantee its persisting performance. In recent years, there has been considerable interest in developing thin film composite membranes (TFC) suitable for OSN via interfacial polymerization (IP). The focus of those studies is to augment the membrane permeability, selectivity, and solvent stability via structural and pore design.[9–18] Numerous methods have been deployed to this aim, such as altering monomers and supports and tuning the cross-linking degree.[9–115]  To date, conventional IP procedures for various types of polymers, such as polyamide, polyimide, polyester, covalent organic framework (COF), and covalent organic polymer (COP), have been explored.[13,19,20]

Polyphosphazene (PPz) is a class of inorganic-organic hybrid polymers known for its robustness, flexibility in its structural design, and tunability of its properties.[21]  It comprises a backbone of alternating nitrogen and phosphorous atoms accompanied by two organic substituents linked to each phosphorous atom.[22] The two main monomers for preparing PPz are hexachlorocyclotriphosphazene (HCCP) and poly(dichlorophosphazene) (PDCP). The chlorine group present in these monomers can easily be substituted via nucleophilic attack by various monomers containing amino or hydroxyl groups.[23] Different PPz architectures have been synthesized, including linear, star-shaped, dendritic, cyclolinear, and cyclomatrix polyphosphazene (CPPz) structures.[24] Accordingly, different kinds of PPz with distinct properties have been designed on a molecular scale. Among

those architects, cyclomatrix polyphosphazene is known for its superior chemical stability and solvent resistance.[25]

To the best of our knowledge, only a limited number of studies have investigated the use of polyphosphazene-based materials as nanofiltration membranes, and only for application in aqueous environments.[26,27] You et al.[26] prepared a positively charged polyamine-based CPPz NF membrane via IP of polyethyleneimine (PEI) and HCCP. They showed that their produced membrane has a water permeance of 3.7 L m$^{-2}$ h$^{-1}$ bar$^{-1}$ and a rejection of up to 97% for MgCl$_2$ and 82% for methylene blue (a chloride salt of a cationic dye with Mw=319.85 g mol$^{-1}$). Allen et al.[27] focused on fabricating linear poly(bis(phenoxy)phosphazene) membranes on a porous support and studied the diffusion of Cr$^{3+}$, Co$^{2+}$, and Mn$^{2+}$ through the membrane. Both studies indicated the technical feasibility of PPz based membranes as NF membranes for aqueous applications. Since these authors only reported the solute rejection in water, to date, there has not been a detailed investigation on the potential of CPPz membranes for OSN applications.

Obtaining a good rejection for small molecules with a $M_w < 400$ g mol$^{-1}$ in combination with acceptable permeance is always challenging for OSN membranes, when they are prepared with IP. To this aim, the membrane should have small and precise well-distributed pores, which often leads to a relatively low solvent flux as a consequence of the often encountered trade-off between selectivity and permeance.[1] To the best of our knowledge, limited studies, such as [10,13,28–38], succeeded in developing membranes with a rejection above 90% for dyes with $M_w$ of 314 g mol$^{-1}$ to 328 g mol$^{-1}$ and acceptable ethanol permeances of more than 1 L m$^{-2}$ h$^{-1}$ bar$^{-1}$.

The goal of this work is to prepare CPPz OSN membranes via IP, with properties that make them suitable for rejecting small solutes with a $M_w$<500 g mol$^{-1}$ in various solvents. To achieve this goal, we consider a recently developed one-step IP method, suitable for preparing ultrathin cyclomatrix poly(phenoxy)phosphazene hybrid membranes for gas separation [39], to be a promising preparation method for OSN membranes as well. In this method, a thin film poly(phenoxy)phosphazene network is formed via a polycondensation reaction on top of the ceramic support. For gas separation

membranes, first, a biphenol or a tri/dihydroxybenzene is dissolved in a DMSO/KOH solution to convert the hydroxyl groups to anions that are crucial for the reaction to proceed.[39,40] In the second step, the formed phenolates react with HCCP in cyclohexane during a nucleophilic substitution reaction in which HCl is eliminated, and a highly cross-linked structure of CPPz is formed. The goal of the current contribution is to demonstrate that selecting larger organic bridges and reducing the extent of cross-linking results in CPPz membranes with NF properties suitable for OSN applications. We hypothesize that the length, flexibility, and reactivity of the phenolates directly affect the chain's mobility, pore size, and distribution. Provided that our hypothesis holds, which we intend to show in this manuscript, the facile nature of the technique used for membrane synthesis allows for tuning the properties of the membrane and changing its applicability from gas separation to nanofiltration.

Furthermore, to the best of our knowledge, it is the first time that it has been tried to prepare CPPz membranes by combining HCCP and 1,1-Tris(4 hydroxyphenyl)ethane (TPE) and use these membranes for OSN application. The membranes have been prepared through IP between TPE and HCCP, creating a thin film composite layer on an alumina or a PAN support. The CPPz TPE-HCCP network has been characterized, and the performance of the prepared membrane has been evaluated in detail with different solvents, including toluene, ethanol, and acetone. The experimental work presented here provides one of the first investigations into the feasibility of implementing CPPz-based nanofiltration membranes in OSN applications.

## 7.2 Experimental

## 7.2.1. Materials

1,1-Tris(4 hydroxyphenyl)ethane (TPE, >98.0%) was purchased from TCI (Belgium). Phosphonitrilic chloride trimer (HCCP, 99%), dimethyl sulfoxide (DMSO, anhydrous, ≥99.9%), Methylene Blue (MB, 97%), sodium chloride (NaCl,≥99%), and poly(ethylene glycol) (PEG) with molecular weights of 400, 600, and 1500 g mol$^{-1}$ were obtained from Sigma-Aldrich (The Netherlands). Brilliant Yellow (BY, 70%) was purchased from Aldrich. Cyclohexane (EMSURE for analysis), sodium sulfate (Na$_2$SO$_4$, anhydrous,

for analysis EMSURE ACS), magnesium sulfate heptahydrate (MgSO$_4$, for analysis EMSURE ACS), PEG 1000 (EMPROVE ESSENTIAL), Rhodamine B (RB) and potassium hydroxide (KOH, pellets extra pure) were acquired from Merck kGaA. Ethanol (EtOH, technical grade) was purchased from Boom. Magnesium chloride hexahydrate (MgCl$_2$.6H$_2$O, 99.0−100.0%, AnalaR NORMAPUR ACS Reag.) was obtained from VWR chemicals (Netherlands). PEG 200 was obtained from Fluka (Germany). All chemicals were used as received.

α-alumina discs (39 mm of diameter, 2 mm of thickness, and pore size of 80 nm) with one polished side were obtained from Pervatech B.V, the Netherlands, and used as supports. A 3µm γ-alumina layer with a typical pore diameter  between 3 to 8 nm was fabricated on the polished surface of the α-alumina, serving as an intermediate layer for preparing the selective polymeric layer, according to the earlier reports (Figure S7.1).[41] Porous polyacrylonitrile (PAN) ultrafiltration supports, UF010104, with a molecular weight cutoff of 10 kDa, were obtained from Solsep, the Netherlands.[42,43]

## 7.2.2. Material fabrication

Both TPE-HCCP free-standing films and membranes on inorganic or polymeric supports were prepared by conducting interfacial polymerization (IP) between 10 w/v% TPE in DMSO (hydroxyl molar ratio of TPE:KOH of 0.85) and 3.5 wt.% HCCP in cyclohexane. First, KOH with the mentioned hydroxyl molar ratio of TPE to KOH was added to a 10 wt.% TPE solution in DMSO and heated for 2.5 h at 80 °C. Subsequently, it was brought into contact with the HCCP solution according to the procedures described below.

## Synthesis of TPE-HCCP free-standing films

The TPE-HCCP free-standing layer was prepared in the following way. A 3.5 wt.% HCCP solution in cyclohexane was gently poured atop the TPE solution to minimize disturbances of the top layer of the TPE solution. A thin layer formed at the interface of the two phases as the two solutions contacted. After 30 min, the films were collected, filtered, and washed 3

times with ethanol, acetone, and water. Then, the solid films were dried in a vacuum oven at 50°C.

## Preparation of alumina-supported TPE-HCCP TFC membranes

TFC membranes were prepared by IP atop the ceramic support using an IP cell reported earlier.[44] The support and IP set-up were warmed up in a closed box located in an oven at 80 °C for 30 min. After this, 5 mL of TPE solution was poured on top of the support, and it was placed in the oven at 80 °C for 15 min. Subsequently, the cell was taken from the oven, and the remaining TPE solution on top of the support was discarded. After that, the surface of the support was dried from the remaining TPE solution droplets using a rubber roller and $N_2$ gun. Then the HCCP solution was poured on top of the support slowly. After 15 min of reaction at room temperature, the HCCP solution was discarded, and the membrane surface was rinsed three times with ethanol. It was dried overnight in a fume hood and then kept in the vacuum oven at 50 °C before further analysis.

## Preparation of PAN-supported TPE-HCCP thin-film composite membranes

PAN-supported TPE-HCCP thin-film composite membranes were fabricated as follows. A 7 cm × 10.5 cm piece of the PAN support was soaked in water overnight to wet the pores and remove any residuals. Subsequently, the water droplets on the support's surface were dried, and the support was placed in an IP cell reported earlier.[45] Then, 25 mL of the TPE solution was poured on top of the support membrane and left to soak for 10 min at room temperature. Subsequently, the remaining TPE solution was discarded, and the surface of the support was dried with an $N_2$ gun and paper tissue to obtain a dry surface. Next, 25 mL HCCP solution was poured on top of the support, and it was left to react for 10 min at room temperature. The remaining solution was removed, and the membranes were rinsed with ethanol. The membrane's surface was dried in a fume hood for 5 min, followed by thermal treatment of the membrane at 65 °C for 5 min. After this temperature treatment it was stored in Milli-Q water before

characterization. It is worth mentioning that the thermal treatment was added to improve membrane rejection.

## 7.2.3. Physical and chemical characterization

The membrane characterization was done according to the procedure previously reported.[46] Field-emission scanning electron microscopy (FE-SEM) images were obtained with Zeiss MERLIN high-resolution scanning electron microscope using an accelerating voltage of 1.4 kV to visualize the thickness and morphology of the membranes. For the sample preparation, membranes were dried overnight in a vacuum oven at 50 ºC and fractured in liquid nitrogen. EDX analysis was performed at 10 kV with >1000 counts/s on the spouter-coated 5 nm Pt/Pd samples. Fourier transform infrared spectroscopy (FTIR) measurement was done on the free-standing film using a PerkinElmer UATR Spectrum Two to examine the chemistry of the free-standing film. The dried free-standing film was scanned between the wave numbers of 4000 to 550 $cm^{-1}$ in reflectance mode at a resolution of 4 $cm^{-1}$ for a minimum of 32 scans. X-Ray Fluorescence (XRF) measurements (S8 Tiger, Bruker) were performed on the free-standing films. Cyclohexane permporometry was used to determine the pore diameter of the support and the prepared membrane using the procedure reported earlier.[47] The zeta potential measurements were performed as reported earlier, [48], with an electrokinetic analyzer SurPASS system (Anton Paar, Graz Austria) and a 0.005 M KCl solution.

## 7.2.4. Membrane performance

Permeance and dye rejection data were collected using Sterlitech stainless steel cells (model HP4750) with a pressure of 5-21 bars. Pure solvent permeance data were determined by weighing the permeate sampled, m (g), during timed intervals using four applied transmembrane pressures between 8 and 21 bar and taking the slope of a linear fit of the collected pressure – flux data forced through the origin. The solvent permeance was calculated using Equation 7.1:

$$P=\frac{m}{\rho \times A \times t \times \Delta p}$$

<div align="right">(7.1)</div>

where $\rho$ (g L$^{-1}$) is the density of the pure solvent obtained from the manufacturer, $A$ (m$^2$) is the effective membrane filtration area, $t$ (h) is the liquid sampling time, and $\Delta p$ (bar) is the applied trans-membrane pressure.

Dyes rejection measurements were conducted using single dye solutions of BY (a divalent anionic sodium salt with $M_w$ = 624.55 g mol$^{-1}$, 50 ppm), RB (a monovalent cation chloride salt $M_w$ = 479.02 g mol$^{-1}$, 50 ppm), and Methylene Blue (MB, a monovalent cation chloride salt with $M_w$ = 319.85 g mol$^{-1}$, 50 ppm) in either water, ethanol or acetone. The rejection was calculated using Equation 7.2:

$$R=1-\frac{C_p}{\frac{(C_R+C_F)}{2}}$$

<div align="right">(7.2)</div>

where $R$, $C_p$, $C_F$ and $C_R$ are the rejection, permeate concentration, feed concentration and retentate concentration. The retentate and permeate samples were obtained at a recovery between 45% to 70%. Between each measurement, the membranes were washed in acetone and ethanol several times, at least for 24 h. Solute concentrations of BY, RB, and MB were calculated from PerkinElmer $\lambda$12 UV−Vis spectrophotometer results at the characteristic wavelengths of 401.3 nm (BY/water), 554.4 nm (RB/water), 664.8 nm (MB/water), 655 nm (MB/ethanol), 552.9 nm (RB/ethanol), 657 nm (MB/acetone), and 556.2 nm (RB/acetone). The dye adsorption during the rejection measurement was calculated as follows:

$$M_{ads}=M_f-M_R-M_p$$

<div align="right">(7.3)</div>

where $M_{ads}$, $M_f$, $M_R$ and $M_p$ are the mass of dyes adsorbed on the membrane and in the feed, retentate, and total permeate, respectively. The adsorbed dye percentages were calculated to be between 0.2% to 4%. Also, to eliminate the dye adsorption on the ceramic support during rejection

measurements, for some measurements, the set-up was filled one more time after reaching the mentioned recoveries for the first run, and the test was repeated.

Salt rejection measurements for both types of membranes were performed in batch mode in a custom-built set-up with an effective membrane area of 7.55 cm$^2$, as reported earlier.[45] The membrane was placed at the bottom of a stainless steel vessel. The vessel was filled with 1 L of salt solution and pressurized to 10 bar with nitrogen gas. During the measurement, the solution was stirred with an overhead stirrer at 500 rpm to minimize concentration polarization. The salt rejection was assessed with 2 g L$^{-1}$ aqueous single salt solutions of MgSO$_4$, MgCl$_2$, Na$_2$SO$_4$, or NaCl. After collecting 10 mL of permeate, the samples were collected from permeate and retentate directly from the cell. The salt rejection was calculated using Equation (7.2). The salt concentration was derived using a 3310 conductivity meter (WTW, Germany).

PEG molecular weight cutoff (MWCO) for both types of membranes was measured using an aqueous solution of PEGs mixtures and the same set-up used for salt rejection. For this purpose, PEGs with mean molecular weights of 200, 400, 600, 1000, and 1500 g mol$^{-1}$ were used, each at a concentration of 1 g L$^{-1}$. After collecting 10 mL of permeate, the samples were collected from permeate and retentate directly from the cell. The PEG concentrations in the feed, the permeate, and the retentate were assessed using gel permeation chromatography (GPC, Agilent Technologies 1200/1260 Infinity GPC/SEC series) according to a previously described protocol.[49] The PEG rejection was then calculated using Equation (7.2) and the MWCO was determined as the molar mass that is retained for 90%. The polystyrene-based MWCO was determined with 0.5 g L$^{-1}$ and 1 g L$^{-1}$ synthesized polystyrene of broad molecular weight between 200-1500 g mol$^{-1}$ in acetone and toluene, respectively and the earlier described procedure was followed to calculate the polystyrene-based MWCO.

In addition, the PEG-based MWCO data can be used to determine the pore diameter of the selective layer.[50,51] PEG molecules can form spheres of a certain radius in the solution, and their molecular weight, $M_w$ (g mol$^{-1}$), can

be related to the PEG radius and diameter, $r$ (Å) and $d$ (Å), via the Stokes-Einstein equation [52]:

$$r=0.1673 \, M_W^{0.557} \tag{7.4}$$

with $d = 2r$ (7.5)

Equations (7.4) and (7.5) can be used to determine $\mu_p$ and $\sigma_p$, the mean effective pore diameter based on the solute radius obtained for a rejection of $R$=50% and the geometric standard deviation, defined as the ratio between the values of the pore diameter at $R = 84.13\%$ and $R = 50\%$, respectively.

Two models have been proposed in literature to calculate the pore size distribution. In the first model, the influence of hydrodynamic and steric interactions between solutes and pore sizes on solute rejection is neglected and the pore diameter is assumed to be equal to the solute diameter ($d_p = d$). The mean pore diameter $\mu_p$ in this case can be determined directly from equations (7.4) and (7.5) by substituting the PEG molecular weight for which a rejection of $R$=50% is obtained in equation (7.4).

In the second model, the steric and hydrodynamic hindrances between solutes and pore sizes on solute rejection are taken into consideration and the relation between the pore diameter and the PEG solute diameter for which $R$=50% is obtained can be expressed as [53]:

$$\mu_p = \frac{d_{R=50\%}}{0.416} \tag{7.6}$$

where the PEG diameter at $R=50\%$, $d_{R=50\%}$, is obtained from the PEG molecular weight for which a rejection of $R$=50% is obtained and equations (7.4) and (7.5).

After substituting $\mu_p$ and $\sigma_p$ in Equation (7.7) and solving this equation, the probability density function and the pore size distribution of the membrane are obtained [54].

$$\frac{\mathrm{d}R(d_\mathrm{p})}{\mathrm{d}d_\mathrm{p}} = \frac{1}{d_\mathrm{p}\ln\sigma_\mathrm{p}\sqrt{2\pi}}\exp\left[-\frac{(\ln d_\mathrm{p} - \ln\mu_\mathrm{p})^2}{2(\ln\sigma_\mathrm{p})^2}\right] \tag{7.7}$$

where $d_\mathrm{p}$ is the pore diameter.

It should be noted that this pore size distribution function has originally been determined for ultrafiltration membranes, but it has been applied for NF membranes regularly as well and its applicability has recently been re-evaluated [53].

## 7.3 Results & Discussion

The results and discussion section is split up into three parts. In the first part, we will discuss the formation and characterization of the TPE-HCCP free-standing films. The second part will focus on the characterization and performance of the alumina-based membrane featuring the solvent permeances and the solute rejections. Finally, in the third part, we will evaluate the formation and performance of PAN-based TPE-HCCP membranes.

## 7.3.1. Formation and characterization of the polyphosphazene free-standing film

Interfacial polymerization between TPE in DMSO and HCCP in cyclohexane results in the formation of a cyclomatrix polyphosphazene TPE-HCCP layer at the interface of the two solutions, as shown in Figure 7.1A. Before the reaction, TPE is deprotonated by KOH, forming readily reactive anions which participate in the nucleophilic substitution of chlorine attached to the triazatriphosphorine ring.[39] One should note that the use of DMSO as solvent is necessary to enhance the nucleophilicity of TPE and, subsequently, to establish the network. At the DMSO-cyclohexane interface, the phenolates react with HCCP to form the cyclomatrix polyphosphazene network, as shown in Figure 7.1B.
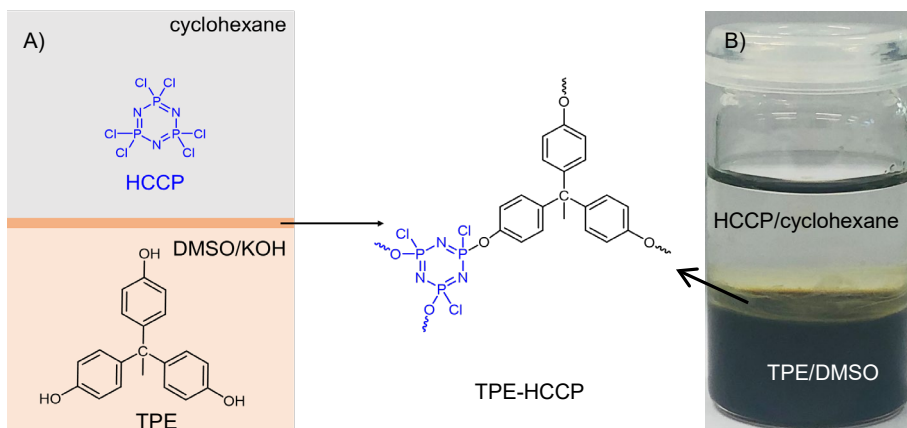
Figure 7.1 (A) Schematic representation of TPE-HCCP free-standing layer's formation. (B) Photograph of glass vial confirming the TPE-HCCP free-standing layer's formation after 10 min.

FTIR is used to evaluate the chemistry of the formed networks. Figure 7.2 shows the FTIR spectrum of the used monomers and prepared networks. The TPE-HCCP network demonstrates the characteristic peaks of both monomers, TPE and HCCP, as well as the new peaks of the formed bonds during the IP reaction. The network reveals two peaks around 1499 cm$^{-1}$ and 1599 cm$^{-1}$ belonging to the C=C stretching vibrations of the aromatic ring of the TPE monomers. Also, the weak band at 2970 cm$^{-1}$ originates from the asymmetric stretching mode of the sp$^3$ C-H bond in the CH$_3$ group.[55,56] The HCCP is apparent from the broad peak at 1100-1200 cm$^{-1}$, ascribed to the asymmetric P=N-P stretching, and a peak at 875 cm$^{-1}$ related to the symmetric P=N-P stretching.[57,58] In addition, the P-Cl bond with the peaks at 595 cm$^{-1}$ and 511 cm$^{-1}$ is to some extent disappeared.[59] Finally, a new peak appearing at 940 cm$^{-1}$ can be assigned to the formation of P-O-Ar bonds.[60] In summary, we can confirm the formation of the TPE-HCCP network with FTIR.
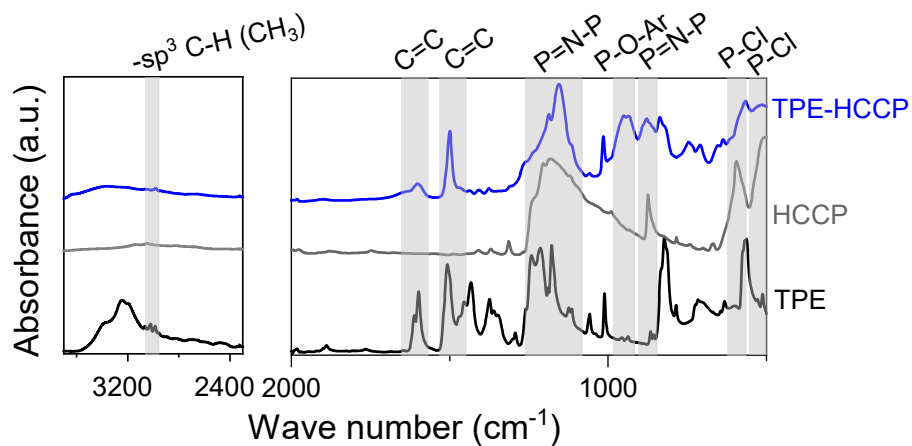
Figure 7.2 FTIR spectra of monomers TPE and HCCP and the formed polyphosphazene network.

Table 7.1 summarizes the result of all the methods used for elemental analysis of the TPE-HCCP free-standing layer. The results from all the methods are in good agreement and show that the number of reacted Cl is between 2-3 per HCCP. The number of reacted Cl was calculated based on the ratio of C/N, P/C, and P/Cl. Though the possibility of Cl hydrolysis in the presence of water and formation of KCl as by-product is high, the calculated reacted Cl based on the ratio of P/Cl, still matches well with other methods calculated based on C/N and P/C ratios. We conclude that the hydrolysis of Cl during preparation is negligible.

Table 7.1 An overview of the outcomes of several methods used for characterization of TPE-HCCP free-standing layer

| Technique | Atomic composition (%) | | | | | | | Number of reacted Cl | | |
|---|---|---|---|---|---|---|---|---|---|---|
| | C | N | O | P | S | Cl | K | C/N | P/Cl | P/C |
| XRF | - | - | - | 34.6 | 5.14 | 39.9 | 20.3 | - | 2-3 | - |
| C,N | 44.3 ±0.2 | 5.6 ±0.1 | - | | | | | 2-3 | - | - |
| EDX | 63.6± 2.2 | 10.2 ±0.6 | 10.1 ±0.5 | 7.3 ±0.6 | 1 ±0.1 | 5.6 ±1.4 | 2.4 ±2.1 | 2 | 3 | 2-3 |

222

## 7.3.2. Formation, characterization and NF performance of alumina-supported polyphosphazene membrane
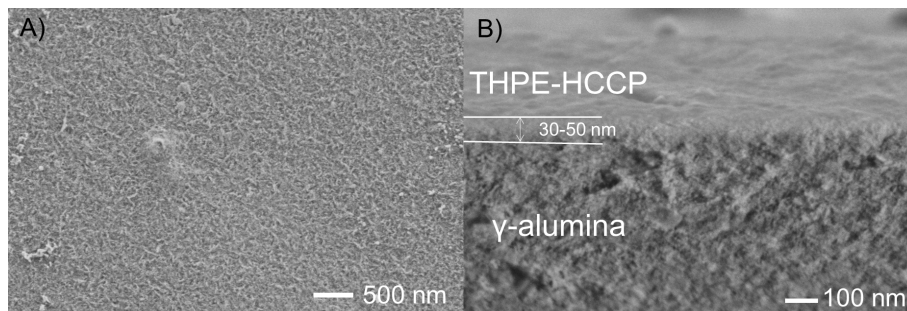


Figure 7.3 (A) FE-SEM picture of the TPE-HCCP membrane surface and (B) Cross-section FE-SEM image.

Figure 7.3A and Figure 7.3B show the surface and cross-sectional FE-SEM pictures of the TPE-HCCP alumina-supported membrane, respectively. Figure 7.3A reveals that the surface morphology of the membrane is relatively rough and homogeneous. The cross-sectional image, Figure 7.3B, shows that the thickness of the TPE-HCCP layer on top of the alumina support is between 30-50 nm. In contrast, cyclomatrix polyphosphazene membranes containing polyhedral oligomeric silsesquioxane (POSS-HCCP) on top of the ceramic support showed a smooth surface and a thickness of about 80 nm.[44] This difference in surface morphology between these membranes could be due to the relatively thin TPE-HCCP layer, reflecting the roughness of γ-alumina morphology rather than that of the TPE-HCCP layer itself.[44] In addition, POSS-HCCP membranes were fabricated by IP between POSS in DMSO/water and HCCP in cyclohexane, whereas TPE-HCCP networks were prepared via IP in DMSO and cyclohexane. Incorporation of water in the fabrication of the POSS-HCCP layer results in growing the layer mostly on top of the ceramic support.[61] For TPE-HCCP, the layer probably behaves differently, and the layer grows inside the pores due to the high solubility of HCCP in DMSO, explaining the differences in thickness.

Figure 7.4A and Figure S7.2 show the MWCO of the prepared alumina-supported TPE-HCCP membranes in different solvents. The polystyrene-based MWCO in toluene and acetone is 503±215 Da and 347±120 Da,

respectively. Also, the PEG-based MWCO of the TPE-HCCP membrane in water was found to be 467±137 Da, fitting well within the typical range of NF membranes.[62] The obtained MWCO is in the range of earlier reported IP TPE-based poly(aryl cyanurate) NF membranes (TPE-cyanuric chloride) which showed a MWCO of 400±83 Da [45]. However, those TPE-cyanuric chloride based NF membranes were not developed for OSN, but for dealing with aqueous solutions at extreme pH conditions instead. Finally, the MWCO in different solvents is comparable (within the accuracy range obtained) and therefore seems to be independent of the type of solvent. It suggests that the alumina-supported TPE-HCCP membranes are suitable for solute separation in solvents, provided that the membrane shows sufficient chemical stability for the applied solvent. Furthermore, the obtained MWCO is smaller than most pharmaceutical and catalyst sizes and comparable to low MWCO OSN membranes.[33,63,64]

The pore diameter of the membrane directly affects the performance of NF membranes. Cyclohexane permporometry is a technique to characterize the active pores of a membrane responsible for the actual membrane performance.[47] Figure S7.3 compares the oxygen permeance of the support and TPE-HCCP membrane as a function of the relative cyclohexane pressure during the desorption step of the permporometry analysis. The data suggest a pore diameter of ~5.9 nm for the support. The pore size of the alumina-supported TPE-HCCP membranes can not be revealed by this method since the detection limit of the set-up is 2 nm.[65] Figure 7.4B shows an estimation for the pore size distribution of the alumina-supported TPE-HCCP membrane based on the two different models, the first obtained based on equations (7.4) and (7.5), giving $\mu_p = 0.5$ nm and $\sigma_p = 1.8$, and the second after correcting this mean pore diameter value for steric hindrance effects as described by equation (7.6), leading to $\mu_p = 1.12$ nm. Both models illustrate that pores smaller than 1 nm own the highest probability density function. As expected, the pore diameter distribution based on model 2, ranging from 0 to 5 nm, is wider than that obtained from model 1 (0 – 2 nm). In addition, the obtained pore size distribution based on model 1 is in line with the reported value for the other types of NF/OSN membranes, where model 1 was used to calculate pore size distribution as well.[50,66]
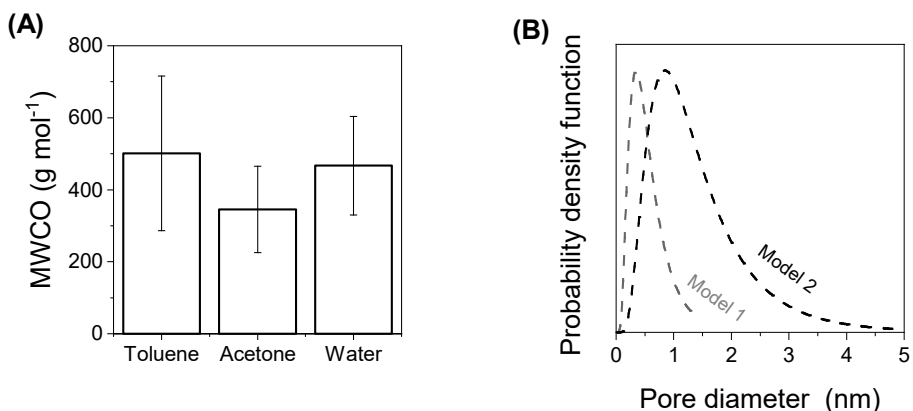
Figure 7.4 (A) MWCO of alumina-supported TPE-HCCP membranes in different solvents. (B) Pore size distribution of the alumina-supported TPE-HCCP membranes calculated based on the PEG rejection in water.

The organic solvent nanofiltration performance of the alumina-supported TPE-HCCP membranes was evaluated by measuring the permeance of different solvents, ethanol, toluene, water, and acetone (see Figure S7.4), followed by determining the rejection of salts and various dyes with different molecular weights in an aqueous solution. Figure 7.5A shows the pure solvent permeance as a function of the solvent's physiochemical properties ($\delta_p \eta^{-1} V^{-1}$), where $\delta_p$ represents the Hansen solubility parameter for polarity, $V$ is the molar volume, and $\eta$ is the dynamic viscosity. A good correlation between the solvent's properties and their permeance can be observed, in line with reported results for other nanofiltration membranes.[20]   As a general trend, a decrease in $\delta_p \eta^{-1} V^{-1}$ (toluene < ethanol < water < acetone) results in an increase in permeance (ethanol < toluene < acetone < water).

The average pure water permeance is 1 L m$^{-2}$ h$^{-1}$ bar$^{-1}$ with a 95% CI (confidence interval) of ±0.1 L m$^{-2}$ h$^{-1}$ bar$^{-1}$, whereas, for the support, this is 7.1 L m$^{-2}$ h$^{-1}$ bar$^{-1}$ with a 95% CI of ±1.6 L m$^{-2}$ h$^{-1}$ bar$^{-1}$. The strong reduction in the water permeance of the membrane compared to that of the support confirms the formation of a dense polymeric network. The obtained water permeance is comparable to other γ–alumina-supported TFC

membranes such as polyimide (~1.7 L m$^{-2}$ h$^{-1}$ bar$^{-1}$) [65], and thioether-based membranes (~0.6 L m$^{-2}$ h$^{-1}$ bar$^{-1}$) [52], as well as PAN-supported membranes such as TPE-cyanuric chloride (1.77 L m$^{-2}$ h$^{-1}$ bar$^{-1}$). [45] Additionally, the membrane has an acetone permeance of 0.7 L m$^{-2}$ h$^{-1}$ bar$^{-1}$ and an ethanol permeance of 0.4 L m$^{-2}$ h$^{-1}$ bar$^{-1}$. The achieved ethanol and acetone permeance are moderately comparable to other IP NF membranes.[65–72] The toluene permeance is 0.55 L m$^{-2}$ h$^{-1}$ bar$^{-1}$ and lower compared to the permeance of IP-prepared polymeric-supported (polyester on top of polyethylene terephthalate) membranes and similar to the permeance of other γ-alumina-supported TFC membranes prepared with grafting.[33,72]

Prior to the dye rejection test, salt rejection measurements were performed for three salts to give an insight into the performance of membranes. The rejection decreases in the order $Na_2SO_4$ (48.6±2.1%) ~ $MgCl_2$ (46.1%) > $MgSO_4$ (43.7%±5%) > NaCl (7.9±10%), suggesting that the rejection is mainly based on the dielectric exclusion since divalent ions are retained more than monovalent ions independent of their charge.[73,74] Size exclusion may play a role as well since $Na^+$ has a significantly smaller size than the other ions and $Cl^-$ is significantly smaller than $Mg^{2+}$,[8,75], which can further explain the relatively high NaCl transport (low NaCl rejection) through the membrane. It is encouraging to compare our results with those found by You et al. [26], the only other HCCP-based IP NF membranes from polyethyleneimine and HCCP. They prepared a positively charged membrane, due to the presence of remaining nitrogen groups originating from the polyethyleneimine as also found for polyethylenemine - cyanuric chloride based NF membranes [76], with salt rejections for $MgCl_2$ (97%) > $MgSO_4$ (88%) > NaCl (87%) > $Na_2SO_4$ (58%) and a permeance of 3.7 L m$^{-2}$ h$^{-1}$ bar$^{-1}$ when tested with a 1 g L$^{-1}$ aqueous salt solution.[26] Although You et al. [26] did not evaluate the molecular weight cutoff or mean pore radius for their membrane, a comparison of the salt rejection measurements suggests that our selective layer on top of the alumina support is more neutral than the positively charged membrane prepared by them, as expected based on the monomers used This lower surface charge could explain the lower salt rejections for our alumina-supported membranes.[8,45] Furthermore, our use of a solution with a higher salt concentration than You et al. [26] probably also reduced the rejection for

some of the salts. Unfortunately, the surface charge for our alumina-supported TPE-HCCP membrane could not be confirmed via zeta potential measurements due to the thickness of the membrane support and equipment limitations of our zeta potential measurement equipment regarding the allowed thickness of the sample.

The performance of the alumina-supported TPE-HCCP membrane is assessed with the dyes (MB, RB, and BY) rejection in water, and the result is shown in Figure 7.5B. The prepared membrane has an excellent dye rejection with 98.2±2.3% for MB, 98.6±1.1% for RB, and 94±9.2% for BY. As expected, the dye rejections of the alumina-supported TPE-HCCP membrane are enhanced substantially compared to the support with an RB rejection of 14% and BY rejection of 76% in water. It again confirms that a tight TPE-HCCP layer formed.[65] Since the difference between the MB, RB, and BY rejection is insignificant, we refrain from interpreting the rejection data in more detail. The membrane performance for RB and MB rejection in ethanol (EtOH) and acetone (Ace) is shown in Figure 7.5B on the right side. The membrane has a high level of rejection for RB in ethanol and acetone, 99.7±0.3% and 99.7±0.0%, respectively. It is similar to the obtained RB rejection in water. However, for MB, the rejection is reduced to 92±1.7% and 93±0.5% in ethanol and acetone, respectively, which can be rationalized by the nature and solubility of MB in different solvents. For example, MB molecules tend to aggregate in an aqueous solution, explaining its high rejection in water compared to other solvents.[77]

In summary, the rejection results show that the alumina-supported TPE-HCCP membranes can reject MB with a molecular weight of 319.8 g mol$^{-1}$ and the smallest and longest molecular dimensions of 1.4 nm and 0.59 nm, respectively, as well as RB with a molecular weight of 479 g mol$^{-1}$ and the smallest and longest molecular dimensions of 0.43 nm and 1.7 nm. Therefore, the swelling of the TPE-HCCP selective layer on top of alumina supports in solvents such as ethanol and acetone is restricted by the extent of cross-linking and the attachment of the layer to the support.[78,79]
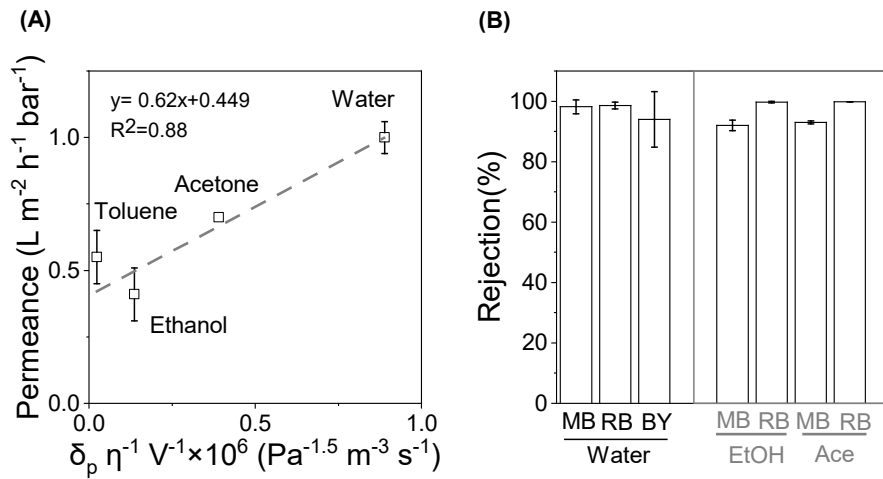
**Figure 7.5** (A) Pure solvent permeance as a function of their solvent properties in terms of $\delta_p \eta^{-1} V^{-1}$ for alumina-supported TPE-HCCP membranes. The gray dashed line shows the hypothetical linear relationships. (B) On the left side, the black frame: the rejection of Methylene Blue (MB), Brilliant Yellow (BY), and Rhodamine B in water for TPE-HCCP membranes. On the right side, gray frame: RB and MB rejection in different solvents, ethanol(EtOH) and acetone(Ace).

In Figure 7.6, the performance of the alumina-supported TPE-HCCP membrane is shown in relation to the performance of other IP-based NF membranes for treating solutions containing small solutes (314 Da< $M_w$ <327 Da). Compared to these other IP NF membranes, alumina-supported TPE-HCCP membranes reveal acceptable permeance with good rejection (above 92%) for a small dye such as MB (with a molecular weight of 319.9 Da) in acetone and ethanol. Notably, the prepared membrane has comparable performance as a polyester (4) and a polyamide (5) TFC membrane.[13,31]

In summary, the new alumina-supported TPE-HCCP membranes seem to be stable in solvents such as toluene, acetone, ethanol, and water with acceptable solvent permeances and good rejection for small dyes such as MB.
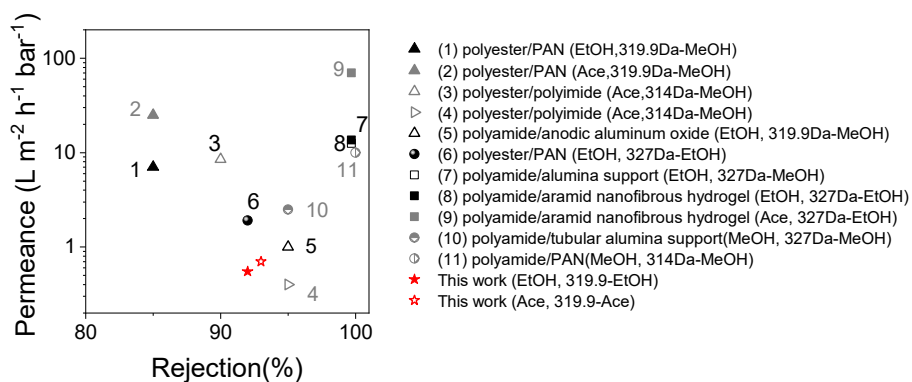
Figure 7.6 Comparison of the prepared alumina-supported TPE-HCCP membrane performance for small solutes (319.9 Da < $M_w$ < 400 Da) from this work with other IP NF membranes reported in the open literature.[10,13,31,32,34-36,38] The legend of each membrane shows polymer type/support type (Solvent for permeance measurement, $M_w$ of solute-solvent used to measure the rejection of solute).
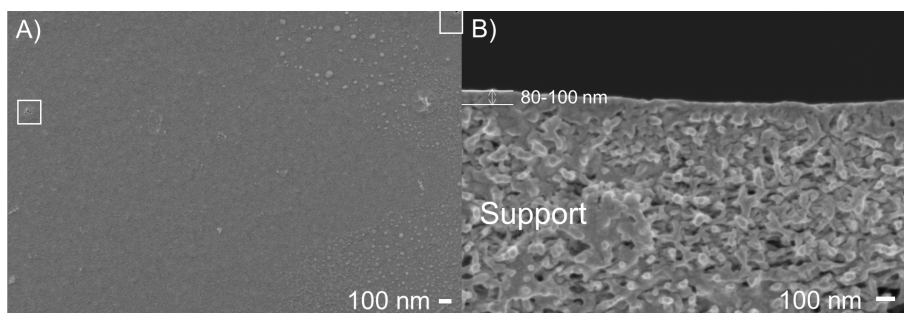
## 7.3.3. PAN-supported polyphosphazene



Figure 7.7 FE-SEM pictures of the PAN-based TPE-HCCP membrane (A) surface and B) Cross-section. The white squares show the pinholes on the surface of PAN-supported membranes.

We have shown the successful formation of alumina-supported TPE-HCCP polyphosphazene membranes and their potential and performance as organic solvent nanofiltration membranes. To go one step further towards economically scaling up the membrane, we prepared TPE-HCCP membranes on a PAN support. Undoubtedly, the physical-chemical properties and structure of the support membranes significantly impact the formation and performance of composite membranes.[80] For this reason, the preparation

procedure has been adapted. To evaluate the morphology, integrity, and thickness of the selective layer, FE-SEM was performed, and the results thereof are shown in Figure 7. The FE-SEM picture confirms the formation of a layer with a few visible pinholes on top of the support, Figure 7A. It indicates that the IP method is not sufficiently optimized, and still, some modification is needed. The PAN supports were soaked in water overnight while the ceramic supports were kept dry before IP. The observed defects could be due to the presence of trapped water in the pores of PAN support during IP, which hinders the formation of the CPPz layer on top of the support. Another reason could be the limited resistance of the PAN support to the DMSO solution, which could have resulted in the formation of defects upon its exposure to the phenolate/DMSO solution. Efforts to prepare PAN-supported membranes based on the procedure used for alumina-supported membranes failed (the top layer was removed) due to the low thermal resistance of the PAN support, making it impossible to pour the phenolate solution on top of the support at 80°C. Figure 7B shows the cross-sectional image of the TFCs membranes. The formed layer on top of the PAN support is in a range of 80 – 100 nm (see Figure 7B), and, therefore, thicker than the obtained TPE-HCCP layer on the alumina support (see Figure 3)
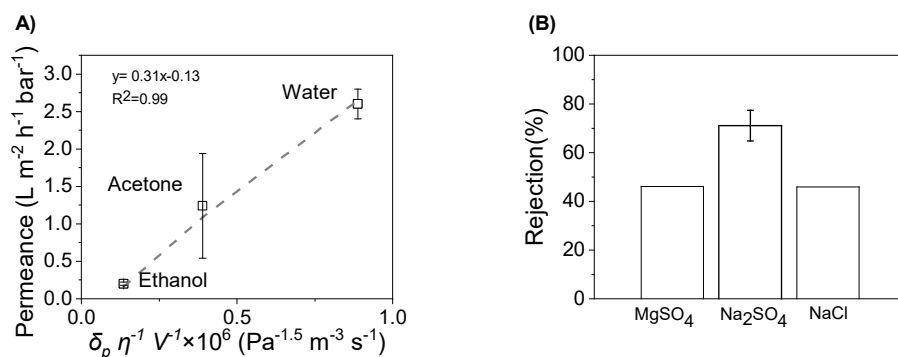


Figure 7.8 (A) Pure solvent permeance as a function of their solvent properties in terms of $\delta_p \eta^{-1} V^{-1}$ for PAN-supported TPE-HCCP membranes. The gray dashed line shows the hypothetical linear relationships (B) Salt rejection for three different salts.

The NF performance of the PAN-supported TPE-HCCP membrane, assessed by measuring the permeance of water, acetone, and ethanol, as well as the rejection of different salts, is shown in Figure 7.8. For the PAN-supported

TPE-HCCP membrane, the solvent permeance as a function of its physiochemical properties ($\delta_p \eta^{-1} V^{-1}$) follows the same order as that for the alumina-supported membranes; the permeance enhances as $\delta_p \eta^{-1} V^{-1}$ increases (Figure 7.8A). This indicates comparable interaction between the polymeric network and the solvents for both membranes. Although the TPE-HCCP layer of the prepared PAN-supported membranes is thicker, these membranes show considerably higher water and acetone permeances (around 1.2 and 2.6 L m$^{-2}$ h$^{-1}$ bar$^{-1}$, respectively) than the alumina-supported TPE-HCCP membranes. However, the ethanol permeance for the PAN-supported TPE-HCCP membrane is lower, with ethanol permeance of around 0.2 L m$^{-2}$ h$^{-1}$ bar$^{-1}$.

The results of the salt rejection measurements for three different salts in single salt aqueous solution experiments are shown in Figure 8B. The salt rejection follows the order of Na$_2$SO$_4$ (71.1%) > MgSO$_4$ (46.2%) ~ NaCl (46%). Before heat treatment, PAN-supported membranes show Na$_2$SO$_4$ rejection of 43%, indicating the effectiveness of heat treatment in the preparation of these membranes. The lower rejection of MgSO$_4$ compared to Na$_2$SO$_4$ indicates that the separation is based on a negative charge repulsion (Donnan-exclusion). Zeta potential results confirm the formation of a negative charge layer on top of the PAN support (Figure S7.5). Also, it illustrates that over the pH range from 3.9 to 9, the zeta potential of the layer remains negative, indicating that the isoelectric point (IEP) of the membrane surface is below 3.9, and the value depends on the solution pH as normally found. It should be noted that both the absolute zeta potential value as well as the slope of the zeta potential with pH are lower than found for typical commercial polyamide membranes such as NF-270.[81] It is good to mention that a negative charge of the membrane might be due to the presence of unreacted phenolate of TPE in the network. Although the PAN-based membrane shows a higher salt rejection than the alumina-based membranes, the rejection is lower than reported for other TFC membranes.[45] If Donnan-exclusion based on the negatively charged membrane surface would be the major contributor to the separation mechanism, it would be expected that MgSO$_4$ would have been rejected to a larger extent than NaCl, due to the stronger repulsion of SO$_4^{2-}$ compared to Cl$^-$ by the negatively charged surface of the membrane.[75] Furthermore,

results from MWCO experiments show that the rejection does not reach 100% for all tested 3 membrane samples (Figure S7.6), confirming the presence of the pinholes. This relatively high MWCO for the PAN supported membranes compared to the low MWCO of the alumina supported membranes may have (negatively) affected the $Mg^{2+}$ rejection to a larger extent than the rejection of the smaller $Na^+$. The higher $Na_2SO_4$ and NaCl rejections for the more open and negatively charged PAN-supported TPE-HCCP membrane compared to the alumina-supported TPE-HCCP membrane and the similar $MgSO_4$ rejections for the PAN-supported and alumina-supported membranes supports our impression that the alumina-supported membrane has a more neutral surface than the negatively charged PAN-supported TPE-HCCP membrane. Also, the RB rejection in water for the PAN-supported TPE-HCCP membranes is only about 50%. Although the lower rejection compared to the alumina-supported TPE-HCCP membrane could partly be caused by the negative charge of the PAN-supported TPE-HCCP membrane, it is more likely that the presence of pinholes for this latter membrane negatively affected the rejection for this cation as well. These rejections can probably be improved by modifying the IP method to form an integrated defect-free selective layer.

These obtained results suggest that the properties of the formed layer depend strongly on the properties of the support. The obtained differences in layer formation and characteristics can be due to the lower hydrophilicity of the PAN support or, more importantly, the significant difference in the pore size of the supports. The ceramic support has a γ-alumina layer with a pore diameter of 5.9 nm on top, while the mean pore size of the PAN support is 54.3 nm.[42] The small pores of supports favor forming a high cross-linking degree. When the support is soaked in the first IP monomer solution, a substantial amount of monomers is trapped in the bigger pores of supports. After exposing the surface to the second solution, the polymer grows in the inner pores more, which hinders the diffusion of monomers to the reaction zone and makes a defective low cross-linked layer.[80] This result is in line with the finding of Sharabati et al.[82] They found that increasing the pore size of the support decreases salt rejection, reduces cross-linking extent, and increases water permeation. Finally, each support provides a different interface for IP that influences the attachment of the IP-formed selective layer to them and dictates the performance and stability of the membrane in

each solvent. Our future research will focus on adapting techniques for preparing TPE-HCCP networks on polymeric supports to enhance membrane integration and rejection.

In summary, although the new TPE-HCCP polyphosphazene membrane is successfully formed on top of alumina supports, for PAN-supported TFC membranes the IP method and/or the chemical stability of the PAN support needs to be updated and improved to prepare a better performing membrane, and additional efforts are required to develop a proper CPPz layer on top of polymeric supports. A solution for potential insufficient chemical stability of the PAN support in DMSO has recently been proposed by Yushkin et al. [83], who showed that the use of infrared heating at 170°C strongly increases the stability of porous PAN in aprotic solvents such as DMSO.

## 7.4 Conclusion

In this work, we show for the first time the preparation of polyphosphazene TFC membranes via IP of TPE and HCCP on top of a ceramic support for OSN application. FE-SEM has confirmed the formation of a defect-free network atop the ceramic support with a film thickness of 30-50 nm. The resulting TPE-HCCP network is highly cross-linked and shows performance in the NF range, making the membrane suitable for OSN application. TPE-HCCP membranes exhibit a high MB (Mw of 319.8 g mol$^{-1}$) rejection of 98.2±2.3% in water, 92±1.7% in ethanol, and 93±0.5% in acetone while maintaining acceptable permeance. Also, the obtained PEG-based MWCO in water and polystyrene-based MWCO in acetone and toluene are comparable and between 300-500 Da. Furthermore, aiming for more cost-effective production of TPE-HCCP NF membranes, the TPE-HCCP layer was formed with IP on top of a PAN support. FE-SEM has revealed the formation of a 80-100 nm layer with a few pinholes on top of the PAN support. The water and acetone permeance of TFC PAN-supported membranes is higher compared to alumina-supported membranes. However, these higher permeances can (partly) be due to the presence of the pinholes. The resulting TPE-HCCP PAN-supported membrane is negatively charged, resulting in a higher rejection of salts. However, a proper MWCO could not be determined, most likely due to the pinholes present in the TFC layer. Finally,

additional attempts are needed to prepare defect-free cyclomatrix polyphophazene TFCs on top of the PAN supports. One of the possibilities to improve these PAN-supported membranes is the use of recently reported infrared heat treated PAN supports with improved chemical stability for DMSO. Our work is among the first attempts to design and evaluate the potential of cyclomatric polyphosphazene networks as a membrane for OSN. It clearly shows that this network has the potential to be used as an alternative to conventional TFC OSN membranes.

## 7.5 Acknowledgement

# 7.6 References

[1] Y. Li, Z. Guo, S. Li, B. Van der Bruggen, Interfacially Polymerized Thin-Film Composite Membranes for Organic Solvent Nanofiltration, Adv. Mater. Interfaces. 8 (2021) 2001671. https://doi.org/10.1002/admi.202001671.

[2] P. Li, H. Lan, K. Chen, X. Ma, B. Wei, M. Wang, P. Li, Y. Hou, Q. Jason Niu, Novel high-flux positively charged aliphatic polyamide nanofiltration membrane for selective removal of heavy metals, Sep. Purif. Technol. 280 (2022) 119949. https://doi.org/10.1016/j.seppur.2021.119949.

[3] K. Nath, H.K. Dave, T.M. Patel, Revisiting the recent applications of nanofiltration in food processing industries: Progress and prognosis, Trends Food Sci. Technol. 73 (2018) 12–24. https://doi.org/10.1016/j.tifs.2018.01.001.

[4] E. Schäfer, Andrea Iris, Fane, Anthony G., Nanofiltration: Principles, applications, and new materials, John Wiley & Sons, Inc., 2021.

[5] S. Chisca, V.-E. Musteata, W. Zhang, S. Vasylevskyi, G. Falca, E. Abou-Hamad, A.-H. Emwas, M. Altunkaya, S.P. Nunes, Polytriazole membranes with ultrathin tunable selective layer for crude oil fractionation, Science (80-. ). 376 (2022) 1105–1110. https://doi.org/10.1126/science.abm7686.

[6] Y. Zhao, T. Tong, X. Wang, S. Lin, E.M. Reid, Y. Chen, Differentiating Solutes with Precise Nanofiltration for Next Generation Environmental Separations: A Review, Environ. Sci. Technol. 55 (2021) 1359–1376. https://doi.org/10.1021/acs.est.0c04593.

[7] G. Bargeman, J.B. Westerink, O. Guerra Miguez, M. Wessling, The effect of NaCl and glucose concentration on retentions for nanofiltration membranes processing concentrated solutions, Sep. Purif. Technol. 134 (2014) 46–57. https://doi.org/10.1016/j.seppur.2014.07.025.

[8] G. Bargeman, J.B. Westerink, C.F.H. Manuhutu, A. ten Kate, The effect of membrane characteristics on nanofiltration membrane performance during processing of practically saturated salt solutions, J. Memb. Sci. 485 (2015) 112–122. https://doi.org/10.1016/j.memsci.2015.03.039.

[9] M.F. Jimenez Solomon, Y. Bhole, A.G. Livingston, High flux membranes for organic solvent nanofiltration (OSN)—Interfacial polymerization with solvent

activation, J. Memb. Sci. 423–424 (2012) 371–382. https://doi.org/10.1016/j.memsci.2012.08.030.

[10] S. Karan, Z. Jiang, A.G. Livingston, Sub–10 nm polyamide nanofilms with ultrafast solvent transport for molecular separation, Science (80-. ). 348 (2015) 1347–1351. https://doi.org/10.1126/science.aaa5058.

[11] K.S. Goh, J.Y. Chong, Y. Chen, W. Fang, T.-H. Bae, R. Wang, Thin-film composite hollow fibre membrane for low pressure organic solvent nanofiltration, J. Memb. Sci. 597 (2020) 117760. https://doi.org/10.1016/j.memsci.2019.117760.

[12] J. Liu, S. Wang, T. Huang, P. Manchanda, E. Abou-Hamad, S.P. Nunes, Smart covalent organic networks (CONs) with "on-off-on" light-switchable pores for molecular separation, Sci. Adv. 6 (2020). https://doi.org/10.1126/sciadv.abb3188.

[13] M.F. Jimenez-Solomon, Q. Song, K.E. Jelfs, M. Munoz-Ibanez, A.G. Livingston, Polymer nanofilms with enhanced microporosity by interfacial polymerization, Nat. Mater. 15 (2016) 760–767. https://doi.org/10.1038/nmat4638.

[14] J. Li, J.-L. Gong, G.-M. Zeng, B. Song, W.-C. Cao, S.-Y. Fang, S.-Q. Tang, Y. Guan, Z.-K. Tan, Z.-P. Chen, X.-Q. Mao, R.-L. Zhu, Thin-film composite polyester nanofiltration membrane with high flux and efficient dye/salts separation fabricated from precise molecular sieving structure of β-cyclodextrin, Sep. Purif. Technol. 276 (2021) 119352. https://doi.org/10.1016/j.seppur.2021.119352.

[15] N.A. Khan, R. Zhang, H. Wu, J. Shen, J. Yuan, C. Fan, L. Cao, M.A. Olson, Z. Jiang, Solid–Vapor Interface Engineered Covalent Organic Framework Membranes for Molecular Separation, J. Am. Chem. Soc. 142 (2020) 13450–13458. https://doi.org/10.1021/jacs.0c04589.

[16] M.H. Abdellah, L. Pérez-Manríquez, T. Puspasari, C.A. Scholes, S.E. Kentish, K.-V. Peinemann, A catechin/cellulose composite membrane for organic solvent nanofiltration, J. Memb. Sci. 567 (2018) 139–145. https://doi.org/10.1016/j.memsci.2018.09.042.

[17] M.F. Jimenez-Solomon, P. Gorgojo, M. Munoz-Ibanez, A.G. Livingston, Beneath the surface: Influence of supports on thin film composite membranes by interfacial polymerization for organic solvent nanofiltration, J. Memb. Sci. 448 (2013) 102–113. https://doi.org/10.1016/j.memsci.2013.06.030.

[18] G.M. Shi, Y. Feng, B. Li, H.M. Tham, J.-Y. Lai, T.-S. Chung, Recent progress of organic solvent nanofiltration membranes, Prog. Polym. Sci. 123 (2021) 101470. https://doi.org/10.1016/j.progpolymsci.2021.101470.

[19] M. Amirilargani, G.N. Yokota, G.H. Vermeij, R.B. Merlet, G. Delen, L.D.B. Mandemaker, B.M. Weckhuysen, L. Winnubst, A. Nijmeijer, L.C.P.M. Smet, E.J.R. Sudhölter, Melamine-Based Microporous Organic Framework Thin Films on an Alumina Membrane for High-Flux Organic Solvent Nanofiltration, ChemSusChem. 13 (2020) 136–140. https://doi.org/10.1002/cssc.201902341.

[20] A. Asadi Tashvigh, N.E. Benes, Covalent organic polymers for aqueous and organic solvent nanofiltration, Sep. Purif. Technol. 298 (2022) 121589. https://doi.org/10.1016/j.seppur.2022.121589.

[21] R.S. Ullah, L. Wang, H. Yu, N.M. Abbasi, M. Akram, Z. -ul-Abdin, M. Saleem, M. Haroon, R.U. Khan, Synthesis of polyphosphazenes with different side groups and various tactics for drug delivery, RSC Adv. 7 (2017) 23363–23391. https://doi.org/10.1039/C6RA27103K.

[22] H.R. Allcock, Recent developments in polyphosphazene materials science, Curr. Opin. Solid State Mater. Sci. 10 (2006) 231–240. https://doi.org/10.1016/j.cossms.2007.06.001.

[23] K.S. Ogueri, H.R. Allcock, C.T. Laurencin, Generational biodegradable and regenerative polyphosphazene polymers and their blends with poly (lactic-co-glycolic acid), Prog. Polym. Sci. 98 (2019) 101146. https://doi.org/10.1016/j.progpolymsci.2019.101146.

[24] H.R. Allcock, N.J. Sunderland, R. Ravikiran, J.M. Nelson, Polyphosphazenes with Novel Architectures: Influence on Physical Properties and Behavior as Solid Polymer Electrolytes, Macromolecules. 31 (1998) 8026–8035. https://doi.org/10.1021/ma9804491.

[25] W. Wei, X. Huang, K. Chen, Y. Tao, X. Tang, Fluorescent organic–inorganic hybrid polyphosphazene microspheres for the trace detection of nitroaromatic explosives, RSC Adv. 2 (2012) 3765. https://doi.org/10.1039/c2ra20263h.

[26] M. You, W. Li, Y. Pan, P. Fei, H. Wang, W. Zhang, L. Zhi, J. Meng, Preparation and characterization of antibacterial polyamine-based cyclophosphazene nanofiltration membranes, J. Memb. Sci. 592 (2019) 117371. https://doi.org/10.1016/j.memsci.2019.117371.

[27] C.A. Allen, D.G. Cummings, A.E. Grey, R.E. McAtee, R.R. McCaffrey, Separation of Cr ions from Co and mn ions by poly (bis(phenoxy) phosphazene) membranes, J. Memb. Sci. 33 (1987) 181–189. https://doi.org/10.1016/S0376-7388(00)80376-2.

[28] C. Liu, J. Yang, B. Guo, S. Agarwal, A. Greiner, Z. Xu, Interfacial Polymerization at the Alkane/Ionic Liquid Interface, Angew. Chemie. 133 (2021) 14757–14764. https://doi.org/10.1002/ange.202103555.

[29] L.F. Villalobos, T. Huang, K.-V. Peinemann, Cyclodextrin Films with Fast Solvent Transport and Shape-Selective Permeability, Adv. Mater. 29 (2017) 1606641. https://doi.org/10.1002/adma.201606641.

[30] S.H. Park, A. Alammar, Z. Fulop, B.A. Pulido, S.P. Nunes, G. Szekely, Hydrophobic thin film composite nanofiltration membranes derived solely from sustainable sources, Green Chem. 23 (2021) 1175–1184. https://doi.org/10.1039/d0gc03226c.

[31] T. Huang, T. Puspasari, S.P. Nunes, K. Peinemann, Ultrathin 2D-Layered Cyclodextrin Membranes for High- Performance Organic Solvent Nanofiltration, Adv. Funct. Mater. 30 (2020) 1906797. https://doi.org/10.1002/adfm.201906797.

[32] Y. Li, E. Wong, A. Volodine, C. Van Haesendonck, K. Zhang, B. Van der Bruggen, Nanofibrous hydrogel composite membranes with ultrafast transport performance for molecular separation in organic solvents, J. Mater. Chem. A. 7 (2019) 19269–19279. https://doi.org/10.1039/C9TA06169J.

[33] L. Xia, J. Ren, M. Weyd, J.R. McCutcheon, Ceramic-supported thin film composite membrane for organic solvent nanofiltration, J. Memb. Sci. 563 (2018) 857–863. https://doi.org/10.1016/j.memsci.2018.05.069.

[34] S. Sorribas, P. Gorgojo, C. Téllez, J. Coronas, A.G. Livingston, High Flux Thin Film Nanocomposite Membranes Based on Metal–Organic Frameworks for Organic Solvent Nanofiltration, J. Am. Chem. Soc. 135 (2013) 15201–15208. https://doi.org/10.1021/ja407665w.

[35] Z. Ali, B.S. Ghanem, Y. Wang, F. Pacheco, W. Ogieglo, H. Vovusha, G. Genduso, U. Schwingenschlögl, Y. Han, I. Pinnau, Finely Tuned Submicroporous Thin-Film Molecular Sieve Membranes for Highly Efficient Fluid Separations, Adv. Mater. 32 (2020) 2001132. https://doi.org/10.1002/adma.202001132.

[36] M.M.A. Almijbilee, X. Wu, A. Zhou, X. Zheng, X. Cao, W. Li, Polyetheramide organic solvent nanofiltration membrane prepared via an interfacial assembly and polymerization procedure, Sep. Purif. Technol. 234 (2020) 116033. https://doi.org/10.1016/j.seppur.2019.116033.

[37] Q. Liu, X. Wu, K. Zhang, Polysulfone/Polyamide-SiO2 Composite Membrane with High Permeance for Organic Solvent Nanofiltration, Membranes (Basel). 8 (2018) 89. https://doi.org/10.3390/membranes8040089.

[38] M.H. Abdellah, L. Pérez-Manríquez, T. Puspasari, C.A. Scholes, S.E. Kentish, K.-V. Peinemann, Effective Interfacially Polymerized Polyester Solvent Resistant Nanofiltration Membrane from Bioderived Materials, Adv. Sustain. Syst. 2 (2018) 1800043. https://doi.org/10.1002/adsu.201800043.

[39] F. Radmanesh, E.J.R. Sudhölter, A. Tena, M.G. Elshof, N.E. Benes, Thin film composite cyclomatrix poly(phenoxy)phosphazenes membranes for hot hydrogen separation, Adv. Mater. Interfaces. (n.d.).

[40] F. Radmanesh, A. Tena, E.J.R. Sudhölter, M.A. Hempenius, N.E. Benes, Non-aqueous interfacial polymerization derived polyphosphazene films for sieving or blocking hydrogen gas, Submitted. (n.d.).

[41] M. ten Hove, M.W.J. Luiten-Olieman, C. Huiskes, A. Nijmeijer, L. Winnubst, Hydrothermal stability of silica, hybrid silica and Zr-doped hybrid silica membranes, Sep. Purif. Technol. 189 (2017) 48–53. https://doi.org/10.1016/j.seppur.2017.07.045.

[42] Y. Ma, S. Velioğlu, Z. Yin, R. Wang, J.W. Chew, Molecular dynamics investigation of membrane fouling in organic solvents, J. Memb. Sci. 632 (2021) 119329. https://doi.org/10.1016/j.memsci.2021.119329.

[43] T.H. Lee, M.G. Shin, J.G. Jung, E.H. Suh, J.G. Oh, J.H. Kang, B.S. Ghanem, J. Jang, J.-H. Lee, I. Pinnau, H.B. Park, Facile suppression of intensified plasticization in glassy polymer thin films towards scalable composite membranes for propylene/propane separation, J. Memb. Sci. 645 (2022) 120215. https://doi.org/10.1016/j.memsci.2021.120215.

[44] F. Radmanesh, M.G. Elshof, N.E. Benes, Polyoctahedral Silsesquioxane Hexachlorocyclotriphosphazene Membranes for Hot Gas Separation, ACS Appl. Mater. Interfaces. 13 (2021) 8960–8966. https://doi.org/10.1021/acsami.0c21968.

[45] M.G. Elshof, E. Maaskant, M.A. Hempenius, N.E. Benes, Poly(aryl cyanurate)-Based Thin-Film Composite Nanofiltration Membranes, ACS Appl. Polym. Mater. 3 (2021) 2385–2392. https://doi.org/10.1021/acsapm.0c01366.

[46] F. Radmanesh, M. Pilz, L. Ansaloni, T.A. Peters, E. Louradour, H. van Veen, D. Høvik, M.A. Hempenius, N.E. Benes, Comparing amine- and ammonium functionalized silsesquioxanes for large scale synthesis of hybrid polyimide high-temperature gas separation membranes, J. Memb. Sci. 637 (2021) 119524. https://doi.org/10.1016/j.memsci.2021.119524.

[47] F.P. Cuperus, D. Bargeman, C.A. Smolders, Permporometry: the determination of the size distribution of active pores in UF membranes, J. Memb. Sci. 71 (1992) 57–67. https://doi.org/10.1016/0376-7388(92)85006-5.

[48] D.M. Reurink, J.P. Haven, I. Achterhuis, S. Lindhoud, E.H.D.W. Roesink, W.M. de Vos, Annealing of Polyelectrolyte Multilayers for Control over Ion Permeation, Adv. Mater. Interfaces. 5 (2018) 1800651. https://doi.org/10.1002/admi.201800651.

[49] M.G. Elshof, W.M. de Vos, J. de Grooth, N.E. Benes, On the long-term pH stability of polyelectrolyte multilayer nanofiltration membranes, J. Memb. Sci. 615 (2020) 118532. https://doi.org/10.1016/j.memsci.2020.118532.

[50] A. Asadi Tashvigh, M.G. Elshof, N.E. Benes, Development of Thin-Film Composite Membranes for Nanofiltration at Extreme pH, ACS Appl. Polym. Mater. 3 (2021) 5912–5919. https://doi.org/10.1021/acsapm.1c01172.

[51] P. Puhlfürß, A. Voigt, R. Weber, M. Morbé, Microporous TiO2 membranes with a cut off <500 Da, J. Memb. Sci. 174 (2000) 123–133. https://doi.org/10.1016/S0376-7388(00)00380-X.

[52] N. Kyriakou, R.B. Merlet, J.D. Willott, A. Nijmeijer, L. Winnubst, M.-A. Pizzoccaro-Zilamy, New Method toward a Robust Covalently Attached Cross-Linked Nanofiltration Membrane, ACS Appl. Mater. Interfaces. 12 (2020) 47948–47956. https://doi.org/10.1021/acsami.0c13339.

[53] B. Sutariya, S. Karan, A realistic approach for determining the pore size distribution of nanofiltration membranes, Sep. Purif. Technol. 293 (2022) 121096. https://doi.org/10.1016/j.seppur.2022.121096.

[54] K.H. Youm, W.S. Kim, Prediction of intrinsic pore properties of ultrafiltration membrane by solute rejection curves: Effects of operating conditions on pore properties., J. Chem. Eng. JAPAN. 24 (1991) 1–7. https://doi.org/10.1252/jcej.24.1.

[55] J.A.V. Donald L. Pavia, Gary M. Lampman, George S. Kriz, Introduction to spectroscopy, Cengage learning, 2014.

[56] F. Alregeb, F. Khalili, B. Sweileh, D.K. Ali, Synthesis and Characterization of Chelating Hyperbranched Polyester Nanoparticles for Cd(II) Ion Removal from Water, Molecules. 27 (2022) 3656. https://doi.org/10.3390/molecules27123656.

[57] A. Deniz, N. Zaytoun, L. Hetjens, A. Pich, Polyphosphazene–Tannic Acid Colloids as Building Blocks for Bio-Based Flame-Retardant Coatings, ACS Appl. Polym. Mater. 2 (2020) 5345–5351. https://doi.org/10.1021/acsapm.0c00574.

[58] E. Maaskant, H. Gojzewski, M.A. Hempenius, G.J. Vancso, N.E. Benes, Thin cyclomatrix polyphosphazene films: interfacial polymerization of hexachlorocyclotriphosphazene with aromatic biphenols, Polym. Chem. 9 (2018) 3169–3180. https://doi.org/10.1039/C8PY00444G.

[59] Jiang, Wang, Luo, Qi, Qiao, Zou, Wang, Design and Application of Highly Efficient Flame Retardants for Polycarbonate Combining the Advantages of Cyclotriphosphazene and Silicone Oil, Polymers (Basel). 11 (2019) 1155. https://doi.org/10.3390/polym11071155.

[60] Y. Zhang, X. Chen, J. Xu, Q. Zhang, L. Gao, Z. Wang, L. Qu, K. Wang, Y. Li, Z. Cai, Y. Zhao, C. Yang, Cross-Linked Polyphosphazene Nanospheres Boosting Long-Lived Organic Room-Temperature Phosphorescence, J. Am. Chem. Soc. 144 (2022) 6107–6117. https://doi.org/10.1021/jacs.2c02076.

[61] Y. Zhang, N.E. Benes, R.G.H. Lammertink, Visualization and characterization of interfacial polymerization layer formation, Lab Chip. 15 (2015) 575–580. https://doi.org/10.1039/C4LC01046A.

[62] P. Marchetti, M.F. Jimenez Solomon, G. Szekely, A.G. Livingston, Molecular Separation with Organic Solvent Nanofiltration: A Critical Review, Chem. Rev. 114 (2014) 10735–10806. https://doi.org/10.1021/cr500006j.

[63] J. Geens, B. De Witte, B. Van der Bruggen, Removal of API's (Active Pharmaceutical Ingredients) from Organic Solvents by Nanofiltration, Sep. Sci. Technol. 42 (2007) 2435–2449. https://doi.org/10.1080/01496390701477063.

[64] A. Asadi Tashvigh, T.-S. Chung, Robust polybenzimidazole (PBI) hollow fiber membranes for organic solvent nanofiltration, J. Memb. Sci. 572 (2019) 580–587. https://doi.org/10.1016/j.memsci.2018.11.048.

[65] N. Kyriakou, L. Winnubst, M. Drobek, S. de Beer, A. Nijmeijer, M.-A. Pizzoccaro-Zilamy, Controlled Nanoconfinement of Polyimide Networks in Mesoporous γ-Alumina Membranes for the Molecular Separation of Organic Dyes, ACS Appl. Nano Mater. 4 (2021) 14035–14046. https://doi.org/10.1021/acsanm.1c03322.

[66] S. Yang, H. Li, X. Zhang, S. Du, J. Zhang, B. Su, X. Gao, B. Mandal, Amine-functionalized ZIF-8 nanoparticles as interlayer for the improvement of the separation performance of organic solvent nanofiltration (OSN) membrane, J. Memb. Sci. 614 (2020) 118433. https://doi.org/10.1016/j.memsci.2020.118433.

[67] Z. Zhou, D. Lu, X. Li, L.M. Rehman, A. Roy, Z. Lai, Fabrication of highly permeable polyamide membranes with large "leaf-like" surface nanostructures on inorganic supports for organic solvent nanofiltration, J. Memb. Sci. 601 (2020) 117932. https://doi.org/10.1016/j.memsci.2020.117932.

[68] Y. Chen, M. Toth, C. He, Facile and fast fabrication of high structure-stable thin film nanocomposite membrane for potential application in solvent resistance nanofiltration, Appl. Surf. Sci. 496 (2019) 143483. https://doi.org/10.1016/j.apsusc.2019.07.225.

[69] X. Cheng, X. Jiang, Y. Zhang, C.H. Lau, Z. Xie, D. Ng, S.J.D. Smith, M.R. Hill, L. Shao, Building Additional Passageways in Polyamide Membranes with Hydrostable Metal Organic Frameworks To Recycle and Remove Organic Solutes from Various Solvents, ACS Appl. Mater. Interfaces. 9 (2017) 38877–38886. https://doi.org/10.1021/acsami.7b07373.

[70] Y. Zhang, X. Cheng, X. Jiang, J.J. Urban, C.H. Lau, S. Liu, L. Shao, Robust natural nanocomposites realizing unprecedented ultrafast precise molecular separations, Mater. Today. 36 (2020) 40–47. https://doi.org/10.1016/j.mattod.2020.02.002.

[71] Z. Yuan, X. Wu, Y. Jiang, Y. Li, J. Huang, L. Hao, J. Zhang, J. Wang, Carbon dots-incorporated composite membrane towards enhanced organic solvent nanofiltration performance, J. Memb. Sci. 549 (2018) 1–11. https://doi.org/10.1016/j.memsci.2017.11.051.

[72] M. Amirilargani, R.B. Merlet, A. Nijmeijer, L. Winnubst, L.C.P.M. de Smet, E.J.R. Sudhölter, Poly (maleic anhydride-alt-1-alkenes) directly grafted to γ-alumina for high-performance organic solvent nanofiltration membranes, J. Memb. Sci. 564 (2018) 259–266. https://doi.org/10.1016/j.memsci.2018.07.042.

[73] J. de Grooth, R. Oborný, J. Potreck, K. Nijmeijer, W.M. de Vos, The role of ionic strength and odd–even effects on the properties of polyelectrolyte multilayer nanofiltration membranes, J. Memb. Sci. 475 (2015) 311–319. https://doi.org/10.1016/j.memsci.2014.10.044.

[74] D.L. Oatley, L. Llenas, R. Pérez, P.M. Williams, X. Martínez-Lladó, M. Rovira, Review of the dielectric properties of nanofiltration membranes and verification of the single oriented layer approximation, Adv. Colloid Interface Sci. 173 (2012) 1–11. https://doi.org/10.1016/j.cis.2012.02.001.

[75] J. Luo, Y. Wan, Effects of pH and salt on nanofiltration—a critical review, J. Memb. Sci. 438 (2013) 18–28. https://doi.org/10.1016/j.memsci.2013.03.029.

[76] K.P. Lee, J. Zheng, G. Bargeman, A.J.B. Kemperman, N.E. Benes, pH stable thin film composite polyamine nanofiltration membranes by interfacial polymerisation, J. Memb. Sci. 478 (2015) 75–84. https://doi.org/10.1016/j.memsci.2014.12.045.

[77] J.A. Caram, J.F.M. Suárez, A.M. Gennaro, M.V. Mirífico, ELECTROCHEMICAL BEHAVIOUR OF METHYLENE BLUE IN NON-AQUEOUS SOLVENTS, Electrochim. Acta. 164 (2015) 353–363. https://doi.org/10.1016/j.electacta.2015.01.196.

[78] J. Canning, G. Huyang, M. Ma, A. Beavis, D. Bishop, K. Cook, A. McDonagh, D. Shi, G.-D. Peng, M. Crossley, Percolation Diffusion into Self-Assembled Mesoporous Silica Microfibres, Nanomaterials. 4 (2014) 157–174. https://doi.org/10.3390/nano4010157.

[79] G.L. Dotto, J.M.N. Santos, I.L. Rodrigues, R. Rosa, F.A. Pavan, E.C. Lima, Adsorption of Methylene Blue by ultrasonic surface modified chitin, J. Colloid Interface Sci. 446 (2015) 133–140. https://doi.org/10.1016/j.jcis.2015.01.046.

[80] F. Liu, L. Wang, D. Li, Q. Liu, B. Deng, A review: the effect of the microporous support during interfacial polymerization on the morphology and performances of a thin film composite membrane for liquid purification, RSC Adv. 9 (2019) 35417–35428. https://doi.org/10.1039/C9RA07114H.

[81] M. Dalwani, N.E. Benes, G. Bargeman, D. Stamatialis, M. Wessling, A method for characterizing membranes during nanofiltration at extreme pH, J. Memb. Sci. 363 (2010) 188–194. https://doi.org/10.1016/j.memsci.2010.07.025.

[82] J. A. D. Sharabati, S. Guclu, S. Erkoc-Ilter, D.Y. Koseoglu-Imer, S. Unal, Y.Z. Menceloglu, I. Ozturk, I. Koyuncu, Interfacially polymerized thin-film composite membranes: Impact of support layer pore size on active layer polymerization and seawater desalination performance, Sep. Purif. Technol. 212 (2019) 438–448. https://doi.org/10.1016/j.seppur.2018.11.047.

[83] A.A. Yushkin, M.N. Efimov, A.O. Malakhov, G.P. Karpacheva, G. Bondarenko, L. Marbelia, I.F.J. Vankelecom, A. V. Volkov, Creation of highly stable porous polyacrylonitrile membranes using infrared heating, React. Funct. Polym. 158 (2021) 104793. https://doi.org/10.1016/j.reactfunctpolym.2020.104793.

## 7.7 Supporting information
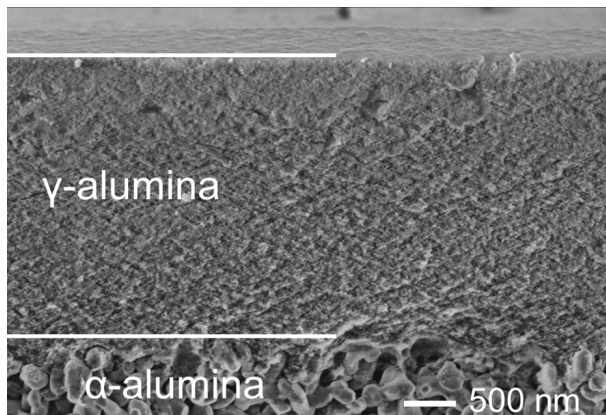


Figure S7.1 FE-SEM picture of a cross-section of the membrane, showing a γ-alumina layer (Øpores = 5 nm, 2.9 μm in thickness) and a part of the α- alumina layer (Øpores = 80 nm, 2 mm in thickness.
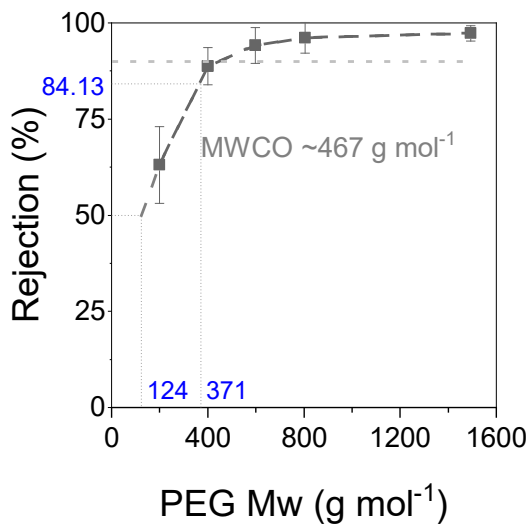


Figure S7.2 PEG rejection of TPE-HCCP membranes in water. The squares indicate the five different molecular weights PEG used for this retention test. The MWCO is a molar mass at which 90% of the PEG is retained.
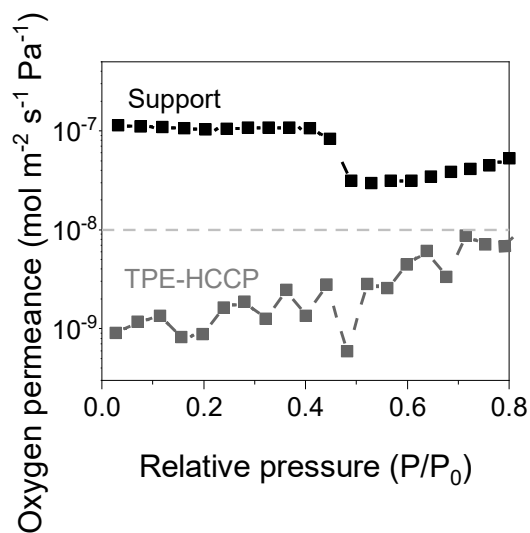
Figure S7.3 Oxygen permeance as a function of the relative cyclohexane vapor pressure for the pristine support and TPE-HCCP membrane. The corresponding average Kelvin pore radius for support using the Kelvin equation is 2.9 nm. The blue dashed line shows the detection limit of the set-up, which is $1 \times 10^{-8}$ mol m$^{-2}$ s$^{-1}$ Pa$^{-1}$.
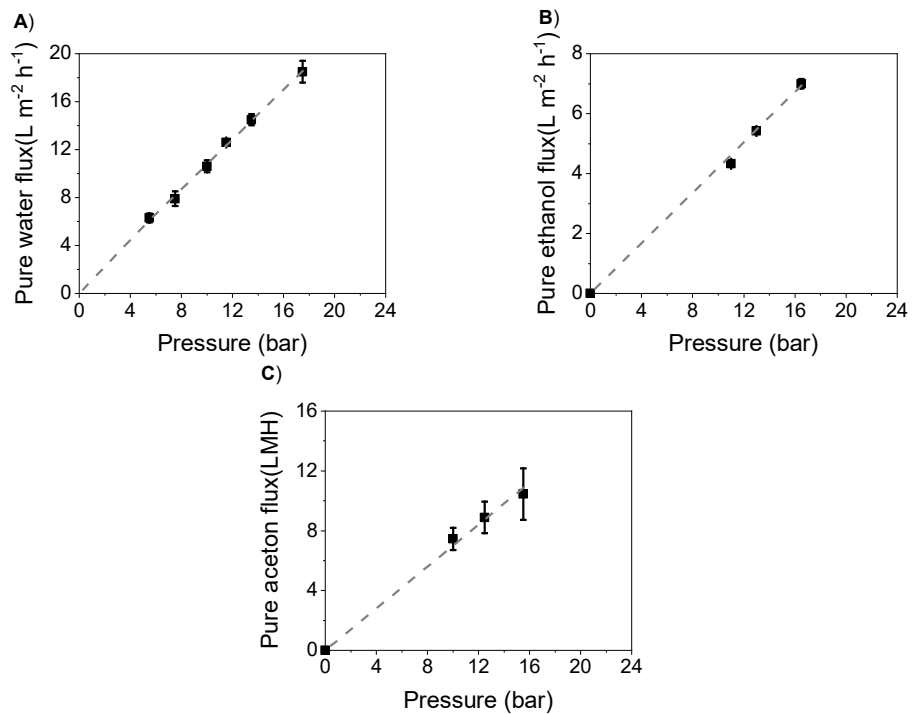
Figure S7.4 Pure solvent flux of TPE-HCCP membranes as a function of pressure (A) water, B) ethanol (EtOH), and (B) acetone (Ac).
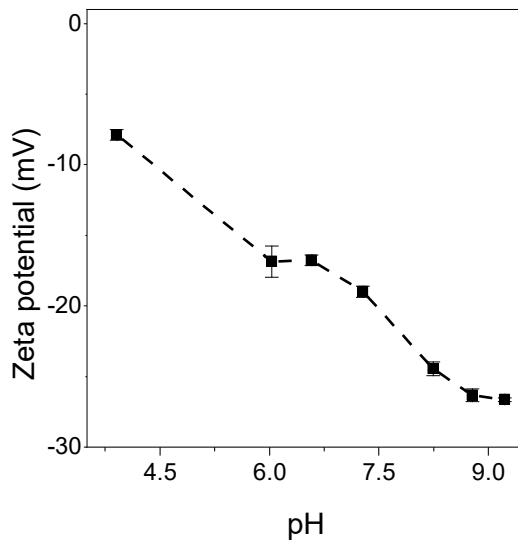
Figure S7.5 Zeta potential as a function of the pH for polymeric-supported TPE-HCCP membrane
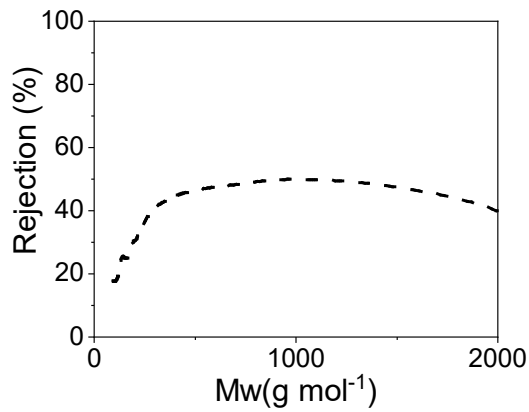


Figure S7.6 PEG retention for PEGs with different molar mass for polymeric-supported TFC membranes.

# Chapter 8

# Conclusions, reflections and perspectives

Interfacial polymerization (IP) allows the use of a wide variety of monomers to synthesize and design an indefinite amount of polymer networks. Various synthesizing parameters can affect the structure, performance, and scale-up potential of these networks. In Chapter 2, the effects of some of these parameters on the properties and the performance of IP-derived polyPOSS-imide thin film composite membranes for hot gas separation are explored, and the scale-up potential of these membranes is evaluated. In the second part of this thesis, a non-conventional IP platform is introduced that makes use of two immiscible organic solvents and provides opportunities for a broadened range of monomer combinations. Through chapters 3 to 7, IP methods are explored to prepare cyclomatrix polyphosphazene networks for a broad range of applications, from hot gas separation to hydrogen barriers and organic solvent nanofiltration. Similar to conventional (aqueous-organic) interfacial polymerization, the process can be easily tuned to obtain tailored molecular structures and film morphologies.

This chapter first provides overall conclusions and concerns about the prepared networks and gives possible directions for further research. This is followed by a section that describes some potentially interesting monomer combinations for non-aqueous IP. Finally, general conclusions and remarks are given.

## 8.1 On the chapter content

This section is split into two distinct parts based on the chemistries of networks. The first part discusses polyPOSS-imide networks, and the second part considers cyclomatrix polyphosphazene (CPPz) networks.

### 8.1.1. PolyPOSS-imide

PolyPOSS-imide membranes are promising for separating $H_2$ from larger molecules ($CO_2$, $N_2$, $CH_4$) at temperatures up to 300 °C. Their fabrication involves two steps: interfacial polymerization of octa amino propyl polyoctahedral silsesquioxane (POSS) and 6FDA, followed by thermal imidization.[1] The unique properties of these networks have been studied in

detail in the previous reports by Raaijmakers et al. [1–4]. Chapter 2 aims to go one step further and scale up these potential networks for the separation of $H_2$ at high temperatures in the industry. For this, two distinct POSS molecules were used: one functionalized with $-NH_3^+Cl^-$ and one with, so far unexplored, $-NH_2$. The ammonium groups are partially deprotonated by using three different bases, LiOH, NaOH, and KOH. The formation, imidization, and performance of polyPOSS-imide membranes atop lab-scaled flat disc and single-channel tubular supports are systematically studied. For flat disc membranes, at 200 °C, the absence of cations results in comparable permeability combined with higher selectivity for $H_2/N_2$. This, and the possibility of discarding adding a base, motivated a scale-up study of the new POSS with $-NH_2$ group. The data show that the new monomer allows more reproducible production of defect-free membranes and has a higher potential for larger-scale polyPOSS-imide fabrication. The result indicates that the production of by-products such as salts does not change the composition and performance of the networks; however, it might promote forming defects in larger scale membranes for which there is lower control over the process.

Aside from the above efforts to industrialize the polyPOSS imide membranes, the following methods have been applied to optimize and enhance the properties, stability, and performance of these membranes.

## The effect of solvent

Solvents selection is one of the important parameters affecting the morphology, cross-linking density, and performance of prepared networks by IP. Many research papers have used co-solvents, for instance, to disturb the liquid-liquid interfaces and enhance the permeability of the final membrane. In the synthesis of polyPOSS-imide membranes, DMSO can be used as a co-solvent for the aqueous phase to disturb the interface, but in addition to increase the reactivity of POSS. For this, we have prepared polyPOSS-imide membranes by the IP reaction of octa amino propyl POSS in DMSO and water (with volumetric ratio 2:3) with anhydride in toluene, followed by thermal imidization. The FE-SEM cross-sectional image of the new membrane shows that the thickness of the formed layer on top of the ceramic support is increased from 60-80 nm to 136 nm, Figure 8.1.
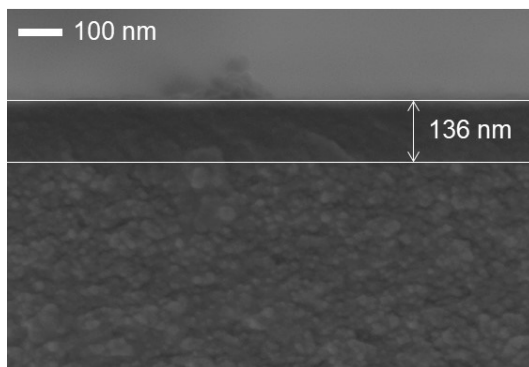
Figure 8.1 FE-SEM image of cross-section polyPOSS-imide membranes prepared with the IP reaction of octa amino propyl POSS in DMSO and water (with volumetric ratio 2:3) with anhydride in toluene, followed by thermal imidization

Gas separation performance was measured at 200 °C and transmembrane pressure of 2 bar. Figure 8.2 compares the performance of water-based and water/DMSO-based membranes. It shows that using DMSO as a co-solvent leads to decreased permeances and enhanced permselectivity, indicating the selective layer has a higher cross-linking degree. The phenomena can be explained by:

1- Increasing the reactivity of POSS,
2- reducing the hydrolysis of the anhydride, and
3- increasing the diffusion of anhydride to the interface due to the dipole-dipole interaction between DMSO and the anhydride group.

Besides, during the imidization step at 300 °C, DMSO can be decomposed and form small sulfur species that might react with unreacted functional groups and participate in further cross-linking. Ultimately, this experiment emphasizes the importance of solvent-pair selections for IP on the performance of final membranes.
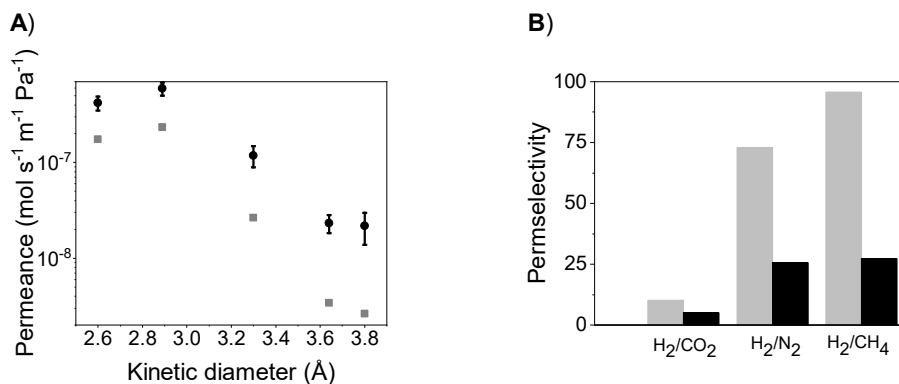
Figure 8.2 Comparing the gas performance of polyPOSS-imide membranes prepared with IP between POSS in water or water/DMSO and 4,4′-(Hexafluoroisopropylidene)diphthalic anhydride (6FDA) in toluene following by imidization. The gas performance is shown at 200 °C and transmembrane pressure of 2 bar. (A) permeance and (B) permselectivity of different gas pairs.

## In situ fabrication of palladium nanoparticles

Palladium membranes are highly effective in separating $H_2$ from $CO_2$. They are exclusively selective toward $H_2$; if they are made thin enough, they will show high hydrogen fluxes. However, they suffer from mechanical instability due to hydrogen embrittlement, their rigid inorganic nature, and the volume expansion that occurs during the transition from α–β phase. One strategy to solve the mentioned issue is embedding Pd nanoparticles (NPs) in a flexible polymeric matrix.[5]

Here, we explore the in-situ formation of palladium NPs in polyPOSS-imide networks using four steps:

1- Dissolving palladium nitrate, $Pd(NO_3)_2$, or palladium acetate, $Pd(OAc)_2$, in the aqueous phase,
2- formation of polyamic acid via IP reaction of POSS and 6FDA; palladium ions interact with the carboxylate group of polyamic acids during this process,
3- reduction of palladium ions to palladium nanoparticles by sodium borohydride ($NaBH_4$), and
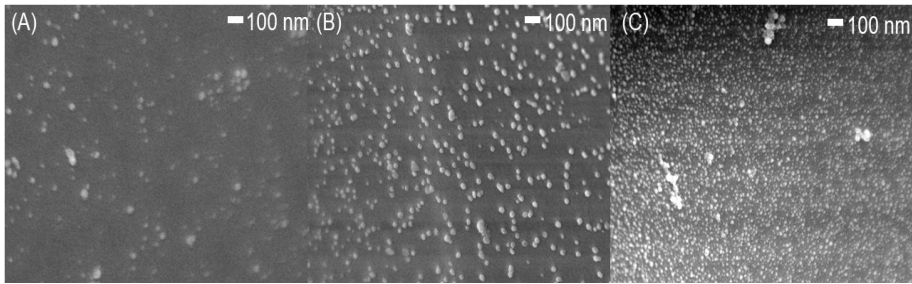4- conversion of polyamic acid to polyimide by thermal imidization.

Figure 8.3 FE-SEM images of palladium NPs embedded in polyPOSS imide matrix. The concentration of $Pd(NO_3)_2$ salts in the aqueous phase was increased from left to right side.

FE-SEM images (Figure 8.3) of free-standing layers show the successful formation of palladium nanoparticles in the polyPOSS-imide matrix on top of the ceramic supports. It is observed that a low concentration of palladium salts results in lower permeances and higher permselectivities, while a high concentration of palladium salts leads to the formation of a defective layer. Yet, the formation of embedded palladium nanoparticles was successful and might be interesting for other applications.

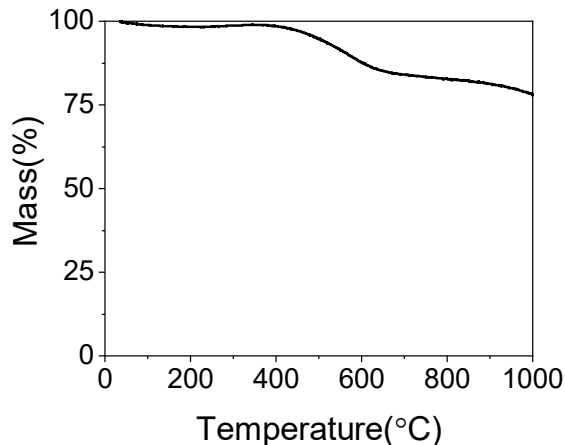## Increasing the thermal stability



Figure 8.4 TGA scan of the polyPOSS-imide free-standing layer with OAPS as the main building block.

The thermal stability of the polyPOSS-imide membranes is constrained by the propyl chains connected to the POSS cages. One solution to enhance thermal stability is to replace the aminopropyl chains with a more thermally stable group, such as aminophenyl. To this aim, octa amino phenyl POSS (OAPS) could be a good option to form polyPOSS-imide membranes. However, OAPS has limited solubility and much less reactivity in water to form a network with the conventional IP method. We used a non-aqueous interfacial polymerization to react OAPS in DMSO/water and 6FDA and form polyamic acid. This was followed by thermal imidization. The thermogravimetric analysis (TGA) data of the obtained polyimide confirms that the thermal stability of the network is enhanced, and no weight loss is observed at temperatures up to 450 °C under $N_2$ atmosphere, Figure 8.4.

The single gas performance of polyPOSS-imide membranes with OAPS, polyOAPS-imide, as the main building block at 50, 100, and 200 °C is shown in Figure 8.5. The permeability of the membrane decreases with the increasing size of the permeant, illustrating the molecular sieving behavior (Figure 8.5A). The gas permeation is thermally activated and the permeance increases with increasing temperature. The Arrhenius plots of the gas permeance (Figure 8.5B) exhibit constant activation energy over the complete temperature range from 50 to 200 °C. The activation energies follow the order $CH_4 > N_2 > He > H_2 > CO_2$, corresponding to the variation in the kinetic diameter of the gas molecules. The exception is $CO_2$ due to the affinity of this gas for the amine and $CF_3$ groups. In Figure 8.5C, the permselectivities of $H_2/N_2$, $H_2/CH_4$, and $H_2/CO_2$ are presented as a function of temperature. Results show that $H_2/N_2$ and $H_2/CH_4$ permeselectivities vary between 20 to 10 at temperatures of 50 °C to 200 °C, respectively. The permselectivities of all the gas pairs decrease as a function of temperature except for $H_2/CO_2$, which increases from 2 to 3 at temperature ranges from 50 to 200 °C. This is due to differences in the activation energies of $H_2$ and $CO_2$.
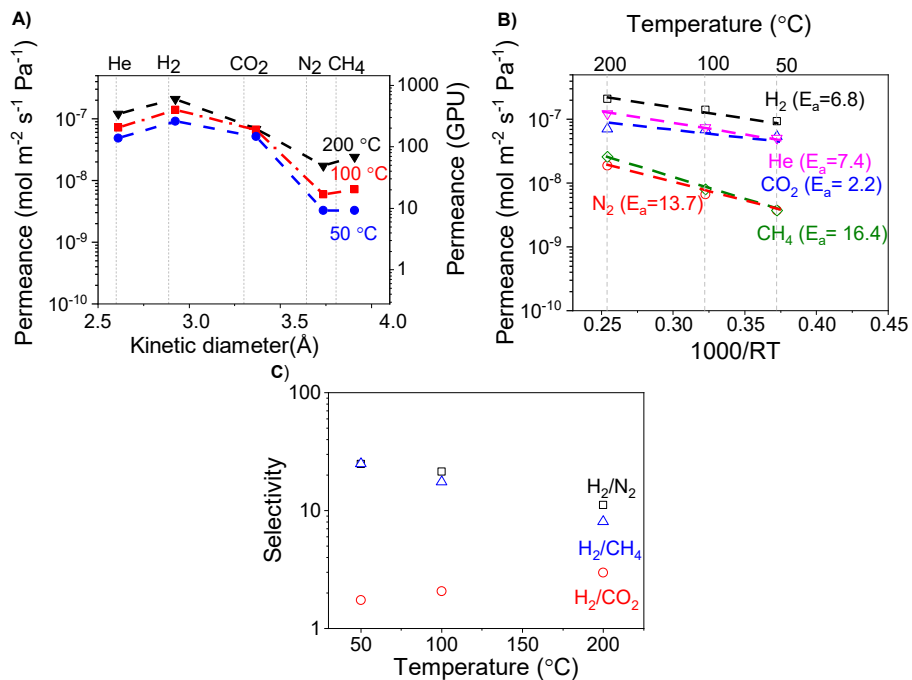
Figure 8.5 (A) Gas permeance as a function of gas kinetic diameter for three different temperatures. (B) Arrhenius plot of pure gas permeances. The unit of activation energies is kJ mol$^{-1}$. (C) Ideal selectivities of the membranes as a function of temperature.

Finally, polyOAPS-imide membranes exhibit lower permeances and permeabilities compared to polyimide membranes. The pathway of diffusion in polyPOSS-imide/polyOAPS-imide structures is via the organic bridges because the POSS cages are too small to allow the transportation of gases. Due to the low number of organic bridges (1 per OAPS cages) in poly OAPS-imide network compared to polyPOSS-imide, gases cannot diffuse freely in polyimide structure, which results in lower permeances.

## 8.1.2. Cyclomatrix polyphosphazene networks

Cyclomatrix polyphosphazene (CPPz) materials are broadly reported in the literature for their flame retardant properties and good thermal stability. However, the formation of films from this network in a single solvent is challenging and mainly results in microspheres. To overcome this issue, IP could offer a platform for in-situ synthesis and film formation in one single

step. However, the number of studies that succeeded in fabricating CPPz films via classical aqueous IP is limited [6,7] because the HCCP molecules are not reactive enough to form a network. In this thesis, we present for the first time the formation of a series of thin cyclomatrix polyphosphazene films with different linkers, via N or O atoms, using non-aqueous IP. The membranes have the potential for a broad range of applications, such as hydrogen separation at high temperatures, organic solvent nanofiltration, and gas barriers. Similar to conventional (aqueous) IP, the process can be tuned to control the properties of the CPPz membranes.

In chapter 3, we present membranes that have been prepared via the interfacial polymerization of a POSS and hexachlorocyclotriphosphazene (HCCP) for gas separation at high temperatures. POSS cages offer additional thermal and mechanical stability to the network, which was shown before by polyPOSS-imide networks. The network is highly cross-linked and shows high thermal stability up to 340 °C under $N_2$ atmosphere. At 250 °C, the POSS-HCCP membranes that we present have higher permselectivites compared to polyPOSS-imide membranes, while the hydrogen permeances are comparable.

In chapters 4, 5, and 7 we introduce a series of poly(phenoxy) CPPz membranes. The structure-property relationships of ploy(phenoxy) CPPz are extensively studied. The length, flexibility, and cross-linking extent of the organic bridges between the HCCP core can be varied via the selection of different precursors. Accordingly, the application of those membranes could be changed from hot hydrogen gas selective membranes to (hydrogen) gas barriers and organic solvent nanofiltration. The general trend from the above chapters is clear: CPPz with short organic bridges and lower cross-linking degrees are suitable for gas barriers. The short-length bridges between the HCCP core hinder the diffusion of gas molecules. In addition, the linear-like structure of these materials leads to denser polymer chain packing and less free volume.

The performance and application of the materials can be changed by changing the aryloxy groups between the HCCP rings. When the hydroxyphenyls are exchanged by biphenols, more permeable gas separation membranes are obtained that are suitable for hydrogen separation at high

temperatures. By further increasing the size and flexibility of the aromatic alcohols, networks can be made that can be used as organic solvent nanofiltration membranes.

Besides changing the precursors, the potassium hydroxide (KOH) concentration is another parameter that can be used to change the network structure, and hence the permeability. The presence of KOH is necessary for the conversion of the aromatic alcohols into aryloxide anions. The IP reaction involves the attack of the aryloxide anions on the P atoms of HCCP, resulting in the formation of CPPz, and KCl as a by-product. With increasing the KOH concentration, the concentration of aryloxide anions increases. This enhances the reaction kinetics and alters polymer chain packing, free volume, and gas permeation.

The importance of the cross-linking degree of CPPz structure in their thermal stability is further reflected in chapter 6. Unreacted hydroxyl and Cl groups connected to the HCCP core facilitate the collapse of the HCCP ring after exposure to a temperature above 250 °C. On the contrary, a fully cross-linked network is more thermally resistant and can stand high temperatures up to 450 °C.

Finally, non-aqueous interfacial polymerization provides a unique platform for synthesizing CPPz films on top of ceramic supports. CPPz networks have distinct and unique properties. The molecular flexibility of the network and pathways for molecular transportation can be adjusted by changing the organic bridges. The number of organic bridges has a critical and pronounced effect on the molecular fluxes.

## Long-term stability of CPPz gas separation membranes

Long-term operational stability under dry and humid conditions is important for membrane application in, for instance, the water-gas shift process since water is then present in the $H_2/CO_2$ separation process. Accordingly, the long-term performance of the POSS-HCCP and BPH-HCCP membranes under dry and wet conditions with mixed gas at 200 °C was performed, Figure 8.6.

Figure 8.6A represents the long-term hydrothermal stability of the POSS-HCCP membranes. The membrane shows stable performance over 100 hr at 200 °C during dry measurement. After introducing the humidity, both $H_2$ and $CO_2$ permeance decreases, and the $H_2/CO_2$ selectivity enhances. Even though a minor drop in permeance is observed during the wet measurement, the selectivity is higher than the initial selectivity observed in the dry feed atmosphere. After removing the humidity at 200 h, the permeance is still lower, and the selectivity is higher than the original values in the dry measurement. These results suggest that, under the operating conditions of 200 °C and transmembrane pressure of 10 bar, physical aging has a limited effect on the separation performance of the POSS-HCCP membranes. This is in line with the hydrothermal stability of polyPOSS-imide.[8]
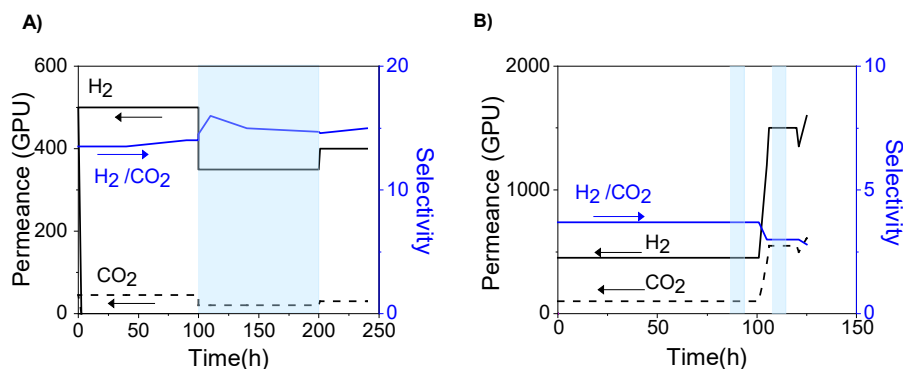


Figure 8.6 Long-term operational stability of membranes for $H_2/CO_2$ separation under dry ($H_2:CO_2:CH_4$ = 40:30:30) or wet feed (applying 10 mol% humidity) at 200 °C and transmembrane pressure of 10 bar. The blue area shows the effect of wet feed on the membrane performance. The experiments were conducted at Sintef Oslo by Dr. T.A. Peters. (A) POSS-HCCP and (B) BPH-HCCP membranes.

The long-term hydrothermal stability of the BPH-HCCP membrane is shown in Figure 8.6B. The data illustrate that the $H_2$ and $CO_2$ permeance is stable under dry conditions over 100 h. However, after introducing humidity, the permeances increase, and $H_2/CO_2$ selectivity reduces. Even after removing the water, neither permeances nor selectivity could not return to their original values. This could be due to the following reasons:

1- Decomposition of the network after exposure to humidity,
2- delamination of the BPH-HCCP layer from the support, and/or

3- the decomposition of the γ-alumina layer after exposure to high temperature and humidity.

To affirm the first assumption, we exposed the BPH-HCCP powder in an oven at 200 °C to the flow of $N_2$ with 10 mol% humidity for 10 h. FTIR and $N_2$ adsorption was measured before and after the heat treatment, and no changes could be detected before and after those treatments. Based on those experiments, we could not confirm the first reason and suggest doing an in situ hydrothermal stability test by thermal gravimetric analysis (TGA) instrument.

To validate assumption number 2 and 3, FE-SEM was done on the surface of tested membranes for long-term hydrothermal stability, Figure 8.7. The image shows that after the test, a defect close to 250 nm is formed on the surface due to the delamination of the BPH-HCCP layer from the support and/or the decomposition of the γ-alumina layer. The loose connection of the layer to the support leads to the separation of the layer from the support. Also, the thickness of the BPH-HCCP layer on top of the γ-alumina support is around 30 nm which offers low protection to the γ-alumina from the steam. Hence, I suggest increasing the thickness of the BPH-HCCP layer and re-evaluating the stability performance.
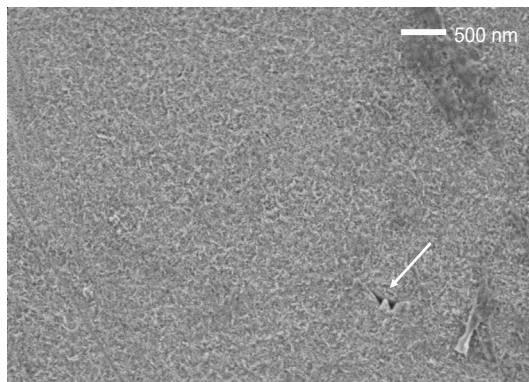


Figure 8.7 The FE-SEM image of the surface of the BPH-HCCP membrane after the hydrothermal performance test. The arrow shows the defect that forms on the surface after the test.

# Gas barriers

In chapter 5 of this thesis, we focus on developing hydrogen barrier via IP of small aromatic hydroxyl compounds in a KOH/DMSO solution and HCCP in cyclohexane on top of ceramic supports. Via the amount of dissolved potassium hydroxide, the extent of deprotonation of the aromatic hydroxyl compounds can be changed to tune the molecular structure and permselective properties of the thin polymer networks from hydrogen/oxygen barriers to gas separation membranes. The formed network has a low degree of cross-linking, providing a lower number of free volumes for gas diffusion. The layer forms on top of the ceramic supports; however, studying the properties of the layer independent of supports might be interesting for barrier application. Hence, developing a single-solvent polymerization method for synthesizing these materials, independent of a porous support, would be of help.

# Pyrolysis of the CPPz network

In chapter 6, we pyrolyzed CPPz networks that were obtained from the IP reaction between 1,3,5-trihydroxybenzene (THB) or *m*-dihydroxybenzene (MDHB) and HCCP. The structural and chemical evolution of the CPPz networks during the heat treatment process is studied in detail. The data show that the unreacted Cl or OH groups connected to the HCCP core facilitate the collapse of the $P_3N_3$ ring at temperatures around 250 °C. To overcome this issue, it would be interesting to replace 2 or 3 of the Cl groups under a controlled condition with aminophenyl, aryloxy, or phenyl groups, before the IP process. In this case, after the reaction of the remaining Cl, the added groups can protect the ring from collapsing.

# Nanofiltration (NF)

In chapter 7, we present organic solvent nanofiltration membranes that have been prepared via interfacial polymerization of 1,1-Tris(4 hydroxyphenyl)ethane (TPE) and HCCP using non-aqueous IP on top of polymeric polyacrylonitrile (PAN) and ceramic alumina supports. What makes this chapter intriguing is the critical role of the support in dictating the formation and properties of the formed layer. Alumina supports allow us to

form a defect-free thin neutral film suitable for separating small dyes with a molecular weight of 320 Da. These supports are hydrophilic and have small pores with a diameter of 3-8 nm. On the other hand, PAN supports are hydrophobic and less resistant toward the super base solution (DMSO and KOH) at 80 °C. They have big pores, which could hold/pass more volume of the first solution during IP. Consequently, the membrane fabrication method was adjusted, and a thermal treatment step was included. The obtained film on top of the PAN support is negatively charged and does not cover the whole surface of the support. Also, the polymer-supported membrane is not as selective as the alumina-supported membranes because of defects. Hence, I strongly suggest optimizing the procedure for making the layer on top of the polymeric supports.

## More questions to answer

Finally, various questions still remain regarding the non-aqueous IP and structure properties of CPPz. In aqueous IP, the interfacial polymerization reaction mainly takes place in the organic phase since the monomer in the aqueous phase has a higher solubility in the organic phase. For the non-aqueous IP, one can expect that the reaction zone will shift, at least partly, towards the DMSO phase. A microfluidic device can simply visualize the formation of free-standing films and subsequently help us to understand the direction of film growth on the supports. Another important question is the sorption behavior of the CPPz membranes toward $CO_2$ and $CH_4$. The sorption of molecules by a polymer causes network dilation of the polymer material and plasticization of the polymer. So, it is one of the essential fields to investigate later. The final question is the effect of cyclic structure of HCCP on the performance of CPPz films. A simple way is to replace the HCCP monomer with poly(dichlorophosphazene) in the IP process to explore if the linear structure of this molecule provides opportunities for improved membrane/gas barrier properties.

## 8.2 Possible monomer combinations for non-aqueous interfacial polymerization

Non-aqueous IP provides a platform to expand the IP technique to monomers with low solubility and reactivity in water. We try to emphasize

the robustness and versatility of this technique by introducing other possible monomer combinations that can be reacted via non-aqueous IP. This section describes preliminary experiments with some of these combinations, and discusses some specific properties of the formed networks, such as their thermal and chemical stability. Abbreviations and molecular structures of the various monomers can be found in Table 8.2.
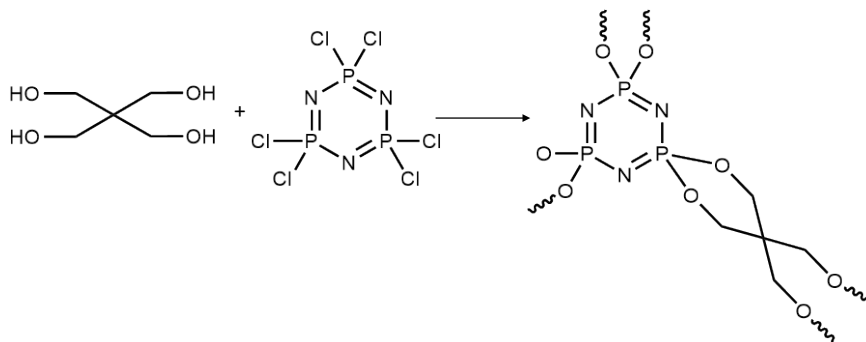
## 8.2.1 Networks based on HCCP



Figure 8.8 The formation of the PEN-HCCP structure.

Non-aqueous IP provides a suitable platform to react pentaerythritol (PEN) in DMSO/ water/KOH with HCCP in cyclohexane, Figure 8.8. The obtained network was analyzed by energy dispersive X-ray spectroscopy (EDX) technique, Table 8.1. The result showed that between 1 to 2 PEN react per HCCP. Considering the low concentration of Cl in the structure, we can conclude a fully cross-linked network form.

Table 8.1 EDX analysis of PEN-HCCP free-standing layers.

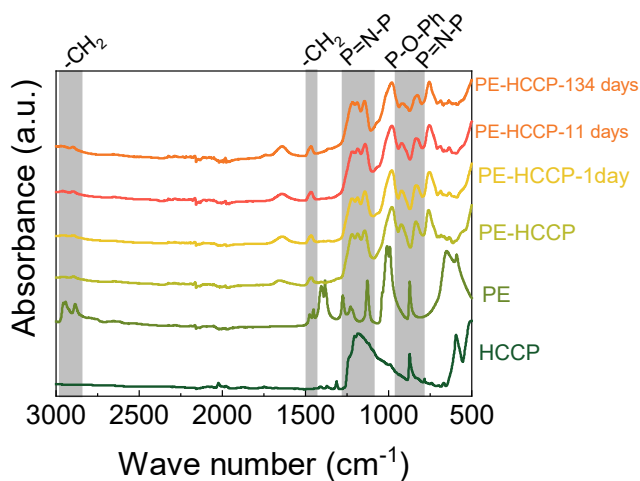| Element | Atomic composition (%) |
|---------|------------------------|
| C | 41.49±0.2 |
| N | 12.9±1 |
| O | 18.7±1 |
| P | 21.5±0.9 |
| S | 0.4±0.1 |
| Cl | 2.2±0 |
| K | 3.4±0.6 |

Figure 8.9 FTIR spectra of PEN-HCCP networks performed at specific times after exposure to 0.1 M NaOH solution.

To study the potential of these networks in high pH conditions, we expose the free-standing powder to 0.1 M NaOH solution for 134 days. The FTIR spectra of this network at specific times after exposure to NaOH is shown in Figure 8.9. The results show that the network is stable, proving the potential of this network to be used at extremely high pH. However, further research is mandatory to fully investigate this technique considering the hydrolysis of P-Cl bonds.

## 8.2.2 Networks based on tetrafluoroterephthalonitrile

We go one step further to test the potential of our non-aqueous system in the formation of networks on chemistries in that HCCP molecules are not involved. For this, tetrafluoroterephthalonitrile (TFTPN) replaces HCCP and reacts with non-conventional IP monomers, listed in Table 8.2, in DMSO. The preliminary results showed that the layer was formed at the interface of two phases with the mentioned monomer combinations.

The formed network in the last row of Table 8.2 might be interesting for the formation of polymers of intrinsic microporosity (PIM).[9] For this, some preliminary characterizations such as FTIR were performed to verify the formation of these networks, Figure 8.10. The result confirmed the presence

of all the characteristic peaks of TTSBI and TFTPN as well as the new bond, P-O-ph. However, further optimization and analysis are required to understand the properties and potential of the materials. For example, the networks might enhance the performance of membranes by providing an open structure.
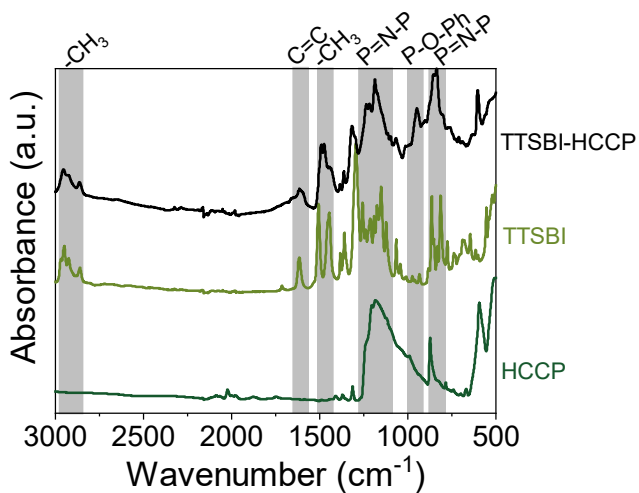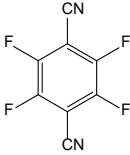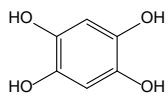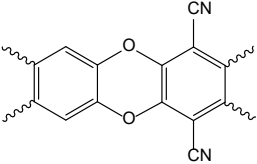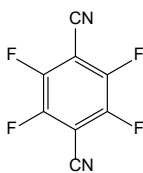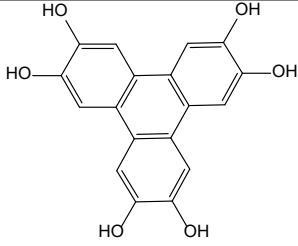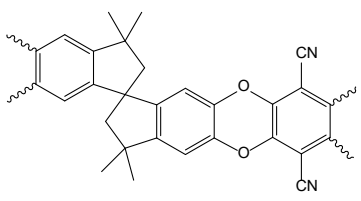


Figure 8.10 FTIR spectra of TTSBI-TFTPN.

Table 8.2 List of suggested monomer combinations and the expected structure after the IP

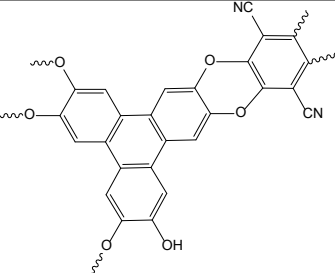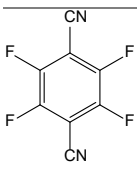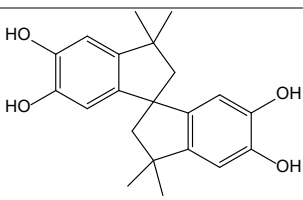| Monomer 1 | Monomer2 | Suggested network |
|---|---|---|
|  TFTPN |  1,2,4,5-Benzenetetrol |  |
|  TFTPN |  2,3,6,7,10,11-Hexahydroxytriphenylene |  |
|  TFTPN |  5,5',6,6'-tetrahydroxy-3,3,3',3'-tetramethyl-1,1'-spirobisindane |  |

# 8.3 General conclusions and remarks

## 8.3.1 Interfacial polymerization

A crucial parameter in IP is the selection of monomers. Monomers determine the flexibility and pore (free-volume) size of the network controlling the final performance of the formed layer. For example, increasing the size of organic bridges in hybrid materials enhances the pore (free-volume) size and shifts the molecular separation from gases to liquids.

The reactivity of monomers plays a vital role in the formation and properties of networks. Monomers with lower reactivity do not react or require more time to react, which influences the thickness and properties of the layer. In this thesis, we found that the solvents strongly influence the reactivity of the monomer and can enhance the kinetics of the reaction. For example, in this thesis DMSO replaces water in conventional IP to facilitate the nucleophile attack and help the formation of layers.

Reaction parameters can influence the properties of the formed layer. For example, we find out that raising the concentration of reactant can intensify the polymer chain packing by increasing the kinetics of the reaction.

## 8.3.2 Cyclomatrix polyphosphazene network

CPPz network is known for its high thermal stability. However, the properties of this material as a potential membrane under harsh conditions have not been completely addressed. The proposed non-aqueous IP in this thesis allows for facile fabrication and detailed study of these materials as films. For example, we found out that by reducing the flexibility and number of organic bridges between the HCCP core, the network could be adjusted for barrier properties. They can be pyrolyzed at 450 °C to form a dense graphitize structure accompanied by P-O bonds. The unreacted free Cl group in CPPz material could facilitate the ring opening of the HCCP core.

## 8.3.3 Industrial application

We hope to go one step further and scale up CPPz materials for industrial applications. However, we need to address some issues before taking this step, including changing the ceramic support to polymeric support and the effect of steam on the long-term hydrothermal stability of those networks, producing self-stand barrier materials.

## 8.3.4 The future potential of the new platform

In this thesis, we have shown that non-aqueous interfacial polymerization provides an opportunity to use monomers with complicated topologies beyond the potential of classical aqueous interfacial polymerization. This

technique, like classical interfacial polymerization, allows control of the structure, properties, and performance of membranes/films based on the applications. It is notable that after successfully preparing films on top of the ceramic supports, we have taken non-aqueous interfacial polymerization a step closer to scaling up by preparing thin film composite membranes with polymeric supports. One could mention that our produced membranes still have some limitations, such as low permeation compared to commercial membranes. However, we should notice that this technique is still new and plenty of modifications can be performed to improve the performance of the final membranes.

## 8.4 References

[1] M.J.T. Raaijmakers, M.A. Hempenius, P.M. Schön, G.J. Vancso, A. Nijmeijer, M. Wessling, N.E. Benes, Sieving of Hot Gases by Hyper-Cross-Linked Nanoscale-Hybrid Membranes, J. Am. Chem. Soc. 136 (2014) 330–335. https://doi.org/10.1021/ja410047u.

[2] M.J.T. Raaijmakers, W. Ogieglo, M. Wiese, M. Wessling, A. Nijmeijer, N.E. Benes, Sorption Behavior of Compressed CO 2 and CH 4 on Ultrathin Hybrid Poly(POSS-imide) Layers, ACS Appl. Mater. Interfaces. 7 (2015) 26977–26988. https://doi.org/10.1021/acsami.5b08286.

[3] M.J.T. Raaijmakers, E.J. Kappert, A. Nijmeijer, N.E. Benes, Thermal Imidization Kinetics of Ultrathin Films of Hybrid Poly(POSS-imide)s, Macromolecules. 48 (2015) 3031–3039. https://doi.org/10.1021/acs.macromol.5b00473.

[4] M.J.T. Raaijmakers, M. Wessling, A. Nijmeijer, N.E. Benes, Hybrid Polyhedral Oligomeric Silsesquioxanes–Imides with Tailored Intercage Spacing for Sieving of Hot Gases, Chem. Mater. 26 (2014) 3660–3664. https://doi.org/10.1021/cm500691e.

[5] L.F. Villalobos, R. Hilke, F.H. Akhtar, K.-V. Peinemann, Fabrication of Polybenzimidazole/Palladium Nanoparticles Hollow Fiber Membranes for Hydrogen Purification, Adv. Energy Mater. 8 (2018) 1701567. https://doi.org/10.1002/aenm.201701567.

[6] E. Maaskant, H. Gojzewski, M.A. Hempenius, G.J. Vancso, N.E. Benes, Thin cyclomatrix polyphosphazene films: interfacial polymerization of hexachlorocyclotriphosphazene with aromatic biphenols, Polym. Chem. 9 (2018) 3169–3180. https://doi.org/10.1039/C8PY00444G.

[7] M. You, W. Li, Y. Pan, P. Fei, H. Wang, W. Zhang, L. Zhi, J. Meng, Preparation and characterization of antibacterial polyamine-based cyclophosphazene nanofiltration membranes, J. Memb. Sci. 592 (2019) 117371. https://doi.org/10.1016/j.memsci.2019.117371.

[8] L. Ansaloni, M. Sarić, E. Louradour, F. Radmanesh, J.W. Dijkstra, M. Pilz, D. Høvik, N.E. Benes, Y. van Delft, T.A. Peters, Stability investigation of polyPOSS-imide membranes for H2 purification and their application in the steel industry, Int.

J. Hydrogen Energy. 47 (2022) 11359–11368. https://doi.org/10.1016/j.ijhydene.2021.09.089.

[9] M. Tamaddondar, A.B. Foster, M. Carta, P. Gorgojo, N.B. McKeown, P.M. Budd, Mitigation of Physical Aging with Mixed Matrix Membranes Based on Cross-Linked PIM-1 Fillers and PIM-1, ACS Appl. Mater. Interfaces. 12 (2020) 46756–46766. https://doi.org/10.1021/acsami.0c13838.

# Acknowledgements

The past four years have been a great and inspiring journey. I grew professionally and personally on many levels and learned many skills. In this part, I would like to express my gratitude to my colleagues, friends, and family for their support and help along this journey.

My first appreciation goes to my supervisor **Nieck Benes** who believed in me and gave me the opportunity to work as a PhD student at Film in Fluids (FiF) group. I am sincerely thankful for the unlimited support and all the scientific discussions throughout these four years. I especially appreciate the huge amount of freedom in directing the flow of my PhD to try different scientific fields and make mistakes. Your particular guidance and remarks made me try my best to achieve as much as I can from my PhD. Not only in the research, but you taught me a lot about managing projects and supervising students.

I would like to thank **Ernst Sudhölter** for supervising me and bringing insightful contributions from the chemist's perspective. It was always a great pleasure to discuss with you my chemistry questions and see your enthusiastic responsiveness and eagerness to go deeper into the subject.

I am grateful to **Alberto Tena** for being critical of my research work. It helped me to be critical, find my weaknesses and think a few steps ahead of my research. I enjoyed our scientific as well as non-scientific discussions.

I would like to thank **Mark Hempenius** for all our chemistry discussions on the chapters two and five. I appreciate that you always made time in your busy schedule to help me out.

**Gerrald Bargeman (Nouryon)**, I am grateful for all your help with chapter seven. I really appreciate the time you took to review my paper and give me suggestions for improvements.

**Thijs Peters** and **Luca Ansaloni (SINTEF),** I thank you for bringing your critical point of view to our research in chapter two. I really appreciate the time you took to review chapter two and turn it into an excellent paper. **Thijs,** thank you for doing more research on the cyclomatrix polyphosphazene membranes and performing long-term gas permeation

measurements on them. I believe these experiments give insight for future directions.

**Genesis 2020** partners, I appreciate all the meetings and comments on thermally stable gas separation membranes. Mainly, I would like to thank Monika Pilz from SINTEF, Thijs Peters from SINTEF, Luca Ansaloni from SINTEF, Eric Lourader from CTI, Dag Høvik from Funzionano AS, and Yvonne van Delft from TNO for all the inputs that you gave.

I also wish to thank the members of my committee, **Suzana Nunes, Katja Loose, Thijs Peters, Gerrald Bargeman, Christian Nijhuis,** and **Mark Hempenius,** for generously offering their time and support to review my thesis.

To my paranymph **Nikos** and **Anne**, I would like to thank you for taking a special place in my ceremony. **Nikos**, it was a great pleasure to have you as a colleague and friend. Our discussions in the lab or during coffee breaks played a great role in my project and scientific perspectives. **Anne**, you are such a kind and friendly person. Whenever I was frustrated or confused, I could always rely on you for a short walk on campus, which calmed me down and helped me to make up my mind.

**Cindy** and **Frank**, I am extremely thankful not only for helping me in the lab but also for all the fun times during breaks. During the past four years, you supported and helped me complete my work in the lab; without you, it would not be possible. Besides, I appreciated the breaks and all the chocolates. **Annet,** I would appreciate your help during my PhD. You are such a friendly person, I am thankful for all the short talks.

**Marie** and **Zainab**, I am extremely grateful for the times we spent together inside and outside the lab. Not only have both of you turn out to be great friends, but you have played a significant role in my professional career.

I would like to thank the former members of FiFs; **Mariël and Kristianne**. **Mariël**, I was lucky to have you for the first two years of my PhD. Thank you for all the lessons about interfacial polymerization. I enjoyed sharing our

scientific and non-scientific thoughts and issues. **Kristianne**, thank you for our discussions and for teaching me ellipsometry.

I would like to thank the remaining current and former members of MST and IM cluster for all the scientific and friendly discussions, as well as pleasant dinners. Thank you **Ameya, Audrey, Lily, Tao, Moritz, Burak, Wouter, Harmen, Wendy, Herman, Ineke, Rob, Tymen, Pelin**, Renaud, **Michiel, Michel, Jurjen, Jurgen, Patrik, Jason, Juri, Matthijs, Hans David, Harm, Dona, Bob, Iske, Dennis, Denys, Antoine, Shuyana, Liniker, Meryll, Timon, Louis, Jeff, Shaur**, **Mieke** and **Chin Yin**.

I owe my gratitude to my family. **Mama**, I would like to thank you for never doubting me for a second. You have always supported me in following my dreams, no matter how difficult it was to be far from each other. I am forever grateful to you! Dear **Baba**, I always love you and will miss you so much. I am grateful to you for all the life lessons. Thank you for all your effort in raising me. My sister **Safoora**, and my brother **Reza**, despite the long distance, your unconditional love, support, optimism, and advice were more valuable than you could imagine. Thanks for always being there for me. **Hadi**,  thank you for your support and love.

My dear husband, **Vali**, words are not just enough to express my gratitude and feeling for you. This work could not have been done without your patience. You always supported my work and encouraged me during the tough and inconvenient time of PhD. You have always listened to my problems and wisely advised me. Your cheerful and positive nature has enlightened my mood and motivated me to continue. You are the light of my life and the most important person to me. I am grateful for everything we have done together and looking forward to the future.

<div align="right">
With Love,<br>
Farzaneh<br>
November 2022
</div>

# About the author

Farzaneh Radmanesh was born on August 29, 1989 in Esfahan, Iran. After graduating high school in the field of mathematics, she started bachelor in Chemical Engineering-polymer industry at the Isfahan University of Technology. For her bachelor's thesis, she conducted research on fabrication and characterization of nanocomposite membranes for gas separation. She gained some teaching experience as a teaching assistant (TA) in different courses during her bachelor studies.

Directly after bachelor, she started her master in 2010 in Chemical Engineering at the same university. During her master studies she was also part-time involved in teaching. After obtaining her master degree in 2013, she started working as a full-time TA and research assistant in the same department at Isfahan University of Technology.

 In 2017, she came to The Netherlands, the University of Twente, to conduct research work on ion exchange membranes at Membrane Science and Technology (MST) cluster with Prof. Wiebe M. de Vos as her supervisor. Her research work was about the fabrication and characterization of cation exchange membranes. In August 2018, she started a Ph.D. at the Film in Fluid (FiF) group under the supervision of prof.dr. Nieck Benes and prof.dr. Ernst Sudhölter in the project named Genesis 2020.

# List of publications

## From this thesis

1. **<u>Farzaneh Radmanesh</u>**, Ernst J.R. Sudhölter, Alberto Tena, Maria G. Elshof, and Nieck E. Benes. "Thin film composite cyclomatrix poly(phenoxy)phosphazenes membranes for hot hydrogen separation." *Advanced Materials Interfaces* (2022)-Accepted.

2. **<u>Farzaneh Radmanesh</u>**, Gerrald Bargeman and Nieck E. Benes. "Cyclomatrix polyphosphazene organic solvent nanofiltration membranes." *Journal of Membrane Science* (2022)-Accepted.

3. **<u>Farzaneh Radmanesh,</u>** Monika Pilz, Luca Ansaloni, Thijs A. Peters, Eric Louradour, Henk van Veen, Dag Høvik, Mark A. Hempenius, and Nieck E. Benes. "Comparing amine-and ammonium functionalized silsesquioxanes for large scale synthesis of hybrid polyimide high-temperature gas separation membranes." *Journal of Membrane Science* 637 (2021): 119524.

4**<u>. Farzaneh Radmanesh,</u>** Maria G. Elshof, and Nieck E. Benes. "Polyoctahedral Silsesquioxane Hexachlorocyclotriphosphazene Membranes for Hot Gas Separation." *ACS applied materials & interfaces* 13.7 (2021): 8960-8966.

5. **<u>Farzaneh Radmanesh,</u>** Ernst J.R. Sudhölter, Alberto Tena, and Nieck E. Benes. "Non-aqueous interfacial polymerization derived polyphosphazene films for sieving or blocking hydrogen gas." Submitted.

6. **<u>Farzaneh Radmanesh,</u>** Alberto Tena, Ernst J.R. Sudhölter, and Nieck E. Benes. "Low temperature pyrolysis of thin film composite polyphosphazene membranes for hot gas separation." Submitted.

## Beyond this thesis

7. **<u>Farzaneh Radmanesh</u>**, Timon Rijnaarts, Ahmad Moheb, Morteza Sadeghi, and Wiebe M. De Vos. "Enhanced selectivity and performance of heterogeneous cation

exchange membranes through addition of sulfonated and protonated Montmorillonite." *Journal of colloid and interface science* 533 (2019): 658-670.

8. Sylvie Neyertz, David Brown, Saman Salimi, **Farzaneh Radmanesh**, and Nieck E. Benes. "Molecular Characterization of Membrane Gas Separation under Very High Temperatures and Pressure: Single-and Mixed-Gas $CO_2/CH_4$ and CO2/N2 Permselectivities in Hybrid Networks." *Membranes* 12.5 (2022): 526.

9. Saman Salimi, **Farzaneh Radmanesh**, Nieck Benes, Monika Pilz, David Brown, and Sylvie Neyertz. "Identifying the meta, para and ortho isomers in octa (aminophenyl) silsesquioxane (OAPS) from joint experimental characterizations and theoretical predictions of the IR and NMR spectra." *Journal of Molecular Structure* 1266 (2022): 133510.

10. Luca Ansaloni, Maria Sarić, Eric Louradour, **Farzaneh Radmanesh**, Jan Wilco Dijkstra, Monika Pilz, Dag Høvik, Nieck E. Benes, Yvonne van Delft, and Thijs A. Peters. "Stability investigation of polyPOSS-imide membranes for H2 purification and their application in the steel industry." *International journal of hydrogen energy* 47.21 (2022): 11359-11368.

11. Sylvie Neyertz, Saman Salimi, **Farzaneh Radmanesh**, Nieck E. Benes, and David Brown. "High-temperature molecular screening of hybrid polyOAPS-imide networks based on octa (aminophenyl) silsesquioxane for increased thermomechanical resistance." *Physical Chemistry Chemical Physics* 23(2021): 11438-11454.

12. Luca Ansaloni, Eric Louradour, **Farzaneh Radmanesh**, Henk van Veen, Monika Pilz, Christian Simon, Nieck E. Benes, and Thijs A. Peters. "Upscaling polyPOSS-imide membranes for high temperature $H_2$ upgrading." *Journal of Membrane Science* 620 (2021): 118875.

13. Sylvie Neyertz, David Brown, Saman Salimi, **Farzaneh Radmanesh**, and Nieck E. Benes. "Molecular characterization of polyOAPS-imide isomer hyper-cross-linked membranes: Free-volume morphologies and sorption isotherms for $CH_4$ and $CO_2$." *Journal of Membrane Science* (2021): 119531.

14. Timon Rijnaarts, Dennis M. Reurink, **Farzaneh Radmanesh**, Wiebe M. De Vos, and Kitty Nijmeijer. "Layer-by-layer coatings on ion exchange membranes: Effect of multilayer charge and hydration on monovalent ion selectivities." *Journal of membrane science* 570 (2019): 513-521.

15. Elisabeth Vaudevire, **Farzaneh Radmanesh**, Annemieke Kolkman, Dennis Vughs, Emile Cornelissen, Jan Post, and Walter van der Meer. "Fate and removal of trace pollutants from an anion exchange spent brine during the recovery process of natural organic matter and salts." *Water research* 154 (2019): 34-44.

16. Amir Ehsanian Mofrad, Ahmad Moheb, Mohammadali Masigol, Morteza Sadeghi, and **Farzaneh Radmanesh**. "An investigation into electrochemical properties of poly (ether sulfone)/poly (vinyl pyrrolidone) heterogeneous cation-exchange membranes by using design of experiment method." *Journal of colloid and interface science* 532 (2018): 546-556.